Analysis Of Factors That Contribute To And Interfere With Bactericidal Properties Of Low-Temperature Atmospheric Pressure Plasmas

Angela Privat Maldonado

Doctor of Philosophy

University of York

Biology

September 2015

ABSTRACT

Bacterial resistance to antibiotics continues to be a significant concern globally. In the search for more effective antibacterial treatments, low temperature plasmas (LTPs) have arisen as an attractive alternative to traditional therapies. LTPs generate a cocktail of reactive nitrogen and oxygen species (RNOS), ultraviolet (UV) photons, electrons and electromagnetic fields. They therefore offer the potential to facilitate the localised delivery of bactericidal agents without contact to the treatment site. However, whether the distribution of RNOS in the gas phase, the presence of organic matter during treatment and the heterogeneity of bacterial populations affect the treatment outcome was unknown.

Single-cell analysis was undertaken throughout to investigate the heterogeneous response of the model system *Salmonella enterica* to treatment with atmospheric-pressure plasma jets. In conjunction with the electrical, optical, and chemical studies, this enabled key mechanisms that drive plasma-bacteria interactions to be explored. My research has demonstrated three main points: **(a)** The level of DNA damage induced in single cells is determined by the spatial distribution of RNOS in the plasma effluent. This was found to be a characteristic of LTPs generated in open air. **(b)** The contribution of UV radiation solely to bacterial elimination and induction of DNA damage is minimal. Therefore, the bactericidal action of LTPs can be ascribed to the RNOS generated in the plasma, although the role of charged species and electric fields cannot be ruled out. **(c)** Preferential redox reactions between plasma-generated RNOS and external biomolecules in the environment decrease the efficacy of the treatment.

This study evidences the importance of the aforementioned conditions for the development of successful antimicrobial plasma therapies. It highlights the usefulness of single cell analysis to assess heterogeneous responses in a bacterial population in response to LTPs treatments. These results were made possible only due to interdisciplinary quantitative approaches used in this project.

TABLE OF CONTENTS

LIST OF FIGURES

Chapter 1: Introduction

Chapter 2: Materials and Methods

Chapter 3: Optimization of the AP-DBD plasma jet for bacterial elimination

LIST OF TABLES

"You have brains in your head. You have feet in your shoes. You can steer yourself any direction you choose"

Dr. Seuss

"You're off to great places! Today is your day! Your mountain is waiting, so get on your way!"

Dr. Seuss

ACKNOWLEDGEMENTS

I would like to thank my four supervisors Dr. Marjan van der Woude, Dr. Roddy Vann, Dr. Deborah O'Connell and Dr. Paul Pryor, who have made my journey through this PhD all the more enjoyable. I appreciate their continuous support during my research, the friendly advice I always received from them and their patience. You are all excellent people and mentors from whom I have learnt much more than just science. I would also like to thank my training advisory panel, Dr. Sangeeta Chawla and Dr. Christoph Baumann, for their feedback and helpful discussions that helped me to progress on my research.

I would like to thank all the members in the van der Woude group, past and present: Nick Donohue, Reyme Herman, Grace Taylor-Joyce, Andy King and all the undergrad and master students that made this place an exceptional group of people to work with. In special, I thank Erica Kintz for her friendship and for being an awesome Master and Commander. Also, I would like to thank everyone in the LTP group, who always made me feel welcome and helped me so much since day one. In especial, I would like to thank James Dedrick, Sandra Schröter, Andy West and Jerome Bredin for their friendship. A big thank you to all the CII residents that made this place an second home for me, in special Shraddha Kamdar, Ana Pinto, Naj Brown and German Leonov who are magnific people, excellent scientists and very good friends. Also, I would like to thank all the members of the Latin American Society, specially Manuel Lopez Pereyra, Cinthia Mena-Duran, Martha Villamizar, Gabriela Gross and Horacio Hoyos for the good energy they all transmit.

I deeply appreciate the invaluable help received from Dr. Kari Niemi, Richard Hermitage, Neil Johnson, Bob Hide and John Emery on solving the problems we had with the plasma sources during these years. Also, I would like to thank Graeme Park, Jo Marrison, Karen Hogg and Karen Hodgkingson for their help with my image analysis and flow cytometry experiments and Phil Roberts for the photography. I would also like to thank Dr. Victor Chechik and his group for giving me the chance to run invaluable experiments that complemented my research.

In particular, I would like to thank the Wellcome Trust and the University of York for sponsoring my research and for giving me the opportunity to develop a set of invaluable interdisciplinary skills I am sure will help me in my future career. I would also like to thank my former mentor Dr. Jorge Arevalo Zelada for believing in my abilities as a young student and supporting my application to the CIDCATS programme.

Finally, I would like to thank my family, specially my mom and grandma for their unconditional love and support, my sisteron Caty and my brotheron Haris for their loving advice and my husband Yury, who I met during my time in York and has supported my efforts to finish this PhD with love, patience and good humour. They have been there for me during the ups and downs of my PhD and I cannot thank them enough for that. Muchas gracias.

AUTHOR'S DECLARATION

All the work presented in this thesis is original and was carried out by myself, with the exception of Figure 3.9 which was prepared by Dr. Kari Niemi and Figures 2.6a, 4.10c and 4.12a, which were prepared by Apiwat Wijaikhum and adapted for this thesis.

I recorded the light emitted from the AP-DBD plasma jet and Dr. Kari Niemi helped with the calculation of the gas temperature. The measurement of the ozone density in the gas phase was done in collaboration with Apiwat Wijaikhum, who did the data analysis. I prepared the samples for EPR spectroscopy and UV-Vis spectrophotometry assays and the acquisition was carried out in conjunction with Dr. Yury Gorbanev in the Department of Chemistry. I prepared the samples for flow cytometry assays and the acquisition was assisted by Dr. Karen Hogg. The image analysis for the DDD Assay was done by myself using an algorithm developed by Dr. Roddy Vann.

None of the work described herein has been presented previously for an award at this, or any other, university.

1 INTRODUCTION

1.1 MOTIVATION OF THE PROJECT

Bacterial resistance to antibiotics continues to be a significant concern globally as it can result in increased costs for the healthcare system and loss of human life (1). This is not a new problem, since the appearance of drug-resistant strains started in hospitals around 1930s (2). In the late 1950s, the appearance of multi-drug resistant *Salmonella spp.*, *Escherichia coli* and *Shigella spp.* was first reported (3). Nowadays, the number of drug-resistant pathogens has increased, partially due to the administration of incomplete treatments or exposure to sub-lethal doses of the drug (2) and this poses a threat to public health. The pipeline for antibiotic development faces a challenging scenario due to the large amount of time, effort, scientific research, and expense required to generate new compounds.

Patients in health-care facilities are at special risk of infections. Burns, open sores and especially surgical wounds are amongst of the most frequently affected sites in health-care facilities and is one of the most common infections acquired in nosocomial settings. These are related to significantly high levels of morbidity and they can progress to systemic infections that lead to death (4). For example, pathogens such as *Pseudomonas aeruginosa*, *Staphylococcus aureus* and beta-haemolytic streptococci that colonize acute and chronic wounds, surgical site wounds and burns (5) are known to develop resistance to antibiotic treatments (6-8). The development of antibiotic resistance in clinically important bacteria complicate the elimination of infections and compromise the healing process (9, 10). The development of alternative or complementary therapies that can effectively eliminate pathogens from skin infections, especially pathogens resistant to single or multiple drugs, that are safe and do not generate resistance to treatment is paramount. New treatments, such as low temperature plasma therapies that can effectively address the polymicrobial nature of wound infections and that do not rely on a single mechanism of action, are especially needed.

The motivation for this project is to contribute towards the development of new topical antibacterial treatments that can be translated to the patients' bedside. With this purpose, this project aims to investigate a new topical antimicrobial therapy based on the use of low temperature plasmas (LTPs) to treat bacterial infections. LTPs are a multitarget therapy that have proved to be effective against microorganisms *in vitro* and *in vivo* (11-15). LTPs could be an effective way to eliminate pathogens from chronic wounds, surgical site infections and burns where conventional antibiotic therapies have failed. Short exposures to this multitarget therapy has also been suggested to be safe for humans, as the exposure to low concentration of reactive nitrogen and oxygen species have stimulating effects in eukaryotic cells (increase of proliferation and migration, promotion of DNA repair) and the UV radiation emitted by plasma does not have major negative effects (16). However, a deeper understanding of the factors that

contribute to or interfere with the efficacy of the treatment is fundamental. This study is an effort to provide insight in this direction.

1.2 STATE OF THE ART - BIOMEDICAL OPTIONS TO TREAT INFECTED WOUNDS

The failure of antibiotics to control wound infections have motivated the interest of the scientific community towards the development of alternative therapies that do not rely on a single mechanism of action. Common bactericidal procedures used to sterilize surfaces such as wet and dry heat, irradiation, UV light, pulsed electric fields, high hydrostatic pressures and ultrasound are effective on inert materials, but are not suitable for patient treatment (17). Novel topical therapies to eliminate pathogens on infected wounds have emerged due to the many advantages they have over systemic antibiotic treatments, especially systemic adverse effects. Topical treatments provide increased target site concentration and allow the use of antimicrobial agents not available for systemic therapy, such as dressings supplemented with silver ions and alginates, vacuum dressings and low temperature plasmas.

The treatments currently available to treat wound infections can be classified into two categories: antibiotics and antiseptics.

1.2.1 Antibiotics

Antibiotics can be described as chemicals compounds that can be produced naturally (by microorganisms for example, e.g. penicillin) or synthetically that can inhibit the proliferation or eliminate microorganisms. Antibiotics have an effect on specific cell targets with a narrow spectrum of activity (18). These compounds are relatively nontoxic, but due to bacterial resistance, they are more prone to losing their effectiveness (10). These include sulfonamides, penicillins, tetracyclines, polymixin, neomycin and chloramphenicol; each of them with specific action over Gram-positive or Gram-negative bacteria. However, bacteria that develop resistance to one or multiple drugs can cause prolonged infections, expensive health care costs, and increase the risk of death, posing a significant threat to public health. New antibiotics are needed to treat skin infections, considering the increasing number of methicillin-resistant *S. aureus* (MRSA) infections in wounds (19).

1.2.2 Antiseptics

These are compounds with antibacterial action that can be applied to intact skin or open wounds to inhibit or kill microorganisms. In contrast to antibiotics that act on specific cell targets, these compounds have multiple targets and are effective against a broad range of microorganisms (10), which makes more difficult the development of resistance to treatment. The mechanisms of antibacterial action of antiseptics used on infected wounds are multiple and include DNA intercalation and induction of DNA breaks, inhibition of DNA synthesis, cross-linking of macromolecules, damage to membrane-bound enzymes, among others (20).

Hydrogen peroxide (H_2O_2): This is a colourless liquid widely used for disinfection that is effective against bacteria (vegetative and spores), yeasts and viruses (20). The bactericidal activity of H_2O_2 is mediated by the induction of oxidative damage in target cells. This effect is *via* direct interaction with sulfhydryl groups in proteins, but mostly *via* indirect generation of highly reactive hydroxyl free radicals (·OH) which attack biomolecules such as lipids in the cell membrane, proteins, and nucleic acids (21). It has been described that Gram-positive bacteria are more sensitive to H_2O_2 than Gram-negative bacteria (10), but tolerance to the treatment can be developed when pathogens are exposed to sub-lethal concentrations of H_2O_2 (22).

Chlorhexidine: Due to its broad-spectrum efficacy and low irritation, it is one of the most widely used compounds for the manufacture of antiseptic products (20). Chlorhexidine affects directly the membrane potential of microorganisms and at high concentrations, it induces the coagulation of intracellular biomolecules (23). The activity of chlorhexidine can be affected by the presence of biomolecules and depends on the pH (24). Although chlorhexidine is widely used and it is an effective antiseptic, it has been suggested that it could select for multi-drug resistant Gram-negative strains and generate hypersensitivity (25).

Iodophors: This term refers to preparations that contain iodine with broad spectrum of activity and no known bacterial resistance. Molecular I_2 can freely cross the cell membrane and inhibit cellular respiration, destabilizes cell membranes, inhibits protein synthesis and denatures nucleic acids (26). Although very effective, iodine compounds can be toxic if significantly absorbed and cause pain. The less irritating compound povidone iodine is usually preferred, but it is less effective than iodine (10).

Silver compounds: Low concentrations of ionic silver (Ag^+) are effective against a broad range of pathogens and cause low toxicity to human cells (27). The bactericidal mechanism of action of silver ions is primarily through the attack to molecules at the cell membrane, collapse of the proton motive force and inhibition of enzymes of the respiratory chain (28). One common product used to support wound healing and bacterial elimination is the use of wound dressings that contain silver. However, the antibacterial action of silver may vary according to the availability of its ionic form and its activity can be affected by the presence of complex biomolecules in the wound site (29). In addition, plasmid-encoded bacterial resistance to silver compounds have been reported (30).

In addition to these antiseptics, new antibacterial agents are constantly developed with the aim of replacing and/or supplementing conventional antibacterial treatments. Some of these new treatments are described below:

Antimicrobial peptides: This therapy takes advantage of the antimicrobial function of naturally occurring peptides that participate in the innate immune response of animals such as *Xenopus*

laevis (31) and antimicrobial peptides found in the saliva of primates and humans, among others (32). These peptides can be synthesized in the laboratory and have proved to possess potent antimicrobial activity against a broad range of parasites, bacteria, fungi and some viruses (33). Antimicrobial peptides target mainly the cell membrane, but also can inhibit cell wall, nucleic acids and protein synthesis, which in combination lead to cell death (34). Because the cell membrane has been named as the main target, researchers have suggested that development of resistance is unlikely since it would require a complete redesign of the cell membrane, which is a 'costly' solution for microbial species (31). However, surface remodelling in response to antimicrobial peptides has been observed, in addition to the expression of proteolytic enzymes to degrade these peptides (34). In the same way as with antibiotics, pathogens can exhibit constitutive and inducible resistance to peptides (35). Therefore the mechanisms responsible of antimicrobial peptide action and development of resistance have yet to be fully understood.

Super-oxidized water: It is obtained by applying an electric current on salty water that result in a solution with high oxidation-reduction potential. It is effective against a wide range of microorganisms due to the presence of hypochlorous acid, hypochlorite ions, and dissolved oxygen, ozone and superoxide radicals. Thus, its activity is mediated by the induction of oxidative stress in cells (36). It has been widely used as a disinfectant in recent years, and it has been suggested to be more effective than other treatments such as povidone iodine (37).

The treatments described above have many advantages but also some limitations. The development of hypersensitivity to the treatment, the toxicity of the compounds or the selection for antibiotic-resistant bacteria have motivated the search for novel therapies. In the search for more effective antibacterial treatments, low temperature plasmas (LTPs) have risen as an attractive alternative or complementary antimicrobial therapy due to their ability to kill pathogens *via* induction of oxidative damage (11, 38-42). The benefits of this technology in biomedicine are multiple, as plasma treatments can be used to deliver topically a rich cocktail of reactive oxygen and nitrogen species, UV photons and electromagnetic fields to treat pathogens from distance (16), damage multiple bacterial targets at the same time (43, 44) and be safe for the treatment of patients (40, 45). This is an advantage over ointments, wound dressings and chemical compounds which direct contact with the wound can interfere with the healing process.

1.3 INTRODUCTION TO PLASMAS

Irving Langmuir was the first to introduce the term plasma in 1928 to describe a highly interacting ionized gas carrying multiple components that would resemble blood plasma carrying white and red blood cells (46). Plasma is the fourth state of matter and it can be generated by coupling sufficient quantities of energy to a gas to induce ionization (47). During

ionization, the atoms or molecules lose one or several electrons, resulting in the generation of a mixture of neutral, excited and charged species that exhibit collective behaviour (11). Neutral species and ions are commonly referred as “heavy” species and electron and photons as “light” due to discrepancies in their mass (the mass of ions and neutrals is higher than the mass of electrons) (48).

Plasma constitutes more than 99 % of the visible universe, i.e., stars, nebulae, and interstellar space (49). Natural terrestrial plasmas also exist, e.g. the aurora borealis. Man-made plasmas can be generated in the laboratory and in industry. Their applications include the manufacture of printed circuit boards, mobile phones, plasma displays, protective coatings for aircraft, ozone generation, medical cauterization, bacterial elimination and wound treatments (50). The specific application of LTPs in bacterial elimination is discussed below more in depth.

Natural and man-made plasmas are generated under a wide range of conditions, including low, atmospheric and high pressures, electron temperatures ranging from 10^2 to 10^8 K and electron densities ranging from 10^3 to 10^{33} electrons/m^3, respectively (50). In plasmas the temperature is determined by the energies of the heavy particles in the plasma and their degrees of freedom (translational, rotational, vibrational and the ones related to electronic excitation) (50). Plasmas can be broadly classified into categories and these are known as thermal and non-thermal plasmas.

Thermal plasmas: In these plasmas, the ionization and chemical processes are determined by the temperature. Thermal plasmas are characterized by being in equilibrium, as the plasma state approaches local thermodynamic equilibrium. This is the case of solar plasma in nature and man-made plasma torches that are used to cut steel, with temperatures above 1500 °C (50).

Non-thermal or low temperature plasmas (LTPs): Commonly referred to as “low-temperature” or “cold” plasmas, LTPs are systems where the electrons and ions are not in thermodynamic equilibrium. The high temperature of the electrons determines the ionization and chemical processes, but the low temperature of heavy particles determine the macroscopic temperature of plasma (50). LTPs can be generated with the application of an electrical discharge to a gas at sub-atmospheric, atmospheric and elevated pressures and also occur in nature, e.g. aurora borealis. Man-made plasmas developed with applications in biomedicine are particularly important. This is the case of atmospheric pressure plasma jets to eliminate pathogens and promote wound healing and coagulation. These plasmas operate at temperatures above 25 °C, but below the tissue thermal damage threshold (43 °C) (11).

1.4 LOW TEMPERATURE PLASMAS FOR BIOMEDICAL APPLICATIONS

The interaction of plasma-generated metastable species, ions and electrons with molecules of oxygen and nitrogen present in the surroundings, leads to the formation of reactive nitrogen and

oxygen species (RNOS), charged particles (ions and electrons), electromagnetic fields and UV photons (51-53). The preferred gases to generate LTPs are noble gases such as argon and helium since they generate stable glow-like discharges with low gas temperatures (54).

LTP sources generate a variety of reactive species. These can be divided into reactive oxygen species (ROS) such as ozone (O_3), superoxide ($O_2^{\cdot -}$), singlet delta oxygen ($O_2(a^1\Delta g)$) and atomic oxygen (O) and reactive nitrogen species (RNS) such as atomic nitrogen (N), peroxynitrite ($ONOO^-$) and nitric oxide (NO). In addition, electronically and vibrationally excited oxygen and nitrogen are generated. The presence of increasing humidity in the environment contributes to the formation of species such as H_2O^+, OH^- anion, ·OH radical and H_2O_2 (55). The generation of radicals is further enhanced by the addition of molecular gases such as O_2 and N_2 to the gas admixture (56, 57). In addition, LTPs generate UV photons that could contribute to the elimination of pathogens. There exists a discrepancy in the literature concerning the role that UV photons play in plasma-induced bactericidal activity (58). The use of distinct plasma sources, each of which generates a different cocktail of RNOS, by different research laboratories as described in the following section contributes to this uncertainty.

1.4.1 Corona discharge

Corona discharges are usually generated on sharp electrodes with imposed high voltage. The plasma is generated between the powered electrode and the anode, formed by living tissue or biological sample (59). The active region in corona discharges is restricted to the region close to the point electrode and is restricted to distance of millimetres. An example is the hairline plasma that produced nanosecond-short current pulses (**Figure 1.1a**) that can access narrow cavities such as tooth root canal, suggesting a possible application in dentistry (60). 'Hybrid' plasmas are a modification of this type of source where a ground mesh electrode is introduced through which the current passes, providing a current-free plasma for medical applications (61).

1.4.2 Microwave discharges

Microwave discharges are generated by the application of frequencies in the GHz range. These plasmas produce a high concentration of reactive species, have a low breakdown voltage and long electrode lifetime (62-64). One example is the coaxial transmission line resonator (**Figure 1.1b**) which has the advantages of low power requirements, low-temperature operation, and operation at atmospheric pressure (65). Another example is the MicroPlaSter beta (Adtec Plasma Technology Co. Ltd., London, United Kingdom), one of the few LTP sources currently certified for medical use (66).

1.4.3 Gliding arc

Gliding arc discharges present characteristics of non-thermal plasmas such as relatively low neutral-gas temperatures and high electric fields, but also possess characteristics of thermal plasmas such as high electron density, current and power (67). The discharge typically occurs

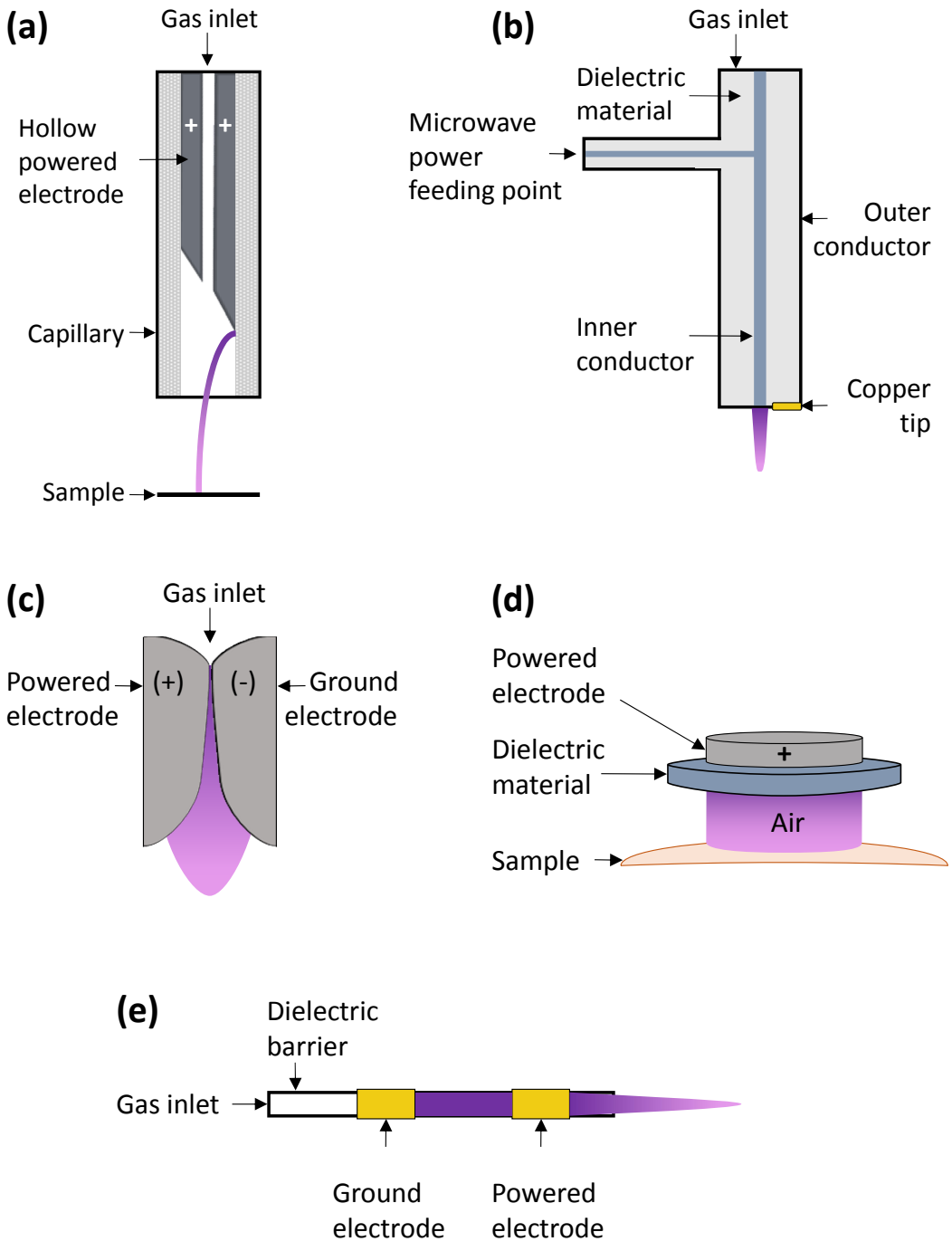

Figure 1.1. ***Schematics of low-temperature plasma sources used on biomedical research.*** **(a)** Hairline plasma corona discharge. **(b)** Microwave discharge coaxial transmission line resonator. **(c)** Gliding arc discharge. **(d)** Dielectric barrier discharge (DBD) plasma arrangement. **(e)** DBD plasma jet with double electrode configuration.

between two diverging electrodes and is transported by flowing gas outside the diverging area (**Figure 1.1c**).

1.4.4 Dielectric barrier discharge (DBD)

DBDs have been used for decades to generate ozone on a large scale and now they find application in biomedicine. In DBDs, a dielectric material (glass, quartz or plastic) is fitted between the powered and grounded electrodes where the discharge takes place. The dielectric material prevents the formation of arcs, which could damage the sensitive samples that are exposed to treatment (**Figure 1.1d**). The electrical breakdown occurring at atmospheric pressure is composed of independent current filaments. The charge accumulates on the dielectric material and helps to sustain the generation of plasma at lower voltages (68). One example is the floating-electrode DBD (FE-DBD) plasma source. Here, the second ungrounded electrode is the biological sample and remains at a floating potential (13). In the PlasmaDerm (Cinogy, Duderstadt, Germany) used for microbial elimination and inducement of wound healing, the human body or sample serves as the second electrode. Different versions of the PlasmaDerm currently exist and it is of particular importance since it has gone through the first clinical trial to prove safety and efficacy on the elimination of pathogens from chronic venous leg ulcers (15).

1.4.5 Plasma jet

This configuration is characterized by the generation of plasma around the powered electrode in a glass or quartz tube that is transported outside the device in propagating ionization waves and forms a stream of active particles discharging as a small jet (**Figure 1.1e**). The plasma can be developed using any type of plasma described above, i.e. DBD, corona, gliding arc or microwave discharge. The plasma generated in jet configuration away from the biological target presents a plasma plume that can extend up to centimetres away from the ignition point. This characteristic of plasma jets allows the topical treatment of specific targets from distance and is an advantage over the conventional plasma sources, where plasma is confined between electrodes (55). Plasma jets such as the plasma pen, plasma torch, the plasma needle and others have been developed and tested against clinically relevant pathogens and purified biomolecules (69-72). One of these plasma sources is the Kinpen (Neoplas GmbH, Greifswald, Germany), which is a small-sized hand piece unit being currently tested to treat wounds, root canal infections and cancer cells (16, 73).

1.5 RNOS IN PLASMA

That main mechanism of action of LTP treatments is the induction of oxidative damage to bacterial cells. RNOS are known to have antibacterial properties as they can damage the structure of proteins, lipids and nucleic acids of microorganisms (74) and have even been

implicated in the mechanisms of cell death of specific antibiotics (75). Some of the various reactive nitrogen and oxygen species generated in the plasma are described below.

1.5.1 Hydrogen peroxide (H_2O_2)

This molecule is soluble in water and can freely diffuse within and between bacterial cells. In addition, H_2O_2 can use aquaporins to cross the cell membrane (76). H_2O_2 is considered a poorly reactive species as it is a weak oxidizing or reducing agent. However, H_2O_2 can directly inactivate enzymes *via* oxidation of –SH groups (74). H_2O_2 that crosses the cell membrane can go through chemical reactions with iron (e.g. iron bound to DNA) and possibly copper ions to generate more damaging species such as ·OH *via* Fenton reaction:

$$H_2O_2 + Fe^{2+} \rightarrow OH^- + FeO^{2+} + H^+ \rightarrow Fe^{3+} + OH^- + \cdot OH$$

In addition, H_2O_2 can indirectly contribute to the oxidation of lipids, proteins and DNA by generating secondary radicals (77).

1.5.2 Hydroxyl radical (·OH)

It is by definition the most biologically active free radical. ·OH radical is a highly reactive and short-lived molecule (78). It can react with virtually any biomolecule present at close proximity. ·OH radicals can be formed in the Haber-Weiss reaction when H_2O_2 and iron ions are present (74). The reaction starts with ferric ion being reduced into ferrous ion:

$$Fe^{3+} + O_2\cdot^- \rightarrow Fe^{2+} + O_2\cdot$$

This reaction is followed by the Fenton reaction described in Section 1.5.1. ·OH radical accounts for most or all of the damage induced in DNA of H_2O_2-treated cells (21). The presence of metal ions on the DNA double strand, specifically iron, favours the site-specific ·OH radical generation, leading to DNA damage that ·OH scavengers find it difficult to protect against. In this case, ·OH directly adds to double bonds in the DNA molecule and abstracts an hydrogen molecule from the methyl group of thymidine and from 2'-deoxyribose (79).

1.5.3 Superoxide ($O_2\cdot^-$)

This species does not react with most biological molecules in aqueous solution and is less reactive than ·OH. However, $O_2\cdot^-$ reacts quickly with other radicals such as NO and iron-sulphur clusters in proteins (74). Thus, it can be said that NO scavenges $O_2\cdot^-$, but at the same time gives origin to a more toxic radical, peroxinitrite ($ONOO^-$). Because it is a charged molecule, it cannot freely cross the cell membrane, but it can be transported into the intracellular compartment by anion exchange proteins present in some cells (21). In liquid solutions under physiological conditions, $O_2\cdot^-$ is dismutated to form H_2O_2 and molecular oxygen and this reaction is favoured at acidic pH (74):

$$HO_2\cdot + O_2\cdot^- + H^+ \rightarrow H_2O_2 + O_2$$

The formation of H_2O_2 by $O_2^{\cdot -}$ can contribute to the formation of ·OH *via* Fenton reaction. Thus, most of the damage induced in cells by $O_2^{\cdot -}$ is mediated by the formation of secondary reactive species.

1.5.4 Singlet delta oxygen ($O_2(a^1\Delta g)$)

Singlet delta oxygen interacts with biomolecules by transferring its excitation energy to them and/or reacting chemically with them (21). In liquid solutions, the excitation energy of $O_2(a^1\Delta g)$ can be transferred to the solvent and its lifetime is affected by the solvent used. $O_2(a^1\Delta g)$ can react with compounds containing C=C bonds and also interact directly with DNA, methionine, cysteine, histidine, tryptophan, azide ion, cholesterol, β-carotene and ascorbate, among others (80). In reaction with molecules containing two conjugated double-bonds separated by a single bond, $O_2(a^1\Delta g)$ can form endoperoxides. These endoperoxides can generate various products of oxidation, including 8-hydroxydeoxyguanosine, a marker of DNA damage (81). $O_2(a^1\Delta g)$ is inefficient at producing strand breakage and attacks only guanine, the base in DNA that is the most sensitive to oxidative damage (82). During lipid peroxidation, peroxyl radicals ($RO_2^{\cdot}$) can form $O_2(a^1\Delta g)$, contributing to the induction of oxidative damage inside the cells (21).

1.5.5 Ozone (O_3)

O_3 is a powerful oxidizing agent that adds directly across double bonds in unsaturated aromatic and aliphatic compounds (i.e. O_3 combines with aliphatic compounds) to generate ozonides, which can be further decomposed to cytotoxic aldehydes (83). O_3 oxidizes proteins attacking –SH groups, tyrosine, tryptophan, histidine and methionine residues, among others and also reacts with polysaccharides (84). In addition, O_3 can fragment DNA and oxidize nucleotide bases (especially G and T) both directly and *via* the formation of ·OH radical in aqueous solutions. The reaction of O_3 with proteins in the respiratory chain, cysteine and methionine can lead to the formation of $O_2(a^1\Delta g)$ and in reaction with lipids, O_3 generates H_2O_2 (83).

1.5.6 Nitric oxide (NO)

NO reacts with molecular oxygen to form $NO_2^{\cdot}$, a far more reactive radical in gas and in solution (21). NO can cross the cell membrane and diffuse between and within cells. NO binds to transition metal ions and it is highly reactive with other radicals, but its reaction with most biomolecules is slow. NO quickly reacts with peroxyl radicals, and therefore it is said that NO can inhibit lipid peroxidation (85). In addition, NO can bind to Fe^{+2} to decrease its reactivity with H_2O_2 to make ·OH *via* Fenton reaction. NO can also lead to the formation of nitrites, known to inhibit bacterial growth (86). Thus, NO acts as an effective scavenger of ·OH, peroxyl radicals and $O_2^{\cdot -}$, as mentioned above, and its damaging effects in biomolecules are related to the formation of additional reactive species.

1.6 BIOLOGICAL TARGETS OF LTP

Bacteria that originate from the environment, normal skin microflora and endogenous sources (e.g. gastrointestinal and oropharyngeal mucosae) (5) can cause infections in disrupted tissue, e.g. wounds, since the wound provides ideal growth conditions for microbial colonization and proliferation with a warm, moist, and nutrient-rich environment (87). Wound infections are polymicrobial and involve both aerobic and anaerobic microorganisms (88). Pathogens such as *P. aeruginosa*, *S. aureus* and beta-haemolytic streptococci are some of the most frequent pathogens found in wounds (89) and development of antibiotic resistance constitutes a major problem in the treatment of acute and chronic wounds (5). In this context, different LTP sources have been demonstrated to effectively eliminate a broad range of microorganisms including antibiotic-resistant pathogens, fungi, Gram-positive and Gram-negative bacteria, and viruses (90). *In vitro* experiments have demonstrated the efficacy of different plasma sources against thin film, planktonic and biofilms forms of *P. aeruginosa* (91), *S.* a*ureus* (14) and *E. coli* (71). It has even been suggested that the application of LTPs could restore antibiotic sensitivity in MRSA (92). In addition, direct application of plasma to chronic wounds has been demonstrated to contribute to the elimination of polymicrobial infections in human patients (93). However, the composition of RNOS in the plasma depends on the type of plasma source used and this has a direct effect on the bactericidal properties of the plasma.

1.6.1 Cell membrane

Because plasma delivers a complex mix of RNOS to the bacterial cell, the cell membrane is the first barrier encountered that is exposed to oxidative damage. The first reports on the application of LTPs for the elimination vegetative bacteria and bacterial spores described morphological changes in plasma-treated cells due to a process referred as ‘etching’, which is caused by the interaction of RNOS with molecules in the cell membrane (94). Morphological changes in plasma-treated bacteria such as *E. coli*, *Bacillus subtilis* and *Streptococcus mutans* have been reported using scanning electron microscopy (95-97), fluorescence microscopy (14) and transmission electron microscopy (98). In addition, it has been demonstrated that the electric field created by some LTP sources can induce electroporation in eukaryotic and bacterial cells which increases the permeability of the cell membrane and could improve the pass of plasma-generated RNOS to the intracellular compartment (99, 100). The permeabilization of the cell membrane also cause loss of intracellular content, as demonstrated by the identification of proteins and nucleic acids leaked into the extracellular environment from plasma-treated MRSA, *Candida albicans* and *P. aeruginosa* (14).

1.6.2 Lipids

These molecules are major targets during oxidative stress and are the main constituents of the cell membrane. Polyunsaturated fatty acids present in membranes are attacked directly by charged reactive species and this initiates lipid peroxidation. The oxidation of lipids in the cell membrane reduces its fluidity, disrupts the proteins embedded in the cell membrane and

therefore affects its structure (21). Although bacterial cell membranes have only monounsaturated fatty acids (101), these molecules can also oxidize upon exposure to free radicals. This process has been reported in membrane-rich fractions of *E. coli* and living *E. coli* bacteria exposed to plasma in liquid suspensions by measuring the amount of malondialdehyde, a product of lipid peroxidation formed upon exposure to LTPs (13, 71).

1.6.3 Proteins

RNOS can affect structure and activity of proteins, specifically by targeting disulphide bonds and metalloproteins (74). At the molecular level, Takai *et al.* have demonstrated that a low-frequency plasma jet induced oxidative damage in purified amino acids, preferentially in sulphur-containing and aromatic amino acids (102). This damage is translated into oxidation of proteins that contain such amino acids, in addition to destruction of the tertiary structure of proteins that determines the catalytic sites of enzymes, e.g. abolishment of the enzymatic activity of purified enzymes such as lysozyme (103) and lactate dehydrogenase (44). The reduction of the enzymatic activity *in vivo* was also described for intracellular glyceraldehyde 3-phosphate dehydrogenase of *E. coli* exposed to a radio-frequency-driven microscale atmospheric-pressure plasma jet (104).

1.6.4 DNA

The oxidative damage induced in the DNA is one of the major causes of cell death and induction of mutations (105). Lesions in the DNA can be caused by single- or double-strand DNA breaks or oxidation of nucleotide bases, which leads to the formation of mutagenic sites (105). Such damage to the DNA accumulates during exposure of bacterial cells to H_2O_2, $O_2^{\cdot -}$, and O_3 formed in the extracellular environment and intracellular compartment as consequence of oxidative damage. For example, ·OH radicals formed as a consequence of the interaction of H_2O_2 with iron *via* Fenton reaction in the intracellular compartment (and specifically in reaction with DNA-bound iron) is one of the main free radicals responsible of oxidative damage to the DNA (77). LTPs have proved to induce single- and double-strand DNA breaks on isolated DNA using techniques such as gel electrophoresis (44, 51), polymerase chain reaction (71) and RAMAN spectroscopy (104). In live organisms, the presence of oxidized nucleotides in bacteria exposed to an FE-DBD plasma has been also reported using ELISA to detect 8-hydroxydeoxyguanosine, a common and stable product of oxidative DNA damage (13).

1.6.5 Gene expression

Studies on *E. coli* exposed to LTP treatment have shown a differential gene expression in bacterial cells immediately after plasma treatment. In these studies, the authors have demonstrated that genes related to the response to oxidative stress and DNA repair processes were up-regulated, whereas those genes related to motility, energy generation, house-keeping and metabolism and virulence were down-regulated (106, 107). These studies support the

participation of plasma-generated RNOS in bacterial elimination and highlight the importance of repair mechanisms in bacterial cells to survive to oxidative damage induced by LTP treatments.

1.7 FACTORS THAT AFFECT THE EFFICACY OF LTP

One of the advantages of LTPs is the possibility of modulating several physical parameters to develop specific treatments (**Figure 1.2**). These are universal factors that affect the efficacy of plasma sources for any given application. Discrete modifications of these parameters have a significant impact on the outcome of LTP treatments. For example, the addition of oxygen to the gas admixture used to generate plasma and increasing treatment times can boost the elimination of bacteria in solid and liquid environments (13, 108, 109). Other factors such as the distance between the regions around the powered electrode where the plasma is generated and the sample (110) and the voltage used to ignite the plasma (108) can be modulated to improve the treatment outcome. In general, variations in the physical parameters used to produce the plasma impact on the chemical composition of plasma, i.e. concentration of RNOS, ions, electrons and UV photons, targeting different cellular components as described above and therefore will directly impact on the mechanisms of action used to kill pathogens. A careful modulation of these parameters is required to ensure the reproducibility of the results, stability of the signal and robustness of the treatment.

In addition, significant differences in the composition of the plasma generated due to the configuration of the plasma sources used should be noted. For example, whereas a DBD plasma jet delivers a rich cocktail of charged and neutral species that is carried outside the device and is transported by the gas (51, 52), a radio-frequency capacitively-coupled plasma provides a charge-free discharge composed of mostly neutral species (111-113).

The biological characteristics of the target sample are also important and can determine the modification of the external parameters required to generate a plasma treatment that is successful against the target cells. In this sense, the differences in cell structure (presence of outer and inner cell membranes in Gram-negative but only inner cell membrane in Gram-positive bacteria), biological state (vegetative or spores) and response to oxidative stress of each species exposed to plasma will determine their resistance or sensitivity to the treatment. For example, it has been suggested that the differences in the structure of the cell membranes make Gram-positive bacteria more tolerant to plasma treatments than Gram-negative bacteria (12). Also, it has been reported that vegetative *S. aureus* are more susceptible to plasma treatment than endospores of *B. subtilis* when exposed to plasma under the same conditions (114). Besides these factors, the concentration of the bacterial population to be treated can determine the treatment outcome, as an increase in the bacterial load exposed to plasma has been related to a decrease in the efficacy of the treatment (115).

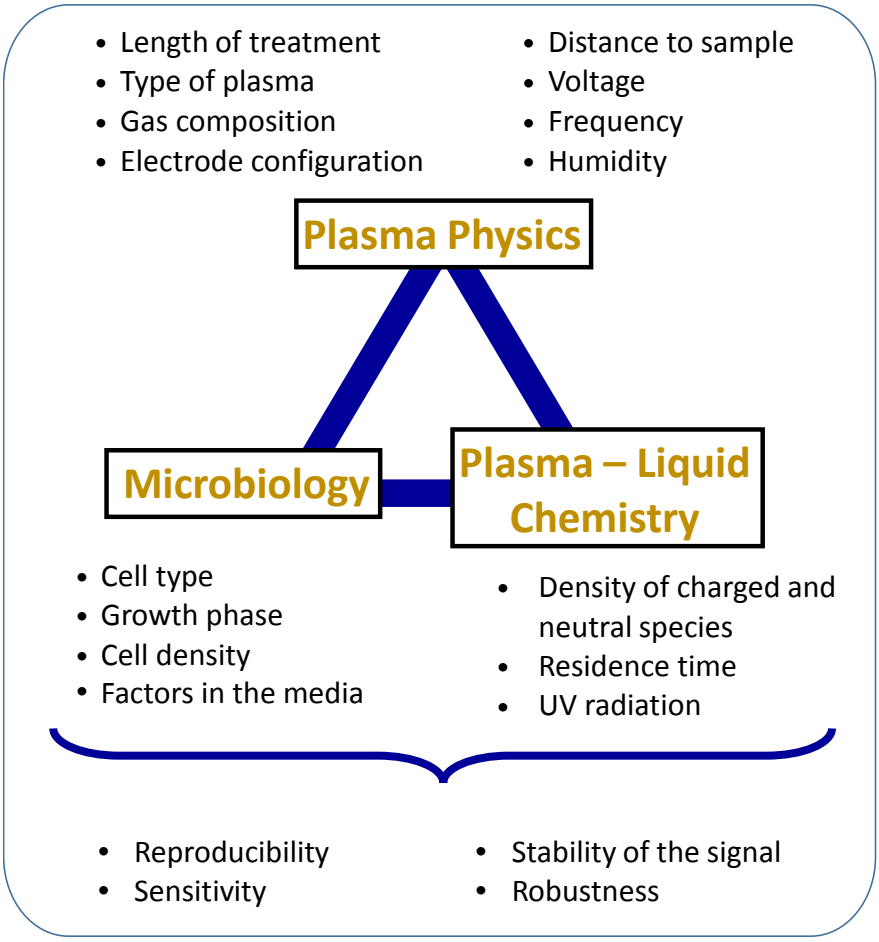

Figure 1.2. ***Parameters that affect the efficacy of antibacterial plasma treatments.***

Another factor to consider is the vehicle in which the sample is exposed to LTP treatments. The composition and chemistry of plasmas in the gas phase varies inevitably when in contact with liquids. This interaction gives origin to a new set of RNOS in the plasma-treated liquid. In this context, the nature and concentration of RNOS delivered to target cells exposed to plasma in solid or liquid environments is different and therefore contribute to the variation in the response of microorganisms to LTP treatments. Taking advantage of the formation of long-lived reactive species in plasma-treated liquids, plasma-activated water has been suggested to have antibacterial properties (116, 117) and plasma-activated medium is being studied on its properties to kill cancer cells and cell lines *in vitro* (118-120).

1.8 LIMITATIONS OF CURRENT APPROACHES

The understanding of how the complex composition of the plasma operates on the biological sample and which are the main biomolecules that should be targeted to induce cell death is pivotal. Oxidative damage in microorganisms such as bacteria has been extensively studied in the past, and the interaction of RNOS and target molecules and their effects in bacteria are well-characterized (80). In contrast, due to the complex chemical composition of low temperature plasmas, the bacterial responses to LTP treatments are not well understood.

The current approaches used to assess the effect of LTP sources on bacterial cells have limitations in their ability to explain the biological effect that underpin bacterial elimination. Reports in the literature are based on the study of the effect of plasma at the population level and does not reflect the oxidative damage induced in individual cells (13, 71, 91). In addition, the use of purified DNA and proteins are not representative of the effect induced in living bacterial cells and results cannot be extrapolated to the effect on molecular targets contained in living cells (44, 102, 121), limiting the understanding on how LTP treatments affect biological systems. Furthermore, it is unknown how the spatial distribution of RNOS in the plasma effluent affects the bactericidal action of LTPs, as the multiple RNOS present in the plasma have different reaction rates with biomolecules. This can determine the pathways used to induce cell death. It has been demonstrated that RNOS in the plasma effluent varies as it diffuses from the main plasma bulk (112, 122), demonstrating that RNOS are not restricted to the visible region of the jet (91). Therefore, it could be expected that such spatial distribution will have an effect on the mechanisms used by the plasma to eliminate bacteria. Finally, there is a lack of information about the interaction of plasma-generated RNOS with external organic molecules in the surroundings of the target cells, even when it is known that these molecules can undergo redox reactions (21).

The existing knowledge on antibacterial LTP treatments contribute only partially to the elucidation of antimicrobial mechanisms of plasmas. The factors mentioned above are particularly important considering the possible applications of plasma treatments on wounds

and surgical site infections, where the complex environment of the infected wound with organic debris and multiple cell types spatially distributed could affect the treatment outcome. In addition, these factors are also relevant in the context of LTP treatments of fresh produce and decontamination of surfaces in health care settings (90). The exposure of bacteria to sub-lethal doses of RNOS could promote the adaptation of microorganisms to the oxidative stress induced by plasma or mutations that could favour the resistance to treatment, an unwanted side effect that should be carefully considered in the development of any antibacterial treatment.

The first clinical trials of LTP treatments in human patients have been carried out, as a variety of studies have demonstrated that LTP sources can kill bacteria *in vitro* and in animal models (12, 14, 71, 91), they do not damage human skin biopsies (123) and promote wound healing (124). These studies aim to assess the efficacy, safety and applicability of the treatments in humans with infected chronic ulcers using the MicroPlaster (93) and the PlasmaDerm (15). This is a great advance for the field of plasma medicine for decontamination of skin wounds, as the interaction of the chemically rich plasma with bacterial targets have been shown to induce multiple effects *in vitro* that involve the alteration of cell structure, gene expression and metabolic pathways. However, there are multiple factors that could affect the interactions of RNOS with bacterial cells *in vivo* that may determine the treatment outcome, e.g. presence of polymicrobial communities in infected wounds, complex environmental conditions in the wound bed and heterogeneity in the response of microorganisms to oxidative stress. To contribute to the understanding of the mechanisms leading to bacterial cell death in bacterial populations in complex environments and to be able to predict the treatment outcome, it is essential to assess the interaction between plasma-generated RNOS and target/non-target cells in such complex environments. The success of plasma treatments will depend on the ability to design plasma treatments that are chemically effective against bacteria, that can be safely applied to patients and that can be tuned to eliminate multiple pathogens.

1.9 MODEL OF INFECTION FOR LTP RESEARCH

1.9.1 *Salmonella* Typhimurium

Salmonella enterica (*S. enterica*) is a Gram-negative flagellated rod-shaped facultative intracellular bacteria that is a major cause of foodborne illness around the world, infecting more than 1.3 billion people every year (125). There are 6 subspecies identified that are further subdivided into serovars (126). The distinction between serovars is based on their flagellar, carbohydrate and lipopolysaccharide structures. These pathogens are typically related to enteric diseases and can cause enteric or typhoid fever (caused by serovars Typhi, Paratyphi and Sendai), bacteraemia (caused by serovars Choleraesuis and Dublin, among others), enterocolitis (caused by most *Salmonella* serovars) and chronic asymptomatic carriage (125).

Salmonella enterica serovar Typhimurium infects both humans and animals *via* ingestion of contaminated food or water. *Salmonella* is a ubiquitous bacteria that can multiply and survive in a variety of environments outside and inside the host. It includes temperatures ranging from 5 to 47 °C, pH from 4 to 9 and environments with low or high amount of water (127). When it reaches the intestinal epithelium, it starts a gastrointestinal disease that in some cases can lead to the infection of phagocytic cells. To survive inside the mononuclear phagocytes, it has evolved numerous defense mechanisms to overcome the oxidative stress induced by the host cell (128). The activated phagocyte produces the first response against the intracellular *Salmonella* by generating $O_2^{\cdot -}$ that is released in the *Salmonella*-containing vacuole. Here, $O_2^{\cdot -}$ is dismutated to H_2O_2 and subsequently converted to the highly reactive ·OH radical. H_2O_2 can be enzymatically converted to hypochlorous acid in the phagocyte. Because of its neutral nature, H_2O_2 diffuses rapidly across the bacterial cell membrane, where in reaction with iron or copper ions generates ·OH radical *via* Fenton reaction. In response to this, *Salmonella* has developed an increased resistance to H_2O_2 mediated by the induction of eleven genes in response to peroxides, in contrast to eight found in *E. coli* (80). In addition, *S.* Typhimurium has two genes for the periplasmic superoxide dismutase Cu,ZnSOD instead of only one found in *E. coli*, which contributes to their survival (129). The second response is mediated by the generation of nitric oxide that inhibits important enzymes that participate in central metabolic pathways (130). NO can either spontaneously or by enzyme-catalysed reactions be converted to a more reactive nitrogen species, including peroxynitrite ($ONOO^-$). $ONOO^-$ can undergo conversion to nitrogen dioxide (NO_2) and ·OH, that can affect *Salmonella* targets (130). In response, *Salmonella* possess direct and indirect mechanisms to antagonize $ONOO^-$. For example, the periplasmic superoxide dismutase indirectly prevents the formation of $ONOO^-$ as it consumes the $O_2^{\cdot -}$ precursor (131), whereas the peroxiredoxin-alkyl hydroperoxide reductase can directly transform $ONOO^-$ to the less toxic NO_2^-, providing protection against reactive nitrogen intermediates (132). Although ROS and RNS can induce oxidative damage in *S.* Typhimurium, the existence of redundant pathways orchestrated by the OxyR and SoxRS systems that control the expression of these genes contribute to the survival of *S.* Typhimurium under disadvantageous conditions (78).

Although *S.* Typhimurium is not related to the pathology of infected wounds, *Salmonella* display abundant mechanisms of defense to scavenge and remove reactive species and quickly promote the repair of biomolecules damaged during oxidative stress (130). For this reason, *S.* Typhimurium was chosen as a model system for this study as it could provide information on the efficacy of LTP treatments against naturally resistant pathogens, contributing to the current knowledge on LTP treatments on *Salmonella* (58, 133-135). Even more, the results obtained in this body of work could be valuable not only for the biomedical field, but also for the food safety field, as *Salmonella* is one of the main causes of food poisoning. In addition, considering the ability of *Salmonella* to infect phagocytic cells, this model could be used in the future to

explore the possible applications of LTP treatments to eliminate intracellular infections *in vitro*. This could serve as a proof-of-principle study that could be translated to other intracellular pathogens responsible of skin wound lesions such as *Leishmania* parasites for which current treatments are toxic and not effective (136).

1.10 OBJECTIVE

Low temperature plasmas are a promising alternative multitarget antibacterial therapy to eliminate pathogens from wounds, surfaces and liquids. The objective of this thesis is to elucidate the factors that interfere with or contribute to the efficacy of LTP treatments, with special focus on the role of the spatial distribution of RNOS in the plasma jet, the effect of external biomolecules present during treatment and the variability in the response to plasma at the single cell level.

1.11 HYPOTHESES

Based on what is known about the effect of plasma on biological samples, three hypotheses were proposed:

(a) The response of a bacterial population exposed to LTP treatment is not homogeneous and therefore different levels of damage are expected in plasma-treated bacterial cells at the single cell level

(b) The spatial distribution of reactive species in the plasma effluent of any given plasma jet have a direct effect on the level of damage inflicted in the biomolecules of bacterial cells and therefore determine the mechanisms of action that lead to bacterial elimination

(c) The presence of external biomolecules present during the exposure of bacteria to plasma treatment, such as proteins, lipids and carbohydrates in wound exudate or culture media, decreases the efficacy of the bactericidal LTP treatment, as they compete with bacterial cells for the reaction with RNOS

1.12 AIM

This piece of work aims to test these hypotheses combining physical, biological and chemical approaches to determine the role of these factors on the efficacy of antibacterial plasma treatments on the bacterial model *Salmonella enterica* serovar Typhimurium. For this purpose, an in-house built atmospheric-pressure dielectric barrier discharge plasma jet (that delivers charged and neutral species) was used as the main plasma source of study and a radio-frequency capacitively-coupled plasma jet (that delivers mostly neutral species only) was used to confirm the role of the aforementioned factors on bacterial elimination.

2 MATERIALS AND METHODS

2.1 ABSTRACT

The experimental methods, equipment, reagents and materials used throughout the project are introduced. Assays for culturing bacteria and assessing bacterial inactivation along with protocols for measuring the chemistry in the gas phase and in plasma-treated liquids are described. General methods used in multiple chapters of this project are described here, while the specific optimization of the parameters of the atmospheric-pressure dielectric barrier discharge (AP-DBD) plasma jet for bacterial elimination is described in Chapter 3.

2.2 CHEMICALS AND SOLUTIONS

LB-Lennox Broth (Fisher BioReagents) containing 10 g tryptone, 5 g NaCl and 5 g yeast extract per litre was prepared for liquid culture of bacteria. LB solid medium contained the same components as liquid LB plus 15 g/L of agar.

Minimal medium (M9) was prepared with 11.3 g M9 minimal salts (Sigma) and supplemented with 0.6 µg Fe citrate, 0.1 mM $CaCl_2$, 0.1 mM $MgSO_4$, 0.001 % (w/v) vitamin B1 and 0.2 % (w/v) glucose per litre. M9 solid medium contained the same components as liquid M9 plus 15 g/L of agar.

Helium (He; >99.996 % purity) and oxygen (O_2; 99.6 % purity) were obtained from BOC.

2.3 BACTERIAL STRAIN AND GROWTH CONDITIONS

Salmonella enterica subspecies enterica serovar Typhimurium ST4/74 (Wellcome Trust Sanger Institute, UK) was grown aerobically overnight at 37°C in LB or M9 minimal medium. Forty microliters of the overnight LB culture or 100 µL of M9 culture were transferred to 2 mL of the corresponding fresh medium and incubated for 3 – 3.5 hours which will correspond to late logarithmic to early stationary phase based on doubling times under these conditions.

2.4 ZONE OF INHIBITION TEST

To test the bactericidal effect of plasma in bacteria on semisolid surfaces, *S.* Typhimurium ST4/74 in LB or M9, late logarithmic phase cultures were diluted in the corresponding culture media to obtain an optical density at 600 nm (OD_{600}) of 0.02 (approximately $1.6x10^7$ CFU/mL). A hundred microlitres was spread on LB or M9 agar plates prior to or post plasma treatment. After treatment, plates were incubated for 24 h (LB plates) or 48 h (M9 plates) at 37 °C. The area of the zone of inhibition was measured considering the shape of the zone of inhibition as an ellipse (measurement of the semi-major and semi-minor axes to calculate the area). Images of each plate were acquired. Experiments were done in duplicates or triplicates. Plasma was generated as described for each experiment.

2.5 BACTERIAL VIABILITY AFTER PLASMA TREATMENT OF BACTERIAL SUSPENSIONS

2.5.1 Experimental conditions

Two hundred microliters of late logarithmic phase culture of *S.* Typhimurium in LB culture medium were washed with 3 mL of the corresponding liquid: filtered distilled H_2O (0.22 µm pore size), PBS, DMEM, DMEM + 10 % (v/v) FCS, LB, or 0.85 % (w/v) NaCl sterile for 3 minutes at 1057 x *g*, room temperature (defined as a temperature in the range of 21 – 24 °C for this study). The pellet was resuspended in the corresponding liquid to obtain an OD_{600} = 0.02 (approximately 1.6 x 10^7 CFU/mL). In all cases, samples were kept on ice prior to plasma experiments. For plasma treatments, 500 µL of each bacterial suspension were placed in 24-well plate well and sealing films were used to protect untreated wells from plasma (SealPlate, Excel Scientific).

Plasma was generated with the AP-DBD plasma jet at 12 kV (peak-to-peak), 30 kHz, 2 standard litres per minute (slm) He + 0.5 vol % O_2. Ambient humidity was 21 %. The distances between the nozzle and the sample was 30 mm. Samples were treated for 90 seconds.

2.5.2 Reduction of colony forming units

This method was used to determine the reduction of colony forming units (CFU) after plasma treatment of *S.* Typhimurium suspensions in liquids containing nutrients, salts and vitamins.

After plasma treatment, a set of serial dilutions was made by mixing 50 µL of the sample with 450 µL of the same liquid used to prepare the corresponding bacterial suspension (H_2O, PBS, DMEM, DMEM + 10 % (v/v) foetal calf serum (FCS) or LB) to generate 1:10 to 1:10^6 dilutions. A 100 µL of each dilution were spread with glass beads on LB plates and incubated overnight at 37 °C. Bacterial colonies were counted in plates with up to 300 CFU/plate and the CFU/mL was calculated using the following formula:

$$\frac{\text{CFU}}{\text{mL}} = \frac{\text{(number of colonies) x (dilution factor)}}{\text{Volume plated (mL)}}$$

Experiments were done in triplicates (three aliquots of the each bacterial suspension exposed to plasma), with two biological replicates (2 independent bacterial colonies).

2.5.3 Live/Dead Bacterial Viability Assay by flow cytometry

The Live/Dead BacLight Bacterial Viability Assay (Molecular Probes) was used to distinguish between live and membrane-damaged *S.* Typhimurium after plasma treatment.

Briefly, 500 µL of each bacterial suspension of *S.* Typhimurium prepared as described in Section 2.5.1 was placed in 24-well plate well and sealing films were used to protect untreated wells from plasma (SealPlate, Excel Scientific). After treatment, the remaining volume was transferred to 1.5 mL microcentrifuge tubes and centrifuged at 9,000 x *g* for 2 minutes. Samples

were washed with 1 mL 0.85 % (w/v) NaCl and centrifuged again at 9,000 x *g* for 2 minutes. Samples were resuspended in 1 mL 0.85 % (w/v) NaCl and stained with 5 µM SYTO9 and 2.25 µM PI. Samples incubated for 15 minutes at room temperature protected from light and were acquired using the Beckman Coulter CyAn ADP flow cytometer with FITC filter (excitation at 488 nm, emission at 530/40 nm) and PE-Texas Red (excitation at 488 nm, emission at 613/20 nm). At least 10,000 events per sample were acquired. *S.* Typhimurium was heat-inactivated for 15 minutes at 100 °C and used as negative control (high damage to cell membrane). Samples were analysed using the Summit version 4.3 software (Beckman Coulter).

2.6 DNA DAMAGE DIFFUSION ASSAY (DDD ASSAY)

A method previously reported for the study of DNA fragmentation in bacteria and yeast (137) was adapted for this study. The modified DDD Assay allows the application of plasma treatment to bacterial samples in a liquid-free environment. An algorithm implemented in Wolfram Mathematica 10.0 1.0 (Wolfram Research Inc.) complements this method for the quantification of the radius of diffusion of DNA originated from single cells.

Late logarithmic phase cultures in LB culture medium (100 µL) were washed with 3 mL PBS for 3 minutes at 1057 x *g*, room temperature. The pellet was resuspended in 2 mL PBS to obtain an OD_{600} = 0.07 (approximately 2.3 x 10^7 CFU/mL).

2.6.1 Glass slides cleaning

Prior to use, glass slides were washed with a solution of 15 % (w/v) potassium hydroxide (KOH) in ethanol to remove traces of dirt and grease. Slides were immersed in the 15 % (w/v) KOH in ethanol solution for 5 minutes and were rinsed 3 times in filtered distilled water (0.22 µm pore size), 5 minutes each. Slides were rinsed with ethanol and dried in a 60°C oven for 1 hour. Clean slides were stored in a slide box with silica gel until use.

2.6.2 Preparation of agarose-coated slides (ACS)

Clean microscope slides were individually immersed in 35 mL 1 % (w/v) agarose solution (Melford) in a 50 mL plastic conical tube to cover up to 80 % of the surface of the slide. Excess of agarose from the back of the slide was removed with a tissue. Slides were allowed to air dry at room temperature for 1 hour before storage in a dry box until use up to 1 month after preparation.

2.6.3 Transfer of bacterial sample to ACS

S. Typhimurium prepared as described in Section 2.6 and spread with glass beads on LB or M9 agar plates, according to the culture conditions of the sample to be tested. A rectangular section of agar of approximately 60 mm x 25 mm was cut with a scalpel and was placed over the ACS. The agar slab was removed and slides were ready for plasma treatment.

2.6.4 DDD Assay

A diagram of the protocol is depicted in **Figure 2.1**. Bacterial samples were transferred to ACS and treated with the plasma jet. Slides were covered with 60 µL of 0.65 % (w/v) low-melting-point (LMP) agarose (Product No. A9414, Sigma) equilibrated at 37 °C, and covered with 24 mm x 50 mm coverslips. Slides were allowed to solidify at 4 °C for 10 minutes. Coverslips were gently removed and slides were incubated at 37 °C for 5 minutes in lysing solution (2 % (w/v) SDS, 0.05 M EDTA, 0.1 M dithiothreitol, pH 11.5). Slides were maintained in horizontal position at all times to avoid DNA stretching. Slides were rinsed with filtered distilled water (0.22 µm pore size) for 3 minutes and dehydrated with ice-cold ethanol at 70 %, 90 % and 100 % (v/v), 3 minutes each. Slides were dried for 4 minutes in a 800 W microwave to promote the attachment of DNA to the slide and incubated in the dark at 80 °C overnight. Bacterial DNA was stained with SYBR Gold (Molecular Probes, Invitrogen) at 1:400 in 1x TBE Buffer (0.09 M Tris-borate, 0.002 M EDTA, pH 7.5) for 5 minutes. Slides were rinsed, mounted in 1x TBE buffer and analysed with an inverted fluorescence microscope (Zeiss) with a 488 nm filter.

Images were collected with a high resolution monochromatic camera (AxioCam HRm, Zeiss), using the Axiovision Release 4.8.1 software. Images were collected below the saturation level, as the presence of saturated pixels would invalidate the analysis. Images of single bacteria were collected from 4 areas in the slide: a) treatment site (defined as the place in the sample towards which the visible fraction of the plasma jet is directed to, d=0 cm in **Figure 2.2a**) and at b) 1 cm, c) 2 cm and d) 3 cm from it. In bacteria without DNA damage, the genomic DNA depleted of proteins is formed by a core and a peripheral halo formed by chromatin in form of DNA loops. Cells with DNA damage present DNA fragments dispersed around the core (**Figure 2.2b**). Cells without DNA damage present an intact genomic DNA (**Figure 2.2b,c**). The level of DNA fragmentation was quantified by calculating the radius of the halo formed by DNA fragments around the core using the following algorithm implemented in Mathematica (version 8.0.1.0, Wolfram) by Dr. Roddy Vann. The mean pixel brightness B as a function of the radius r from the centre of the halo can be modelled by the following expression:

$$B = B_0\left(\exp\left(-\frac{r}{r_0}\right)+\mu\right)$$

Where B_0 denotes a brightness scale; μ denotes the background noise (normalised to B_0); r_0 denotes the halo size (or, strictly speaking, the halo intensity decay scale length). This technique allows an objective analysis of the images, as it subtracts the background noise and is independent of the absolute level of illumination.

A positive control of DNA damage was prepared by treating samples with recombinant DNase I (NEB). Samples in agarose-coated slides were treated with 70 µL of 3 U/mL recombinant DNase I in 50 mM Tris-HCl. Slides were covered with a coverslip and incubated for 10 minutes

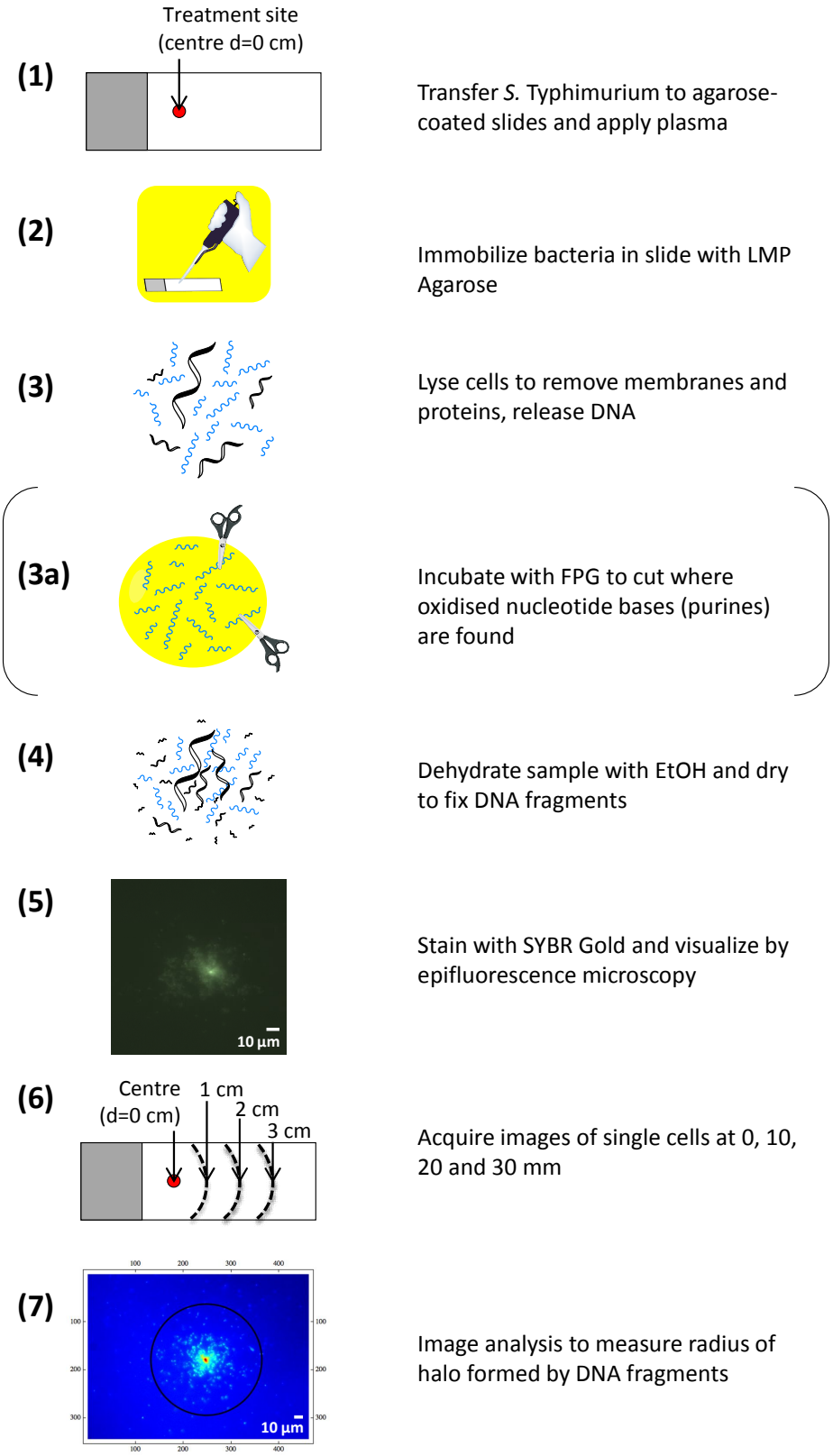

Figure 2.1. ***Schematic of the modified DNA Damage Diffusion Assay (DDD Assay) for plasma experiments.*** The workflow for the analysis of double-strand DNA damage in bacteria at the single cell level is here shown from **1-7**. For the identification of oxidized purines, an additional step **(3a)** corresponding to the incubation of the sample with FPG was added to the protocol. Scale bar 10 µm.

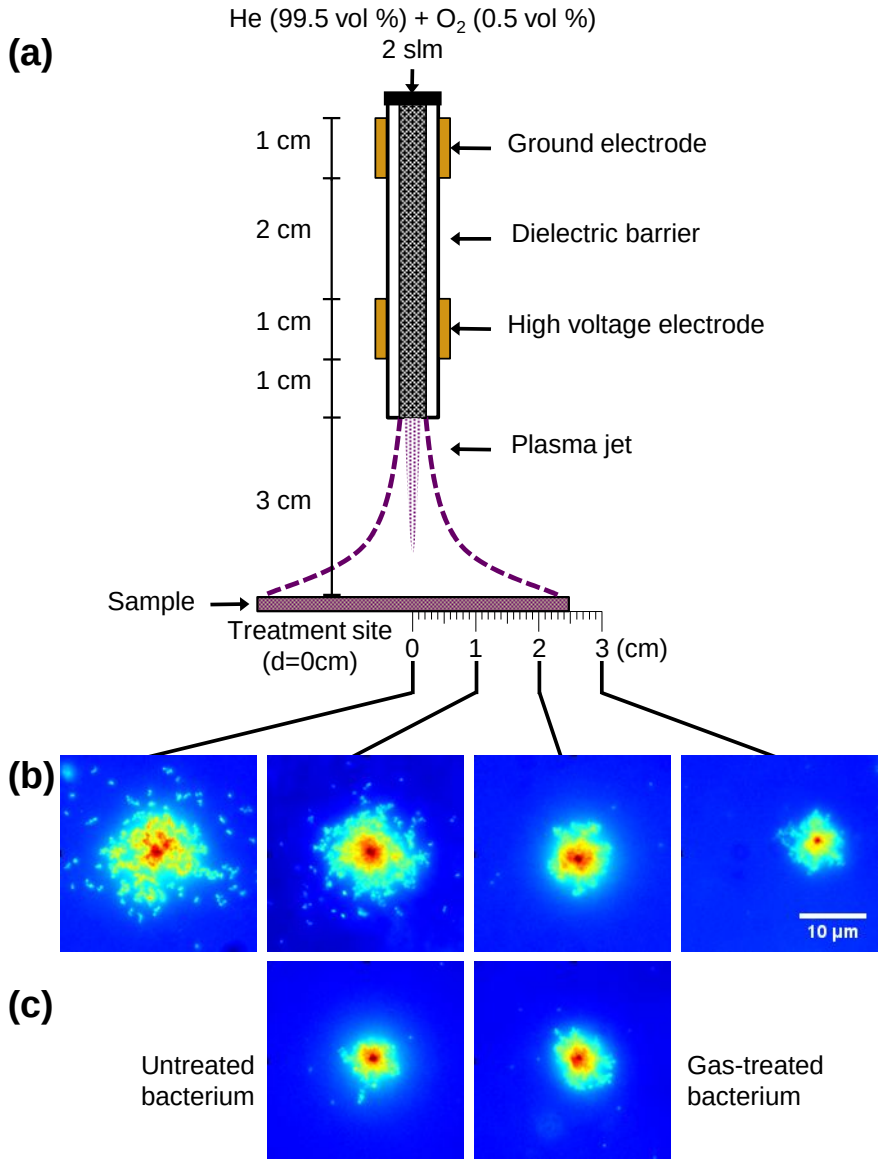

Figure 2.2. ***Schematic of the AP-DBD plasma jet and the effect of plasma treatment on bacterial DNA integrity.*** **(a)** Schematic of the experimental arrangement for the AP-DBD plasma jet. Representative false colour images obtained for the DNA damage diffusion assay of DNA corresponding to single cells for **(b)** plasma-treated *S.* Typhimurium; **(c)** untreated and gas-treated *S.* Typhimurium. The degree of DNA damage derives from the area occupied by the fluorescently stained DNA fragments and varies as a function of the distance to the treatment site (d=0 cm). Scale bar 10 µm.

at room temperature. After incubation, samples were covered with 70 µl of LMP agarose and protocol was followed as described above.

2.6.5 Data analysis

To compare the level of DNA damage obtained at different distances from the treatment site and between experiments, the ratio of DNA damage of single cells in relation to the untreated cells for each experiment was calculated using the following formula:

$$\text{Ratio DNA damage of single cells} = \frac{\text{Radius plasma-treated cell } (\mu\text{m})}{\text{Mean radius untreated cells } (\mu\text{m})}$$

Because the results present unequal variances across groups, the natural logarithm of the ratio (Log_e) was calculated to obtain a distribution that tends to normality for further statistical analysis.

2.6.6 Modified DDD Assay for the identification of damaged nucleotide bases

The DDD Assay previously developed was modified to detect oxidised nucleotide bases as a result of plasma treatment. Formamidopyrimidine-DNA glycosylase (FPG) is an enzyme that cleaves the DNA where an oxidised purine is found. This allows the identification of oxidized purines in addition to DNA breaks directly induced by plasma.

Samples were transferred to the agarose-coated slides, covered with LMP agarose and lysed as described in Section 2.6.4. After lysing the bacterial cells, slides were rinsed 3 times with filtered distilled water (0.22 µm pore size) and 3 times with 1x Reaction Buffer (40 mM HEPES, 0.1 M KCl, 0.5 mM EDTA, 0.2 mg/mL BSA, pH 8.0 with KOH), 3 minutes each. Excess of liquid was removed and 1mL/slide of FPG (1:1000 dilution; NEB) was added to the sample and covered with a coverslip (**Figure 2.1, 3a**). Slides were incubated for 30 minutes at 37°C in a moist box after which they were rinsed with filtered distilled water (0.22 µm pore size) and the protocol was continued as described above.

2.7 ELECTRON PARAMAGNETIC RESONANCE (EPR)

Spin traps were used to determine the concentration of radicals in plasma-treated solutions. The spin traps and reagents described in **Table 2.1** were used for this set of experiments.

2.7.1 EPR calibration

EPR calibration was performed using aqueous solutions of the stable radical TEMPO using concentrations of 4, 10, 20 and 200 µM. The calibrations curves were built and the linear equations with zero intercept to the data were obtained. The values for the linear equation were averaged and a single formula (y=0.9x) was used to calculate the concentration of radicals trapped (**Figure 2.3**).

Abbreviation	Reagents (purity)	Species measured	Provider
DMPO	5,5-dimethy-1-pyrroline-N-oxide (≥ 99 %)	·OH	FLUKA, Sigma
MGD-Fe^{2+} complex	N-Methyl-D-glucamine dithiocarbamate (≥ 98 %) complex with Fe^{2+}	NO/NO_2^-	Santa Cruz Biotechnology Inc.
DEPMPO	5-(Diethoxyphosphoryl)-5-methyl-1-pyrroline-N-oxide (≥ 99 %)	·OH	Santa Cruz Biotechnology Inc.
TEMP	2,2,6,6-Tetramethylpiperidine (≥ 99 %)	$O_3/O/O_2(a^1\Delta g)$	Sigma Aldrich
TEMPO	2,2,6,6-Tetramethylpiperidine 1-oxyl (98 %)	standard radical for calibration	Sigma Aldrich

Table 2.1. ***Spin traps and standard reagents used for EPR spectroscopy.***

(a)

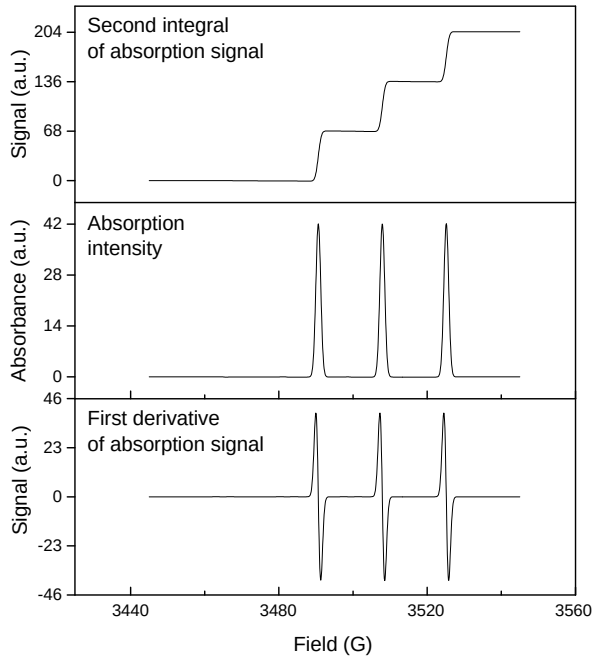

(b)

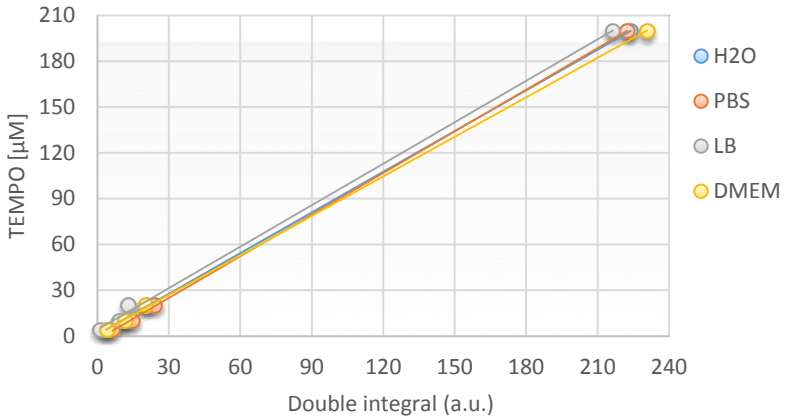

(c)

	H_2O	PBS	DMEM	LB
Linear equations	y = 0.90x	y = 0.8974 x	y = 0.8675 x	y = 0.9272 x
R^2 values	0.9999	0.9994	0.9998	0.9972

Figure 2.3. ***TEMPO calibration for the estimation of the concentration of radicals in plasma-treated liquids.*** **(a)** Calculation of the concentration of spin radical adduct present in the sample using TEMPO. ***Bottom:*** First derivative of the absorption signal (experimentally obtained spectrum). ***Centre:*** Absorption signal, obtained through integration of the first derivative. ***Top:*** Area under the absorption signal, obtained by further integration of the absorption signal. The value obtained is proportional to the number of radicals present in the sample. **(b)** EPR calibration was done using the radical TEMPO in H_2O, PBS, DMEM and LB, as described in Section 2.7.1. **(c)** Corresponding linear equations for TEMPO in each liquid. An average of all the linear equations was calculated (y=0.9x) and used for the estimation of radical concentration in samples.

2.7.2 Experimental conditions

Plasma was generated with the AP-DBD plasma jet at 12 kV (peak-to-peak), 30 kHz, 2 slm He + 0.5 vol % O_2. Ambient humidity was in the range of 20 – 24 %. The distances between the nozzle and the sample was 30 mm. Samples were treated for 30, 60 or 90 seconds.

0.1 M solutions of spin traps were freshly prepared in PBS, DMEM, DMEM + 10% (v/v) FCS, LB and filtered distilled H_2O (0.22 µm pore size) prior to use. For all plasma experiments except MGD_2-Fe^{2+}, 500 µL of each spin trap solution were added to a 24-well plate for treatment. DMEM without phenol red was used in all experiments (Gibco). For all plasma experiments with MGD_2-Fe^{2+}, 250 µL of 0.1 M MGD was mixed with 250 µL 0.02 M $FeSO_4.7H_2O$.

2.7.3 Detection of hydroxyl and superoxide radicals

5,5-dimethy-1-pyrroline-N-oxide (DMPO) was used as it forms radical adducts with O-centred radicals that have a distinguishable EPR spectra. Besides DMPO, 5-(Diethoxyphosphoryl)-5-methyl-1-pyrroline-N-oxide (DEPMPO) was used for the detection of O-centred free radicals (**Table 2.1**). DEPMPO has a longer life-time than DMPO and higher affinity for ·OH radical. Both spin traps were used for the detection of ·OH and O_2·$^-$ in plasma-treated liquids.

To test the role of ionic strength and pH in the formation of ·OH, 500 µL of 0.1 M DMPO in 0.5x, 1x and 4x PBS were plasma-treated. To determine the stability of the DMPO-OH adduct in the different tested liquids, 500 µL of 0.1 M DMPO in H_2O, PBS and LB were treated with the plasma for 90 seconds and analysed immediately after treatment, and at 5 and 10 minutes post-treatment.

2.7.4 Detection of ozone, singlet delta oxygen and atomic oxygen

$O_2(a^1\Delta g)$ was detected indirectly by electron paramagnetic resonance spectroscopy of 2,2,6,6-tetramethylpiperidine-1-oxyl (TEMPO) (**Table 2.1**) formed by the reaction of 2,2,6,6-tetramethylpiperidine (TEMP) with $O_2(a^1\Delta g)$. Because TEMP can be oxidized by reactive species other than $O_2(a^1\Delta g)$ such as ozone and atomic oxygen, sodium azide (NaN_3) (a known scavenger of $O_2(a^1\Delta g)$) was used to identify oxidation of TEMP (Sigma Aldrich) due to other reactive oxygen species. NaN_3 (≥99.5 % purity) were purchased from Fluka.

Spin trap solutions were freshly prepared in argon-saturated liquids. 0.1 M TEMP and 0.1 M TEMP + 0.1 M NaN_3 solutions were plasma-treated as described in Section 2.7.2.

2.7.5 Detection of nitric oxide and nitrite ion

N-Methyl-D-glucamine dithiocarbamate (MGD) in combination with iron(II) sulphate ($FeSO_4$) was used to measure NO and NO_2^- in plasma treated liquids (**Table 2.1**). Upon the addition of $FeSO_4$, MGD forms the MGD_2-Fe^{2+} complex, which is a NO/NO_2^- spin-trapping reagent. Because this complex is sensitive to the redox state of Fe and the presence of O_2, oxidation was

prevented by using a reducing agent. After plasma treatment, 250 µL 0.1 M $Na_2S_2O_4$ (reducing agent) was added to the reaction and mixed for 1 minute. Additionally, MGD, $FeSO_4$ and the reducing agent were added after treating H_2O, PBS, DMEM and LB with plasma for 60 seconds to determine the presence of NO and NO_2^- post-treatment.

2.7.6 Acquisition of the EPR signal

After each plasma treatment, a sample of the plasma-treated liquid was immediately collected in an 80 mm x 1.0 mm capillary tube (Marienfeld Laboratory Glassware). The overall time after the exposure and before recording the spectrum was 2 minutes.

Electron paramagnetic resonance measurements were carried out on a Bruker EMX Micro EPR spectrometer with Bruker WinEPR Acquisition software version 4.40. EPR spectra were recorded using the following conditions: modulation frequency = 100 kHz; microwave power = 3.17 mW (31.7 mW for MGD_2-Fe^{2+}); modulation amplitude = 0.1 G; time constant = 40.96 ms, and magnetic field scan of 100 G for DMPO, TEMPO and TEMP, MGD_2-Fe^{2+} and 170 G for DEPMPO. The absence of signal saturation with MGD_2-Fe^{2+}-NO adducts at elevated power was tested in the power range of 3.17 to 31.7 mW and no saturation was observed. The hyperfine coupling constants for EPR spectra simulations are presented in **Table 2.2**.

2.7.7 Data analysis

For MGD_2-Fe^{2+}-NO adducts the spectra were corrected by subtracting the background (solution of MGD_2-Fe^{2+} complex in respective media).

The amount of $O_2(a^1\Delta g)$ generated by the AP-DBD plasma jet in liquids was estimated from the difference between the EPR measurements of TEMP solution and TEMP + NaN_3 solution. The combined amount of atomic oxygen and O_3 was obtained from the EPR measurement of TEMP + NaN_3 solutions. Concentration was calculated and a correction was made for the loss of volume due to evaporation during plasma treatment.

To confirm the proposed assignments of the spin trap adducts found in each sample, EPR spectra simulations were performed on NIH P.E.S.T. WinSIM software ver. 0.96 (138). This analysis allows one to compare the experimental spectra obtained with that of reference in the literature. Simulated spectra were analysed using SpectrumViewer Plus ver. 2.6.3 (Spectrum Viewer program and documentation written by Erwin Timmerman). The hyperfine coupling constants for the simulations were obtained from a database available online (http://tools.niehs.nih.gov/stdb/index.cfm).

2.8 COLORIMETRIC ASSAYS FOR H_2O_2 AND NO_2^-

UV-Vis spectrophotometry was used for the quantitative determination of H_2O_2 and NO_2^- in plasma-treated solutions as described below.

	Hyperfines		
Spin adduct	**a_N (G)**	**a_H (G)**	**a_P (G)**
DMPO-OH	14.94	14.74	--
DEPMPO-OH	14.00	13.17	47.15
DEPMPO-OOH	-	-	-
$(MGD)_2$-Fe^{2+}-NO complex	12.68	--	--
TEMPO	17.24	--	--

Table 2.2. ***Hyperfine coupling constants for EPR spectra simulations.***

2.8.1 Experimental conditions

For plasma treatment, 500 µL of each liquid were added to a 24-well plate prior to treatment. Plasma was generated with the AP-DBD plasma jet at 12 kV (peak-to-peak), 30 kHz, 2 slm He + 0.5 vol % O_2, 20 – 25 % ambient humidity, and 30 mm distance from nozzle to sample. Samples were treated for 30, 60 or 90 seconds.

UV measurements were performed on a UV-1800 Shimadzu UV-VIS Spectrophotometer with Optical Glass Precision Cells (10 mm light path) provided by Hellma Analytics, using Shimadzu UVProbe software version 2.34. The baseline was pure medium. The background was subtracted from all samples.

2.8.2 Measurement of hydrogen peroxide

The reaction of titanium(IV) salts with H_2O_2 to form a yellow-coloured complex detected by colorimetry was used to determine the concentration of H_2O_2 formed in plasma-treated solutions (139). Calibrations were done using a mixture of 500 µL titanium(IV) solution and 300 µL aqueous H_2O_2 solutions in a range of concentrations 0.0979 – 4.895 mM. H_2O_2 solutions were prepared in each of the following liquids: filtered distilled H_2O (0.22 µm pore size), PBS, DMEM, DMEM + 10 % (v/v) FCS or LB (**Figure 2.4a**). H_2O_2 (30 % (v/v)) and sulphuric acid H_2SO_4 (> 95 % purity) were purchased from Fluka. Potassium oxodioxalatotitanate(IV) dihydrate ($K_2[TiO(C_2O_4)_2]\cdot 2H_2O$) was obtained from Alfa Aesar. To prepare the titanium(IV) solution, 3.54 g of potassium bis(oxalato)oxotitanate(IV) dihydrate was added to a mixture of 27.2 mL of sulphuric acid and 30 mL of filtered distilled H_2O (0.22 µm pore size). The resulting solution was taken to a total volume of 100 mL and left to cool down before use.

After plasma treatment, 500 µL titanium(IV) solution were mixed with 300 µL of the plasma-treated liquid and immediately analysed. The spectra of the titanium(IV) – peroxide complex was collected in the wavelength range between 325 to 800 nm, with 0.5 nm increments. The intensity value of the peak at 400 nm was used.

The amounts of H_2O_2 in plasma-treated samples were also studied after 15 and 30 minutes of plasma treatment of H_2O and LB to determine whether the stability of the molecule in the solutions varied due to the presence of biomolecules.

Catalase was added to plasma-treated DMEM and LB to a final concentration of 32 U/mL and 100 U/mL to confirm the specificity of the assay to detect H_2O_2 and no other peroxides formed in the solution.

2.8.3 Detection of nitrite ion with Griess reagent

Calibration curves for the detection of NO_2^- in liquids (filtered distilled H_2O (0.22 µm pore size), PBS, DMEM, DMEM + 10 % (v/v) FCS or LB) were obtained using 400 µL of the Griess reagent (Sigma Aldrich) and 400 µL aqueous sodium nitrite ($NaNO_2$, Sigma Aldrich, ≥ 97.0 % purity) solution in a range of concentrations from 3.125 – 100 µM (2-fold dilutions) (**Figure**

(a)

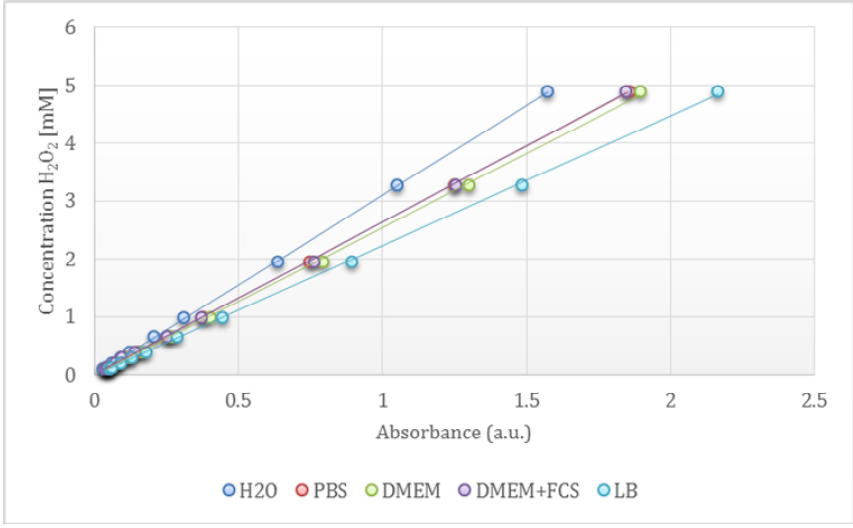

	H_2O	PBS	DMEM	DMEM+FCS	LB
Linear equations	y = 3.1079x	y = 2.6282x	y = 2.5473x	y=2.634x	y = 2.2354x
R^2 values	0.9999	1	0.9994	0.9997	0.9996

(b)

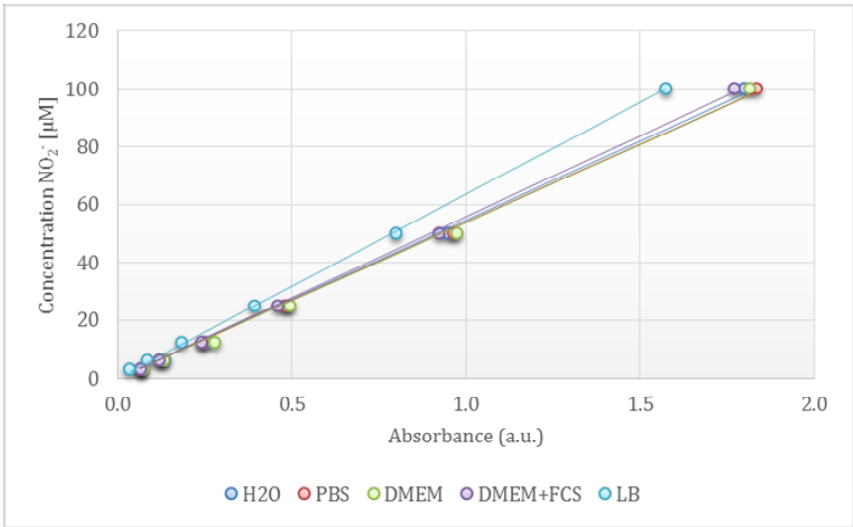

	H_2O	PBS	DMEM	DMEM+FCS	LB
Linear equations	y=54.648x	y=53.843x	y=53.91x	y=55.887x	y=63.454x
R^2 values	0.9982	0.9991	0.9968	0.9992	0.9996

Figure 2.4. ***Calibration curves for the estimation of the concentration of H_2O_2 and NO_2^- in plasma-treated liquid samples and corresponding linear equations.*** Data for **(a)** H_2O_2 and **(b)** NO_2^-. Each dot represent a single measurement.

2.4b). For plasma-treated samples, 400 µL of each sample was used for this experiment. Calibration standards or plasma-treated samples were mixed with Griess reagent and incubated for 5 minutes in the dark at room temperature. Afterwards, samples were mixed and immediately analysed. Spectra were collected in the wavelength range between 350 to 800 nm, with 0.5 nm increment. Intensity values of the peak at 526 nm were used. To determine the formation of NO_2^- in liquids during treatment, Griess reagent was added to H_2O and PBS before plasma treatment.

2.8.4 Data analysis

In each assay, the background spectrum for filter distilled H_2O (0.22 µm pore size), PBS, DMEM, DMEM + 10 % (v/v) FCS or LB was subtracted from the spectra of plasma-treated samples. The resulting linear equations from the calibration curves (**Figure 2.4**) were used to convert absorbance of the plasma-treated sample into concentration of H_2O_2 and NO_2^-.

2.9 STATISTICAL ANALYSIS

One-way ANOVA followed by Tukey's multiple comparisons test was performed using GraphPad Prism v. 4.00 for Macintosh (GraphPad Software) for the analysis of DDD Assay and flow cytometry results. Statistical significance was set at $P<0.05$.

2.10 DETERMINATION OF PLASMA TEMPERATURE

Optical emission spectroscopy and a thermocouple were used for the quantitative determination of the temperature of the plasma effluent as described below.

2.10.1 Optical emission spectroscopy (OES)

Measurements targeting the visible spectral region of the plasma were performed at 21 mm from the nozzle. A UV-visible spectrometer HR2000+ High-Speed Miniature Fiber Optic Spectrometer with wavelength range of 200 – 1100 nm, and the HR4000 High resolution Miniature Fiber Optic Spectrometer with wavelength range of 200 – 400 nm were used. Data was acquired using the SpectraSuite software (Ocean Optics), considering an integration time of 60 seconds, 5 and 10 averages per measurement. The macroscopic temperature of the plasma was obtained by measuring the rotational temperature of the second positive system of N_2, which corresponds to the transition between the electronic states C $^3\Pi_u$ and B $^3\Pi_g$. Spectra were analysed in the range between 376 – 382 nm as this band dominates in this spectral region. Results were analysed by Kari Niemi with an algorithm developed in the LabVIEW platform (140).

Plasma was generated with the AP-DBD plasma jet at 5.6 kV (peak-to-peak) using the double electrode configuration (Section 3.3.1), 123 kHz, 2 slm He + 0.5 vol % O_2. Ambient humidity was 16 – 20 %.

2.10.2 Thermocouple

The Tenma 72-2060 thermocouple (K probe, accuracy ± 0.3 % + 1 °C) with wire diameter of 1 mm was used to measure the temperature of the plasma. The probe was located directly under the plasma jet (x=0 mm) at different distances from the nozzle in the axial direction (y=20, 25 and 30 mm from nozzle) at x=0 mm and x=10 mm. The thermocouple was placed over a LB agar plate to determine the temperature the sample would experience during treatment. Measurements were taken every 30 seconds for 120 seconds.

2.11 MEASUREMENT OF UV RADIATION EMITTED BY AP-DBD PLASMA JET

The UV radiation emitted by the AP-DBD plasma jet was measured with a shortwave meter (Blak-Ray Ultraviolet meter, UVP) in the range 220 – 290 nm, with maximum sensitivity at 254 nm and a minimum detection limit of 20 μW/cm². A Tungsten mesh (Goodfellow Cambridge Ltd.) with 0.2 mm nominal aperture and 0.05 mm wire diameter (64 % open area, 99.95 % purity) was placed between the detector and the plasma jet to shield the detector from electromagnetic fields. The mesh was grounded to the aluminium base of the plasma box.

Plasma was generated with the AP-DBD plasma jet at 5.5 kV (peak-to-peak) using the double electrode configuration (Section 3.3.1), 123 kHz, 2 slm He + 0.5 vol % O_2. The distances between the nozzle and the shortwave meter were 10 mm, 20 mm and 30 mm. UV emission was measured for 60 seconds and the temperature was controlled with a thermocouple (65 °C at ignition).

2.12 TREATMENT WITH PLASMA-GENERATED UV RADIATION ONLY

A magnesium fluoride (MgF_2) window with transmittance ≥ 55 % at 121 nm (Crystran Ltd.) was then used to assess the effect of plasma-generated UV radiation on bacteria. The MgF_2 window was fitted to the lid of a Petri dish to create a sealed chamber with the dish (**Figure 2.5**). Agarose-coated slides for the DDD Assay or LB agar plates to assess bactericidal activity were enclosed in this chamber for plasma treatment with the AP-DBD plasma jet and μAPPJ. The chamber was sealed and air inside the chamber was replaced with Helium + 0.5 vol % O_2 prior to treatment. This was done to ensure UV transmittance through an environment with similar O_2 characteristics as where plasma was generated. The input of gas to the chamber was maintained during treatment. The gas exited the chamber through a tube located at the opposite side of the input conduct.

2.13 UV-ABSORPTION SPECTROSCOPY

UV-absorption spectroscopy is a technique commonly used to measure ozone density. Ozone has a high cross section at Hartley bands between 200 – 320 nm in the ultraviolet with a

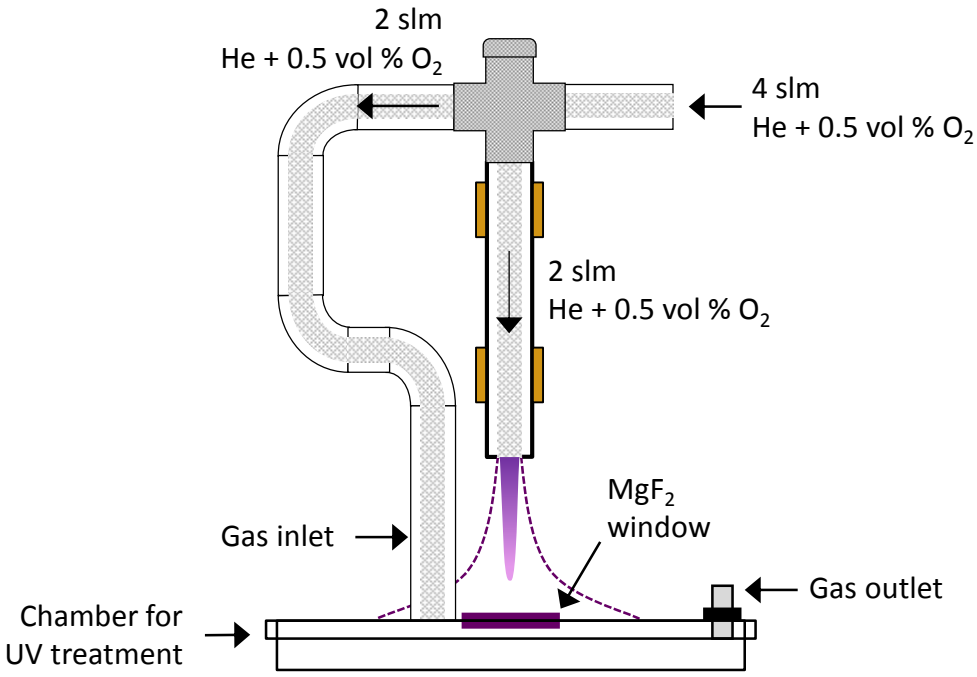

Figure 2.5. ***Experimental design for the treatment with plasma-generated UV radiation.*** The effect of the UV radiation emitted by the AP-DBD plasma jet and the µAPPJ on bacterial cells was assessed using a MgF_2 window fitted to a Petri dish to create a sealed chamber. The MgF_2 window allowed the pass of light above 121 nm with a transmittance ≥ 55 %. The air in the chamber was replaced with the gas admixture used to generate plasma 2 minutes before treatment.

maximum absorption at 255 nm (141). This method is widely used for the measurement of the ozone density in plasmas (142-144).

The determination of ozone density in the AP-DBD plasma jet was done with Apiwat Wijaikhum as part of a collaborative work between the Centre for Immunology and Infection and York Plasma Institute. For this purpose, the AP-DBD plasma jet was housed in a metallic box with a metallic mesh at the top, as described in Section 3.2. The ultraviolet (UV) light source (UV-LED UVTOP TO18 LED 250) was mounted in an electronic control box (ThorLABS TCLDM9). The LED was controlled by two parameters via the connections to the temperature control box (TED200C) and current control box (LDC205C). The UV-LED at light source position was imaged by 100-mm focusing lens to the effluent region of the plasma defined as a probe beam *via* UV beam splitter (BS; UVFS, 50/50, BBAR 250 – 450 nm, fused silica plate, BSW20, Thorlabs) (**Figure 2.6a**). It was assumed that the probe beam was parallel throughout the effluent region. The reference beam was also split by the UV beam splitter and was imaged at the middle between the UV beam splitter and the mirror (MR). Both beams were symmetrically reflected, split and imaged to the slit position, but on different vertical positions. The two beams at the slit were resolved by the dispersing element grating with a groove density of 2399 lines/mm (optical resolution) blazed at 300 nm in the Czerny-Turner spectrograph with 0.5-m focal length (Andor SR-500i) and were imaged by the CCD camera (Andor, Newton DU940P-BU2, 2048 x 512 pixels, pixel size 13.5 µm x 13.5 µm).

The Beer-Lambert law for absorption spectroscopy was used to determine the ratio of transmitted light (I_T) and incident light (I_0):

$$\frac{I_T}{I_0} = \frac{I_{PL} - I_P}{I_L - I_{BG}} = \exp(-n.L.\sigma(T,\lambda))$$

Where n denotes the density of O_3, L denotes the absorption length of the plasma and σ denotes the cross section of O_3 centre at 255 nm. To calculate the absorbance of UV light by the plasma, 4 measurements were taken:

- $\boldsymbol{I_{PL}}$**:** Emission UV-LED light ON, plasma ON
- $\boldsymbol{I_P}$**:** Emission of plasma ON, UV-LED light OFF
- $\boldsymbol{I_L}$**:** UV-LED light ON, plasma OFF
- $\boldsymbol{I_{BG}}$**:** Room background, UV-LED light OFF, plasma OFF

The length of treatment used for bacterial assays was used for the acquisition of each of the aforementioned measurements, capturing 36 images per measurement. Absorbance of UV light by ozone produced in the plasma effluent was measured in the axial direction at 1, 10, 20 and 30 mm distance from the nozzle and in the radial direction starting from the treatment site (radial position = 0 mm) up to 40 mm, in 5 mm steps. The absorption profiles were transformed by two

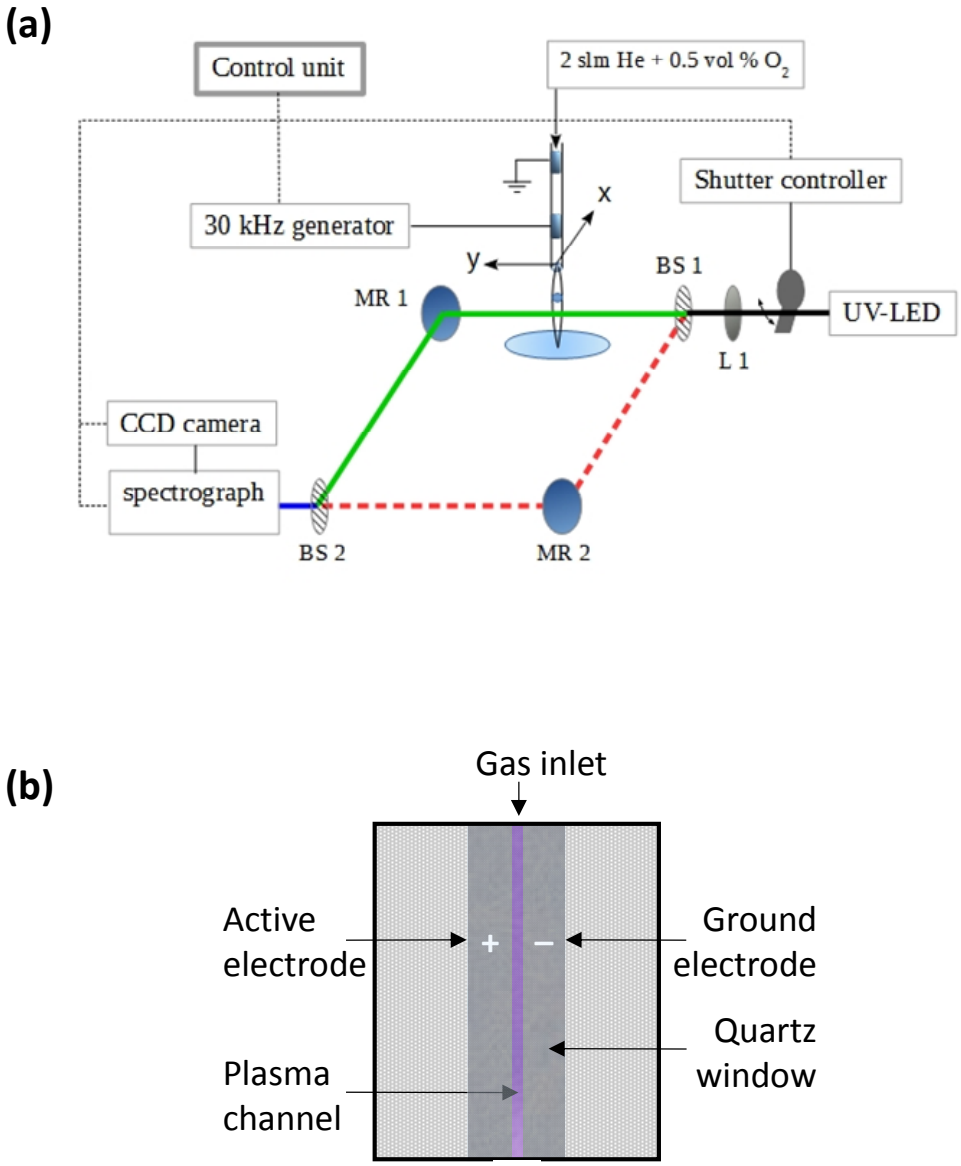

Figure 2.6. ***Schematics for experimental methods.*** **(a)** UV-LED absorption spectroscopy method used. The UV-LED light is split by the beam splitter BS1 and equally directed towards the mirrors MR1 and MR2. The signal collected from the probe beam and reference beam were collected by a spectrograph and imaged by a CCD camera. Image adapted from Wijaikhum *et al.* (unpublished data). **(b)** Schematic of the µAPPJ source.

algorithms of Abel inversions (described in (145, 146)) into radial O_3 density distribution profiles.

2.14 RADIO-FREQUENCY ATMOSPHERIC PRESSURE PLASMA JET (μAPPJ)

The μAPPJ has been described in detail in (147) (**Figure 2.6b**). The homogeneous, low gas temperature glow-mode plasma generated with the μAPPJ has been well characterized with experimental (148) and *in silico* analyses of the plasma parameters including gas temperature, electron properties, O, $O_2(a^1\Delta g)$, O_3, and helium metastables densities (113, 149). Plasma was generated in a plasma channel of 30 mm long and 1 mm x 1 mm cross-section created by two plane parallel stainless steel electrodes mounted in between two quartz windows (148). Two slm He + 0.5 vol % O_2 where supplied to the channel to generate plasma, using 13.56 MHz radio-frequency voltage provided to the active electrode *via* an impedance matching network. The plasma configuration is such that the electric field direction is perpendicular to the gas flow and to the plasma channel exit nozzle. This confines the charged particles within the electrode gap inside the core plasma region. With no direct power input and very short mean free paths for charged particles, the plasma effluent is devoid of charged carriers and neutral species and UV radiation dominate the effluent characteristics (51). Preliminary data indicates the temperature of the plasma is under 40 °C at distances higher than 5 mm from the nozzle in the axial direction (150).

3 OPTIMIZATION OF THE AP-DBD PLASMA JET FOR BACTERIAL ELIMINATION

3.1 INTRODUCTION

In this chapter, the experimental plasma setup used throughout the dissertation is introduced. The atmospheric-pressure dielectric barrier discharge (AP-DBD) plasma jet is described and diagrammed. The aim of this chapter is to gain a better understanding of the antibacterial potential of the AP-DBD plasma jet by examining the various physical and biological parameters that determine the antimicrobial effectiveness against bacteria in solid and semi-solid environments. The AP-DBD plasma jet was optimized to study its bactericidal activity considering the radial distribution of plasma species over the bacterial sample. This is further addressed in Chapter 4. Results are reported using an atmospheric pressure dielectric barrier discharge plasma jet, generated with helium and small percentage admixtures of molecular oxygen. Bacterial load, media composition, distance from nozzle to sample, composition of the feed gas, length of treatment, electrode configuration, voltage, frequency, current and dielectric barrier configuration were considered and optimized for plasma treatment of bacteria. The antimicrobial effectiveness for each condition was studied using *S.* Typhimurium as a model organism.

3.2 DESCRIPTION OF THE PLASMA SOURCE

The AP-DBD plasma jet is a linear-field device where the flow field and the electric field run in parallel (151). The plasma jet is sustained through a streamer-like mechanism. A high electric field region at its tip propagates the plasma in the helium channel outside the plasma tube (152, 153). These types of plasmas usually consist of transient plasmas and as this source is driven by a sinusoidal voltage source we expect multiple breakdowns per applied cycle.

A schematic diagram depicting the arrangement of the AP-DBD plasma jet is shown in **Figure 3.1a**. The plasma jet is housed inside a plasma box the contents of which are fixed and grounded, with interlock installed. Outside the plastic plasma box (**Figure 3.1b**), an oscilloscope (Agilent Technologies DSOX 2004A) with a signal function generator provides sinusoidal waveforms of frequencies from Hz to kHz into an audio amplifier connected to a DC power supply. The amplifier increases the amplitude of the input signal, typically outputting voltages of 10 to 20 Volts. The output from the amplifier feeds into the plastic plasma box; every conducting pathway has an impedance less than 0.5 Ohms.

In one compartment of the plastic plasma box, the amplifier is connected to the primary coil of a frequency-dependent transformer (Plasma Technics Inc.). The transformer has a turns ratio of 1:10 but the secondary voltage produced exceeds this ratio due to the stray capacitance of the secondary coil of the transformer. A 470 pF capacitor that reduces the resonant frequency of the

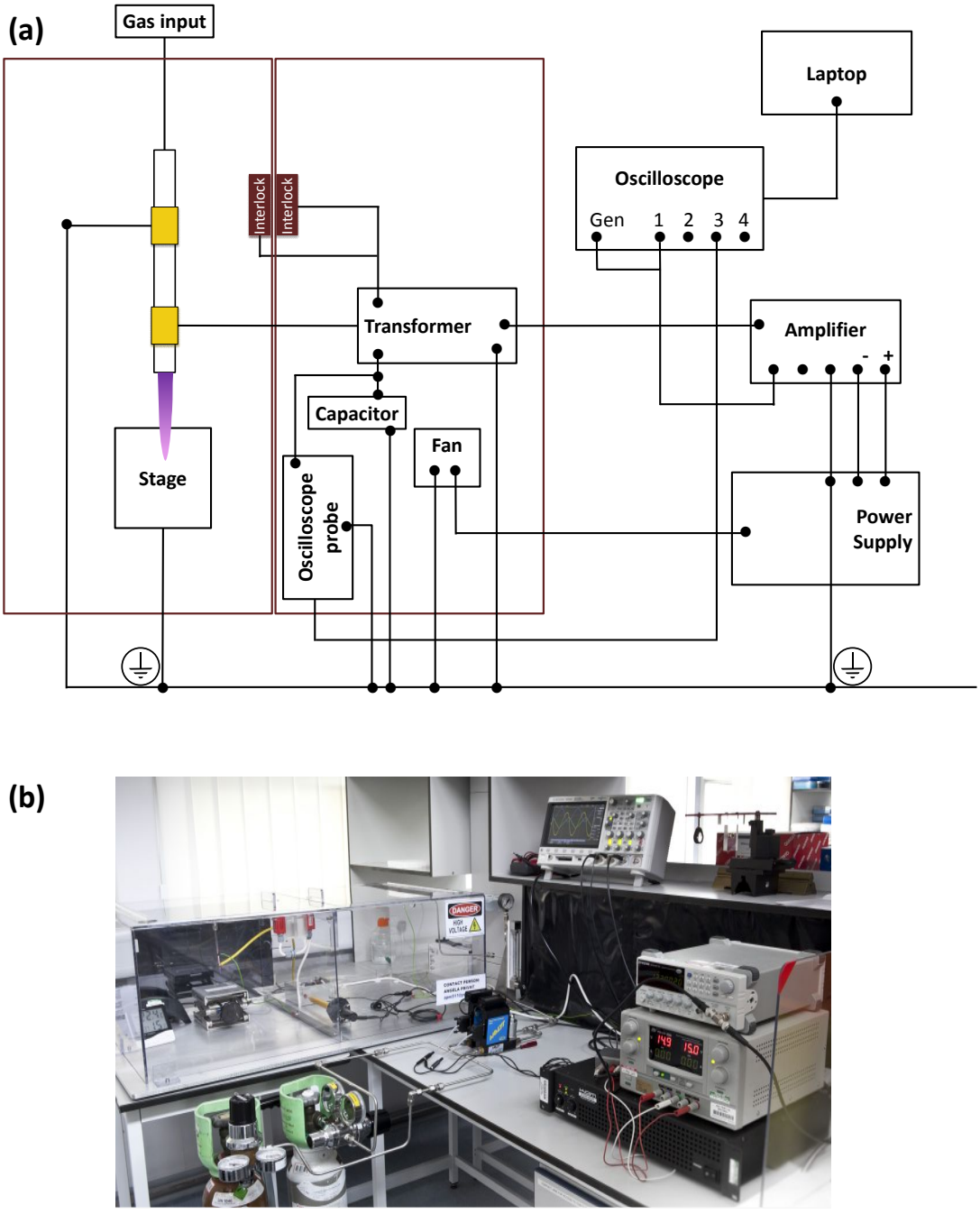

Figure 3.1. ***Schematic and picture of the atmospheric pressure dielectric barrier discharge (AP-DBD) plasma jet built in-house in a plastic plasma box.*** **(a)** The plastic box was divided into two parts, providing a space for sample treatment and another compartment for the electronic components of the plasma. **(b)** Picture of the AP-DBD plasma setup. Power supply, oscilloscope, amplifier and mass flow controllers were located outside the plastic box as shown in picture. ***(Continues in the following page.)***

(c)

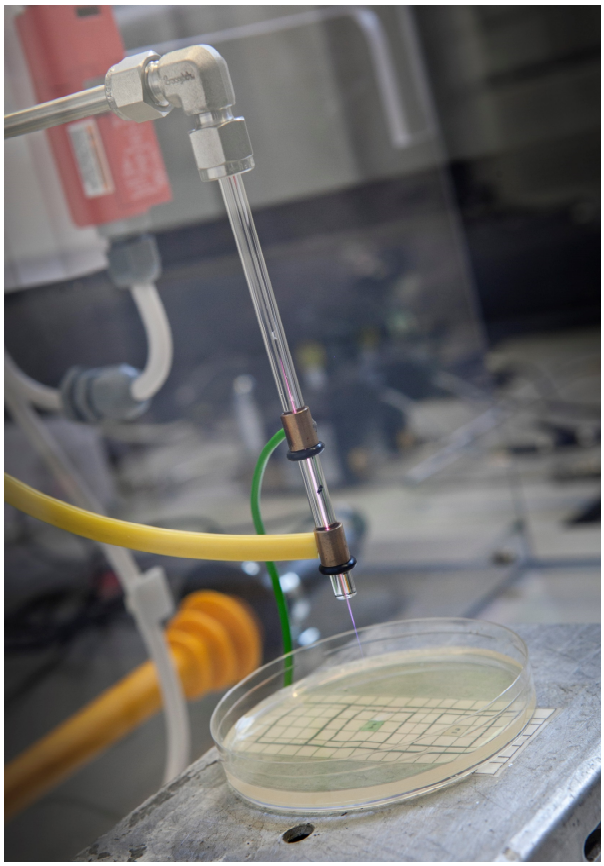

Figure 3.1. (cont.) (c) Picture showing the plasma jet generated between the powered and the ground electrode with the AP-DBD plasma jet. For this picture, plasma was ignited at voltages higher than those used in experiments for demonstration purposes only.

transformer from 124 kHz to approximately 30 kHz (4.1-fold decrease) is connected to the secondary coil of the transformer to reduce the resonant frequency (**Figure 3.2a**; see also Section 3.3.7). The 470 pF capacitor was selected among a set of capacitors since it can reduce the resonant frequency and generate a plasma with gas temperature below 40 °C. A comparison between the experimental data and a fit curve model for an ideal transformer demonstrates that the reduction in the resonant frequency of the system was obtained as a consequence of the stray capacitance in the secondary coil of the transformer (**Figure 3.2b**). Because the capacitance is temperature-dependent, a fan cools down the capacitor to preserve the capacitance and therefore the stability of the signal. The transformer sends the voltage to the powered electrode with amplitudes between 5.00 and 12.00 kV (± 0.1; peak-to-peak), measured with a high voltage probe (Tektronix P6015A) connected to the oscilloscope. The plasma is generated in the second compartment of the plastic plasma box. In this compartment, two symmetrical copper electrodes of equal length (10 mm) are wrapped around a hollow dielectric glass tube of 1 mm inner diameter and 6 mm outer diameter (**Figure 3.1c**). The powered electrode is placed 10 mm above the nozzle of the quartz tube. The grounded electrode is located upstream of the active electrode with 20 mm separation between electrodes and the corresponding wires were oriented in opposite directions to prevent the formation of electromagnetic fields. The feed gas flows at 2 standard litres per minute (slm) in the axial direction. The feed gas consists of an admixture of He with O_2 and the flow rate is controlled by mass flow controllers (Brooks; GFC) located outside the box. The gas passes through the electric field generated by the electrodes and becomes ionized as it travels in the axial direction. Biological samples are placed on an adjustable metallic stage that is grounded to the aluminium base. The generation of plasma is controlled from a laptop connected to the oscilloscope. A code is executed from the laptop to find the resonant frequency as the voltage increases to the desired value (set in the code, expressed in kV) and to register overheating of the capacitor. The plasma is generated and a stable signal at the desired high voltage is produced.

For the measurement of the ozone density in the gas phase and its correlation with the bactericidal activity of the plasma, the AP-DBD plasma jet was installed with a different electrical arrangement (**Figure 3.3**). For this arrangement, the plasma was housed inside a metallic box grounded to the aluminium base. The dielectric tube and an adjustable stage were installed in a motorized support that allowed the mobilization of both structures in the axial and radial direction. The powered electrode connected to the transformer passed through an orifice in the metallic box that was properly insulated. The top part of the box was covered with a metallic mesh, grounded to the aluminium base. Outside the metallic box, a plastic box contained in a similar arrangement the oscilloscope probe, transformer, capacitor and fan. The contents of the plastic box were grounded, with an interlock installed. Outside the plastic box, the oscilloscope, amplifier and power supply were connected as indicated before.

(a)

Capacitance (pF)	Resonant Frequency (kHz)	Voltage IN (mV)	Voltage OUT (V)
0	124.10	112.00	42.60
22	92.82	70.00	35.60
100	58.00	39.00	22.80
220	42.22	46.00	16.30
470	31.03	31.50	12.40
1,000	21.37	25.40	8.60
2,000	15.17	20.40	6.20
100,000	2.12	11.50	0.92

(b)

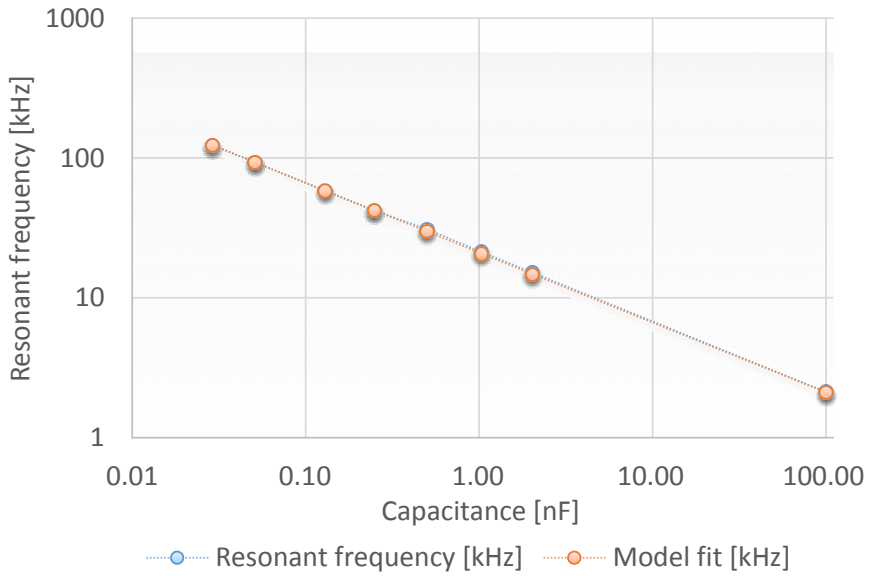

Figure 3.2. ***Identification of the resonant frequency for capacitors coupled to the secondary coil of the transformer at low voltages.*** **(a)** Measurement of the resonant frequency for capacitors ranging from 22 to 100,000 pF. **(b)** Fit curve of experimental and model data that demonstrate that the reduction in the resonant frequency of the system is due to the stray capacitance in the secondary coil of the transformer.

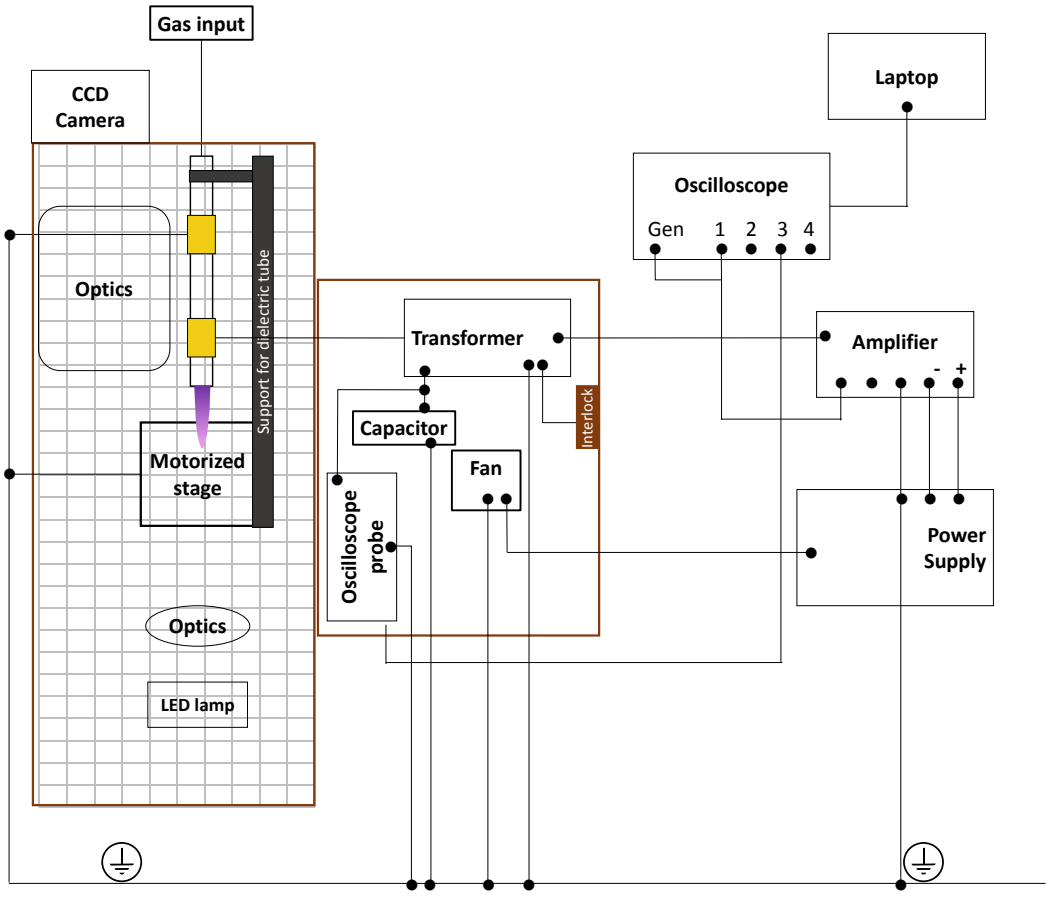

Figure 3.3. ***Schematic of the atmospheric pressure dielectric barrier discharge (AP-DBD) plasma jet installed in an open box with a protective mesh.*** The plasma was generated inside a metallic box was divided into two parts, providing a space for sample treatment and another compartment for the electronic components of the plasma. Power supply, oscilloscope and amplifier were located outside the plastic box.

The setup for the AP-DBD plasma jet was improved over the time and the conditions were optimized as described in the following section. The final version of the AP-DBD plasma jet is depicted in **Figures 3.1 and 3.3**, according to the electrical arrangement in each of the boxes where the components were housed. The conditions for plasma treatment of *S.* Typhimurium were optimized and maintained in either electrical arrangement. The experimental conditions for the optimization of each parameter studied here are individually stated in each of the following subsections.

3.3 OPTIMIZATION OF CONDITIONS FOR PLASMA TREATMENT OF *S.* TYPHIMURIUM

As plasma is rich in neutral and charged particles, electrons and UV radiation, plasma can initiate a cascade of biological and chemical events in the treated microorganism. The antimicrobial activity of plasmas can be affected by several physical, biological and chemical factors. It is well accepted that these factors can determine the bactericidal action of plasmas (154, 155). Thus, the rate and type of the chemical reactions occurring in the gas or liquid phase and the characteristics of the sample can determine the effect of plasma on the biological target (156).

The biological and physical conditions that can determine the antimicrobial activity of the AP-DBD plasma jet were studied. Conditions for the treatment of *S.* Typhimurium were standardized considering reference conditions from the literature (13, 109, 110, 135, 157-166). For this purpose, the zone of inhibition after treatment of bacteria on an agar plate was used. Samples were prepared and the zone of inhibition was assessed as described in Section 2.4, unless otherwise stated.

3.3.1 Electrode configuration

The configuration of the electrodes used to generate the plasma jet can determine the propagation of the jet in the axial direction, the reactive species produced and the overall bactericidal activity of the plasma. It has been suggested that in DBD sources, the jet resembles a positive streamer (153, 167), where the discharge starts from the powered electrode and extends both in the axial direction towards the sample and in the upstream direction. The addition of a grounded electrode to the DBD plasma source could modify the propagation of the jet (157) and therefore impact on the bactericidal properties of the plasma.

The effect of different electrode configurations on the bactericidal effect of plasma was determined. Three configurations were tested (**Figure 3.4**):

a) Single powered electrode, 10 mm from end of nozzle

b) Double electrode, powered electrode 10mm from end of nozzle, grounded electrode 20 mm upstream powered electrode

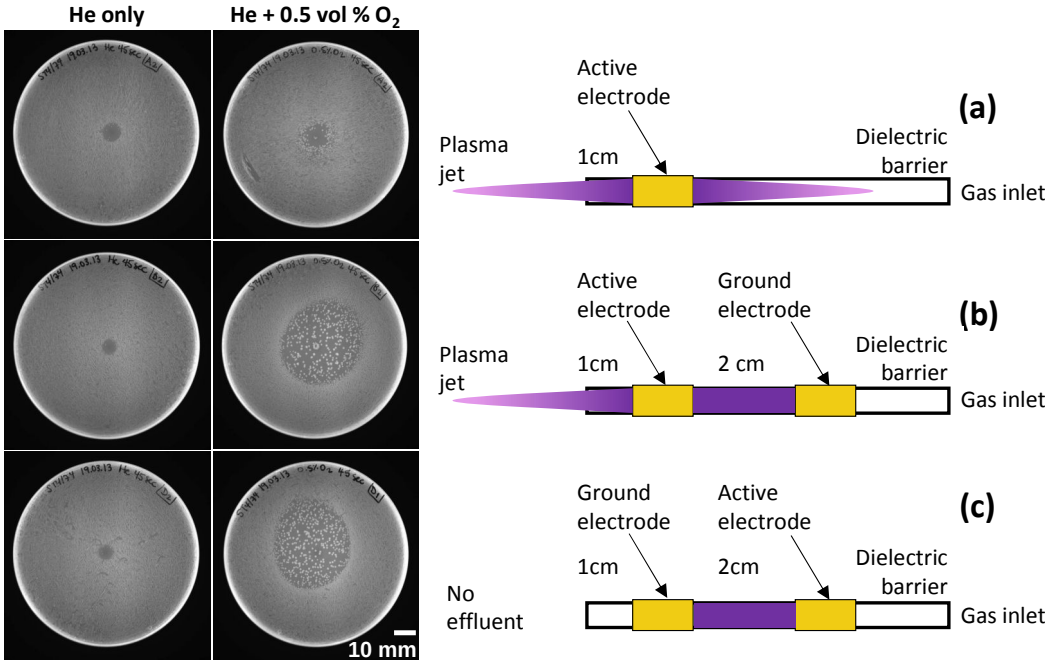

Figure 3.4. ***Optimization of electrode configuration for the AP-DBD plasma. Left:*** Representative agar plates of samples treated for 45 seconds with the AP-DBD plasma jet using 2 slm He or He + 0.5 vol % O_2. ***Right:*** Schematic of the electrode configurations used. Plasma was generated with the **(a)** single electrode configuration, **(b)** conventional double electrode configuration and **(c)** an inverted double electrode configuration. The distances between the nozzle and the sample were 25 mm. Results are representative of two experimental repeats. Scale bar 10 mm.

c) Double electrode, grounded electrode 10mm from end of nozzle, powered electrode 20 mm upstream grounded electrode

Plasma was generated with the AP-DBD plasma jet at 5 kV (peak-to-peak), 123 kHz, using 2 slm He only or He + 0.5 vol % O_2. Ambient humidity was 15 %. Samples were treated for 45 seconds. The distances between the nozzle and the sample were 25 mm.

The plasma ignites around the powered electrode due to the strong electric fields in this region and propagates in both directions along with He (condition **(a)**). The addition of a grounded electrode to the dielectric tube (conditions **(b)** and **(c)**) modified the propagation of the plasma on the direction of the grounded electrode, as no visible plasma was observed beyond the point where the grounded electrode was placed. This phenomenon has been explained for DBD plasmas (168, 169), where the propagation of positive ions in the positive streamer in the direction of the grounded electrode induced the polarization of the dielectric. This leads to the deposition of charges at the inner edge of the grounded electrode. The deposited surface charges can induce a surface ionization wave that propagates on the inside of the dielectric surface when the applied voltage is large enough. If the voltage does not exceed this threshold, the charge build up and the associated electric field is not sufficient to launch the ionization wave, and the plasma terminates inside the dielectric tube at the grounded electrode.

For conditions **(b)** and **(c)**, no visible plasma was observed beyond the grounded electrode. Plasma generated with the grounded electrode in the downstream region (condition **(c)**) did not present a visible plasma jet outside the nozzle, however this does not mean neutral species cannot reach the sample. Reactive neutral species produced by the plasma confined inside the tube can be carried to the sample with the feed gas and were observed to be effective against bacteria (**Figure 3.4c**). The addition of a grounded electrode to the system increased the area treated by the plasma, increasing the zone of inhibition 5.4 times (condition **(b)** 1216 mm^2 and **(c)**: 1244 mm^2). The resulting zones of inhibition in plates treated with conditions **(b)** and **(c)** were of similar size and presented similar number of CFU in this region. This was true for plasma treatments generated with He + 0.5 vol % O_2, but not for plasma generated with He only (**(b):** 39 mm^2 and **(c):** 39 mm^2) (**Figure 3.4**).

The fact that configurations **(b)** and **(c)** provided similar antibacterial activity when O_2 was added to the feed gas could represent a significant participation of neutral species in the elimination of bacteria, specifically those derived from oxygen. The participation of charged species and neutrals delivered for a plasma jet generated using the configuration **(b)** was further studied and is described in Chapters 4 and 5.

The bactericidal activity of plasma was limited to a small region when plasma was generated using the single electrode configuration. For further experiments, the conventional double electrode configuration **(b)** (grounded electrode 10mm upstream end of nozzle, powered electrode 20 mm upstream grounded electrode) was used as it provided an increased area of

bactericidal action. This is in agreement with other devices used for biomedical applications (44, 170).

3.3.2 Bacterial concentration

It has been demonstrated that the initial concentration of bacteria (CFU/ml) determines the dose of antibacterial treatment required to eliminate bacteria (171). The microbial load can also limit the time of exposure to chemical germicides (172). For biomedical plasmas, Fernandez *et al.* demonstrated that the rate of inactivation decreased when increasing concentration of *S.* Typhimurium deposited in polycarbonate membrane filters where exposed to plasma (135). For a pulsed spark plasma, higher deposited energies levels in the plasma jet were required to achieve 1-$\log_{10}$ reduction in the bacterial concentration when treating 10^8 CFU/mL compared with 10^6 CFU/mL *E. coli* in water (115). Thus, the efficiency of plasma treatments to kill bacteria could depend on the size of the initial inoculum.

To determine the initial concentration of bacteria to use for plasma experiments with the AP-DBD plasma jet, 100 µL $1.6x10^9$ CFU/mL, $1.6x10^8$ CFU/mL and $1.6x10^7$ CFU/mL late logarithmic phase *S.* Typhimurium were spread in LB plates and plasma treated. Plasma was generated with the AP-DBD plasma jet at 6 kV (peak-to-peak) using the single-electrode configuration (Section 3.3.1), 123 kHz, 2 slm He + 0.5 vol % O_2. Ambient humidity was 17 %. The distances between the nozzle and the sample were 25 mm.

The zones of inhibition for all three conditions presented a similar area (approx. 300 mm^2). However, plasma-treated agar plates containing 100 µL $1.6x10^7$ CFU/mL presented a zone of inhibition with less bacterial growth and more defined edges than those with higher initial inoculum (**Figure 3.5**). Total clearance of bacterial growth in the zone of inhibition was not obtained, as bacterial colonies could be observed even at the lowest initial inoculum tested.

Deng *et al.* suggested that an increased bacterial load of *B. subtilis* spores in polycarbonate filters could favor the formation of multiple layers of cells, where those in the outer layer are directly affected by the plasma and protect spores underneath, contributing to their survival (173). For the experiments presented here, we could consider that the average size of the rod-shaped *Salmonella* bacterium is 2 – 5 microns long by 0.5 – 1.5 microns wide (174). Then, 100 µL of 1.6 x 10^9 CFU/mL would occupy a surface area of approximately 786 mm^2. Since the surface area of a Petri dish is 5800 mm^2, the chances that multiple layers of bacteria were formed in agar plates prior to plasma treatment are limited. However, the formation of bacterial clumps at higher bacterial concentrations has been suggested to provide a physical protection against plasma treatment to bacteria deposited on membrane filters (135). In cell aggregates, it is possible that peroxidation of phospholipids and polysaccharides occurs in a limited surface area and the membrane damage could be repaired in cells that recover in a nutrient-rich environment. This hypothesis could be supported by the findings of Dobraynin *et al.* that suggest that the main target of charged species is the cell membrane (156). However, the

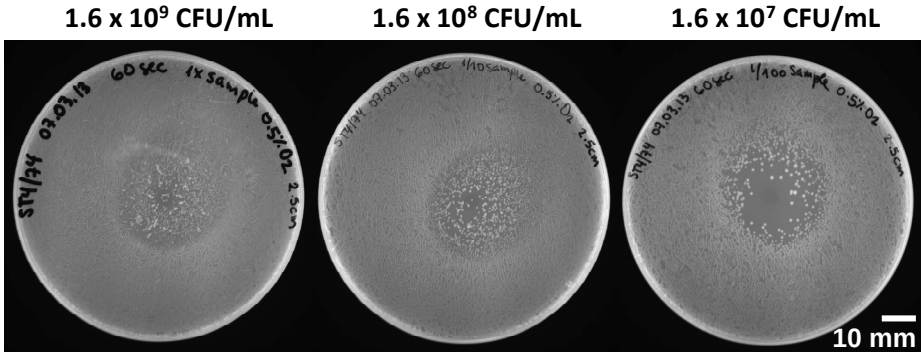

Figure 3.5. ***Effect of bacterial concentration in the killing effect of plasma.*** Three concentrations of late logarithmic phase cultures of *S.* Typhimurium (1.6 x 10^9, 1.6 x 10^8 and 1.6 x 10^7 CFU/mL) were used to test the bactericidal activity of the AP-DBD jet. One hundred microliters of each dilution were plated in LB agar plates. Samples were plasma-treated for 60 seconds and cultured overnight at 37 °C. Scale bar 10 mm.

number of bacterial cells plated at the highest concentration in the present study covered only 14 % of the total surface area of a Petri dish. The aggregation of bacterial cells could be minimal. Therefore, bacterial aggregation might not be the only factor contributing to an increased survival of bacteria to plasma treatment and other factors may be involved in this process.

Based on these results, the lowest initial concentration of bacteria here tested ($1.6x10^6$ CFU/plate) was used for all further experiments, unless otherwise stated. The chosen bacterial concentration lies within the range 10^5 – 10^7 CFU/mL commonly used for the study of antibacterial treatments (158). The possible interaction of plasma with the nutrients in the culture media was explored as described in Section 3.3.3 and further studied in Chapter 5.

3.3.3 Media composition

The different challenging environments where bacteria live and multiply require the adaptation of bacterial cells to variations in nutrient availability, pH, temperature and other stress conditions (175). Under these circumstances, bacterial cells can induce physiological and genetic changes to facilitate the response to multiple stress signals, including oxidative stress (176). It has been suggested that bacteria exposed to nutritional and oxidative stress may adjust their regulatory systems to adapt to exogenous oxidative stress rather than starvation (177). That is the case of the stringent response, activated by the absence of basic nutrients such as iron, phosphate, carbon source or fatty acids in the environment. This response is characterized by down-regulation on the expression of house-keeping genes and up-regulation on the expression of survival genes to adequately administer the resources available (178). In Gram-negative bacteria, the stringent response could represent an increase in the defense against oxidative stress upon exposure to antimicrobials (179). Thus, the nutritional state of bacteria at the time of exposure to oxidative stress induced by the plasma could determine the outcome of the treatment.

While a nutrient-rich environment is beneficial for cell growth and development, the nutrients in the media could also be oxidized or reduced during plasma treatment. It has been described that the culture media RPMI used for eukaryotic cell culture interfered with experiments aiming to induce oxidation of low density lipids *in vitro* (180). In the plasma field, it has been demonstrated that plasma treatment of amino acids in solution induced preferentially the oxidation of sulphur-containing and aromatic amino acids (102). Additionally, low temperature plasma induced structural changes in proteins and amino acids in solution due to oxidation processes (181). Thus, it is possible that the bactericidal activity of plasmas is affected by the nutrient composition of the media.

To determine the effect of the media during bacterial elimination by plasma, two culture media were used. Lennox Broth (LB) was used as a rich source of peptides, lipoproteins, amino acids, salts and carbohydrates derived from yeast extract and is known to allow fast growth. The second medium used was the minimal medium M9 that contains the minimum nutrients

possible for bacterial growth. It has a basic source of carbon (glucose as the only source), nitrogen and salts, from which bacteria can synthesize amino acids and nucleic acid bases. Briefly, 100 µL $1.6x10^7$ CFU/mL late logarithmic phase *S.* Typhimurium cultured in LB or M9 were spread on LB or M9 plates, respectively. Plasma was generated with the AP-DBD plasma jet at 5.5 kV (peak-to-peak), 123 kHz, 2 slm He + 0.5 vol % O_2, using the double-electrode configuration (Section 3.3.1). Ambient humidity was 16 %. The distance between the nozzle and the sample was 25 mm. Samples were plasma-treated for 30 seconds and incubated for 24 (LB) and 48 hours (M9) at 37 °C overnight.

Results showed that *S.* Typhimurium treated in M9 plates presented an increased zone of inhibition compared to those treated in LB plates (**Figure 3.6b,f**). In these zone of inhibition, colony forming units (CFU) were observed, each of them originated from a single bacterium. The presence of CFU in the zone of inhibition might represent the efficacy of plasma to kill bacteria in the treated area. Plasma treatment was more efficient in eliminating bacteria when bacteria were treated in M9 agar plates, observing approximately 80 CFU in the zone of inhibition 48 hours post-treatment. In addition, the area of the zone of inhibition (2027 mm^2) was clearly delimited. In contrast, *S.* Typhimurium treated in LB agar plates presented a zone of inhibition of 123 mm^2 with more than 200 CFU.

Changes in the availability of basic nutrients such as phosphate, nitrogen and carbon and variations in the pH level and oxygen can trigger physiological and morphological changes in the bacterial cell to allow their adaptation to the new environment for survival (182). Bacteria growing in minimal culture medium such as M9 can change their metabolism to promote the biosynthesis of basic biomolecules, primarily the amino acid biosynthetic pathways. These metabolic changes are usually translated into the up-regulation and down-regulation of genes associated with growth and increased expression of genes involved in bacterial survival and biosynthetic pathways (178). In turn, bacteria growing in a nutrient-rich media such as LB can grow fast and increase their protein synthesis (183). Results showed that plasma-treated bacteria in M9 agar plates presented slower growth rates than those in LB plates. In M9 agar plates, CFU were observable in the zone of inhibition only after 48 hour post-treatment (**Figure 3.6f,i**). The preferentially biosynthetic metabolism displayed by bacteria growing in minimal medium is controlled by *RpoS*, a sigma factor that confers resistance to several stress and starvation treatments and helps to maintain redox homeostasis (184). Thus, although bacteria in minimal medium redirect their metabolism to promote biosynthesis, it provides resistance to external insults that include oxidative stress. This includes the upregulation of *dps*, a protein that affects gene expression and protects chromosomal DNA from oxidative stress (185) and an increase in the expression of antioxidant enzymes such as superoxide dismutase, catalase and glutathione reductase, among others (22). Therefore, the differences in the metabolism of bacteria grown in both culture media may not be solely responsible for the increased bactericidal activity of plasma on M9 agar plates.

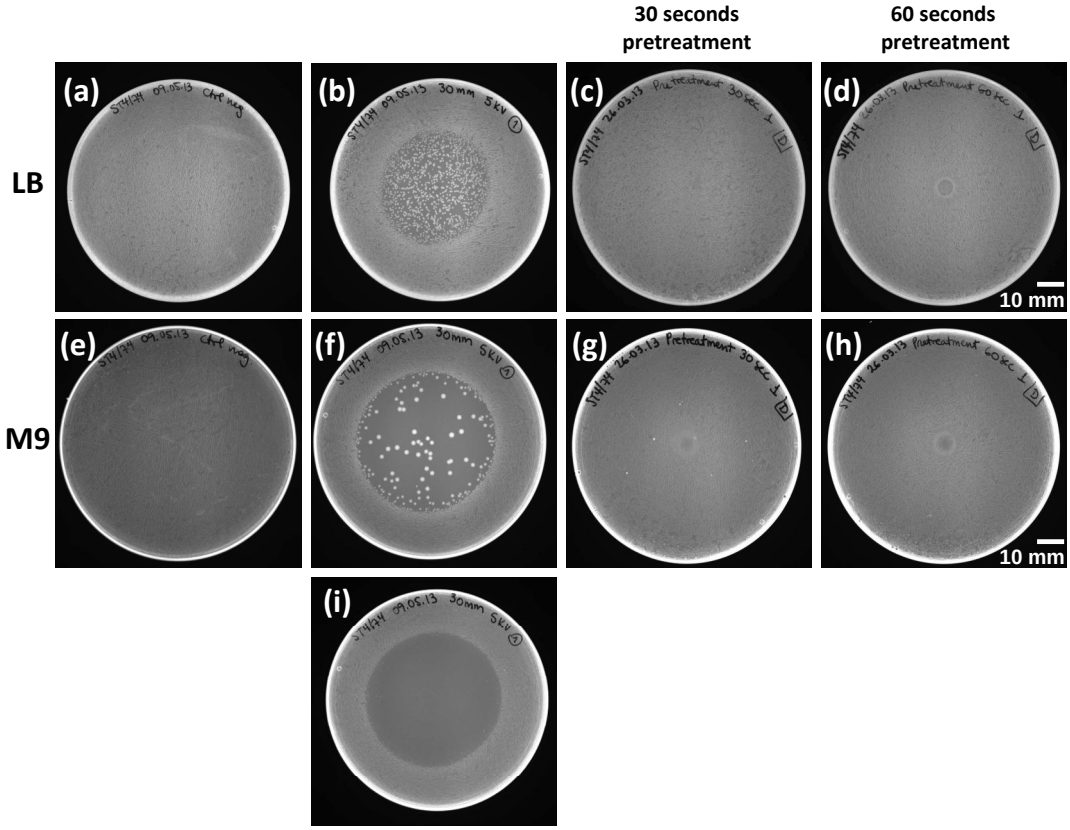

Figure 3.6. ***Effect of media composition in plasma treatments.*** *S.* Typhimurium was spread on **(a-d)** LB and **(e-h)** M9 agar plates. **(a, e)** Untreated samples presented confluent growth. **(b)** LB agar plate treated with the plasma for 30 seconds presented a kill zone with > 200 CFU, whereas **(f)** plasma-treated M9 plates presented a wider, well-defined kill zone with approx. 80 CFU after 48 h incubation. **(c, g)** Plates pre-treated for 30 seconds or **(d, h)** 60 seconds did not present inhibition of growth. **(i)** M9 plate after 24 h incubation. Results are representative of two experimental repeats. Scale bar 10 mm. Pre-treated agar plates **(c, d, g, h)** had a central indentation due to local heating of the agar exposed to the plasma jet, but confluent bacterial growth was observed.

RNOS can react with lipids, proteins, nucleic acids and carbohydrates and do not discriminate between cell components or nutrients in the culture medium. Thus, it is possible that the nutrients in culture media are oxidized during plasma treatment. This reaction could represent a reduction in the amount of RNOS available to interact with bacterial cells and a decrease in the antibacterial activity of plasma. It has been reported that plasma can oxidize and induce structural changes in proteins, amino acids and DNA in solution (51, 186), and the oxidation of proteins can promote the formation of secondary reactive free-radicals (187, 188).

It could be possible that the exposure of nutrients in the culture media to plasma contribute to the formation of toxic secondary reactive species. To determine if the bactericidal effect of plasma was enhanced by the formation of secondary reactive species due to the oxidation of nutrients in the media, LB and M9 plates were pre-treated for 30 and 60 seconds under the same conditions. *S.* Typhimurium was plated immediately after plasma treatment. Although it has been proposed that plasma can induce the formation of toxic compounds as the result of amino acid peroxidation in liquid cultures (189), pre-treatment of LB and M9 agar plates did not affect *Salmonella* growth and plates presented similar growth to untreated plates (**Figure 3.6a,c,d,e,g,h**). The contribution of secondary reactive species formed upon oxidation of nutrients in the media towards bacterial elimination could be limited and it could not observed under these conditions. These results could suggest that the elimination of bacteria in culture media with plasma is related to the direct interaction of plasma species with bacteria.

It is likely that the bactericidal activity of plasma is reduced as a result of the competition for RNOS between nutrients in culture media and bacterial cells during plasma treatment. The effect of external biomolecules during plasma treatment for bacterial elimination was further studied and is described in Chapter 5. LB agar plates were chosen for further experiments as they are routinely used for antimicrobial susceptibility testing (159, 160).

3.3.4 Distance from nozzle to sample

It has been demonstrated that the ability of low temperature plasmas to kill bacteria is affected by variation of distance between the powered electrode and the surface of the bacterial sample (110, 163). Schneider *et al.* described a decrease in the absolute atomic nitrogen density in the effluent of a µAPPJ operated with He and small admixtures of molecular nitrogen with increasing distances from the nozzle (190). Using a similar device, it has been reported that atomic oxygen density declines and O_3 density increases with distance to the nozzle (108, 149). In addition, a decrease in the discharge power was observed with increasing distances between the powered electrode and the sample for a DBD plasma setup, results correlated with the decrease in the antibacterial activity and gas temperature of the plasma (191). Thus, there is evidence that the composition of the plasma varies as it travels away from the nozzle and this affects the bactericidal activity of plasma. However, it is important to consider that although plasma is more effective when the distance from nozzle to sample is reduced, the temperature of

the plasma may be higher at smaller distances from the nozzle (191). Thus, careful measurements of the gas temperature at the contact point with the sample needs to be performed and monitored when optimizing the distance between nozzle and surface of sample for bacterial elimination.

To determine the optimal distance at which samples should be placed for plasma treatment, LB agar plates containing 100 µL $1.6x10^9$ CFU/mL *S.* Typhimurium were placed at 25, 30, 35 and 40 mm distance from the nozzle. Plasma was generated with the AP-DBD plasma jet at 5 kV (peak-to-peak) using the single electrode configuration (Section 3.3.1), 123 kHz, 2 slm He + 0.5 vol % O_2. Ambient humidity was 17 %. Samples were treated for 60 seconds. The temperature of the sample during plasma treatment was measured with a thermocouple placed on an agar plate.

Bacterial elimination in plasma-treated agar plates was inversely proportional to the distance between the powered electrode and the surface of the sample. Plasma-treated plates that were placed at 25 mm from the nozzle, presented more defined zones of inhibition than plates located at 40 mm, as shown in **Figure 3.7a**. None of the treatments tested were able to completely eliminate bacterial growth in the zone of inhibition, but the high bacterial load used in this experiment could explain this. A lower initial inoculum (100 µL $1.6x10^7$ CFU/mL) was also tested, generating more defined zones of inhibition with > 200 CFU (**Figure 3.7b**). There was no visual difference between the zones of inhibition of LB agar plates plasma-treated at 25 and 30 mm from the nozzle. However, the temperature of the plasma at 25 mm from the nozzle (contact point with the sample) was 47 °C after 60 seconds of treatment. This temperature is above the thermal tissue damage threshold (43 °C) (192), a value that has to be considered for the design of plasma treatments with biomedical purposes. Therefore, a treatment 30 mm distance from the nozzle was chosen as plasma was able to eliminate bacteria with similar efficiency at lower temperatures (37 °C).

Results are in agreement with the literature, supporting the effect of the distance to sample on bacterial inactivation (110, 193). For further experiments, samples were placed at 30 mm from the nozzle to prevent interference of the temperature on bacterial elimination.

3.3.5 Composition of the feed gas

Noble gases like helium are relatively easily ionized compared with molecular gases at atmospheric pressure. Helium is one of the preferred gases to generate plasmas at atmospheric pressure because it possesses high heat conductivity and contributes to the generation of plasmas that maintain low temperatures (194). Metastable helium, an electronically excited state, acts as an energy reservoir for Penning ionization (113), which is one of the dominant plasma sustaining mechanisms for the generation of RNOS in the plasma. It has been reported that the addition of small percentages of O_2 to the feed gas of the plasma contributes to the

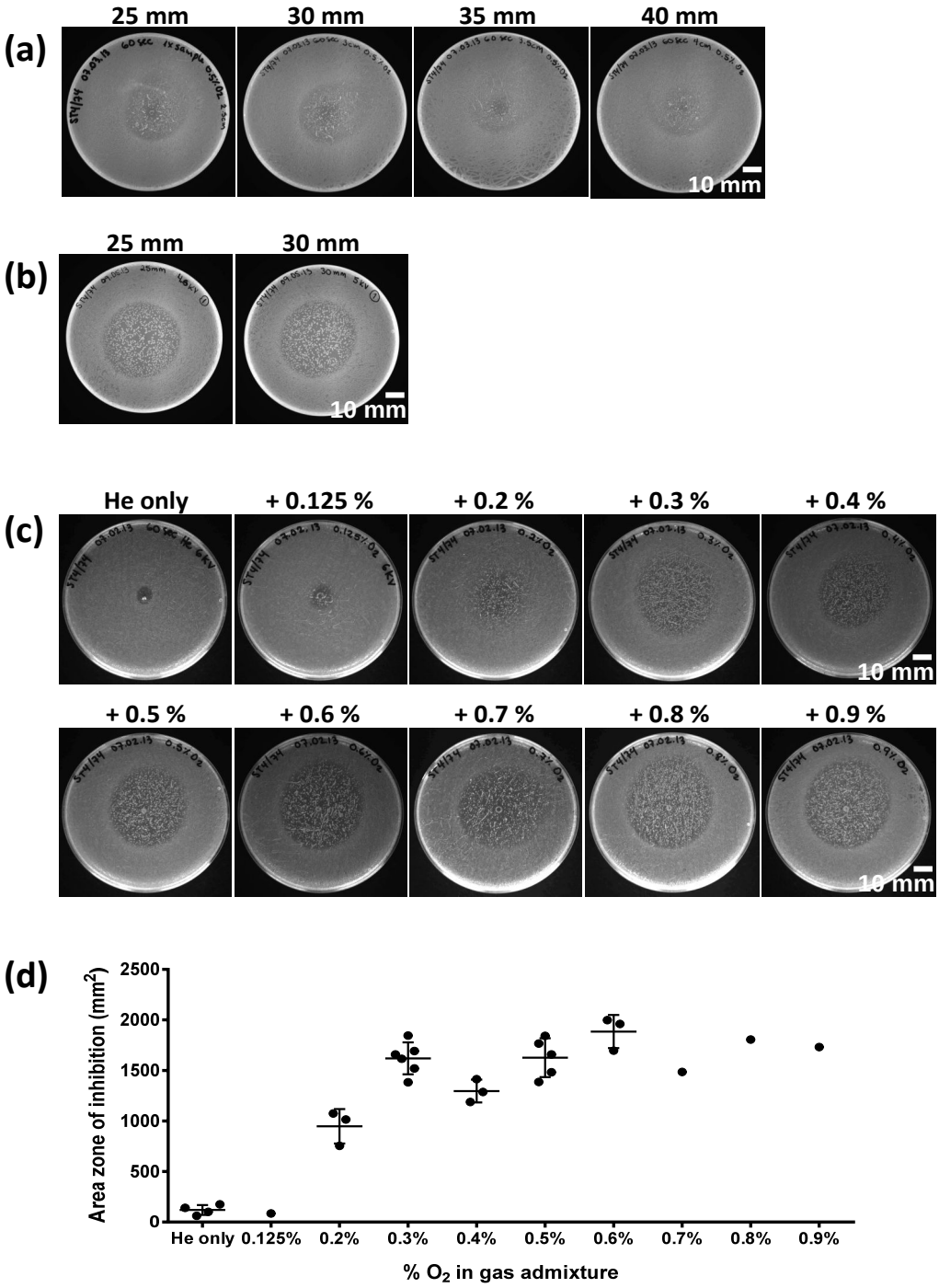

Figure 3.7. ***Optimization of distance from nozzle to sample and composition of feed gas.*** LB plates treated with plasma **(a)** placing samples at different distances from the nozzle (25, 30 35 and 40 mm) using 1.6 x 10^9 CFU/mL as initial inoculum; **(b)** placing samples at different distances from the nozzle (25 and 30 mm) using 1.6 x 10^7 CFU/mL as initial inoculum. **(c)** Effect of variation in the composition of the feed gas (2 slm He + (0 to 0.9) vol % O_2); **(d)** Area of the zone of inhibition as a function of the concentration of O_2 in the feed gas, expressed in mm^2. Each dot represents one plate, bars represent mean values ± S.D. Scale bar 10 mm. Due to technical reasons, it was only possible to test single agar plates for plasma generated with > 0.6 vol % O_2 in gas admixture.

production of O, $O_2(a^1\Delta g)$ and O_3 in the effluent (195). An increase in the concentration of reactive species could potentiate the bactericidal activity of plasmas (108).

To determine the concentration of O_2 in the feed gas required to increase the bactericidal effect of the plasma, different values of vol % O_2 were added to the feed gas. Briefly, 100 µL $1.6x10^{10}$ CFU/mL overnight culture *S.* Typhimurium were spread on LB plates. Plasma treatment was done for 60 seconds. Plasma was generated at 6 kV (peak-to-peak), 123 kHz, 2 slm He + (0 – 0.9) vol % O_2, using the single electrode configuration described in Section 3.3.1. Ambient humidity was 18 %. The distance between the nozzle and the sample was 20 mm. The distance between the nozzle and the sample differ from the value chosen in the previous section for further experiments, thus the temperature of the plasma jet may have played a role in the treatment outcome. It was not possible to ignite the plasma jet with values above 0.9 vol % O_2 under these conditions.

A plasma jet generated only with helium, no oxygen admixture, killed *S.* Typhimurium in a restricted area of approx. 100 mm^2. The killing zone increased with the addition of O_2 to the feed gas. A plateau was reached around 0.5 vol % O_2 and further addition of O_2 to the feed gas did not increase the size of the zone of inhibition (**Figure 3.7c,d**). Complete elimination of bacteria in the zone of inhibition was not obtained for any of the gas admixtures tested here, possibly due to the high concentration of initial inoculum used for this experiment. However, results consistently demonstrate that an increase in the concentration of O_2 in the gas admixture can improve the bactericidal activity of the plasma jet.

The enhancement of the inactivation and bactericidal activity of reactive species generated by the plasma when 0.5 vol % O_2 is added to helium has been previously reported (161, 162, 166). The results obtained here were consistent with the literature (164) and a gas feed containing He + 0.5 vol % O_2 was used for further experiments.

3.3.6 Length of treatment

It has been previously demonstrated that increasing the treatment time can increase the bactericidal activity of plasmas and it depends on the plasma source and the biological and physical conditions used. This correlation has been shown for *E. coli* treated with different plasma sources in solid and liquid environments (13, 109).

To determine the optimal plasma treatment time to kill *S.* Typhimurium with the AP-DBD plasma jet, LB agar plates were treated with the AP-DBD plasma jet for 30, 60, 90 and 120 seconds. Plasma was generated with the AP-DBD plasma jet at 6 kV (peak-to-peak), 123 kHz, 2 slm He + 0.5 vol % O_2, using the double electrode configuration described in Section 3.3.1. Ambient humidity was 34 %. The distance between the nozzle and the sample was 30 mm.

Results demonstrated that the area of the zone of inhibition increased with treatment time (1810 mm^2 for 30 seconds, 2552 mm^2 for 120 seconds) (**Figure 3.8**). The area of the zone of inhibition

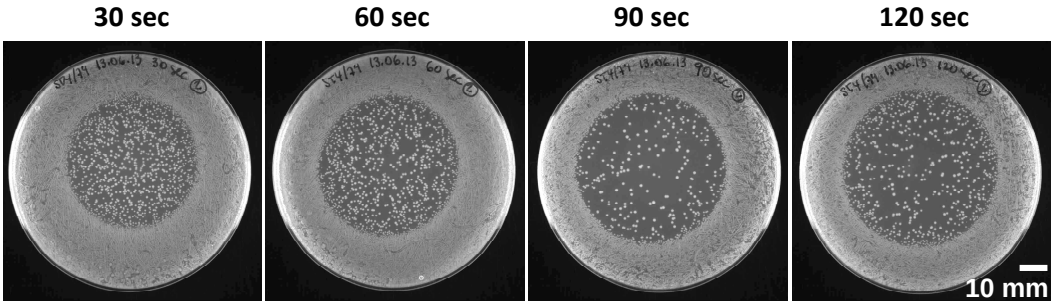

Figure 3.8. ***Optimization of treatment time for*** **S.** ***Typhimurium with the AP-DBD plasma jet.*** Representative agar plates treated with the AP-DBD plasma jet for 30, 60, 90 and 120 seconds (sec). Plasma was generated at 6 kV (peak-to-peak) using the double electrode configuration for DBD (Section 3.3.1), 123 kHz, 2 slm He + 0.5 vol % O_2. The distances between the nozzle and the sample were 30 mm. Results are representative of two experimental repeats. Scale bar 10 mm.

was similar for agar plates treated for 90 and 120 seconds (2290 vs. 2552 mm^2, respectively). In the same way, longer treatments decreased the number of CFU in the zone of inhibition (260 CFU for 120 seconds and > 350 CFU for 30 seconds, respectively).

Thus, a short treatment of 90 seconds was chosen for further experiments considering the possible increase of the sample temperature with longer treatments. In addition, short treatments that can eliminate *S.* Typhimurium could be used to target intracellular bacteria in future applications with a reduced impact on the host cell.

3.3.7 Voltage, frequency and temperature of the plasma

An increase in the voltage of the plasma jet has been related to increasing gas temperatures at the surface of the sample (165). Increasing the voltage can improve the generation of active species in the plasma (108), increase the electron energy (150) and the length of the plume (196). Changes in plasma parameters could all contribute to bacterial elimination. However, the risk of increasing the voltage resides on the possibility of inflicting thermal damage to the sample or host tissue. For biomedical applications of plasma, it is important that the treatment provided does not exceed the thermal tissue damage threshold.

The initial version of the setup operated with a resonant frequency of 123 kHz. Plasma was generated with the AP-DBD plasma jet at this frequency and 5.5 kV (peak-to-peak), using 2 slm He + 0.5 vol % O_2. Samples were treated for 90 seconds at 30 mm distance between the nozzle and the sample.

The macroscopic temperature of the plasma is similar to that of heavy neutrals and ions (in contrast to the high temperature of electrons) (50). The temperature of the plasma can be determined by measuring the rotational temperature of N_2 by optical emission spectroscopy (OES). The results presented below refer to the macroscopic temperature of the gas measured by OES or a thermocouple, as described in Section 2.10.

The results of OES demonstrated that the use of this method is restricted to the visible spectral region of the jet, as it relies on the detection of the second positive system of N_2. The temperature obtained with OES for a plasma generated at 5.5 kV and 21 mm distance from the nozzle was 74 ± 14 °C (**Figure 3.9**). Because the acquisition of the data for these measurements takes place over approximately 5 to 10 minutes (based on the integration time and number of averages used), results could provide a value that might not represent the temperature the sample would actually experience during a treatment of 90 seconds. A temperature more equivalent to the temperature a sample would experience was measured with a thermocouple at 25 mm and 30 mm distance from the nozzle in the axial direction and at 0 and 10 mm distance from the treatment site (d=0 mm) in the radial direction. At this distance, the temperature of the plasma after 30 seconds of exposure was below 40 °C (**Table 3.1**). The working voltage was determined based on the temperature of the plasma jet at the contact point with the sample. The

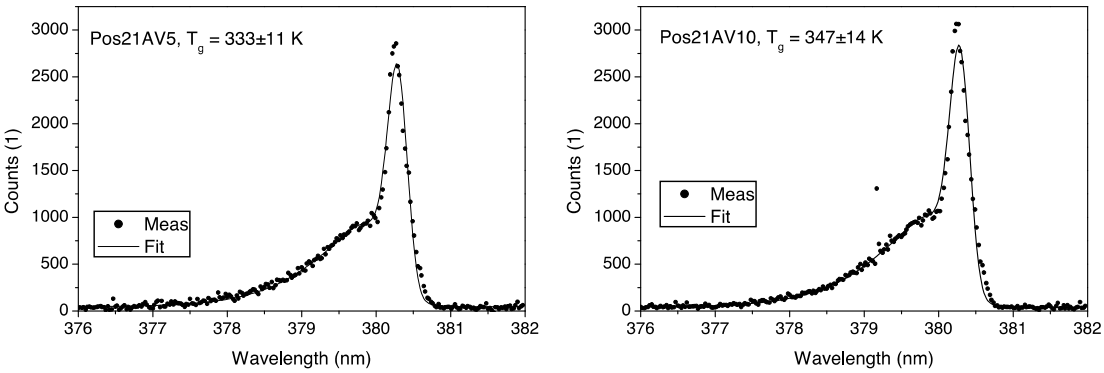

Figure 3.9. ***Measurement of plasma temperature with OES.*** The macroscopic temperature of the plasma was obtained by measuring the second positive system of N_2 around 380 nm. Graphics represent the measurements done at 21mm from the nozzle with ***Left***: 5 averaged readings or ***Right:*** 10 averaged readings. Temperature expressed in degree Kelvin.

	OES	Thermocouple		
	Treatment site (d=0 mm)	**Treatment site (d=0 mm)**		**d=10 mm**
	5.5kV	**5.0kV**	**5.5kV**	**5.0kV**
20 mm	74±14°C	--	--	--
25 mm	--	28°C	50°C	30°C
30 mm	--	27°C	37°C	22°C

Table 3.1. ***Temperature measurement of the plasma at different axial and radial distances from nozzle.*** The temperature of the plasma at the contact point with the sample (d=0 mm) was measured by optical emission spectroscopy (OES) in the visible fraction of the plasma jet and with a thermocouple at further distances in the axial direction. Results show the average of triplicate measurements of the plasma temperature, measured at different distances from the nozzle in the axial direction and in the radial direction. Plasma generated for 30 seconds at 123 kHz. (--) = not measured.

temperature of the plasma jet was measured with a thermocouple as described in Section 2.10.2. The working voltage was set at 5.5 – 6 kV (peak-to-peak) for 90 seconds treatments.

The final version of the setup described in Section 3.2 was modified to operate at lower frequencies to decrease the gas temperature. By reducing the frequency, less individual plasma breakdowns occur. As the gas is exposed to less plasma, the gas temperature remains low. The AP-DBD plasma jet was tested using a 470 pF coupled capacitor. Plasma was generated at 10 kV (peak-to-peak), 30 kHz, 2 slm He + 0.5 vol % O_2, using the double electrode configuration described in Section 3.3.1. Ambient humidity was 36 %. The distance between the nozzle and the sample was 30 mm. Plasma treatment was applied for 120 seconds. The gas temperature at 30 mm from the nozzle (contact point with the sample) was 39°C after 120 seconds, measured with a thermocouple. This reduction represents a decrease of from 63 °C to 37 – 43 °C from the gas temperature obtained when operating at 123 kHz (**Figure 3.10**). Capacitors with higher capacitances were also tested. However, this idea was discarded as further reduction of the resonant frequency did not allow plasma ignition.

To improve the stability of the signal, the ignition of the plasma jet was controlled remotely using a code written by Dr. Roddy Vann. The advantage of controlling the plasma jet from a laptop is the adjustment of the oscillating resonant frequency in real-time to deliver a constant voltage to the system. After finding the resonant frequency at the desired voltage, the code automatically adjusts the oscillating resonant frequency to deliver a stable signal to the system. The operating voltage was increased from 10 kV to 12 kV (peak-to-peak) and the gas temperature was measured with a thermocouple at 30 mm from the nozzle for 120 seconds. With the addition of the 470 pF capacitor to the system, the gas temperature at 30 mm from the nozzle was reduced to 36.5°C. The addition of a fan to cool down the capacitor improved the stability of the signal and allowed a further reduction in the gas temperature from 36.5 °C to 29.5 °C.

The working voltage for the final version of the setup was set at 12 kV (peak-to-peak) for the AP-DBD plasma jet with a 470 pF capacitor coupled to the secondary coil of the transformer and the corresponding cooling system for the capacitor. These conditions were used for further experiments, unless otherwise stated.

3.3.8 Current measurement

The parameters of the external electrical circuit and the presence of the dielectric barriers can influence the voltage and current of DBD plasma jets (197). The AP-DBD plasma jet described here was generated inside a plasma box for a set of experiments. To perform experiments to measure the ozone density in the gas phase, the plasma jet was installed to fit in an open box covered with a protective mesh (shown in **Figure 3.3**). For this purpose, the electric circuit was rearranged to fit the conditions of the new box and therefore the electrical parameters were altered.

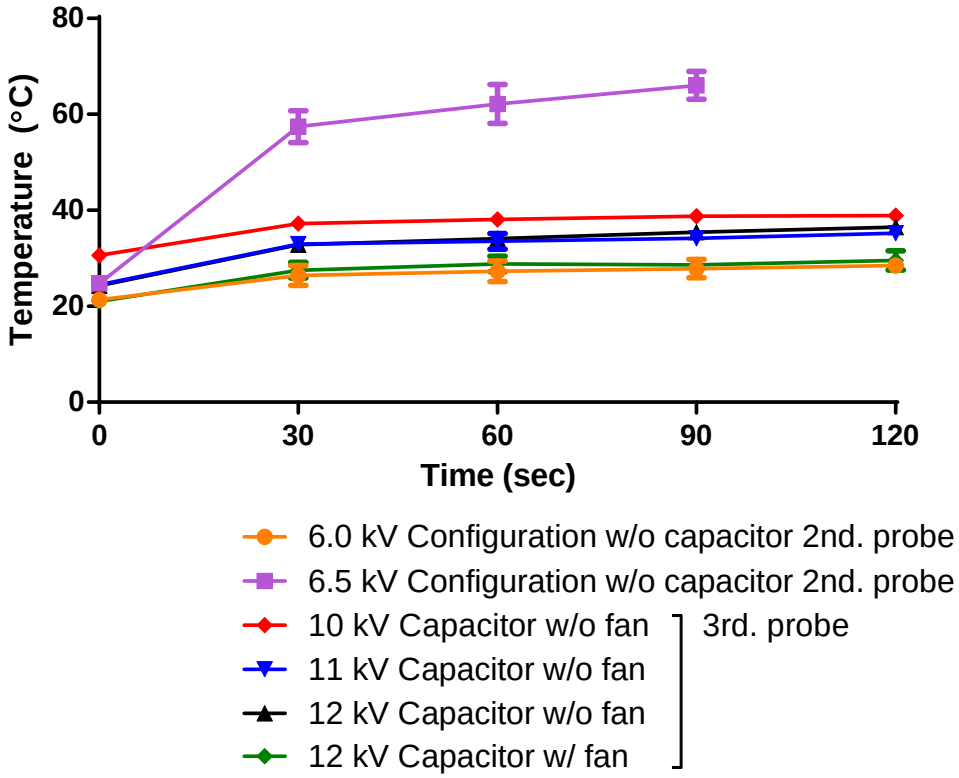

Figure 3.10. ***Reduction of the temperature of the plasma.*** Temperature of the plasma at 30 mm from the nozzle with a plasma generated with or without the addition of 470 pF capacitor and cooling fan to the system. Each dot corresponds to the mean value of triplicate measurements, vertical bars represent S.D. w/o = without. Data are representative of three experimental repeats. Time expressed in seconds (sec).

The current in the plasma setup in both electrical arrangements was monitored when possible. The current in the AP-DBD setup was measured using a current transformer (CM-100-L, IPC), with 50 Ohms sensitivity into the external and an equivalence of 1 Amp per Volt. The current probe was connected to a high-resolution oscilloscope (LeCroy WaveRunner 204Mxi-A). For the measurements, the cable connecting the grounded electrode (current-carrying conductor) to the aluminium base of the plasma box was passed through the current probe opening.

Plasma was generated at 12 kV (peak-to-peak), 30 kHz, using the double electrode configuration described in Section 3.3.1. Ambient humidity was 21 %. The distances between the nozzle and the sample were 30 mm. Plasma was generated with 2 slm He + 0.5 vol % O_2. The current and voltage were recorded over one cycle with the plasma ignition (generation of plasma) and extinction (no feed gas, no ionization).

Results demonstrated that varying the electrical circuit arrangement of the plasma setup affected the current in the system. **Figure 3.11** shows both the sinusoidal driving voltage and the current through the discharge. The plasma generated inside the plastic plasma box presented an amplitude 12 times higher than the plasma generated in the open box covered with a protective mesh (12 mAmp and 1 mAmp, respectively). In OFF mode, the non-plasma waveforms are near sinusoidal (**Figure 3.11c,d**). The signal presents multiple plasma breakdowns when the plasma ignited (**Figure 3.11a,b**). The negative jet current pulse during the voltage rise time could represent the main breakdown that give rise to the streamer propagating from the tube; the positive current pulses could represent a more homogeneous plasma, as the current is maintained for longer (169).

The presence of a stage to support the dielectric and the position of the powered electrode in relation to this stage modified the capacitance of the system. This could have led to a change of current and electric field, as reported before (50).

It has been demonstrated that variations in the current has a direct impact in the electric field and plasma streamer velocity (198), which can alter the chemical reactions in the plasma and consequent formation of RNOS. For this reason, the same electrical arrangement was maintained between experiments that needed to be compared. For experiments described in Chapter 4, plasma was generated in the plastic box, whereas experiments described in Chapter 5 the plasma was generated in the open box covered with a protective mesh.

3.3.9 Delivery of plasma species with different dielectric barrier discharge arrangements

Plasma rich in reactive oxygen and nitrogen species is generated during the ionization process in the surroundings of the powered electrode. Classic DBD plasmas use a straight glass tube connected to a powered and a grounded electrode, as in condition **(b)** in Section 3.3.1. In this configuration, the plasma leaves the dielectric and the plasma-generated electrons, metastables and UV radiation can freely react with molecules present in ambient air. Other configurations of

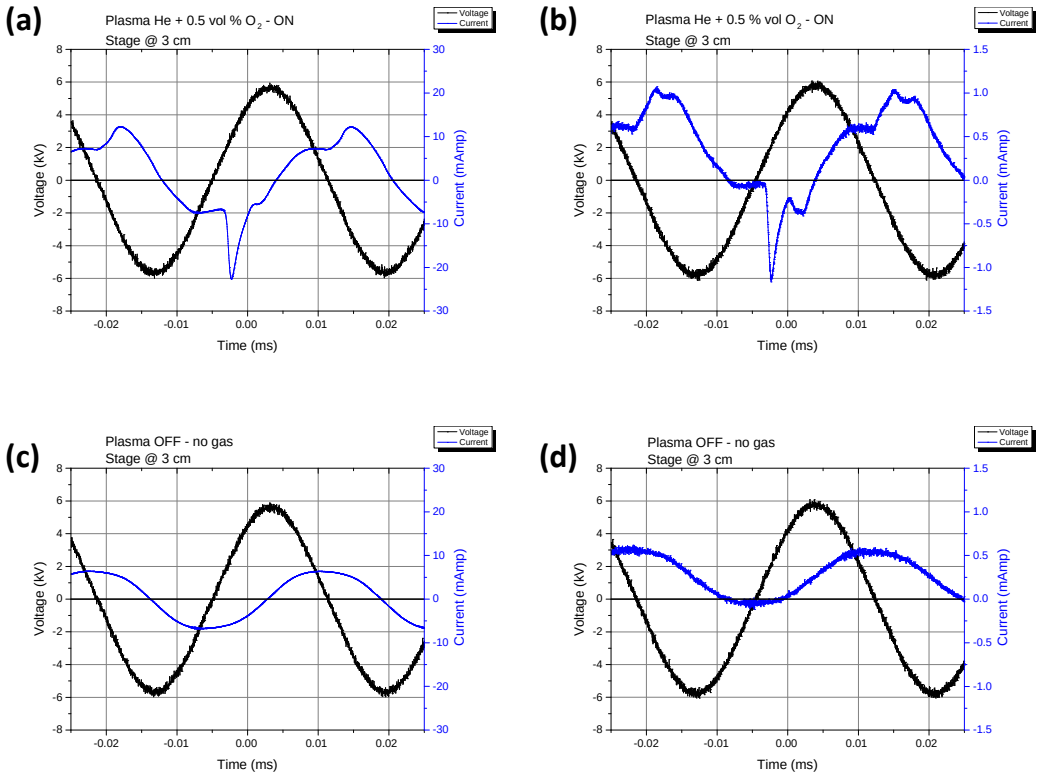

Figure 3.11. ***Measurement of the current and voltage of the AP-DBD plasma jet.*** The current and voltage were recorded over one cycle with **(a,b)** ignition of the plasma and **(c,d)** OFF (no feed gas, no ionization). **(a,c)** Data collected for the AP-DBD plasma jet installed in the plastic plasma box. **(b,d)** Data collected for the AP-DBD plasma jet installed in the open box with a protective mesh shown in **Figure 3.3**.

the dielectric or the nozzle downstream the electrodes to deliver only UV radiation, reactive species or both to the sample have been used. In the case of a modified radio-frequency-driven μAPPJ (X jet), the plasma generated between the two electrodes passes through a glass channel connected downstream from the electrodes (199). The plasma effluent is diverted to one side, whereas the UV radiation continue traveling in straight line towards the sample (200). A similar modification to the nozzle allows the delivery of the plasma effluent and not UV radiation to the sample (104). Zhang *et al.* suggest the use of an inverted funnel-shaped nozzle to concentrate plasma RNOS to improve the delivery of reactive species produced by a DBD plasma needle (201). However, the formation of RNOS in the plasma effluent depends on many factors as mentioned in the previous sections, including the composition of the feed gas and the interaction of plasma species with oxygen, nitrogen and water molecules in ambient air. Thus, limiting the interaction of UV radiation with the plasma in the downstream region or limiting the access of oxygen, nitrogen and water molecules to the plasma effluent could impact on the outcome of plasma treatment of bacteria.

To determine the effect of the dielectric arrangement for the treatment of bacteria with the AP-DBD plasma jet, three conditions were tested (see **Figure 3.12**):

a) Straight glass tube (1 mm inner diameter, 6 mm outer diameter)

b) Glass tube with a curvature of 60° on the downstream region under the powered electrode (1 mm inner diameter, 6 mm outer diameter, prepared by a glassblower)

c) Glass funnel (rim diameter 35 mm, VWR) fused to the nozzle of the glass tube

The direct delivery of plasma RNOS in combination with UV radiation (condition **(a)**) can effectively inhibit bacterial growth, as shown before (combined treatment). The curvature on the downstream region of the dielectric glass tube in condition **(b)** aimed to dissociate the bactericidal effect of UV radiation from the effect of plasma-generated RNOS. As light travels in straight line, the dielectric glass tube with a curvature of 60° at the downstream region prevents the delivery of UV radiation, but allows the delivery of RNOS to the sample (particles-only treatment). No visible light was observed outside the nozzle for this condition. Condition **(c)** was developed to restrict the interaction of plasma with ambient air, concentrate and control the delivery of RNOS to the sample. For this condition, the funnel was placed 2 mm above the agar plate and ambient air was removed from the funnel by flushing the feed gas for 2 minutes prior to plasma treatment.

Plasma was generated with the AP-DBD plasma jet at 123 kHz, 2 slm He + 0.5 vol % O_2, using the double-electrode configuration described in Section 3.3.1. Ambient humidity was 20 %. The distances between the nozzle and the sample were 30 mm. Samples were treated for 90 seconds. For conditions **(a)** and **(b)**, plasma was generated at 6 kV (peak-to-peak) and for condition **(c)** at 5 kV (peak-to-peak). LB agar plates containing *S.* Typhimurium were placed under the funnel

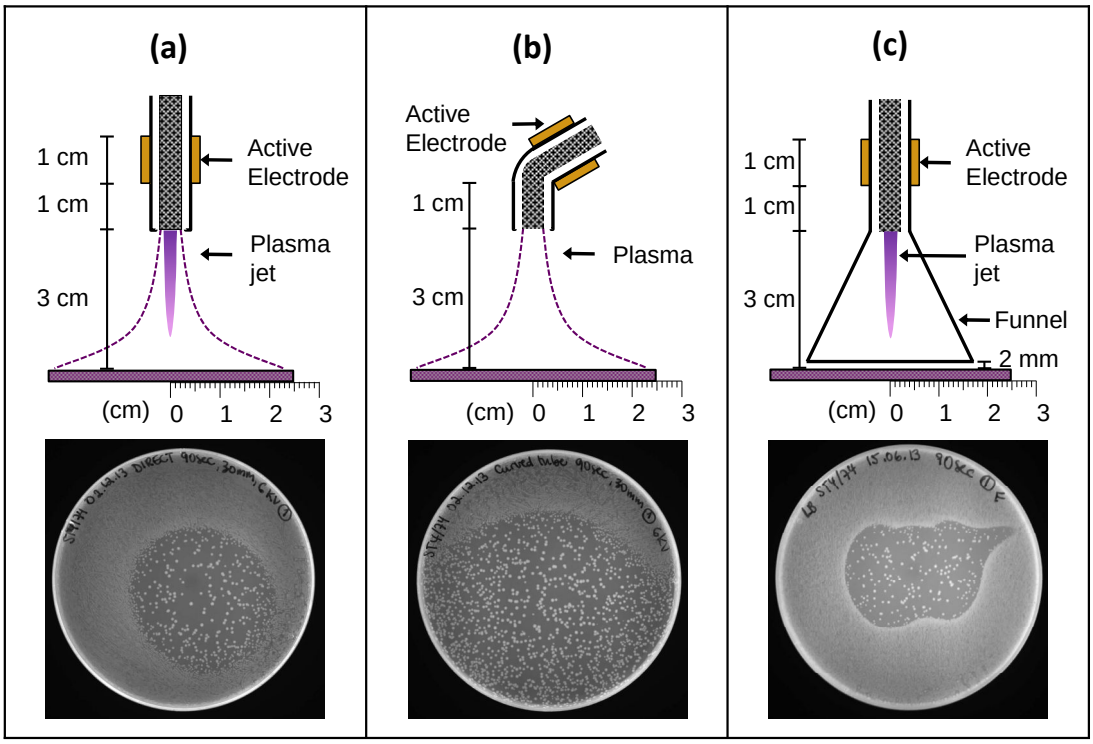

Figure 3.12. ***Comparison of different dielectric arrangements for the AP-DBD plasma jet.*** Representative agar plates treated with plasma generated **(a)** in the straight dielectric glass tube; **(b)** with a glass tube with a curvature of 60° on the downstream region; **(c)** with a glass funnel fused to the nozzle. Experiments done with the double-electrode configuration described in Section 3.3.1.

with 2 mm distance between the rim and the plate to allow the evacuation of the plasma, with a total distance of 30 mm from the nozzle.

LB plates treated with condition **(a)** presented a zone of inhibition of 1806 mm^2 (**Figure 3.12a**). Samples treated with condition **(b)** presented an increased zone of inhibition (2210 mm^2), possibly because the dielectric tube was not perpendicular to the sample (**Figure 3.12b**). This could have promoted the diffusion of plasma towards one side of the plate that increased the size of the zone of inhibition. Alternatively, this effect could be caused by the deformation of the inner compartment of the dielectric glass tube during its preparation. Agar plates treated with condition **(b)** presented 1.8-fold increase in the number of CFU found in the zone of inhibition when compared to condition **(a)**. Because the transmittance of UV radiation was reduced by the curvature in the downstream region of the dielectric in configuration **(b)** and UV radiation contributes to the formation of reactive species (199, 200), it is likely that the composition of the plasma differs between configurations **(a)** and **(b)**. Nevertheless, both configurations showed antibacterial activity that can be attributed to the effect of RNOS and charged species delivered to the sample.

Plates treated with condition **(c)** presented a zone of inhibition of approximately 1350 mm^2 with defined borders and irregular shapes between replicates (**Figure 3.12c**). The number of colonies was reduced in agar plates treated with this condition, but it was not possible to anticipate the shape of the zone of inhibition. Complete elimination of bacteria in the zone of inhibition was not achieved with any of the dielectric arrangements tested here. Agar plates treated presented zones of inhibition with irregular shapes with homogeneous distribution of CFU. This could be explained by a possible recirculation of plasma inside the funnel that could not be fully evacuated through the 2 mm gap. The lack of small CFU growing at the edges of the zone of inhibition (as observed for plates treated with the other two configurations) could be explained by the exit of the plasma through the 2 mm gap. The incoming gas forces the plasma-generated reactive species to exit the funnel through a small gap, exposing the bacteria located at the rim region to higher concentrations of reactive species than those obtained when not using the funnel. The formation of reactive species inside the funnel relied on the composition of the feed gas. Since only oxygen was added to the feed gas to generate the plasma, these results could support the importance of reactive oxygen species for the elimination of bacteria with plasma treatments.

The use of a straight glass tube as a dielectric present the advantage of delivering a combined treatment of RNOS, charged species and UV radiation. The use of a glass tube with a curvature downstream the powered electrode was not considered further as UV radiation contributes to the formation of RNOS in the effluent and therefore should be considered. The contribution of UV radiation in the induction of DNA damage and bacterial elimination was further studied as described in Chapter 4. Finally, the use of a funnel fused to the downstream region of the

dielectric to deliver plasma demonstrated to provide homogeneous clearance in the zone of inhibition, but generated irreproducible zones of inhibition between replicates. Based on these results, a straight glass tube was used for all further experiments.

3.4 DISCUSSION

One of the most interesting applications of LTPs that operate below the thermal damage threshold is their use in biomedicine. The multiple reactive species, charged particles and UV photons produced in the plasma are effective biocidal agents. In this regard, the field of biomedicine could benefit from the development of new therapies that employ LTPs that can be administered topically to treat target pathogens from a distance.

The efficacy of LTP treatments depends on a range of physical parameters, as described here. These parameters can be modulated to generate antimicrobial treatments. In the same way, the characteristics of the target sample such as cell type, concentration and composition of the surrounding environment can contribute to the outcome of plasma treatments. In this chapter, the various physical and biological parameters that determine the antimicrobial effectiveness against bacteria were investigated and the conditions to eliminate *S.* Typhimurium from solid and semi-solid surfaces were determined.

The AP-DBD plasma source designed and built in-house was optimized for the treatment of *S.* Typhimurium in solid and semi-solid surfaces. Results demonstrated that an increase in the initial inoculum exposed to plasma decreased the efficacy of the treatment (Section 3.3.2) and is in agreement with the literature (135, 173). In the plasma treatment of bacteria on solid surfaces, the decrease in the efficacy of plasma treatment with increasing concentration of bacteria could be explained by the formation of multiple layer of bacterial cells that provide protection from oxidative stress to those located at the bottom. Although multiple layers of cells could aid the survival of bacteria after plasma treatment, the highest concentration of bacteria used here (1.6×10^8 CFU/plate) covered less than 15 % of the surface area of the plate. Thus, the formation of multiple layers of cells is unlikely. The decrease in the efficacy of the treatment could correspond to other factors such as bacterial aggregation, as proposed by Fernandez *et al.* (135) and the physiological state of the culture or accumulation of metabolic by-products for antibiotic treatments as proposed by Udekwu *et al.* (202). For the plasma treatments applied here, late logarithmic phase bacteria cultures were diluted 100-fold in fresh media and vortexed prior to plating to avoid aggregation. Experiments were restricted to the use of bacterial cultures in late logarithmic phase, reducing the variability in the response to treatment due to variations in the growth phase. As samples were diluted prior to plating, it would be expected that the amount of molecules secreted by bacteria that could contribute to cell aggregation present in the sample would be minimal.

In addition to bacterial concentration, it was observed that the composition of the surrounding environment where bacteria were exposed to plasma had an effect on the treatment outcome. The results presented here demonstrated an increased bactericidal activity of the AP-DBD plasma jet on *S.* Typhimurium treated in minimal medium M9 plates than *S.* Typhimurium treated in LB plates. Nosenko *et al.* reported that *E. coli* in PBS suspensions required shorter plasma treatments to achieve 100% elimination than *E. coli* in LB suspension when treated with a plasma torch (203). This could be due to the presence of proteins, lipoproteins, carbohydrates and vitamins in the culture media that oxidize in the same way as bacterial components. These reactions between plasma species and nutrients could lead to a reduction in the amount of RNOS available to interact with bacterial cells and therefore, a decrease in the antibacterial activity of plasma. In addition, the metabolic state of bacterial cells growing in the presence of abundant or minimal nutrients might also play a role in the response to oxidative damage induced by plasma, as discussed in Section 3.3.3.

Although it has been proposed that toxic compounds could be formed in liquid cultures as a consequence of amino acid peroxidation (189), the pre-treatment of LB and M9 agar plates did not affect the growth of *Salmonella* and plates presented similar growth to untreated plates. Variations in the composition of the culture media does not only affect the amount of RNOS interacting with cell components, but also affects the metabolism of bacteria. Variations in the concentration of carbon, nitrogen and phosphate sources in the culture media can induce changes in the physiology (redirecting their metabolism to cope with nutritional stress) and morphology (delay of cell division and septation) of bacterial cells (204). Thus, considering that bacteria recover from plasma treatment in the presence of nutrients in a nutrient-rich (LB) or minimal media (M9), the metabolic differences between both cultures could contribute to the effect observed here. Further analysis of the composition of the reactive species in plasma-treated media and their effect on the bactericidal action of plasma treatments is described in Chapter 5.

One of the advantages of LTPs resides in the ability to modulate the several physical parameters to develop specific treatments, specifically their operation at low temperatures for their application in biomedicine. Because the plasma setup was built in-house, it was possible to test different dielectric barrier and electrode configurations, modify the electrical arrangement of the electronic components and replace parts when needed. In the same way, the composition of the feed gas, voltage, frequency and distance to sample were investigated for the elimination of *S.* Typhimurium. However, the operation of LTPs can be affected by small variations in any of these parameters and such changes can have a direct impact on other parameters for the generation of plasma. For example, the results obtained here showed that the gas temperature of the plasma was affected by the voltage and quickly reduced as the plasma dissipated away from the nozzle in the axial and radial direction (described in Section 3.3.7). A decrease in the distance between the powered electrode and the sample also increased the temperature of the

plasma. These results are in agreement with the literature, as previous reports identified an increase in the temperature of the plasma with increasing values of discharge power, voltage and decrease in the distance between the powered electrode (191).

The results presented in this chapter reflect a number of all the possible parameters that can be modified to improve the bactericidal action of the AP-DBD plasma jet (for example, voltage, distance to sample, gas composition, and bacterial load, among others). These parameters were chosen based on their impact on the antibacterial properties of the plasma and on the resources available at the time for this study.

Different DBD plasma sources have been tested in the past for the elimination of bacteria, but the use of different conditions for the generation of plasma poses a challenge for data interpretation and reproducibility of scientific results with different plasma sources. Thus, it is important to acknowledge that these parameters are not independent from each other. Therefore, the participation of UV radiation generated by the AP-DBD plasma jet might not directly compromise the integrity of bacterial samples, but contributes to the chemical reactions to generate more reactive nitrogen and oxygen species that contribute towards bacterial elimination. These reactions are boosted by the interaction of ambient air and water molecules with the plasma plume that propagates in the axial direction outside the nozzle. Thus, although the conditions for the generation of plasma with different devices described in the literature are variable, it is possible to identify trends in the bactericidal activity of LTPs. These trends contribute towards the understanding of the mechanisms of action of plasma for bacterial elimination and the development of effective therapies. Altogether, these results demonstrated the importance of the optimization and characterization of plasma parameters for the development of antibacterial treatments and the development of common and standardized guidelines to assess the bactericidal properties of LTPs.

The effect of plasma treatment with the AP-DBD plasma jet on bacterial DNA at the single cell level and the role of the nutrients present during treatment in the surroundings of the sample are described in Chapter 4 and Chapter 5.

For the treatment of *S.* Typhimurium with the AP-DBD plasma jet in the following chapters, the plasma was generated using the double electrode configuration (Section 3.3.1, configuration (b)), 2 slm He + 0.5 vol % O2. Samples were treated for 90 seconds. The voltage and frequency used for experiments is described in each section, corresponding to either the operation of the plasma prior to (5.5 – 6 kV and 123 kHz) or after the replacement of the oscilloscope probe and addition of the capacitor (12 kV and 30 kHz).

4 DNA DAMAGE AND THE SPATIAL DISTRIBUTION OF RNOS IN THE PLASMA EFFLUENT

4.1 INTRODUCTION

Low temperature plasma treatments have been demonstrated to induce DNA damage in bacteria via oxidative stress (13, 44). The RNOS produced by LTPs can induce two types of damage to the DNA: damage to the sugar-phosphate backbone of the DNA that result in detrimental DNA breaks and oxidation of nucleotide bases that may not result in DNA breaks but can cause mutations if left unrepaired (205). The methods most commonly used to determine DNA damage in plasma-treated samples (purified DNA or bacteria at the population level) are gel electrophoresis to identify single- and double-strand DNA breaks (44, 51), enzyme-linked immunosorbent assay (ELISA) to detect 8-hydroxydeoxyguanosine (oxidized nucleotide base) (13), polymerase chain reaction to identify DNA damage that blocks polymerase progression (71) and RAMAN spectroscopy to identify DNA modifications at the molecular level (104).

The current approaches used to investigate the induction of DNA damage in plasma-treated samples present four limitations: **a)** Only few reports have studied the effect of LTP treatments on DNA in the context of living bacterial cells (13, 206). Most of the studies are done on purified DNA that is not representative of the modifications to the DNA in the context of living bacterial cells. **b)** The study of plasma-treated bacteria in liquids does not represent the direct effect of the RNOS delivered by the plasma, since the chemical reactions in the plasma-liquid interaction modifies the composition of the RNOS delivered to the sample (207). **c)** The study at the population level that assesses the averaged response could mask the effect caused by LTP treatments on individual cells. Because heterogeneity is an inherent characteristic of bacterial populations, it is expected that individual cells will respond in different ways to oxidative stress. These existing approaches provide little or no information about the effect of LTP treatments at the single cell level. **d)** Studies on the gas phase of LTPs have demonstrated that the RNOS produced in plasmas are spatially distributed in the effluent (112, 122). However, there is a lack of information about the effect of the spatial distribution of RNOS in the plasma effluent and the damage induced to DNA in bacterial cells. To date, there are only two reports on the effect of the spatial distribution of RNOS in the plasma on purified DNA (121, 208).

In this chapter, the effect of LTP treatments on the integrity of bacterial DNA at the single cell level is described. This chapter has two aims: firstly, to identify the factors that determine the level of DNA damage in plasma-treated bacterial cells at the single cell level and secondly, to assess whether the level of DNA damage inflicted in bacterial cells is affected by the spatial distribution of RNOS in the plasma effluent. For this purpose, the DNA damage diffusion assay (DDD Assay, Section 2.6) was adapted for the quantitative study of DNA damage in bacteria in dry surfaces at the single cell level after plasma treatment and complemented with the

measurement of the 2-dimensional distribution of O_3 in the plasma effluent. Two plasma sources were used here to compare their effect on bacterial DNA: the AP-DBD plasma jet (delivering charged and neutral species; see Chapter 3) and µAPPJ (delivering mostly neutral species; see Section 2.14).

4.2 LTP INDUCED DNA DAMAGE IN *S.* TYPHIMURIUM IN A RADIAL-DEPENDENT MANNER

To assess the role of the radial distribution of RNOS in LTPs, DNA damage induced by plasma treatment was studied with the DDD Assay at the single cell level as function of distance to the treatment site. With this method, DNA breaks obtained as a consequence of damage to the DNA sugar-phosphate backbone can be detected. Bacteria treated with the AP-DBD plasma jet or the µAPPJ were immobilized and lysed *in situ* and the DNA fragments diffused through the agarose. The distance the DNA fragments diffuse through the agarose is dependent on size, and thus a readout of the presence of DNA double-strand breaks as a result of plasma-induced damage. The radius of diffusion of DNA originating from single cells was quantified, with higher diffusion distance relating to smaller fragments, as described in Section 2.6. The ratio of the radius of plasma-treated cells to the mean radius of untreated cells was calculated and is expressed as Log_e (see Section 2.6.5).

The AP-DBD plasma jet induced statistically significant DNA damage in *S.* Typhimurium located directly under the plasma jet ($P<0.0001$) and up to 10 mm from the centre of the treatment site (**Figure 4.1a**). When compared to the zone of inhibition produced in LB agar plates, 10 mm distance from the treatment site corresponded to 40% of the zone of inhibition. No double-strand breaks in bacterial DNA were detectable beyond this point. Controls that were treated with the feed gas only (2 slm He + 0.5 vol % O_2) at 5 mm from the nozzle with the AP-DBD plasma jet setup did not present detectable DNA damage ($P>0.05$) (**Figure 4.2a left**). Exposure of LB agar plates to the feed gas only did not inhibit bacterial growth either (**Figure 4.2a right**). *S.* Typhimurium treated with the µAPPJ presented detectable DNA damage only in cells located directly under the plasma ($P<0.01$) (**Figure 4.1b**). DNA damage was not detected in other regions beyond this point ($P>0.05$). The µAPPJ inhibited bacterial growth in LB agar plates in an area with 15 mm radius, beyond the point where DNA damage was observed in plasma-treated agarose-coated slides. A positive control of DNA damage obtained with recombinant DNase I confirmed that the fragments observed around the core were indeed DNA fragments originated by the breakage of DNA (**Figure 4.2b**). In addition, DNA damage induced by recombinant DNase I was independent of the location of bacterial cells in the agarose-coated slide.

Altogether, these results demonstrate that the levels of DNA damage induced in *S.* Typhimurium by the AP-DBD plasma jet and the µAPPJ were inversely correlated to the distance to the treatment site, and thus independent of the LTP source used.

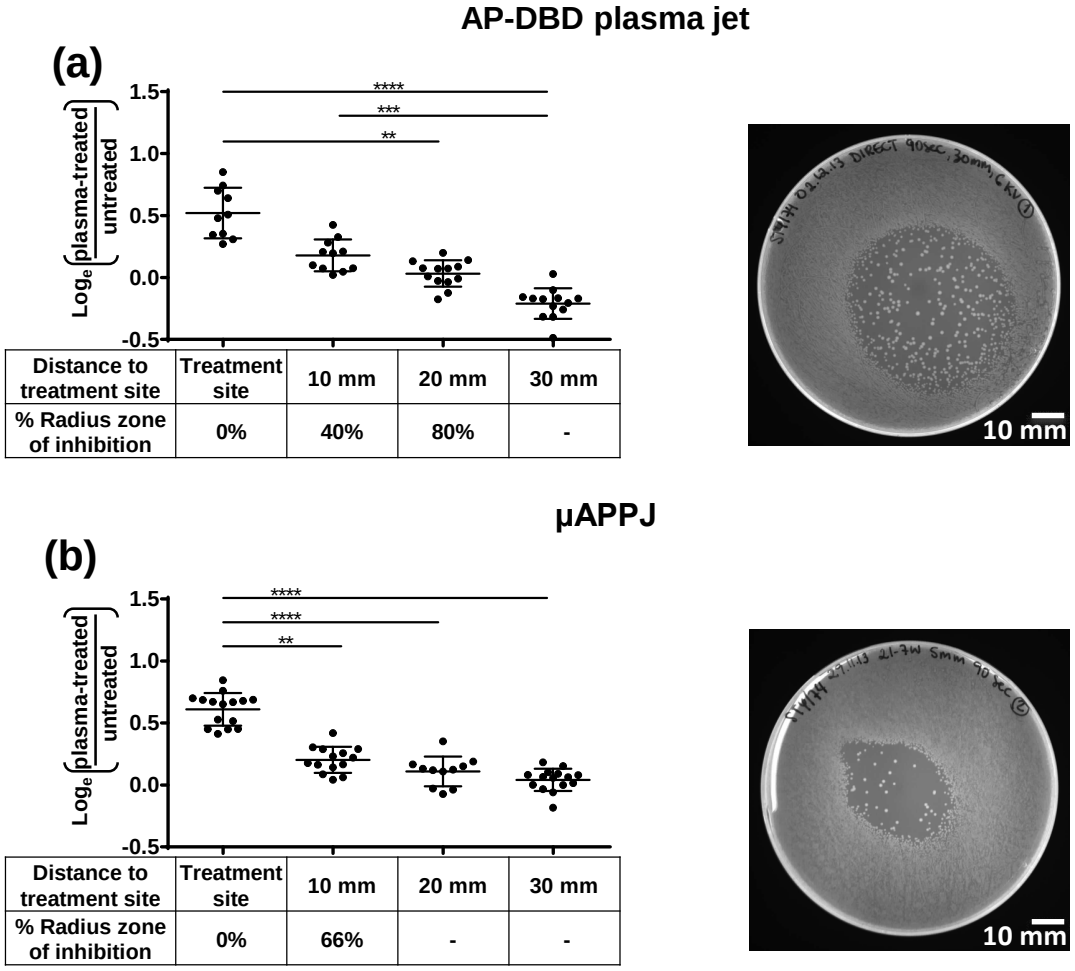

Figure 4.1. ***Plasma induced DNA damage in* S. *Typhimurium in a radially-dependent manner.*** DNA damage at the single cell level was assessed with the DDD Assay. *S.* Typhimurium treated with **(a)** the AP-DBD plasma jet, **(b)** the µAPPJ. ***Left:*** Plots show the level of DNA damage on plasma-treated bacteria at the single cell level as a function of their position to the treatment site (d=0 mm). Each dot represents a single cell; horizontal bars: mean values ± S.D.; ****: P<0.0001; ***: P<0.001; **: P<0.01. Ratio expressed as Log_e (radius plasma-treated cells/mean radius untreated cells). ***Right:*** Representative agar plates for *S.* Typhimurium treated with the AP-DBD plasma jet or µAPPJ. Scale bar 10 mm.

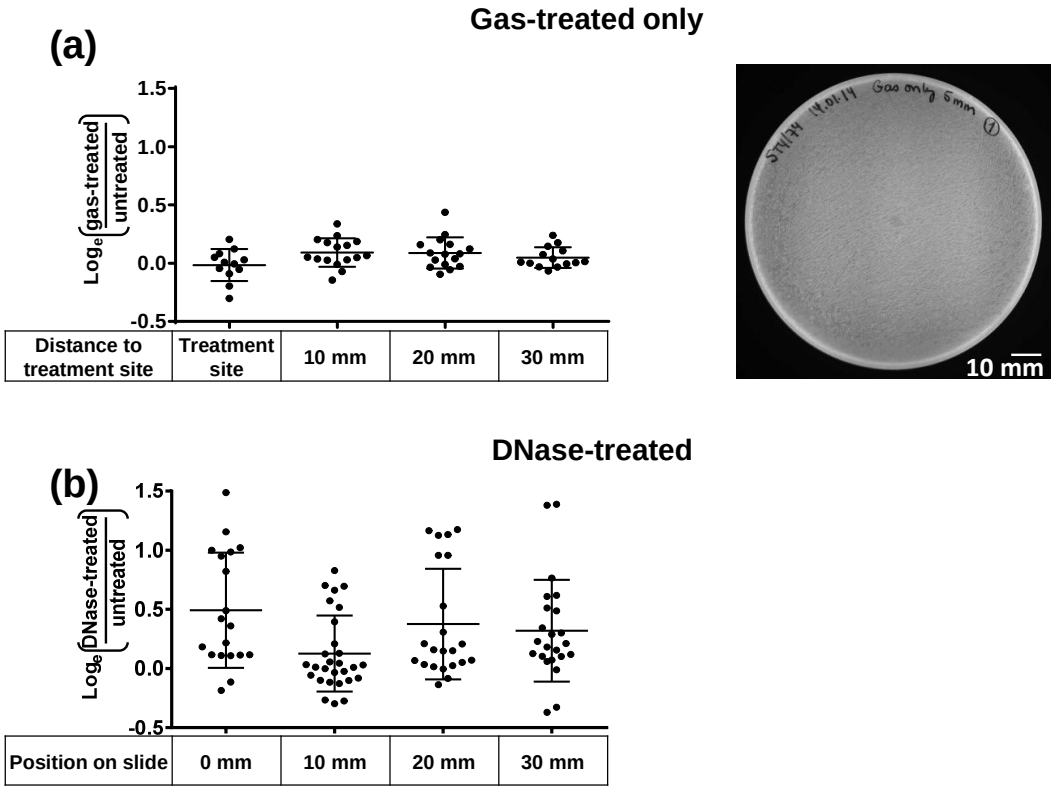

Figure 4.2. ***Controls of DNA damage in gas-treated or DNase-treated samples. Left:*** Plots show the level of DNA damage on **(a)** samples treated with the feed gas only (He + 0.5 vol % O_2) at 5 mm from the nozzle with the AP-DBD setup and **(b)** DNase-treated samples. Each dot represents a single cell; horizontal bars: mean values ± S.D.; P>0.05. Ratio expressed as Log_e (radius plasma-treated cells/mean radius untreated cells). ***Right:*** Corresponding LB agar plate for *S.* Typhimurium exposed to 2 slm gas only at 5 mm distance from nozzle. Scale bar 10 mm.

4.3 PLASMA INDUCED DAMAGE TO NUCLEOTIDE BASES OF CELLS LOCATED UNDER THE PLASMA JET

Cells exposed to oxidative stress can present damage to the DNA sugar-phosphate backbone that result in DNA breaks, as shown here with the DDD Assay (Section 4.2). However, the nucleotide bases can also be affected, leading to the formation of mutagenic base by-products that can be dangerous to cells. Thus, the DDD Assay was modified to identify damage to nucleotide bases induced by the AP-DBD plasma jet. The enzyme formamidopyrimidine-DNA glycosylase (FPG) can detect and remove mutagenic base by-products that occur as a result of exposure of purines to reactive oxygen species, creating a nick in the DNA strand. FPG was added to the protocol for the DDD Assay to identify damaged purines as a consequence of plasma treatment (See Section 2.6.6). If plasma treatment induced the oxidation of purines in addition to the damage of the sugar-phosphate backbone, it would be expected to observe an increase in the level of DNA fragmentation observed in single cells and therefore, an increase in the radius of the halo formed by DNA fragments around the core. The protocol described in **Figure 2.1** including step 3a was followed to identify oxidized purines and damage to the sugar-phosphate backbone of bacterial DNA. The regular DDD Assay was performed in parallel to identify only damage to sugar-phosphate backbone of bacterial DNA. Experiments were done using the final version of the AP-DBD plasma setup housed in the metallic box as described in Chapter 3.

Using the regular DDD Assay for the identification of damage to the sugar-phosphate backbone, it was observed that plasma treatment induced DNA damage in bacterial cells located only at the treatment site ($P<0.05$; **Figure 4.3a**). In this experiment, no DNA damage was observed in cells located at 10 mm distance from the treatment site in the radial direction, as described in Section 4.2. Plasma-treated samples processed with the modified DDD Assay for the identification of oxidized purines and damage to the sugar-phosphate backbone presented high levels of DNA damage in cells located at the treatment site and therefore it was not possible to measure the radius of diffusion of DNA fragments in the samples (**Figure 4.3b**). No DNA fragmentation was detected in samples located at 10 mm, 20 mm or 30 mm from the treatment site.

These results suggest that oxidation of purines and DNA breaks occur in bacterial cells directly located at the treatment site as no increase in the level of DNA fragmentation due to oxidized purines was detected in cells a distance of 10 mm away from this point. Thus, mutations in bacterial DNA as a result of oxidative damage to purines might appear in bacterial cells located at the treatment site that survive to LTP treatment. In contrast, it is less likely that cells located at positions away from the treatment site (where the digestion with FPG enzyme did not produced detectable DNA fragmentation) could develop mutations as a consequence of LTP-induced purines oxidation.

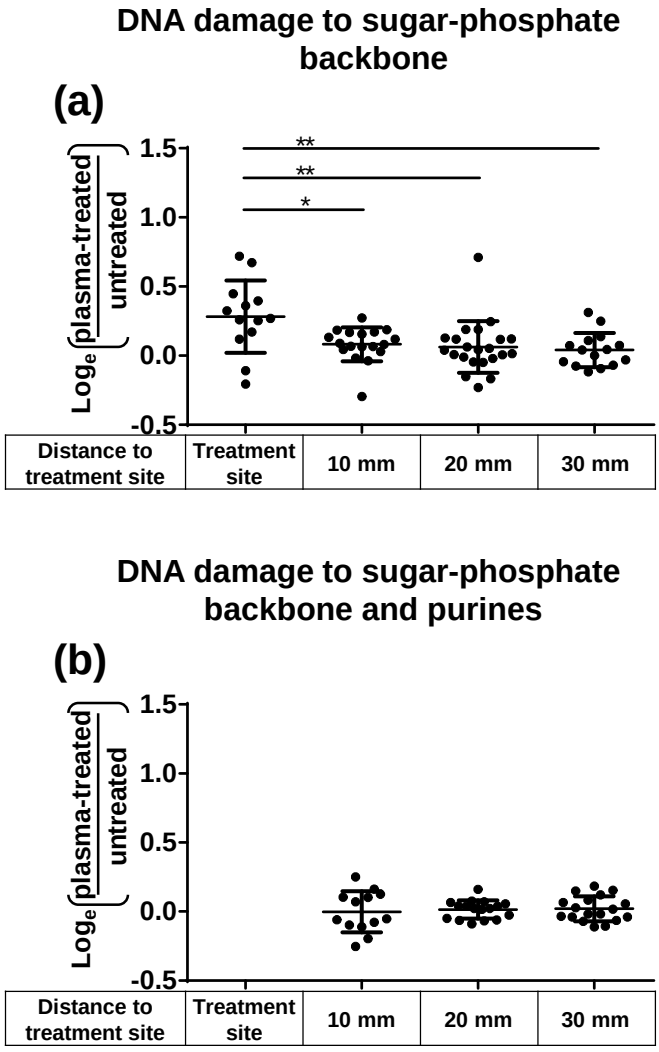

Figure 4.3. ***Damage to purines in DNA was only detectable in cells that also present damage to sugar-phosphate backbone.*** Plots show the level of DNA damage on plasma-treated samples to detect **(a)** single- and double-strand DNA breaks due to damage to the sugar-phosphate backbone and **(b)** single- and double-strand DNA breaks due to damage to purines and sugar-phosphate backbone. DNA damage could not be measured in samples located at the treatment site due to extreme fragmentation. Each dot represents a single cell; horizontal bars: mean values ± S.D.; **: $P<0.01$; *: $P<0.05$. Ratio expressed as Log_e (radius plasma-treated cells/mean radius untreated cells).

4.4 LONGER TREATMENTS WITH LOW PERCENTAGES OF O_2 IN THE GAS ADMIXTURE GENERATED HIGHER LEVELS OF DNA DAMAGE

To assess the role of the gas composition and length of treatment on DNA damage induced by the plasma, *S.* Typhimurium was treated with the AP-DBD plasma jet varying the percentages of O_2 in the gas admixture and the treatment time. Plasma was generated with the AP-DBD plasma jet at 5.5 kV (peak-to-peak), 123 kHz, 2 slm He only, He + 0.3 % vol O_2 and He + 0.5 vol % O_2, using the single electrode configuration (Section 3.3.1). The distance between the nozzle and the sample was 25 mm. Samples were treated for 30, 60 or 120 seconds. DNA damage was assessed in bacterial cells located at the treatment site (0 mm) and at 10, 20 and 30 mm from this point as described in **Figure 2.2**.

In agreement with the results shown in Section 4.2, an inverse correlation between the level of DNA damage and the radial distance to the treatment site was observed, with the highest DNA damage found in bacteria located directly at the treatment site (0 mm). This was observed in all samples treated with the plasma generated with different concentrations of O_2 in the feed gas (**Figure 4.4**). Statistically significant differences were found in the level of DNA damage between cells located at different distances to the plasma jet ($P<0.0001$). Cells located at 30 mm from the treatment site presented compact DNA loops around the core and no detectable fragmentation, similar to the untreated controls.

Samples showed an inverse correlation between the concentration of O_2 in the feed gas and the level of DNA damage inflicted in bacteria located a distance of up to 20 mm from the plasma jet. Thus, plasma generated with He + 0.5 vol % O_2 induced DNA damage in cells located up to 10 mm from the treatment site, whereas samples exposed to plasma generated with He + 0.3 vol % O_2 presented detectable DNA damage in cells located up to 20 mm from the treatment site (120 seconds treatment; $P<0.0001$; **Figure 4.5b,c bottom**). For plasma generated with He only, an increase in the $\log_e$ radius for cells located at 20 mm from the treatment site was observed, but no statistically significant difference was found (120 seconds treatment; $P>0.05$; **Figure 4.5a bottom**). Values for cells located at 30 mm from the treatment site were comparable to results obtained for untreated samples or bacterial cells exposed to the feed gas only (He only) for 30 and 60 seconds (**Figure 4.6**). Exposure of bacterial cells to the feed gas for 120 seconds affected the integrity of bacterial DNA, as an increase in the radius of diffusion of DNA was observed ($P<0.05$).

As expected, an increase in the length of treatment with the AP-DBD plasma jet generated with any of the feed gas compositions increased the DNA damage induced in bacterial cells (**Figure 4.5**). Longer plasma treatments evidenced the variation in the level of DNA damage obtained in bacterial cells located at different distances from the treatment site.

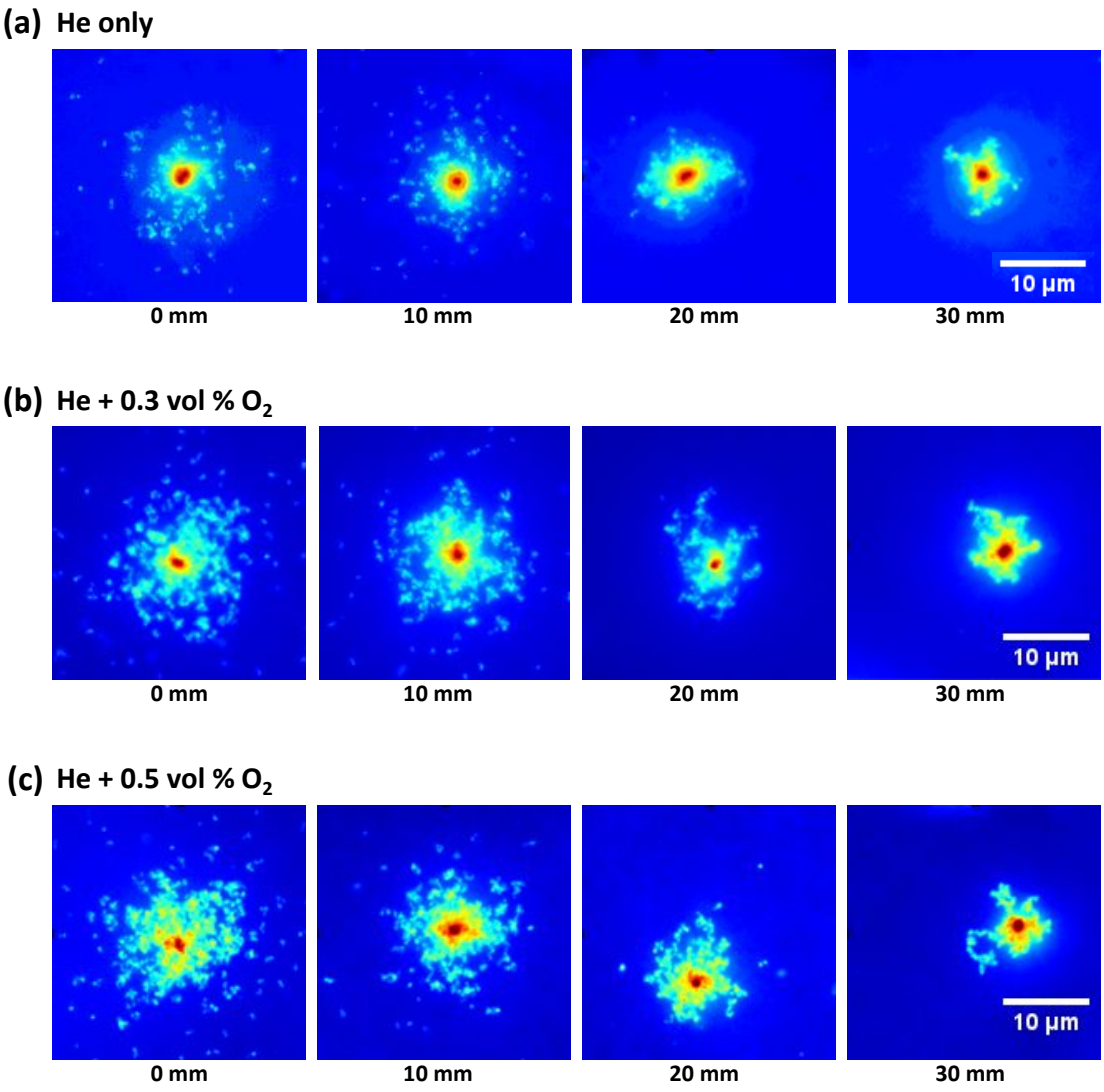

Figure 4.4. ***Effect of composition of the feed gas on DNA integrity of plasma-treated bacterial cells at the single cell level.*** Representative images of DNA damage observed in single cells at the treatment site (0 mm) and at 10 mm, 20 mm and 30 mm from it. *S.* Typhimurium was treated for 120 seconds with the AP-DBD plasma jet, generated with the single electrode configuration and 2 slm **(a)** He only, **(b)** He + 0.3 vol % O_2 and **(c)** He + 0.5 vol % O_2. DNA damage was assessed with the DDD Assay. False colour images of DNA corresponding to single cells are presented.

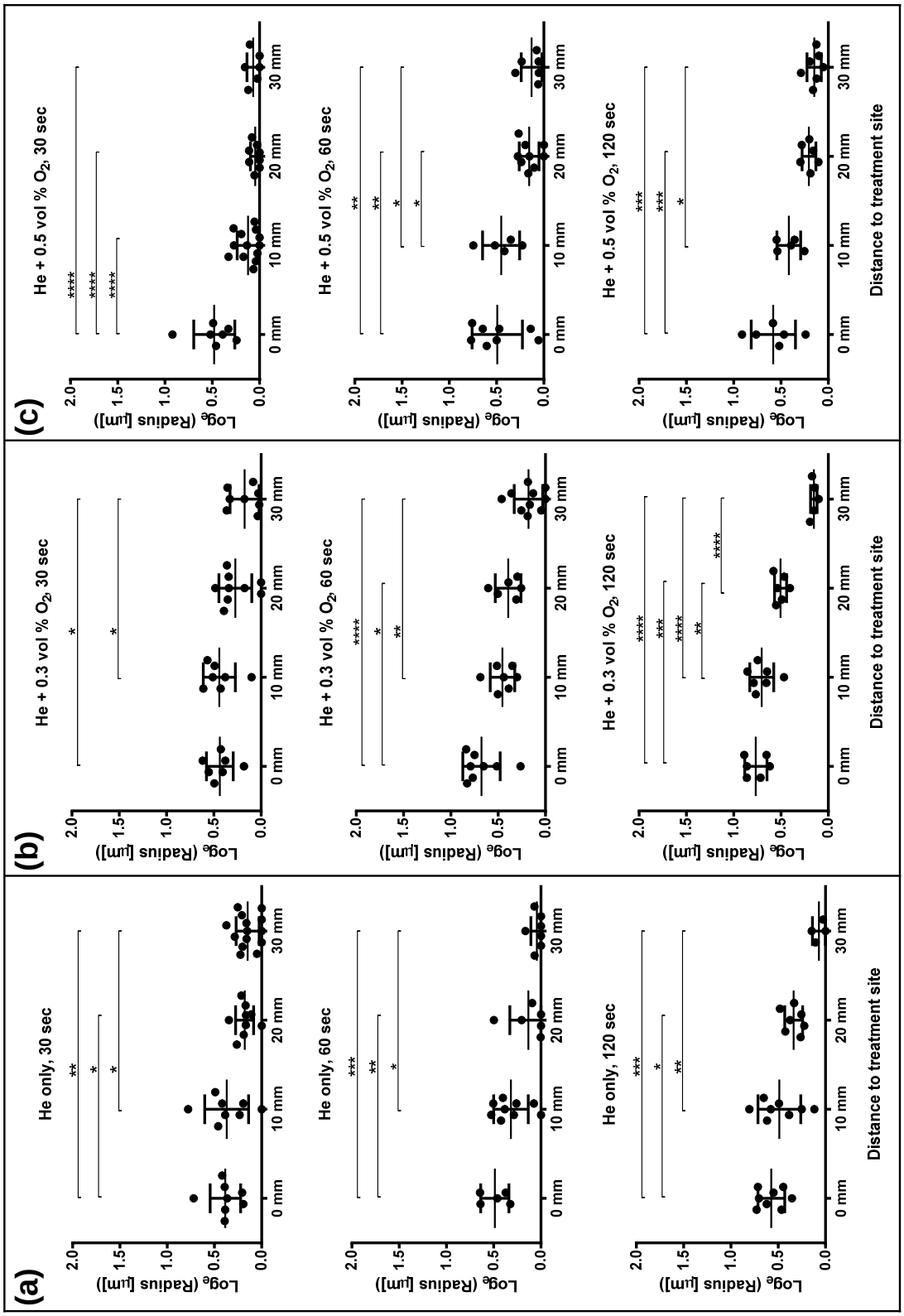

Figure 4.5. (Caption overleaf.)

Figure 4.5. ***Effect of composition of feed gas and length of treatment on DNA damage in S. Typhimurium.*** DNA damage at the single cell level was assessed with the DDD Assay. Samples were treated with the AP-DBD plasma jet generated with the single electrode configuration and 2 slm **(a)** He only, **(b)** He + 0.3 vol % O_2 and **(c)** He + 0.5 vol % O_2. Three lengths of treatment were tested for each condition (30, 60 and 120 seconds). Each dot represents a single cell; horizontal bars: mean values ± S.D.; Radii values expressed as $\log_e$. ****: P<0.0001; ***: P<0.001; **: P<0.01; *: P<0.05.

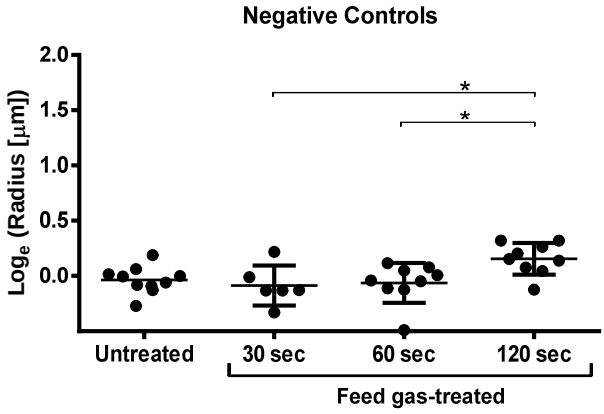

Figure 4.6. ***Controls of DNA damage in untreated and gas-treated*** **S.** ***Typhimurium.*** DNA damage at the single cell level was assessed with the DDD Assay. DNA damage was assessed in untreated and gas-treated samples (He only). Each dot represents a single cell; horizontal bars: mean values ± S.D.; Radii (μm) values expressed as $\log_e$.*: P<0.05.

4.5 PLASMA-GENERATED UV RADIATION DID NOT SOLELY CONTRIBUTE TO DNA DAMAGE DETECTED IN BACTERIAL CELLS

UV photons produced in LTPs can propagate through the helium feed gas used to generate the plasma without being absorbed, as UV photons are absorbed by oxygen and ozone molecules. It is well known that UV radiation can kill bacteria by breaking molecular bonds within DNA, producing thymine dimers that can lead to cell death. UV radiation has been used for decades to disinfect surfaces and air (209). In the range 320 - 400 nm, UV photons can induce DNA damage indirectly by promoting the formation of reactive oxygen species, whereas UV in the range 10 – 320 nm can directly induce DNA lesions, particularly pyrimidine dimers (210, 211). To determine if the AP-DBD plasma jet generated UV radiation and if so, to measure its contribution to the bactericidal effect and DNA damage, three approaches were taken. In the first place, UV radiation emitted by the AP-DBD plasma jet was measured with a shortwave sensor. In the second place, samples were placed in a sealed chamber to allow exposure to UV radiation generated by the AP-DBD plasma jet and the µAPPJ, but not to plasma-generated RNOS or charged species. Lastly, plasma generated with the AP-DBD plasma jet using a dielectric glass tube with a curvature of 60° on the downstream region under the powered electrode (described in Section 3.3.9; **Figure 3.12**) was used to treat samples with plasma-generated RNOS without direct exposure to UV radiation. Using these approaches, DNA damage and inhibition of growth in *S.* Typhimurium were assessed.

4.5.1 UV radiation in the range 220 – 280 nm was not detected in the AP-DBD plasma jet

As mentioned above, UV radiation can directly and indirectly affect the DNA integrity. Therefore, it is necessary to assess if the AP-DBD plasma jet can emit UV photons that contribute to the induction of DNA damage. UV radiation emitted by the AP-DBD plasma jet was measured with a shortwave meter (range 220 – 290 nm; maximum sensitivity at 254 nm, minimum detection limit 20 µW/cm²) shielded by a tungsten mesh, as described in Section 2.11. No UV radiation was detected by the sensor after 30 and 60 seconds of exposure at 10 mm, 20 mm and 30 mm distance from the nozzle.

4.5.2 UV radiation induced low levels of DNA damage and did not inhibit bacterial growth

A chamber with a MgF_2 window installed on the top compartment was used to expose samples (bacteria in agar plates or agarose-coated slides) to the UV radiation emitted by the AP-DBD plasma jet and the µAPPJ, but not to RNOS or charged species (MgF_2 transmittance $\geq$ 55% at 121 nm; Section 2.12). UV radiation with wavelengths below 180 nm in the range of vacuum UV are readily absorbed in air by oxygen molecules (174), and thus does not contribute to the observed effects under these conditions.

The induction of DNA damage and inhibition of growth in *S.* Typhimurium were assessed in samples treated with plasma-generated UV radiation for 90 seconds, the same length of treatment used to assess the effect of direct treatment with LTP. To compensate for the limited transmittance of the MgF_2 window, a longer exposure to UV photons generated by the µAPPJ plasma jet was also carried out for 180 seconds. For both plasma sources, exposure to only the UV radiation generated for 90 or 180 seconds was insufficient to cause a zone of inhibition on agar plates (**Figure 4.7, right**). Furthermore, there was no statistically significant difference in samples treated for 90 seconds with either LTP source and therefore LTP treatments did not induce significant DNA fragmentation in bacterial cells ($P>0.05$, **Figure 4.7a,b**). Bacterial cells exposed to the µAPPJ for 180 seconds presented low levels of DNA fragmentation in cells located at the treatment site ($P<0.05$; **Figure 4.7c**). However, this level was not significantly higher than the levels observed at the same site for a 90 second exposure to UV only generated by either plasma, and still was significantly lower than for the level obtained in samples exposed to all components of the plasma for only 90 seconds ($P<0.0001$; **Figure 4.1**).

It can be concluded that direct interaction of LTP-generated UV photons with DNA of living bacterial cells is not a significant contributor to the overall amount of DNA fragmentation observed. Plasma-generated RNOS could be the main factor that leads to DNA damage in LTP-treated bacteria. These results are in agreement with the literature (199, 200). UV radiation could participate in the generation of reactive species in the plasma, and exert an indirect contribution to bacterial elimination. Thus, a synergistic activity of UV photons and RNOS delivered to bacterial cells was considered.

4.5.3 Particle-only treatment induced similar DNA damage to combined plasma treatment

The AP-DBD plasma jet uses a straight glass tube to generate and deliver the plasma to directly expose samples to UV radiation, RNOS and charged species (combined treatment). In this way, plasma components act synergistically on target cells. To assess the effect of plasma treatment on DNA in bacterial cells independently of direct exposure to plasma-generated UV radiation, a dielectric glass tube with a curvature of 60° at the downstream region was used as described in Section 3.3.9 (**Figure 3.12a,b**). This configuration blocks the propagation of UV radiation and visible light emitted by the plasma outside the tube, but allows the interaction between UV radiation and plasma species upstream the curvature. With this configuration, the treatment is composed of RNOS and charged species only (particles-only treatment).

The DDD Assay was used to study the effects of combined treatment or particles-only treatment on the integrity of DNA in bacterial cells. These experiments shown that both treatments induced DNA damage in bacterial cells located up to 10 mm from the treatment site (combined treatment: $P <0.0001$; particle-only treatment: $P <0.01$; **Figure 4.8a,b**), as presented above. Cells located at 20 mm and 30 mm distance from the treatment site did not present detectable

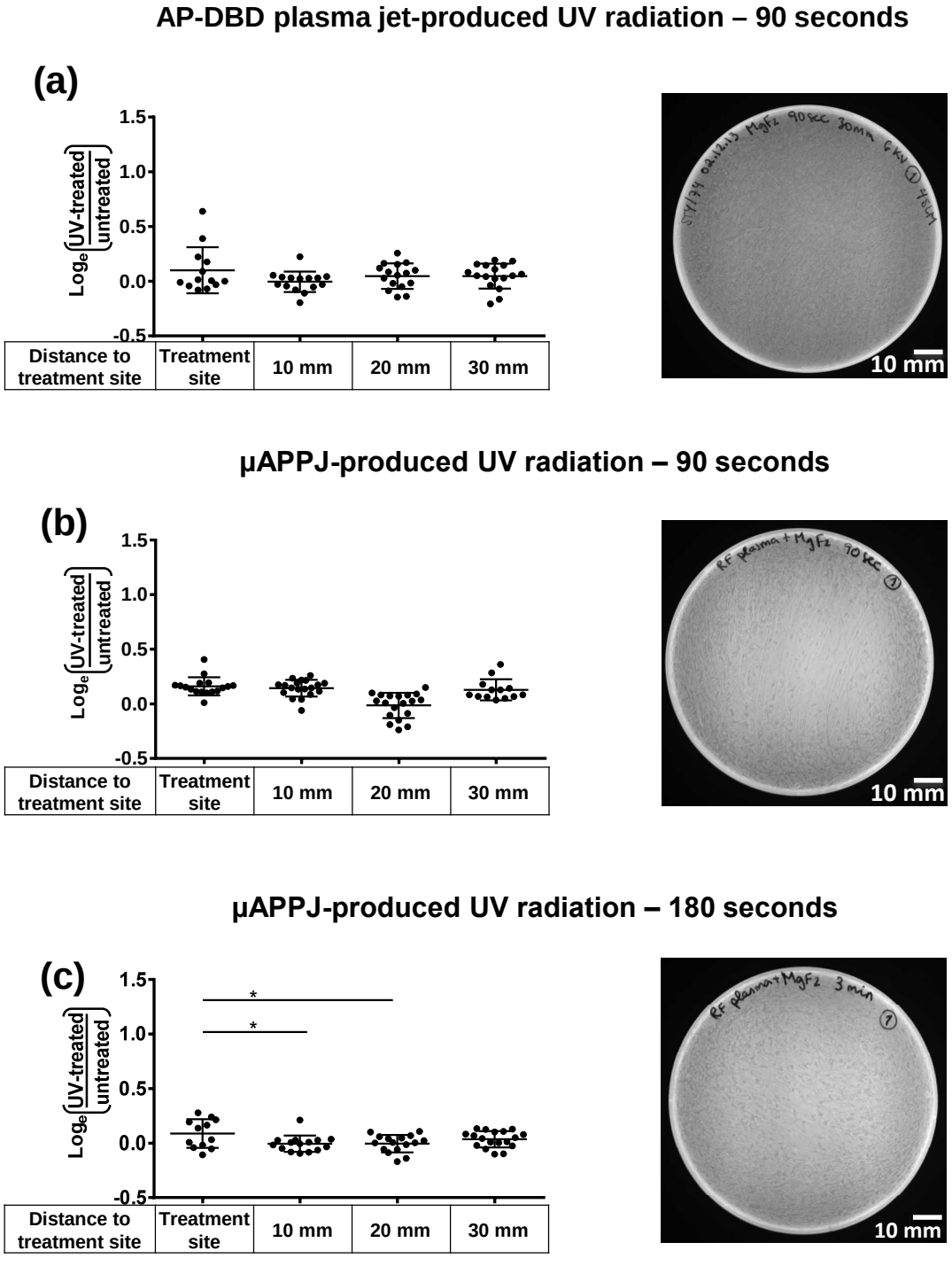

Figure 4.7. ***UV radiation induced low levels of DNA damage and did not inhibit bacterial growth.*** The effect of plasma-generated UV radiation above 121 nm on bacterial DNA at the single cell level was examined using the DDD Assay. ***Left:*** Radii of dispersion of bacterial DNA for S. Typhimurium treated with **(a)** the AP-DBD for 90 seconds, **(b)** μAPPJ for 90 seconds and **(c)** μAPPJ for 180 seconds. Each dot represents a single cell; horizontal bars: mean values ± S.D. *: $P<0.05$. Ratio expressed as Log_e (radius treated cells/mean radius untreated cells). ***Right:*** Representative agar plates for *S.* Typhimurium treated with UV radiation generated by the AP-DBD plasma jet or μAPPJ. Scale bar 10 mm.

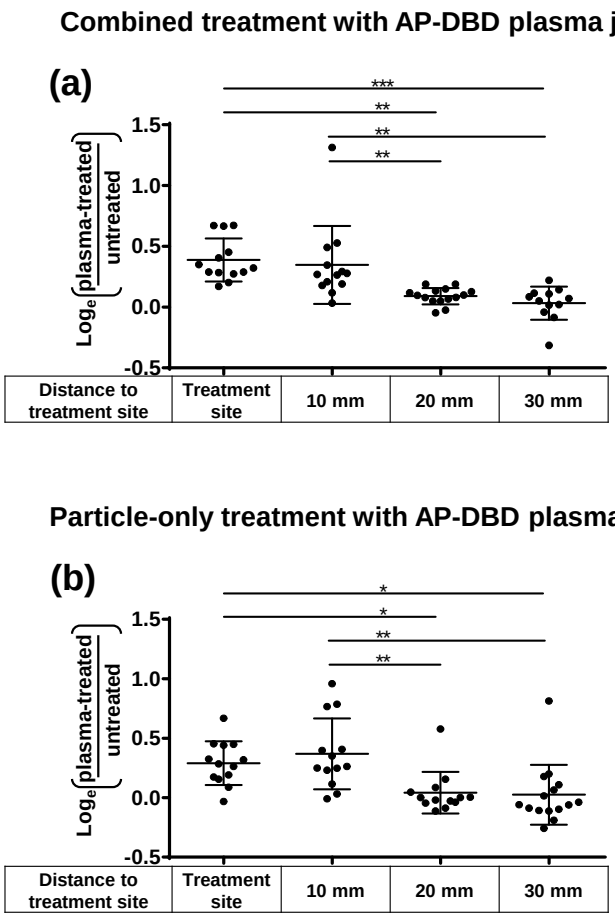

Figure 4.8. ***Combined and particle-only treatment induced similar levels of DNA damage in bacteria.*** The DDD Assay was used to assess the synergistic effect of plasma-generated UV radiation, RNOS and charged species and the effect of RNOS and charged species only. DNA damage induced by the AP-DBD plasma jet generated using **(a)** combined treatment (delivery of plasma and UV radiation) or **(b)** particle-only treatment (delivery of RNOS and charged species only). Experiment done using the 60° curved dielectric tube, as described in Section 3.3.9b. Each dot represents a single cell; horizontal bars: mean values ± S.D. Ratio expressed as Log_e (radius plasma-treated cells/mean radius untreated cells). ***: P<0.001, **: P<0.01; *: P<0.05.

DNA damage. Both treatments had similar bactericidal action against *S.* Typhimurium in LB agar plates as described in Section 3.3.9. These results demonstrate that similar levels of DNA damage were obtained in bacterial cells exposed to the combined and particle-only treatments (no UV photons). These results suggest that DNA damage is mainly caused by the direct effect of RNOS delivered in plasma and not exclusively by exposure to plasma-generated UV photons.

From the set of results obtained in this section, it can be concluded that UV radiation generated by the plasma does not induce significant levels of DNA damage in *S.* Typhimurium and does not impair bacterial growth. These results provide evidence that it is effectively the presence of RNOS in the plasma which is responsible for DNA damage and cell death observed in plasma-treated *S.* Typhimurium.

4.6 ROLE OF NUTRIENTS ON DNA DAMAGE DURING PLASMA TREATMENT

Bacteria exposed to nutritional stress can change their metabolism to adapt to the nutritional restrictions present in the environment. Such modifications can alter the way bacteria respond to and protects themselves from oxidative stress (183). In addition, the presence of external biomolecules during plasma treatment of bacteria could interact with RNOS produced by the plasma, reducing their bactericidal action (see Section 3.3.3). Thus, to determine how the culture media where bacteria were cultured affects the level of DNA damage induced by the AP-DBD plasma jet, two culture media were used. *S.* Typhimurium was grown in LB and minimal media M9 as described in Section 2.3, and prepared for plasma treatment as described in Section 2.6. Bacteria were plated in the corresponding media agar plates and transferred to agarose-coated slides for plasma treatment.

DNA damage in cells grown in LB and M9 was observed in cells located under the plasma jet and up to at 10 mm from it ($P<0.0001$) (**Figure 4.9**). In addition, comparing the data from **Figure 4.9a,b**, it was observed that bacterial cells grown in M9 presented higher levels of DNA damage than those grown in LB at 0mm and 10 mm ($P<0.001$ and $P<0.0001$, respectively). The level of DNA damage for cells located at 20 and 30 mm from the treatment site was comparable to values obtained for the corresponding untreated controls. These results demonstrate an increase in the levels of DNA damage in bacterial cells grown in M9 located at 10 mm distances from the treatment site compared to those grown in LB.

4.7 CORRELATION BETWEEN SPATIAL DISTRIBUTION OF O_3 IN PLASMA AND DNA DAMAGE

The chemical composition of the plasma effluent can change as the plasma leaves the dielectric and interacts with air and water molecules in the surrounding environment, in addition to the variation in the electric field and presence of UV photons. Thus, it is possible that at different

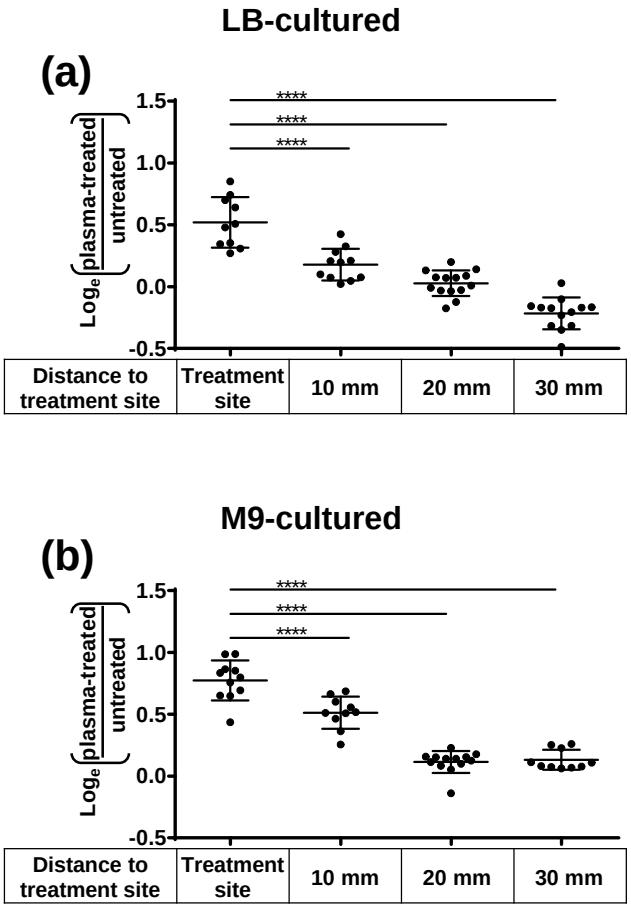

Figure 4.9. ***Bacteria cultured in minimal media were more susceptible to DNA damage than bacteria cultured in nutrient-rich media.*** The effect of growth state and nutrient composition in culture media on plasma-induced DNA damage at the single cell level was examined using the DDD Assay. DNA damage in plasma-treated *S.* Typhimurium previously cultured in **(a)** LB or **(b)** M9 media. Plasma treatment done using the AP-DBD plasma jet. Each dot represents a single cell; horizontal bars: mean values ± S.D. Ratio expressed as Log_e (radius treated cells/mean radius untreated cells). ****: P<0.0001.

axial and radial positions from the plasma jet, the bactericidal properties of the plasma change due to variations in the type and concentration of RNOS present.

Ozone (O_3) is one of the toxic molecules formed in the plasma that can damage the DNA. The distribution of O_3 in the plasma effluent was measured in collaboration with Apiwat Wijaikhum using UV-absorption spectroscopy, as described in Section 2.13. To determine the relationship between the spatial distribution of O_3 and the DNA damage induced by the plasma, two approaches were taken: **a)** To place samples perpendicular to the plasma jet to determine DNA damage in cells as a function of their radial position to the plasma jet (**Figure 4.10a**). For this condition, 3 feed gas compositions were used: He + 0.2 vol %, 0.5 vol % and 1.2 vol % O_2. **b)** To place samples parallel to the plasma jet to determine DNA damage in cells as a function of their axial and radial position to the plasma jet (**Figure 4.10b**). For this condition, plasma was generated using He + 0.5 vol % O_2.

Experiments were done using the final version of the AP-DBD plasma setup housed in the metallic box, as described in Chapter 3. The DDD Assay was used to determine DNA damage in bacterial cells and the zone of inhibition assay was performed to confirm bactericidal activity of plasma treatments.

4.7.1 The radial distribution of O_3 did not correlate with DNA damage

The relationship between O_3 density and the level of DNA damage in plasma-treated bacterial cells as a function of their radial position to the plasma jet was investigated. The O_3 density was measured at 30 mm distance from the nozzle in the axial direction, at the surface of the sample. The O_3 density was measured at both sides of the treatment site (0 mm). These experiments demonstrated symmetry in the distribution of O_3 in the plasma effluent at different positions in the radial direction (**Figure 4.10c**). Increasing the concentration of O_2 in the gas admixture increased the amount of O_3 detected (**Figure 4.10c**). The plasma jet generated using 0.2 vol % O_2 in the gas admixture showed the lowest levels of O_3 (5 ppm). In contrast, the plasma jet generated using 1.2 vol % O_2 in the gas admixture presented up to 12 ppm O_3.

S. Typhimurium were treated with the AP-DBD plasma jet as described in **Figure 4.10a**. The highest levels of DNA damage in treated *S.* Typhimurium were observed in samples treated with plasma generated with 0.2 vol % O_2 in the gas admixture (**Figure 4.11a, left**). The levels of DNA damage decreased with increasing concentrations of O_2 in the gas admixture (**Figure 4.11b,c, left**). DNA damage in bacterial cells was highest at the treatment site and was detectable up to 10 mm from the treatment site for all treatments.

The bactericidal activity of plasma generated with the three gas admixtures used here was also assessed in relation to the O_3 density in the plasma jet. *S.* Typhimurium in LB agar plates exposed to the plasma jet generated with 0.2 vol %, 0.5 vol % and 1.2 vol % O_2 in the gas admixture presented zones of inhibition of 226 mm^2, 1450 mm^2 and 3340 mm^2, respectively

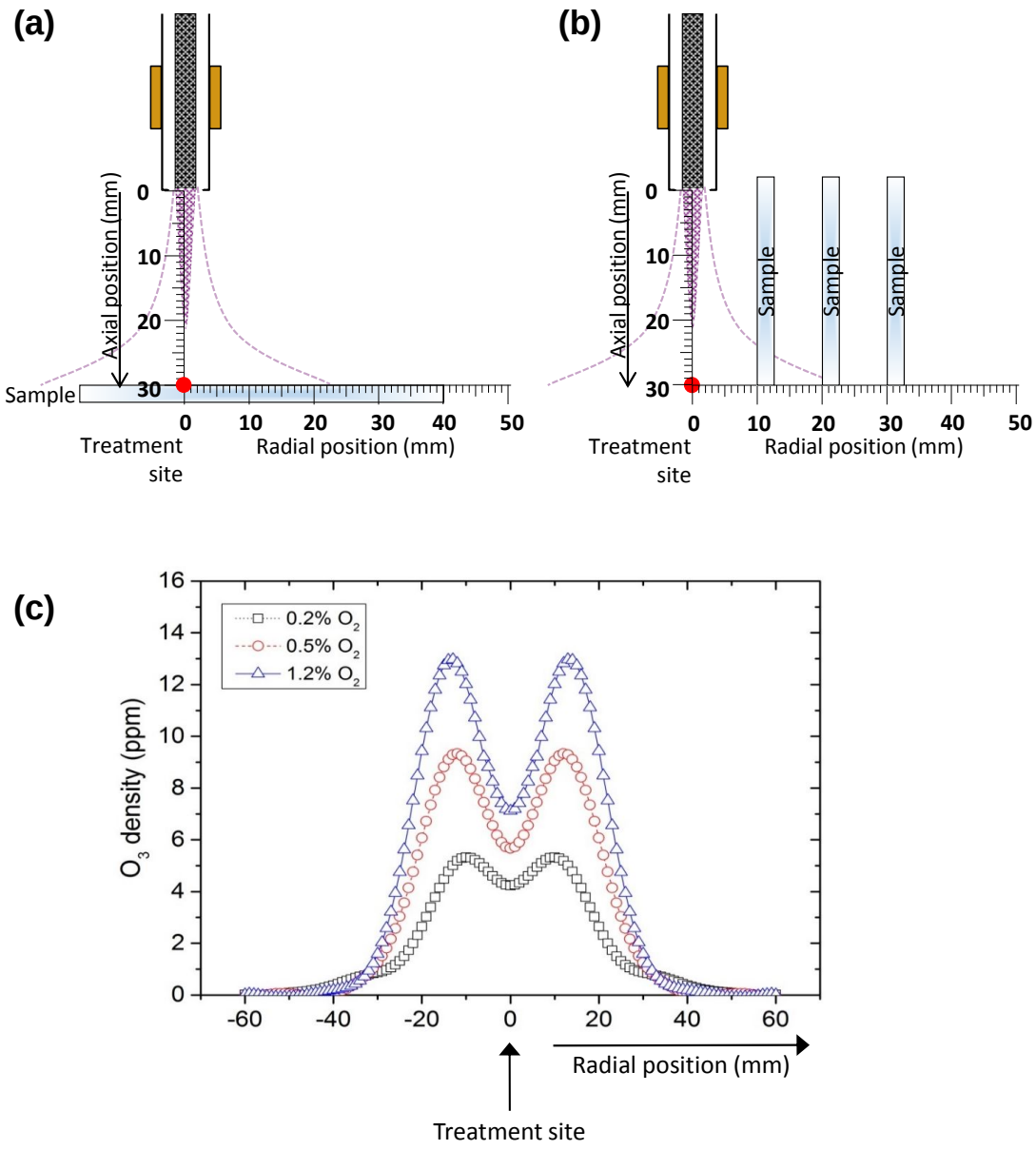

Figure 4.10. ***Experimental designs and measurement of O_3 density.*** Experimental designs for the measurement of O_3 density, DNA damage and bacterial elimination **(a)** in the radial direction, with sample placed in the horizontal position at 30 mm from the nozzle; **(b)** in the axial and radial directions, with samples placed parallel to the plasma jet at 10 mm, 20 mm and 30 mm distance from the treatment site (red dot), using an aluminium support to keep the sample in vertical position. **(c)** O_3 density was measured by UV-Absorption spectroscopy at 30 mm distance from the nozzle, as described in **(a)**. Plasma was generated using 2 slm He + 0.2 vol % O_2, 0.5 vol % O_2 and 1.2 vol % O_2. O_3 density expressed in parts per million (ppm). Image **(c)** adapted from results obtained in collaboration with Apiwat Wijaikhum.

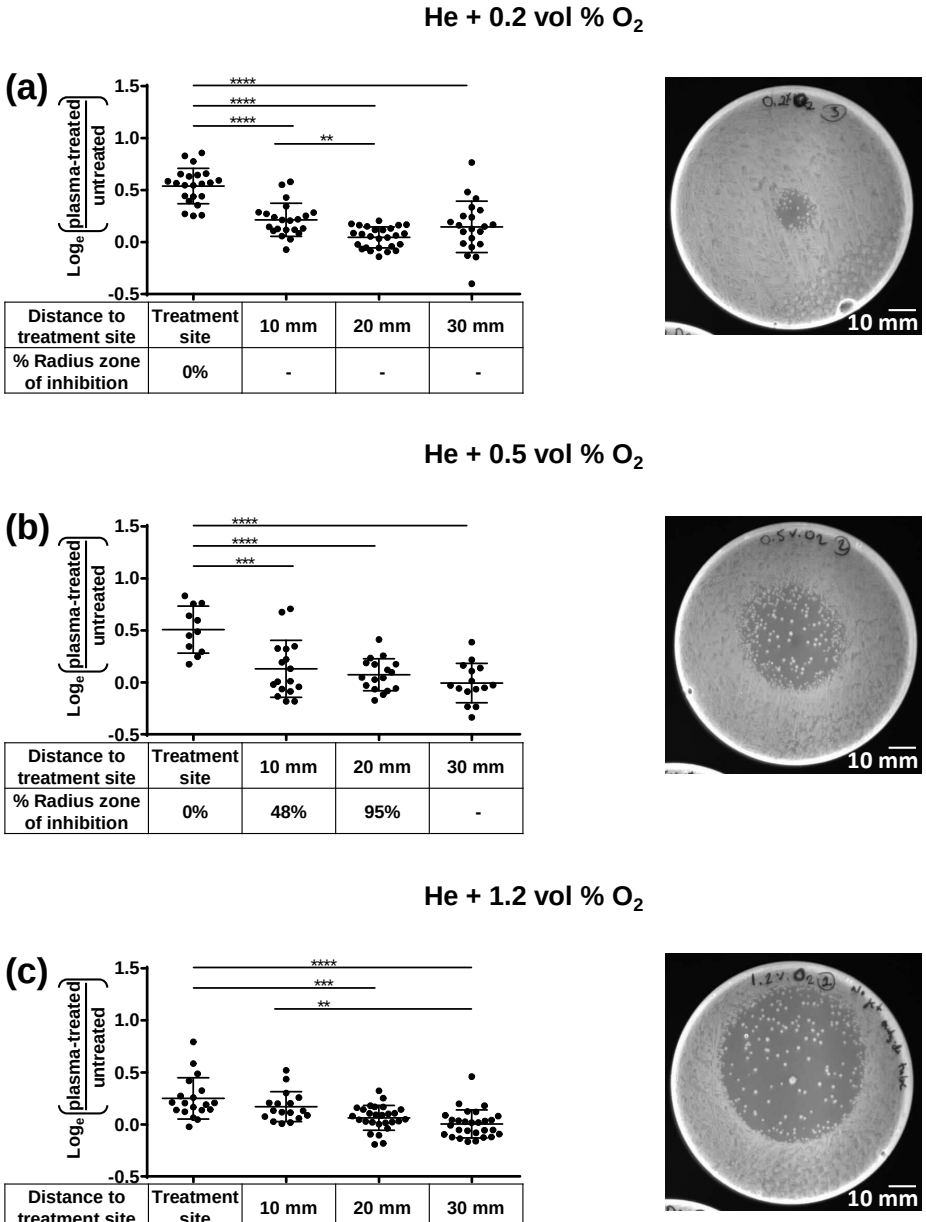

Figure 4.11. ***O_3 at the surface of the sample was not responsible for DNA damage but for bacterial inactivation.*** *S.* Typhimurium were treated with The AP-DBD plasma jet generated with **(a)** He + 0.2 vol % O_2; **(b)** He + 0.5 vol % O_2 and **(c)** He + 1.2 vol % O_2. ***Left:*** Plots show the level of DNA damage on plasma-treated bacteria at the single cell level as a function of their radial position to the treatment site (d=0 mm). Each dot represents a single cell; horizontal bars: mean values ± S.D.; ****: P<0.0001; ***: P<0.001; **: P<0.01. Ratio expressed as Log_e (radius plasma-treated cells/mean radius untreated cells). ***Right:*** Representative agar plates with *S.* Typhimurium treated for 90 seconds with the plasma jet generated with the corresponding gas admixtures. Scale bar 10 mm.

(**Figure 4.11, right**). These results correlated with those presented in Section 3.3.5, as an increase in the percentage of O_2 in the gas admixture increased the size of the zone of inhibition. The radial position of the edges of the zones of inhibition in LB agar plates correlated with the presence of 3 – 6 ppm O_3 for the three gas admixtures tested. Thus, for plasma treatments generated with 0.2 vol % O_2 in the feed gas, LB agar plates presented a zone of inhibition with radius 8 mm that corresponds to 5 ppm O_3 in that position. For 0.5 vol % O_2, the radius of the zone of inhibition was 21 mm, corresponding to 5 – 6 ppm O_3. For 1.2 vol % O_2 the radius of the zone of inhibition was 28 mm, corresponding to 3 – 4 ppm O_3.

These results suggest that O_3 may not be directly responsible of the DNA damage observed in bacterial cells, as increasing concentrations of O_3 in the plasma did not increase the levels of DNA damage induced in plasma-treated bacterial cells. However, these results suggest the participation of O_3 in bacterial elimination with a possible threshold between 3 – 5 ppm O_3 in the plasma effluent required to achieve bacterial inactivation in agar plates.

4.7.2 Abundance of O_3 in the axial direction did not correlate with DNA damage

The relationship between the 2-dimensional distribution of O_3 in the plasma effluent and the levels of DNA damage in cells as a function of their axial and radial position to the plasma jet were investigated. O_3 density was measured in the axial direction at 10, 20 and 30 mm distance from the nozzle and in the radial direction starting from the treatment site (axial position = 30 mm from nozzle; radial position = 0 mm) up to 40 mm, with 5 mm steps. A plastic Petri dish was placed at this distance to preserve the flow dynamics of the plasma, since samples were placed parallel to the plasma jet. This experiment demonstrated that O_3 was more abundant at 25 – 30 mm from the nozzle in the axial direction and at 0 – 20 mm in the radial direction (**Figure 4.12a**). The concentration of O_3 was 6 ppm at the treatment site. A maximum concentration of 9 ppm O_3 was found at 30 mm from the nozzle in the axial direction and 10 mm from the treatment site in the radial direction.

To assess the effect of the spatial distribution of O_3 in the plasma effluent on DNA damage in *S.* Typhimurium, samples were placed parallel to the plasma jet and the level of DNA damage in cells was measured as a function of their axial and radial position to the plasma jet. *S.* Typhimurium in agarose-coated slides were placed vertically at 10 mm, 20 mm and 30 mm from the treatment site in the radial direction using aluminium supports (Thorlabs Inc.) (**Figure 4.10b**). DNA damage was only detected on the slide placed at 10 mm from the treatment site in the radial direction, specifically in bacterial cells located at 27 mm in the axial direction ($P<0.0001$; **Figure 4.13a**). In this region, the concentration of O_3 was 7 – 8 ppm. No DNA damage was detected in cells located in other locations of the sample. Slides placed vertically at 20 mm and 30 mm from the treatment in the radial direction did not present detectable levels of DNA damage (**Figure 4.13b,c**).

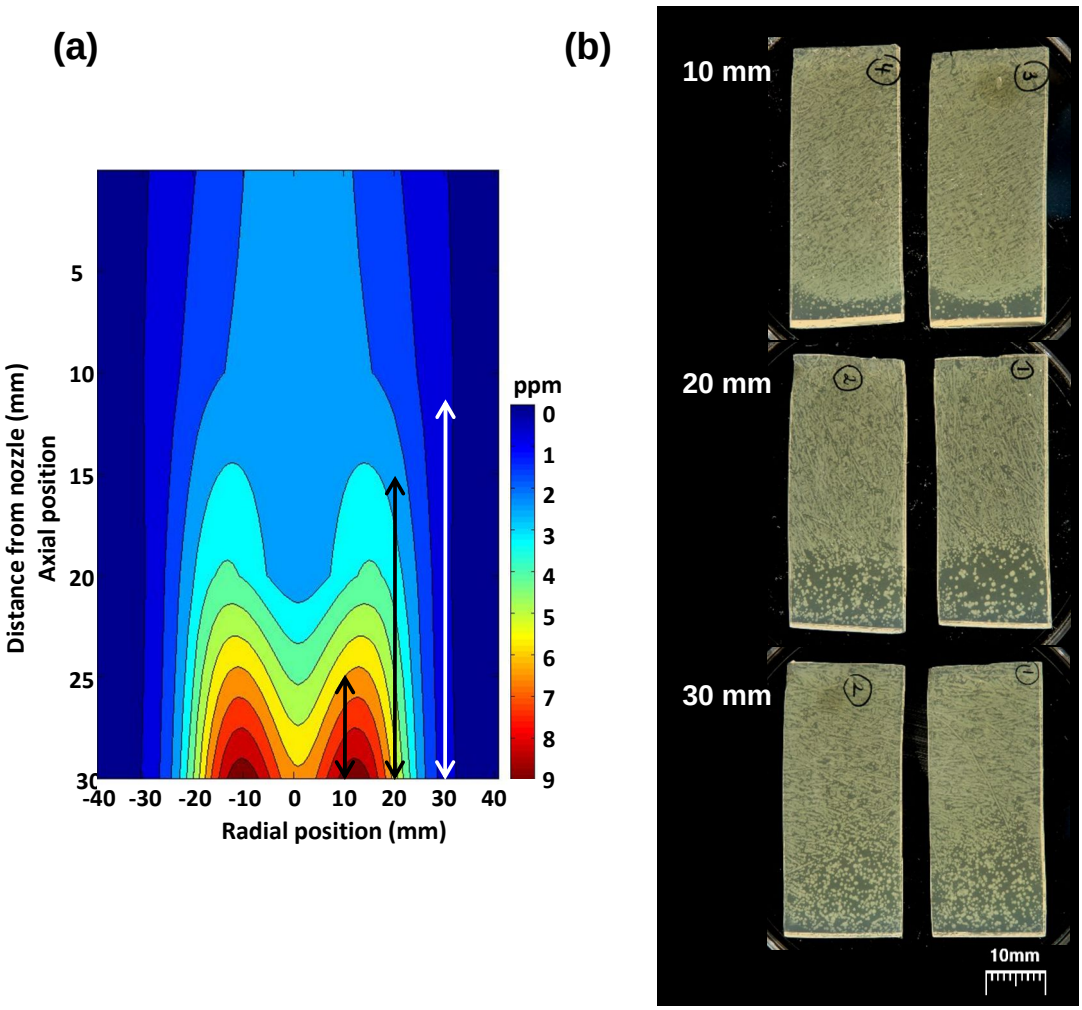

Figure 4.12. ***Elimination of* S. *Typhimurium in vertical agar sections did not correlate with O_3 distribution in plasma effluent.*** **(a)** Spatially-resolved O_3 density in the effluent region for a plasma generated within 30 mm distance from nozzle. O_3 density expressed in parts per million (ppm). **(b)** Representative vertical plasma-treated agar sections containing *S.* Typhimurium at 10, 20 and 30 mm from treatment site in the radial position, treated for 90 seconds with the AP-DBD plasma jet. Scale bar: 10 mm. Arrows in **(a)** indicate the zone of inhibition achieved in plasma-treated vertical agar sections at each radial position. Image **(a)** adapted from results obtained in collaboration with Apiwat Wijaikhum.

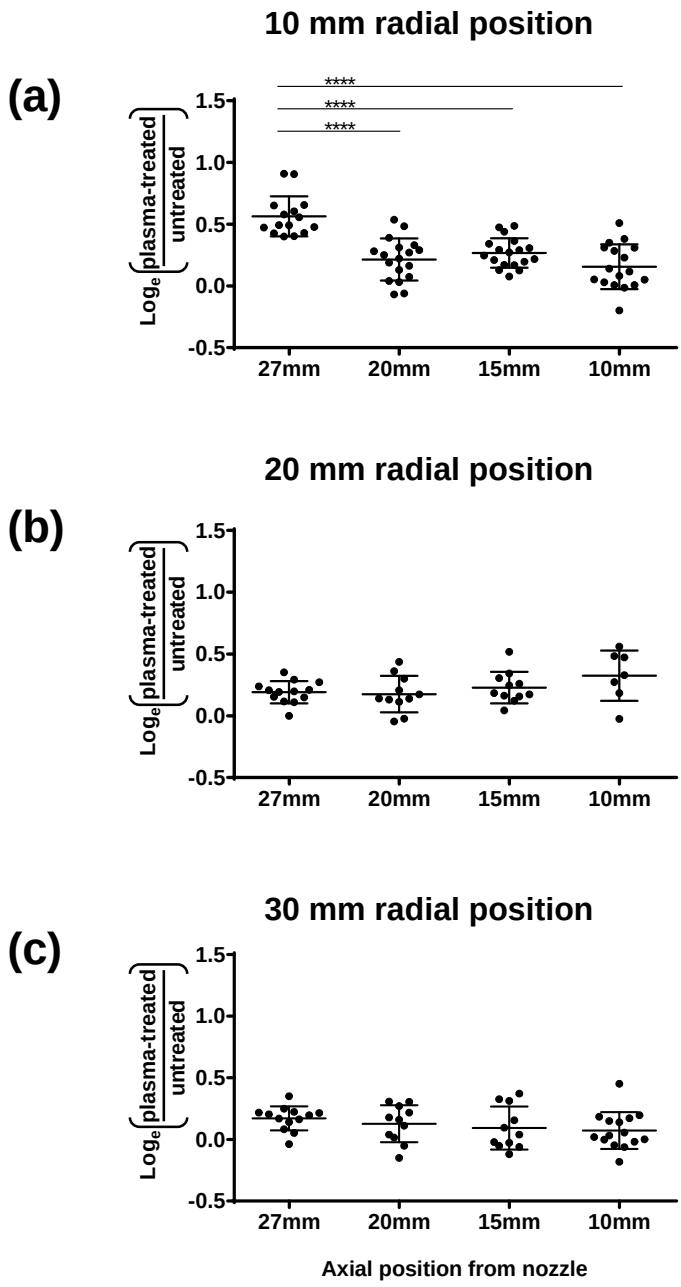

Figure 4.13. ***DNA damage in vertical samples was only induced in regions close to the treatment site.*** Plots show the level of DNA damage on plasma-treated bacteria at the single cell level as a function of their axial position to the nozzle and radial position to the treatment site. Agarose-coated slides containing *S.* Typhimurium placed parallel to the plasma jet at **(a)** 10mm; **(b)** 20 mm and **(c)** 30 mm in the radial direction. Each dot represents a single cell; horizontal bars: mean values ± S.D.; ****: P<0.0001. Ratio expressed as Log_e (radius plasma-treated cells/mean radius untreated cells).

The bactericidal activity of plasma considering the spatial distribution of O_3 in the plasma effluent was also studied. Agar sections carrying *S.* Typhimurium were fixed parallel to the plasma jet at 10 mm, 20 mm and 30 mm from the treatment site in the radial direction, as described above. Zones of inhibition were observed at the three radial positions (**Figure 4.12b**). Vertical agar sections treated at 10 mm from the treatment site in the radial direction presented a well-defined zone of inhibition starting at 25 mm in the axial direction (**Figure 4.12b**). The shape of the zone of inhibition indicates that the presence of the agar section at close proximity to the treatment site interfered with the flow of gas to the sides, generating a u-shaped zone of inhibition. In this region, the corresponding concentration of O_3 was between 6 – 9 ppm. No inhibition of growth was observed in other parts of the agar sections. Vertical agar sections treated at 20 mm from the treatment site in the radial direction presented zones of inhibition starting at 15 mm in the axial direction with observable CFU in this region. The corresponding concentration of O_3 was 2.5 – 6 ppm. The bactericidal action of plasma decreased at 30 mm distance in the radial direction, as agar sections presented zones of inhibition starting at 18 mm in the axial direction with undefined edges and an increase in the number of CFU. At this position, there was only 0 – 1 ppm O_3, but bacterial growth was still inhibited. These results indicate the participation of other RNOS spatially distributed in the plasma effluent on bacterial elimination.

The results of DNA damage in bacterial cells in the context of the spatial distribution of O_3 suggests that at least O_3 alone does not participate in the induction of DNA damage in plasma-treated bacteria and other RNOS spatially distributed in the plasma effluent, either solely or in combination, would be responsible for this damage. Results of the zone of inhibition assays suggest that other RNOS present in the plasma in the axial position would contribute to bacterial elimination, certainly in regions where O_3 is present at low concentrations below 1 ppm.

4.8 DISCUSSION

The aim of this chapter was to identify the factors that determine the level of DNA damage in plasma-treated bacterial cells and to assess whether the level of DNA damage induced was affected by the spatial distribution of RNOS in the plasma effluent. For this purpose, a modified and improved version of the DDD Assay was used to quantify the damage to the DNA sugar-phosphate backbone and oxidized purines in single bacterial cells.

The DDD Assay was previously used for the identification of DNA damage in microorganisms exposed to antimicrobial treatments in solution (137). This method was optimized here for the study of DNA damage in bacteria exposed to plasma treatments in dry environments and it was improved by the addition of a quantitative analysis of DNA damage and enzymatic treatment with FPG for the detection of the oxidized nucleotide bases purines. The method allows the

identification of damage to the DNA sugar-phosphate backbone that can be lethal for the cells, as the open ends are more prone to physical and chemical assaults. The addition of FPG to the protocol allowed further identification of damage to purines, another type of injury to the DNA that does not result in DNA breaks but generates mutagenic base by-products that can be dangerous to cells (205). This modified method has demonstrated to be a valuable tool for the study of DNA damage in plasma-treated samples that preserves information about the effect of spatially-distributed RNOS in the plasma jet. Current approaches to identify oxidized nucleotide bases in bacterial populations (13), single- and double-strand DNA breaks (51) or modifications at the molecular level (104) in plasma-treated samples have provided insight in the general effect of plasma over DNA (purified or in the context of bacterial cells in a population). However, none of these provided information of the level of oxidative damage each cell was exposed to.

To the best of my knowledge, this is the first report addressing the effect of LTP treatments in the integrity of DNA in bacterial cells at the single cell level that considers the distribution of RNOS in the plasma effluent. A combination of different approaches to study the lesion inflicted by LTP treatments in bacterial cells could provide valuable information about the effect of oxidative damage at the single cell level and how this correlates with the bactericidal effect observed at the population level, considering the heterogeneity of the responses displayed in a population of cells. Even more, efforts to improve the sensitivity of the modified DDD Assay presented here could allow the identification of low numbers of single- and double-strand DNA breaks that currently cannot be detected by this method but could still be mutagenic or deleterious.

The results presented here demonstrated that the level of DNA damage induced by the AP-DBD plasma jet and the µAPPJ in *S.* Typhimurium was inversely correlated to the distance to the treatment site and is characteristic of LTPs generated in open air. This was never demonstrated in the context of living bacterial cells at the single cell level, as the only two reports existing on the effect of the spatial distribution of RNOS in DNA were done using purified DNA and analysed by electrophoresis to identify single- and double-strand DNA breaks (121, 208). The DNA damage reported here was found to be at the DNA sugar-phosphate backbone level (single- and double-strand DNA breaks) and at the nucleotide base level, specifically due to oxidation of purines. Whereas double DNA breaks can be irreversible and lead to cell death, oxidation of purines can induce lethal and non-lethal mutations in the DNA. Both types of lesions to the DNA were observed in bacterial cells located at the treatment site but not in those located at further distances. This data suggest that oxidation of purines might not occur at high rates in plasma-treated bacterial cells located away from the treatment site that are still exposed to RNOS, and therefore the chances of inducing mutagenic lesions in DNA could be limited. However, it is worth to mention that even one single mutation can be mutagenic. Highly sensitive methods to detect lesions to the DNA (such as fluorescent protein reporters that

specifically bind to double-strand breaks; (212)) could provide further insight in the type of lesion inflicted to the DNA of plasma-treated bacterial cells.

The AP-DBD plasma jet was able to induce DNA breaks in cells located up to 10 mm distance from the treatment site, whereas the µAPPJ only induce these lesions in cells directly located at the treatment site. This could be explained by the different characteristics of both plasma sources (electrode arrangement, plasma generation, frequency, among others). The µAPPJ delivers mostly neutral species and the AP-DBD plasma jet deliver neutral and charged species. However, both plasma sources induced DNA damage in a radial-dependent manner. These results contrast with those obtained for plasma-treated *S.* Typhimurium in agar plates, where it was not possible to identify a gradual decrease in the antibacterial activity of plasmas in the radial direction. Other mechanisms of action could dominate the bactericidal effect of plasma influenced by the radial distribution of RNOS, as bacteria were killed in regions where corresponding DNA damage was not detected by the DDD Assay.

Evidence obtained from the study of other LTP sources indicate that the concentration of ROS varies in the axial and radial direction (112, 122), demonstrating that RNOS are not restricted to the visible region of the jet (91). Ozone is a relatively long-lived species that induces oxidative damage to bacteria and is one of the toxic reactive species produced in plasma (104, 200). Experimental and *in silico* analysis of a modified µAPPJ have shown that O_3 and can be found up to centimeters away from the plasma jet (108, 213). It could be expected that higher levels of damage to the DNA, proteins, lipids and carbohydrates in plasma-treated bacteria would be found where the concentration of RNOS is higher in the plasma. The collaborative work done with Apiwat Wijaikhum provided insight on the spatial distribution of O_3 on the effluent of the AP-DBD plasma jet and its correlation with DNA damage. These experiments demonstrated that O_3 may not be solely related to the DNA damage observed in bacterial cells, as increasing concentrations of O_3 in the axial and radial direction did not increase the levels of DNA damage induced in bacterial cells.

The DNA damage induced by plasma treatments may be due to the combined effect of RNOS delivered to the sample and not solely due to O_3. The presence of other RNOS in the plasma effluent can be inferred from the results obtained for plasma-treated agar sections in the axial direction, where bacterial elimination was achieved in regions with less than 1 ppm O_3. In addition, it is possible that after reaching the surface of the sample and being transported by advection and diffusion processes, the various RNOS generated in the plasma are lifted together with He, which could explain the increase in the size of the zone of inhibition in agar sections in the axial direction (**Figure 4.12**). In any case, the high levels of DNA damage found in cells located at the treatment site could be the result of the exposure to a high concentration of RNOS produced by the plasma. It could be then expected that the level of oxidative damage induced in

proteins, lipids and carbohydrates in bacterial cells would depend in the same way on the spatial distribution of RNOS in the plasma effluent.

The participation of UV radiation in the mechanisms leading to bacterial elimination was also studied. It is well-known that UV radiation can induce damage to the DNA, including double-strand breaks and mutagenic lesions (205). The contribution of plasma-generated UV radiation to DNA damage was minimal, since bacteria exposed to the combined treatment (particles and UV radiation) presented similar levels of DNA damage than bacteria exposed to the particle-only plasma treatment. The differences in the chemistry of the plasmas generated with the straight and curved tube should be considered. However, these results suggest that RNOS are the main agents leading bacterial elimination. Lackmann *et al.* described that the combined treatment of UV radiation and particles and the particle-only treatment generated with a μAPPJ induced similar damage to the cell envelope of *B. subtilis*, supporting that RNOS and not UV radiation are responsible of the bactericidal action of plasmas (104). The same study showed that the treatment with the complete jet was more effective than UV-only treatment on inducing modifications to plasmid DNA at the molecular level. Thus, it is possible that the UV radiation generated by the LTP sources used here has a minimal or no contribution to the bactericidal action of LTPs rather than directly damaging bacterial targets.

The presence of external biomolecules during plasma treatment could compete with biomolecules in bacterial cells and therefore interfere with the treatment outcome, as suggested in Section 3.3.3. Bacteria cultured in LB or M9 were plated in the corresponding media agar plate prior to transference to the agarose-coated slide for treatment. Results here demonstrated that bacteria cultured in M9 presented higher levels of DNA damage than those cultured in LB. These results could be due to the presence of nutrients transferred to the agarose-coated slide together with the bacterial cells, since RNOS could react with nutrients in the medium rather than with biomolecules in bacterial cells, as suggested in Section 3.3.3. Ingram and Haines described that larger concentrations of O_3 were required to inhibit bacterial growth in the presence of nutrients than without nutrients (214). The authors suggested that the first action of O_3 was on the nutrients in the medium, therefore decreasing its antibacterial properties. The short plasma treatments described here produce low concentrations of O_3, but the interaction of O_3 with nutrients is still expected to interfere with the induction of DNA damage and bacterial elimination. The sensitivity of bacterial cells to DNA damage could be also affected by the metabolic state of bacteria, as cells exposed to nutritional stress change their metabolism to adapt to a nutrient-limited environment (183). These changes include the up-regulation of biosynthetic pathways and limitation of growth, but also an enhanced response to oxidative stress. However, DNA damage in plasma-treated bacteria was measured immediately after exposure and bacterial cells were not allowed to recover. Thus, it is then possible that the differences in DNA damage found between the two populations of bacteria are a consequence

of the reduction of RNOS available to interact with bacterial cells due to the oxidation of nutrients present during treatment, rather than due to the metabolic state of the cells.

As demonstrated in Chapter 3, small variations in the parameters required to generate plasma can affect the bactericidal action of LTPs. Here, it was observed that the addition of O_2 to the gas admixture increased the O_3 density, but decreased the levels of DNA damage induced in *S.* Typhimurium. These results contrast with those obtained for the elimination of *S.* Typhimurium, as more O_2 in the gas admixture correlated with an increased zone of inhibition. The O_3 density represents the formation and destruction processes occurring in the gas phase and that determine the amount of O_3 measured in the plasma. As O_3 is formed in a three-body reaction that involves molecular oxygen (215):

$$O + O_2 + M \rightarrow O_3 + M$$

It can also dissociate *via* the reactions with O and H, as described for a RF-driven DBD plasma jet (143):

$$O + O_3 \rightarrow 2\ O_2$$

$$H + O_3 \rightarrow O_2 + {\cdot}OH$$

The increase in the O_3 density observed here due to the combined effect of both processes could have an impact on the density of other reactive species that are more important for the induction of DNA damage in cells, such as ·OH radical and singlet oxygen. Alternatively, the increased levels of DNA damage at low percentages of O_2 in the gas admixture could be a consequence of the presence of other long-lived species in the plasma such as H_2O_2 that can induce the formation of intracellular ROS *via* Fenton reaction in interaction of H_2O_2 with iron ions (like those bound to the DNA molecule). This particular reaction generates the highly damaging agent ·OH radical that can effectively damage DNA. However, the chemical reactions occurring in the plasma effluent of different plasma sources cannot explain the formation of O_3 in the AP-DBD plasma jet used here, since the composition of the gas phase vary between plasmas due to inherent differences in the LTP source and parameters used. Therefore, experimental and *in silico* approaches to understand the chemistry of the gas phase in this AP-DBD plasma jet should be carried out in the future (216, 217). Together with biological experiments described here, this could provide insights on the type of reactive species and concentrations required to induce fragmentation of DNA in bacterial cells.

The study of the spatial distribution of O_3 on the plasma effluent and its correlation with bacterial inactivation demonstrated that bacterial elimination correlated with the presence of a minimum of 3 – 5 ppm O_3 in the plasma effluent, in addition to other RNOS. The concentration of O_3 in the plasma effluent was the highest at 30 mm in the axial direction, which corresponds to the position of the surface of agar plates. The O_3 density increased with the addition of O_2 to the gas admixture, as shown in **Figure 4.10** and this also increased the size of the zones of

inhibition in plasma-treated agar plates (**Figure 4.11**). Interestingly, the edges of the zone of inhibition obtained in agar plates correlated with the presence of 3 – 5 ppm O_3. These results indicate that a minimum concentration of O_3 in this range would be required to inactivate bacteria with the AP-DBD plasma jet. The presence of O_3, free radicals produced by the breakdown of O_3 and additional RNOS in the plasma would act synergistically to kill bacteria. This is an advantage over other antimicrobial treatments using exclusively O_3, where higher concentrations and longer treatments are required to achieve complete elimination of bacteria (214, 218, 219). Altogether, the data presented here highlights the participation of O_3 in the mechanisms leading to bacterial elimination with LTP treatments and the beneficial synergistic action of the rich 'cocktail' of RNOS produced by plasmas.

UV radiation emitted by both LTP sources used here did not produce a zone of inhibition in agar plates when administrated in an RNOS-free environment. It should be considered however that the plasma jet was generated in a 1 mm gap compartment (1 mm inner diameter of the dielectric in the AP-DBD plasma jet; 1 mm gap between electrodes in the µAPPJ). It is expected that the bulk of UV photons produced by both plasma sources is delivered to the region immediately under the nozzle (i.e. treatment site). However, because the area exposed to UV photons might be of restricted size, it is possible that if UV photons inhibited the growth of some bacterial cells in agar plates, it was masked by the proliferation of neighbouring cells.

In summary, these results indicate that the RNOS in the plasma jet, and not the UV radiation emitted, are the main agents leading to bacterial inactivation and DNA damage. These results are in agreement with the literature, as a number of reports describe the role of plasma-generated RNOS in bacterial elimination (13, 71, 104). Even more, the results presented here evidence that the antibacterial activity of plasmas is directly dependent on the spatial distribution of RNOS in the effluent. The novel approach used here to identify DNA damage at the single cell level contributes to the understanding of the mechanisms of action of LTPs to eliminate bacteria. This approach has an advantage over previous studies assessing the effect of plasma at the population level (13) or on purified DNA (121, 208), since discrete variations in the level of DNA damage inflicted to single cells by LTP treatments can be identified. Whereas most of the information available on the spatial distribution of RNOS in LTPs is dissociated from the mechanisms of action that lead to bacterial elimination (71, 112, 122, 200), the current study successfully combined approaches from physics and biology to determine DNA damage and bacterial elimination achieved as a function of the spatial distribution of RNOS in the plasma effluent. The data presented here highlight the importance of studying the effect of plasma at the single cell level and the spatial distribution of RNOS in the plasma effluent for the development of effective antibacterial treatments.

5 EFFECT OF EXTERNAL BIOMOLECULES DURING PLASMA TREATMENTS

5.1 INTRODUCTION

The study of the gas phase of LTPs has provided valuable information on the species produced by different plasma sources that could mediate the bactericidal action of LTPs (91, 112, 122). LTP sources have demonstrated their antibacterial action *in vitro* in solid and liquid environments (13, 71, 220) and *in vivo* to kill pathogens from infected wounds (15). However, the biomedical application of LTP treatments of skin wounds or infected tissue should consider the presence of interfering agents such as organic molecules (such as those in the wound exudate) and non-target cells in the surroundings of the population to treat that could affect the efficacy of the treatment.

While a nutrient-rich environment is necessary for the survival of bacterial cells, the nutrients in the media can also get oxidized or reduced during plasma treatment and act whether as a further source of radicals or as scavengers of reactive species (187, 188). In the same way, carbohydrates that depolymerize in reaction with RNOS can contribute to the formation of carbon-centred radicals (221) and exert pro-oxidant effects in proteins (21). It has been reported that plasma treatment induced structural modifications on purified amino acids and proteins in water suspensions, especially in sulphur-containing and aromatic amino acids (102, 114, 181). In the context of biologically relevant solutions, Tresp *et al.* demonstrated that in plasma-treated RPMI (culture media for eukaryotic cells rich in amino acids, vitamins, glucose and salts), NO_2^- and H_2O_2 were more abundant than in plasma-treated NaCl and PBS which was attributed to the interaction of RNOS with nutrients in the solution (222). For bacterial elimination, Nosenko *et al.* reported that *E. coli* in PBS suspensions required shorter plasma treatments to achieve 100% elimination than *E. coli* in LB suspension, highlighting the role of the chemical composition of liquids on the treatment outcome (203). The results presented in Chapter 2 and 3 support the idea that the nutrient composition of the media where bacteria is exposed to plasma affects the outcome of the treatment. *S.* Typhimurium in LB treated with the AP-DBD plasma jet presented an increase in the number of CFU that survived to the treatment in agar plates (Chapter 3). In addition, the level of DNA damage induced in bacteria treated in the presence of LB was higher than those obtained in bacteria treated in the presence of minimal medium M9 (Chapter 4). Thus, it is possible that the bactericidal activity of plasmas is affected by the composition of the nutrient media.

To understand the mechanisms underlying oxidative damage in plasma-treated bacteria and anticipate the treatment outcome in the presence of organic molecules, it is necessary to detect and characterize the RNOS formed. There are different analytical approaches to detect RNOS such as chemiluminescence, fluorescence and electron paramagnetic resonance (EPR) (223, 224). Fluorescence and chemiluminescent probes with high sensitivity are useful to monitor

changes of RNOS (225) and they can be used in fluorometry, flow cytometry and fluorescence microscopy (226). However, EPR spectroscopy is considered the gold standard method for the specific detection of free radicals due to its high sensitivity (micromolar concentrations) (227).

EPR is a powerful method that can detect species with one or more unpaired electrons by measuring the absorption of electromagnetic radiation in the microwave frequency region of the spectrum (227, 228). In combination with spin trapping, transient radicals such as ·OH, $O_2^{\cdot-}$ and NO (that under normal conditions would not be detected) react with organic molecules called spin traps to form stable spin adducts. These adducts have characteristic spectra that allows their identification and quantification by EPR spectroscopy (228). This method has been demonstrated to be useful for the direct detection of radicals formed during plasma treatment (229-231). It is important to note that the amounts of spin-trapped free radical species do not represent the entire amount of radicals introduced in the studied sample due to the many side reactions of the radicals (232). However, under similar conditions, the changes of the amount of spin adducts will correspond to the respective changes of the amount of free radicals.

Other long-lived toxic species can be easily detected with colorimetric assays. That is the case of H_2O_2 that in reaction with titanium(IV) reagent forms a yellow-coloured complex that can be detected at 400 nm (139) with a lower limit of 10 µM and upper limit of 2 mM (139). Using this method, Luke *et al.* reported a reduction in the bacterial load of plasma-treated *E. coli* in a water suspension that correlated with the presence of H_2O_2 and peroxynitrite (220). In the same way, it is possible to measure the formation of the product of NO oxidation, nitrite (NO_2^-), in reaction with Griess reagent (223).

The results presented in previous chapters (Chapter 3 and 4) suggested that the presence of organic molecules during plasma treatment of *S.* Typhimurium in agar plates decreased the ability of the AP-DBD plasma jet to induce DNA damage and eliminate bacteria. The present chapter has two aims: firstly, to determine the role of organic molecules during plasma treatment in the amount of RNOS detected and secondly, to determine their effect on the elimination of plasma-treated bacterial cells. For this purpose, five liquids with different composition of organic molecules and salts were chosen:

- H_2O: no buffering properties, no organic molecules
- PBS: buffering properties, no organic molecules
- DMEM: buffering properties, amino acids, vitamins, salts and carbohydrates
- DMEM + 10 % FCS: buffering properties, amino acids, proteins, lipoproteins, vitamins, salts and carbohydrates
- LB: no buffering properties, vitamins, peptides, lipoproteins, salts and carbohydrates

Because it was not possible to quantify the concentration of RNOS produced on solid and semi-solid surfaces, the formation of short- and long-lived species in plasma-treated samples was assessed in liquids. This was done using EPR spectroscopy and colorimetric assays, acknowledging the inherent differences between RNOS formed in the gas phase and those formed in plasma-treated liquids. Furthermore, the antibacterial action of the AP-DBD plasma jet was assessed in planktonic cultures of *S.* Typhimurium prepared in the aforementioned solutions to quantify cell membrane damage and determine bacterial elimination.

5.2 IDENTIFICATION OF RNOS BY EPR

It is possible that the efficacy of LTP treatments to eliminate bacteria is affected by the presence of external organic molecules during treatment, as these molecules can also participate in redox reactions (21). EPR spin trapping was used to determine the effect of organic molecules during plasma treatment of liquids on the concentration of RNOS measured. ·OH radical, O_3/O, $O_2(a^1\Delta g)$, NO and NO_2^- were determined. Samples were prepared and plasma-treated as described in Section 2.7.2. Experiments were carried out using the final version of the AP-DBD plasma setup housed in the plastic box, as described in Chapter 3. Simulations confirmed the presence of only one distinctive EPR spectrum per spin trap that was characteristic of the particular radical trapped (**Figure 5.1**). The concentrations of spin trap radical adducts measured are presented in **Table 5.1**.

The results obtained for EPR analysis of plasma-treated liquids were used here to identify a trend in the formation of RNOS in the presence of organic molecules rather than to compare absolute values between the different RNOS detected. This approach was taken since each spin trap possesses different reaction rates for each radical and therefore results can only be compared within experiments using the same spin trap.

5.2.1 Concentration of ROS in plasma-treated liquids was reduced in the presence of organic molecules

DMPO and DEPMPO are two of the commonly used spin traps for the detection of hydroxyl and superoxide radicals in biological milieu. While DMPO does not form a stable radical adduct with superoxide radical (DMPO-OOH adduct decays overtime into DMPO-OH, which may contribute to the measured amount of DMPO-OH), the adduct DEPMPO-OOH formed upon reaction of DEPMPO and $O_2^{\bullet -}$ is significantly more stable and in most cases can be detected using EPR (227). Notably, in the experiments done for this study, no DEPMPO-OOH was observed even in plasma-treated water, thus suggesting that the superoxide radical was not present in plasma treated solutions.

The spin traps DMPO and DEPMPO were used to detect ·OH. Results showed an increase in the concentration of spin trap radical adducts with increase of the length of treatment. This shows that despite the different reactivity of each spin trap with ·OH, an increase in the

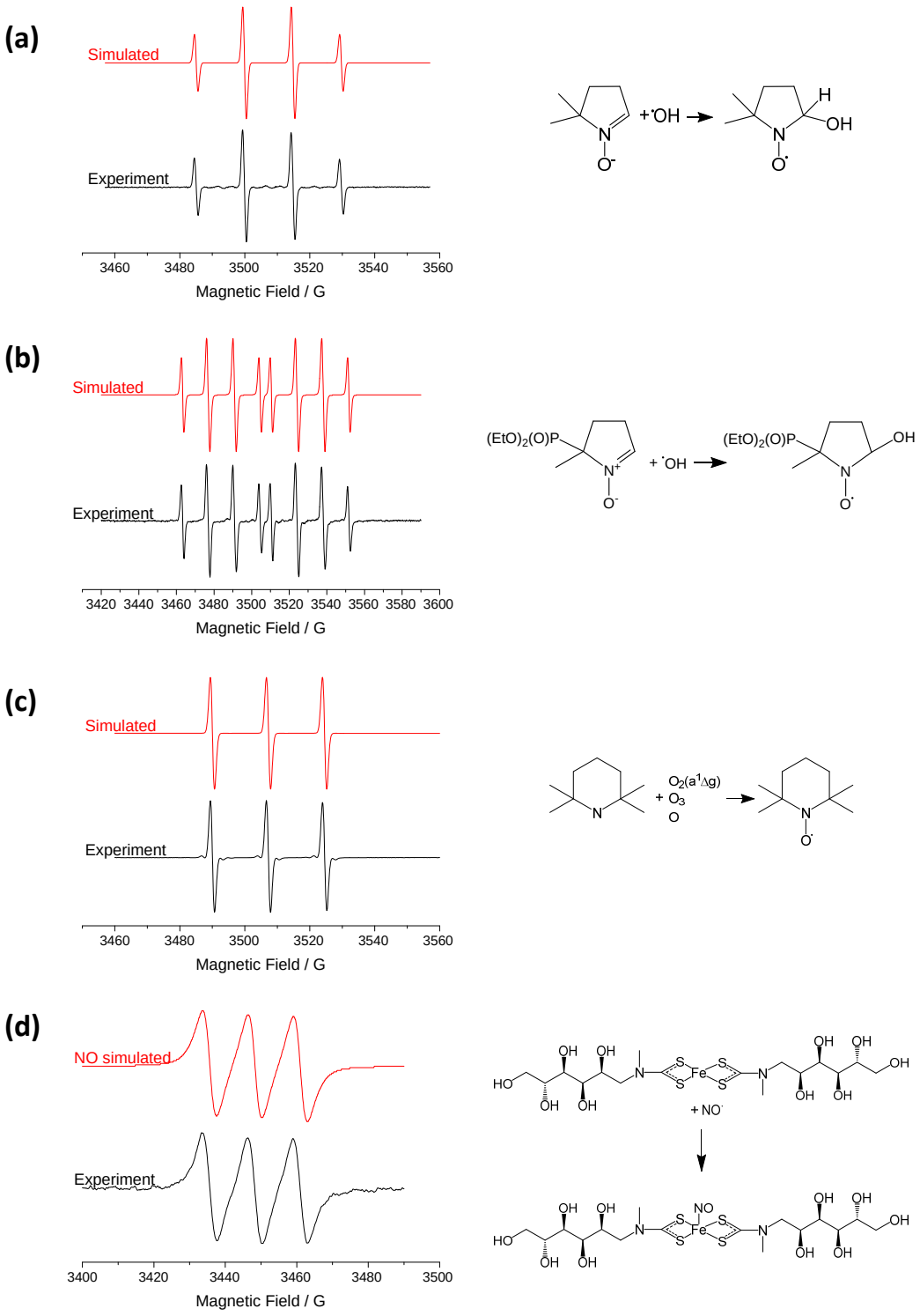

Figure 5.1. ***EPR spectra of radical adducts and chemical reactions. Left:*** Representative computer-simulated (red) and experimental (black) first-derivative spectra of **(a)** DMPO-OH adduct; **(b)** DEPMPO-OH adduct; **(c)** TEMPO from $O_2(a^1\Delta g)$, O_3 and O; **(d)** $(MGD)_2$-Fe^{2+}-NO complex formed in plasma-treated aqueous solutions. ***Right:*** Corresponding chemical reactions for the formation of spin trap radical adducts.

	DMPO-OH (µM)			DEPMPO-OH (µM)			TEMPO from O_3 and O (µM)			TEMPO from $O_2(a^1\Delta g)$ (µM)			$(MGD)_2$-Fe^{2+}-NO complex (µM)		
	30 sec	**60 sec**	**90 sec**	**30 sec**	**60 sec**	**90 sec**	**30 sec**	**60 sec**	**90 sec**	**30 sec**	**60 sec**	**90 sec**	**30 sec**	**60 sec**	**90 sec**
H_2O	2.6	3.8	6.7	5.2	11.8	19.6	32.2	59.8	89.8	29.3	35.6	30.8	7.3	16.2	22.3
PBS	7.0	14.0	17.4	12.0	20.7	33.0	30.9	56.4	68.3	10.5	8.3	15.5	2.9	8.8	1.5
DMEM	6.4	12.8	16.7	16.9	30.1	43.7	39.9	65.3	76.2	18.9	22.6	37.3	0.0	2.7	0.0
DMEM + FCS	3.6	1.8	4.7	-	-	-	15.4	35.8	46.5	5.6	2.4	6.7	1.1	2.8	4.7
LB	0.6	0.9	1.1	-	-	-	15.6	28.2	37.6	2.1	6.3	6.4	13.2	22.3	12.0

Table 5.1. (Caption overleaf.)

Table 5.1. ***Concentration of spin trap radical adducts measured by EPR.*** Samples were treated for 30, 60 and 90 seconds with the AP-DBD plasma jet and the formation of spin trap radical adducts was assessed by EPR. Values expressed in μM. Single measurements for 30 and 60 seconds, averaged values of triplicate samples treated for 90 seconds. Volume treated: 500 μL for all experiments except DEPMPO (150 μL).

concentration of DMPO-OH and DEPMPO-OH adducts formed in plasma-treated liquids was obtained (**Figure 5.2a,b**). The concentration of DMPO-OH adduct was higher in plasma-treated H_2O, PBS and DMEM than in the nutrient-rich liquids DMEM + 10 % (v/v) FCS and LB after 90 seconds of treatment (**Figure 5.2a**). The formation of the spin adduct DEPMPO-OH was measured only in H_2O, PBS and DMEM to confirm the trend observed for the detection of ·OH radical with DMPO (**Figure 5.2b**). Differences between the levels of spin trap radical adducts formed with DEPMPO and DMPO were due to the differences in the volumes used for experiments (500 µL DMPO solutions and 150 µL DEPMPO solutions), kinetic constants of reaction for each spin trap with ·OH and the stability of the respective radical adducts.

In order to investigate if the pH or the ionic strength of the solutions influenced the levels of DMPO-OH adduct detected in plasma treated liquids, three liquid samples containing 500 µL of 0.1 M DMPO in 0.5x, 1x and 4x PBS were plasma-treated. An increase in the levels of DMPO-OH were observed with increasing ionic strength of the solution (**Figure 5.3a**). The pH of the solution decreased only 0.5 points (post-treatment) in all the three experiments, suggesting that the ionic strength (and not the pH) affected the formation and stability of the DMPO-OH adduct in plasma-treated liquids, or the availability of the radical. To estimate the stability of the spin adduct formed, the decay of DMPO-OH adduct over time was also measured. After 10 minutes post plasma treatment, the concentration of the spin adduct was reduced in 28 % for H_2O and PBS and 50 % for LB (**Figure 5.3b**). The latter was likely due to the high organic and inorganic content of LB medium. However, in all cases only 10 – 15 % decay was observed 5 minutes after treatment, confirming the stability of the spin adduct during the time required to process the samples by EPR after plasma treatment.

2,2,6,6-tetramethylpiperidine (TEMP) was used to measure the amount of ROS in plasma-treated liquids, specifically $O_2(a^1\Delta g)$, O and O_3. Takamatsu *et al.* suggested that 2,2,5,5-tetramethyl-3-pyrroline-3-carboxamide (TPC), an amine with similar structure and properties to TEMP, could be converted into respective nitroxide by various oxidising species (229). Preliminary control experiments demonstrated that superoxide (added as KO_2), hydrogen peroxide or a combination of the two did not produce TEMPO from TEMP. Ozone, however, did oxidise TEMP to TEMPO (Gorbanev *et al.*, unpublished data). Thus, to discriminate between TEMPO formed due to $O_2(a^1\Delta g)$ and ozone/atomic oxygen, sodium azide (NaN_3; a known scavenger of $O_2(a^1\Delta g)$ (21, 229)) was used. The amount of $O_2(a^1\Delta g)$ generated by the AP-DBD plasma jet in liquids was determined from the difference between the EPR measurements of exposed solutions of TEMP and TEMP + NaN_3.

The nutrient-rich liquids DMEM + 10 % (v/v) FCS and LB displayed the lowest levels of TEMPO from $O_2(a^1\Delta g)$ after 90 seconds treatment (6.7 and 6.4 µM, respectively; **Figure 5.2c**).The highest levels of the spin adduct TEMPO from $O_2(a^1\Delta g)$ were obtained in plasma-treated H_2O, DMEM and PBS (30.8, 37.3 and 15.5 µM, respectively). TEMPO formed in the

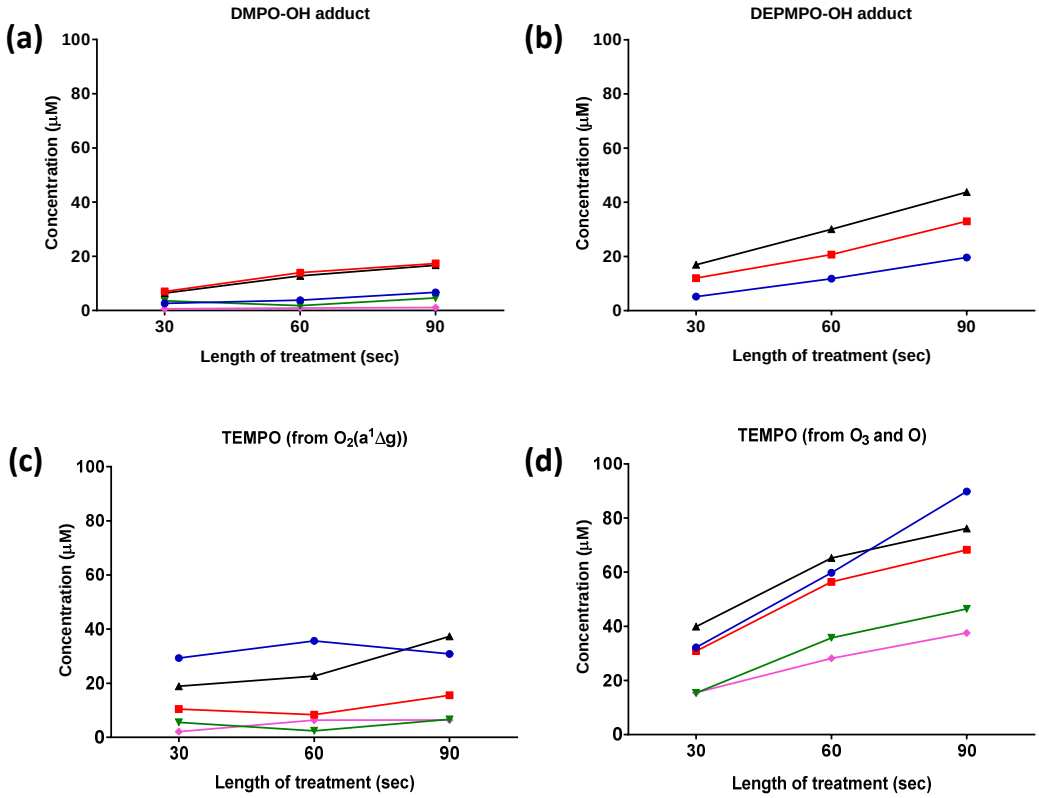

Figure 5.2. ***Detection of oxygen-centred radical adducts in plasma-treated solutions by EPR.*** Experiments to detect the formation of spin trapped radical adducts in 500 µL plasma-treated H_2O (blue), PBS (red), DMEM (black), DMEM + 10 % (v/v) FCS (green) and LB (magenta). Samples were treated for 90 seconds with the AP-DBD plasma jet. **(a)** DMPO-OH adduct; **(b)** DEPMPO-OH adduct; **(c)** TEMPO from reaction with $O_2(a^1\Delta g)$; **(d)** TEMPO from O_3 and O. Data represent single values for 30 and 60 seconds treatments and mean values for 90 seconds treatment ($n \geq 2$). Length of treatment expressed in seconds (sec).

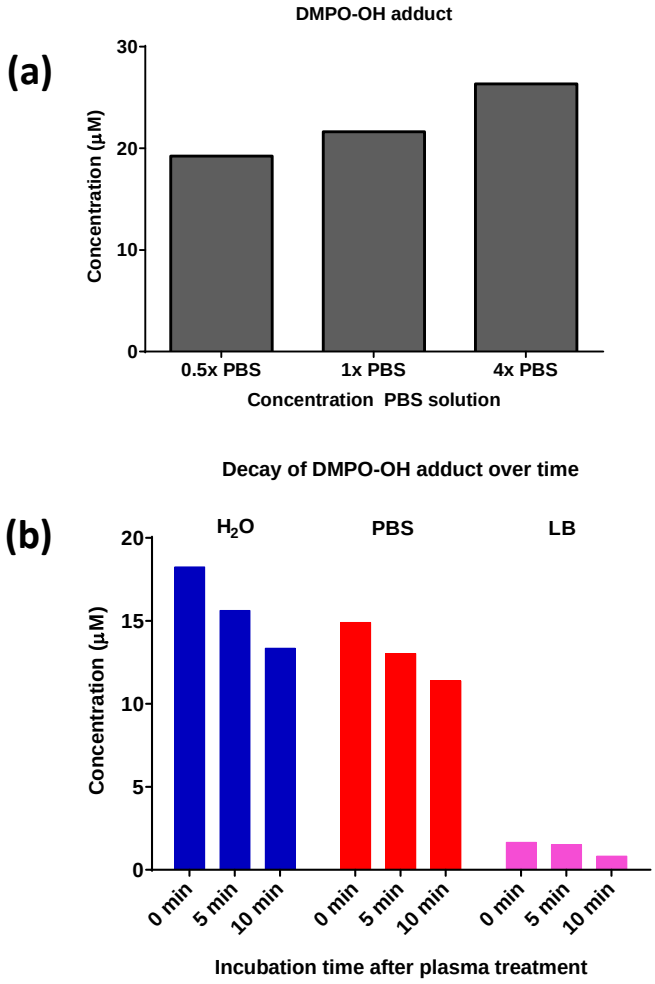

Figure 5.3. ***Features of DMPO-OH formation.*** **(a)** EPR experiments in 500 µL 0.5x, 1x and 4x PBS to determine the effect of the ionic strength on the formation of DMPO-OH adduct. **(b)** Decay of DMPO-OH adduct over time in H_2O (blue), PBS (red) and LB (magenta) measured after 0, 5 and 10 minutes (min) after treatment. Samples were treated for 90 seconds with the AP-DBD plasma jet. Data represent single measurements.

absence of $O_2(a^1\Delta g)$ was ascribed to the reaction of TEMP with ozone and/or atomic oxygen. The combined amount of O and O_3 was estimated from the EPR measurement of TEMP + NaN_3 solutions. Similarly to hydroxyl radical trapping experiments, an increase over time in the levels of TEMPO from O_3/O was observed in all plasma-treated samples (**Figure 5.2d**). The highest levels of TEMPO from O_3/O after 90 seconds treatment where obtained in H_2O, DMEM and PBS (89.8, 68.3 and 76.2 µM, respectively). Similarly to the results observed for TEMPO from $O_2(a^1\Delta g)$, the lowest levels of TEMPO from O_3/O were obtained in the nutrient-rich liquids DMEM + 10 % FCS and LB (46.5 and 37.6 µM, respectively). Although sodium azide is often described as a specific $O_2(a^1\Delta g)$ quencher, it was reported to react with ozone under basic conditions (233). The solutions of TEMP used were at pH 12 (due to TEMP dissolution), and thus it was possible that the amount of TEMPO formed with the additions of sodium azide in the reaction mixture would not be representative of the real concentration of ozone present in the sample due to the enhanced ozone decay observed in solutions with alkaline pH.

To determine if TEMP could trap ROS at physiological pH, 100 mM TEMP solutions prepared in H_2O and PBS were adjusted to pH 7 using phosphoric acid and treated with the AP-DBD plasma jet for 30, 60 and 90 seconds, with and without sodium azide for the detection of $O_2(a^1\Delta g)$. No TEMPO was detected under these conditions (0 µM detected in all samples). These results suggest that at pH 7 TEMP may be protonated, preventing its interaction with ROS. Therefore, it was not possible to determine the formation of ROS at physiological pH using this approach.

The results presented here suggest that the levels of ROS in liquids decreased when organic molecules were present in the plasma-treated solutions and that the ionic strength of the solution can influence the availability of plasma-generated ·OH upon plasma treatment. The generation of ROS in plasma-treated liquids demonstrated a build up with increasing treatment times, as most of the species measured here increased with longer plasma treatments. However, the levels of O, $O_2(a^1\Delta g)$ and O_3 trapped in plasma-treated liquids should be carefully interpreted, as sodium azide could affect the concentrations of ozone in the samples and therefore the concentration of TEMPO formed.

5.2.2 Formation of NO species was independent of the presence of organic molecules

The $(MGD)_2$-Fe^{2+} complex, a NO spin-trapping reagent was used for the detection of NO and NO_2^- in plasma-treated liquids (234). Results demonstrated that the levels of the $(MGD)_2$-Fe^{2+}-NO complex were higher in samples treated for 60 seconds and then decreased in all samples treated for 90 seconds, except H_2O (**Figure 5.4a**). H_2O and LB possessed the highest levels of $(MGD)_2$-Fe^{2+}-NO complex after 60 seconds of plasma treatment (16.2 and 22.3 µM, respectively). The two solutions do not exhibit buffering properties, but do have different ionic strengths. Experiments where the $(MGD)_2$-Fe^{2+} complex was added after 60 seconds of plasma

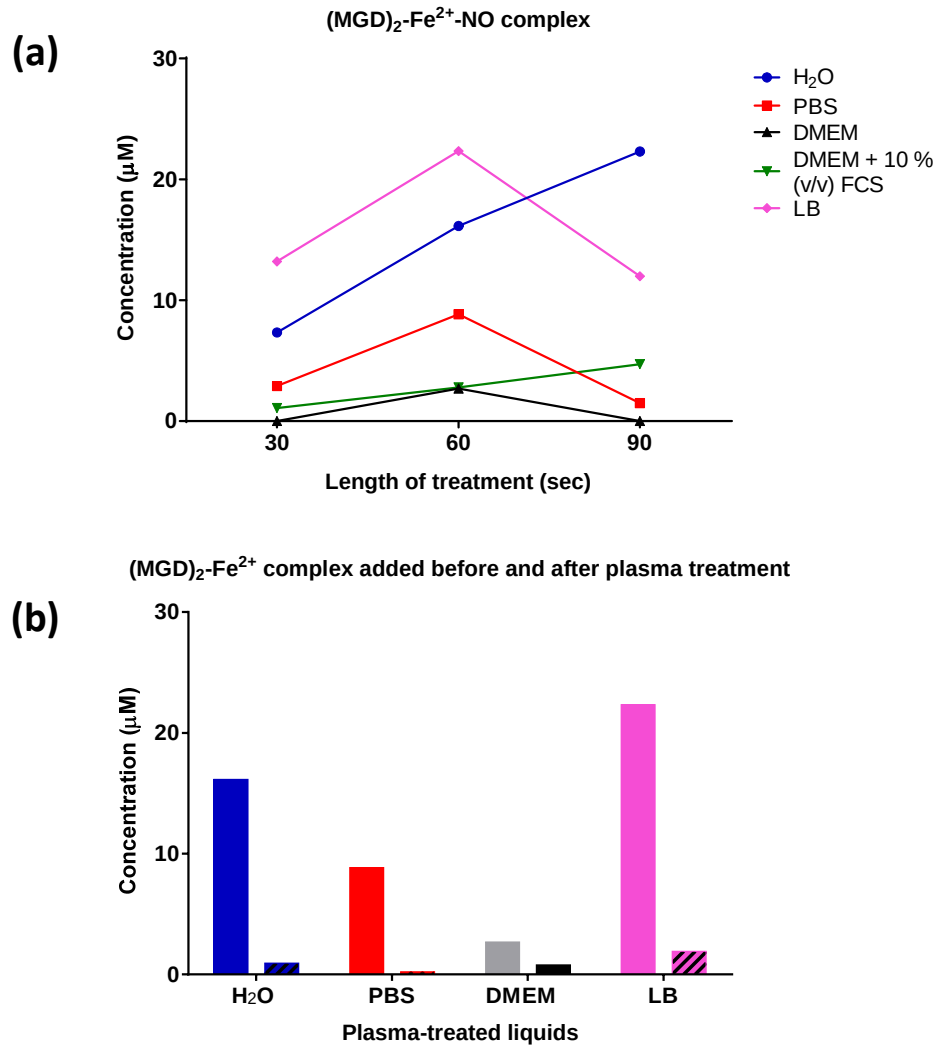

Figure 5.4. ***Detection of NO and NO_2^- by EPR in plasma-treated solutions.*** **(a)** Experiments to detect the formation of $(MGD)_2$-Fe^{2+}-NO complex for NO· and NO_2^-. in 500 µL plasma-treated H_2O (blue), PBS (red), DMEM (black), DMEM + 10 % (v/v) FCS (green) and LB (magenta). Samples were treated for 90 seconds with the AP-DBD plasma jet. Data represent single values for 30 and 60 seconds treatments and mean values for 90 seconds treatment ($n \geq 2$). **(b)** Comparison of the formation of the $(MGD)_2$-Fe^{2+}-NO complex when $(MGD)_2$-Fe^{2+} complex was added before (solid bars) or after (pattern-filled bars) 60 seconds plasma treatment. Data represent single measurements. Length of treatment expressed in seconds (sec).

treatment showed a reduced level of $(MGD)_2$-Fe^{2+}-NO complex compared to the values obtained when the $(MGD)_2$-Fe^{2+} complex was added prior to plasma treatment (**Figure 5.4b**).

These results demonstrate that the concentration of $(MGD)_2$-Fe^{2+}-NO complex in plasma-treated samples was reduced in buffered solutions, especially in those with high concentration of organic molecules, but the reduction of the pH of the plasma-treated solutions contributed to the formation of $(MGD)_2$-Fe^{2+}-NO complex in non-buffered solutions, even in the presence of high organic content (H_2O and LB; **Figure 5.4a**). Here, however, $(MGD)_2$-Fe^{2+} complex could react with nitrite anion, thus increasing the amount of $(MGD)_2$-Fe^{2+}-NO complex measured (234). Therefore, the decrease observed in $(MGD)_2$-Fe^{2+}-NO complex in liquids treated for 90 seconds or samples where $(MGD)_2$-Fe^{2+} complex was added after plasma treatment suggested that $(MGD)_2$-Fe^{2+} complex interacted predominantly with NO and not NO_2^-. Alternatively, NO_2^- anion introduced into liquid sample during plasma treatment underwent further oxidation to NO_3^- during plasma exposure. Either of these would result in reduced amount of detected adduct when the $(MGD)_2$-Fe^{2+} complex was added after the treatment. In other words, there is no direct evidence that NO radical was detected by this method in these experiments. This does not imply that NO radical was not present in the liquid; in fact, its introduction explains the presence of nitrite anion. However, when introduced into the liquid sample, nitric oxide could potentially be completely converted into nitrite *via* interaction with water (which is in large excess to the spin-trapping complex) and oxygen species. However, the results obtained here do not allow the exclusion of the participation of NO radical in the formation of adducts.

5.3 IDENTIFICATION OF RNOS BY COLORIMETRY

NO and H_2O_2 can cross membranes and diffuse between and within cells and give rise to more reactive free radicals to attack bacterial cells (21). The detection of NO· is often achieved by the indirect measurement of its further oxidation product NO_2^- (235) or in combination with NO_3^- (236), whereas H_2O_2 can be directly detected in liquids (139). To determine the presence of NO_2^- and H_2O_2 in plasma-treated solutions, the Griess assay and titanium(IV) oxalate were used. The formation of an azo dye and titanium(IV)-hydrogen peroxide complex for the detection of NO_2^- and H_2O_2 respectively was assessed colorimetrically by UV-Vis spectrophotometry in liquids after plasma treatment (described in Section 2.8). Samples were prepared and plasma-treated as described in Section 2.8.1. Experiments were carried out using the final version of the AP-DBD plasma setup housed in the plastic box, as described in Chapter 3. The concentrations of titanium(IV)-peroxide complex and azo dye measured are presented in **Table 5.2**.

5.3.1 Nutrient-rich solutions presented higher levels of NO_2^-

The presence of NO_2^- in plasma-treated liquids was assessed with the Griess assay to indirectly detect NO radical and the toxic NO_2^- itself, as described in Section 2.8.3. The detected azo dye

	Azo dye (NO_2^-) (µM)			Titanium(IV) – peroxide complex (µM)		
	30 sec	**60 sec**	**90 sec**	**30 sec**	**60 sec**	**90 sec**
H_2O	2.6	2.7	4.1	6.0	20.5	41.1
PBS	1.2	1.7	1.7	12.1	17.0	21.0
DMEM	4.2	10.9	14.8	25.7	57.5	74.5
DMEM+FCS	4.7	9.4	17.1	0.0	12.4	60.8
LB	6.9	12.3	20.4	25.8	44.1	83.9

Table 5.2. ***Measurement of NO_2^- and H_2O_2 by colorimetry.*** Results of UV-Vis spectrophotometric experiments to detect the formation of Azo dye and titanium(IV) – peroxide complex for the identification of NO_2^- and H_2O_2 in plasma-treated solutions, respectively. Measurements done by colorimetry after plasma treatment with the AP-DBD plasma jet. Concentration expressed in µM. Single measurements for 30 and 60 seconds, averaged values of triplicates for 90 seconds treatments. Volume treated: 500 µL for all the experiments.

was formed in plasma-treated liquids as the consequence of the reaction of NO_2^- and Griess reagent. Results demonstrated a time-dependent increase in the concentration of the azo dye formed in all plasma-treated samples when Griess reagent was added after plasma treatment (**Figure 5.5a**). After 90 seconds of treatment, the highest levels were observed in the nutrient-rich liquids LB, DMEM + 10 % (v/v) FCS and DMEM (20.4, 17.1 and 14.8 µM, respectively). Levels below 5 µM were observed in H_2O and PBS (4.1 and 1.7 µM, respectively).

Griess reagent was also added to the liquids prior to plasma treatment to investigate the possibility of detecting NO_2^- during treatment with this method. Results demonstrated that higher levels of azo dye were detected in H_2O and PBS using this approach (**Figure 5.5b**). However, the signal obtained increased with reaction time. Here, Griess reagent was present in the liquids during plasma treatment which adds to the total reaction time. Additionally, some of the Griess reagent, or even the azo dye, was likely degraded by the plasma-generated species. Thus, the addition of Griess reagent prior to plasma treatment might not be useful for the *in situ* determination of NO_2^-. Nevertheless, the main contribution to the increased levels of azo dye was likely due to the increased amount of reactive NO_2^- which decreases after exposure, similar to what was described above for $(MGD)_2$-Fe^{2+} complex and NO (Section 5.2.2).

These results demonstrate that plasma-treated nutrient-rich liquids presented higher levels of NO_2^- than H_2O and PBS. This suggests the oxidation of NO_2^- to NO_3^- occurred at lower rates in the nutrient-rich media, or that the by-products of transformed organic components in these media also contributed to the levels of azo dye detected.

5.3.2 H_2O_2 was increased in plasma-treated nutrient-rich solutions

The presence of H_2O_2 in plasma-treated liquids was quantitatively determined using the titanium(IV) oxalate method (139) as described in Section 2.8.2. Samples exposed to the AP-DBD plasma jet presented a time-dependent increase in the concentration of the titanium(IV)-hydrogen peroxide complex. After 90 seconds of plasma treatment, the highest levels were obtained in LB, DMEM and DMEM + 10 % (v/v) FCS (83.9, 74.5 and 60.8 µM, respectively). The lowest levels were obtained in H_2O and PBS (41.1 and 21 µM, respectively) (**Figure 5.6a**). The levels of titanium(IV)-peroxide complex decreased approximately 50 % in plasma-treated H_2O 30 minutes after plasma treatment, in contrast to a decrease of 30 % in plasma-treated LB (**Figure 5.6b**).

Potentially, organic components of the nutrient-rich media could undergo chemical transformations and form peroxo-compounds or contribute to the formation of H_2O_2 by the reaction of O_3 with lipids (21). Therefore, catalase (a specific H_2O_2 scavenger enzyme) was added to plasma-treated DMEM and LB to a final concentration of 32 U/mL and 100 U/mL to confirm the specificity of the assay to detect H_2O_2. Results showed that the addition of the enzyme reduced (and with 100 U/ml, abrogated) the amount of titanium(IV)-peroxide complex detected, demonstrating the specificity of the reaction (**Figure 5.6c**).

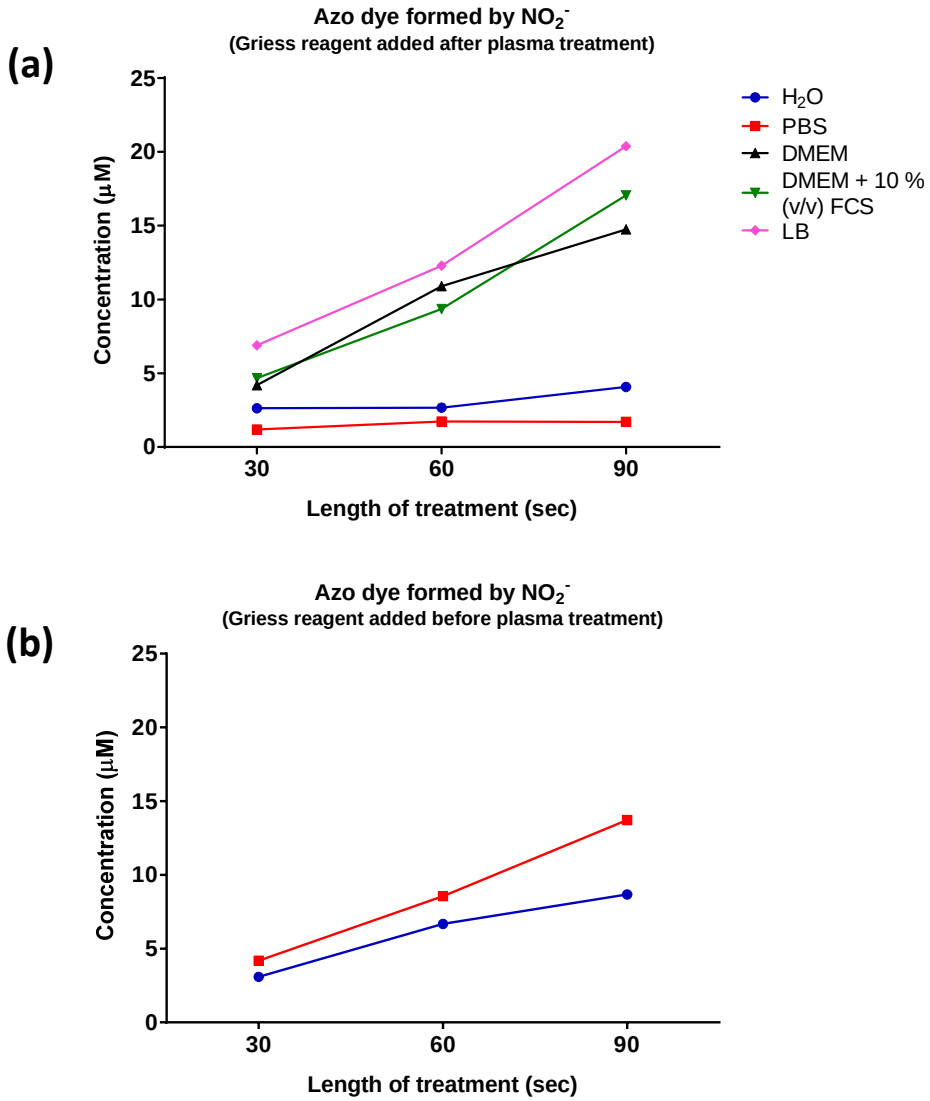

Figure 5.5. ***Detection of NO_2^- by colorimetry.*** Experiments to assess the formation of azo dye formed by the reaction of NO_2^- with Griess reagent. **(a)** NO_2^- measured with Griess reagent added after plasma treatment and **(b)** measured with Griess reagent added before plasma treatment. 500 µL plasma-treated H_2O (blue), PBS (red), DMEM (black), DMEM + 10 % (v/v) FCS (green) and LB (magenta). Samples treated for 90 seconds with the AP-DBD plasma jet. Data represent single values for 30 and 60 seconds treatments and mean values for 90 seconds treatment ($n \geq 2$). Length of treatment expressed in seconds (sec).

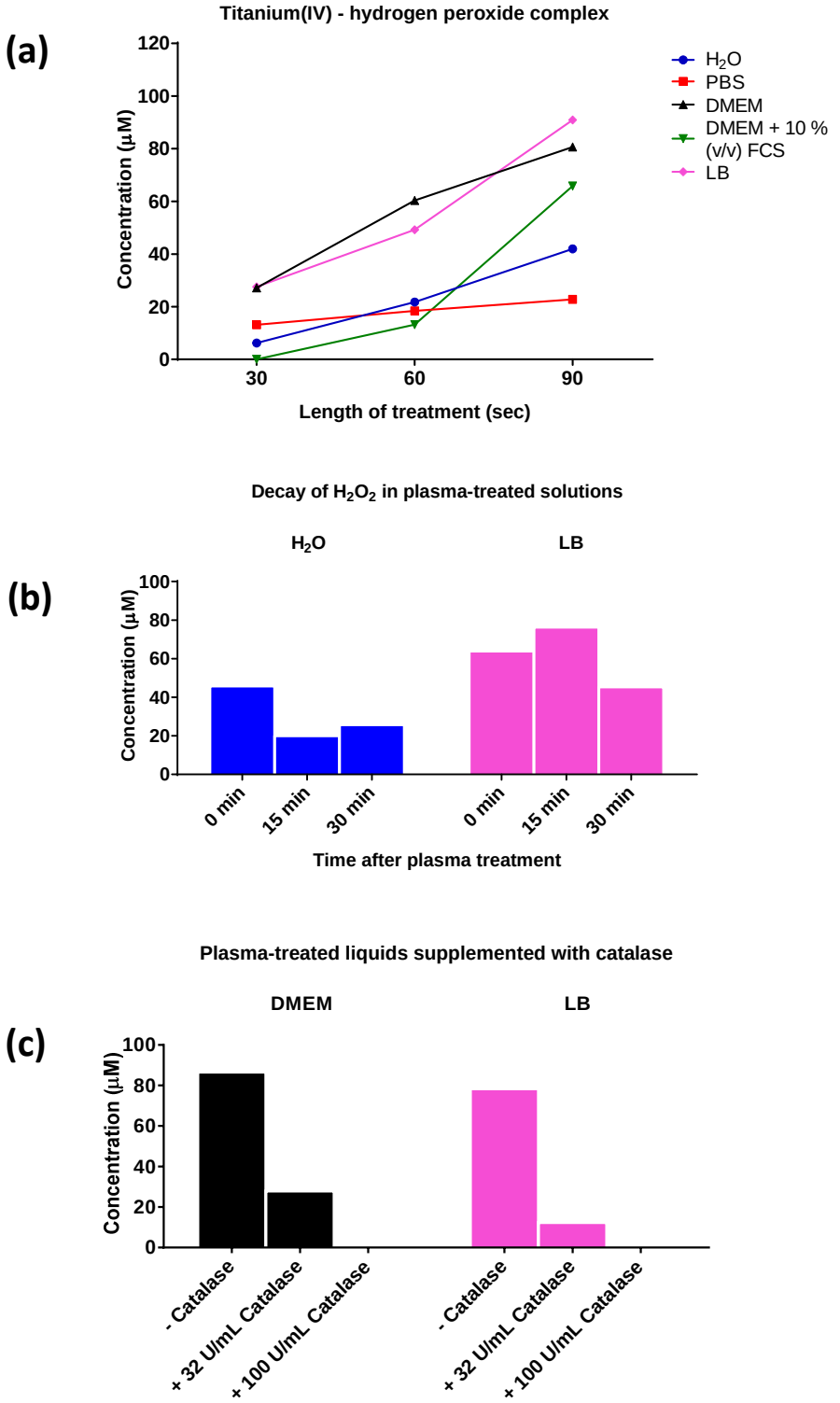

Figure 5.6. ***Measurement of H_2O_2 in plasma-treated liquids, stability and specificity of the reaction.*** Colorimetric experiments to quantify H_2O_2 by the reaction with titanium(IV). **(a)** titanium(IV)-hydrogen complex formed in plasma-treated H_2O, PBS, DMEM, DMEM + 10 % (v/v) FCS and LB. **(b)** Decay of H_2O_2 after 0, 15 and 30 minutes of plasma treatment in H_2O and LB. **(c)** Plasma-treated DMEM and LB supplemented with catalase after treatment for the detection of H_2O_2. 500 µL of each solution treated for 90 seconds with the AP-DBD plasma jet. Data represent single measurements.

The performed experiments indicated that plasma-treated nutrient-rich liquids possessed higher levels of H_2O_2 than H_2O and PBS, suggesting the participation of nutrients in the formation of secondary ROS in liquids. In addition, the specificity of the method to detect H_2O_2 and not possible organic peroxides formed in the plasma-treated solutions was demonstrated, as the addition of catalase to the samples abrogated the detection of H_2O_2.

5.4 EFFECT OF EXTERNAL ORGANIC MOLECULES DURING BACTERICIDAL LTP TREATMENT

The bactericidal action of low temperature plasmas in liquid suspensions has been demonstrated in planktonic cultures and solid surfaces (44, 237-240). However, it is unclear whether the bactericidal action of LTPs is affected by organic molecules present in the surroundings of the sample during treatment. The experiments described in Section 5.2 and 5.3 for the detection of RNOS in plasma-treated liquids demonstrated that the presence of nutrients during treatment affected the levels of RNOS measured. It would be expected then that plasma treatments of bacteria in nutrient-rich solutions were less effective.

To understand the effect of external biomolecules on the bactericidal activity of the AP-DBD plasma jet, three approaches were taken. In the first place, the reduction of colony forming units (CFU) in bacterial suspensions was assessed. In the second place, the damage to the cell membrane was assessed by flow cytometry, using the Live/Dead Assay immediately after treatment. Lastly, the addition of scavengers to agar plates prior to plasma treatment was tested to indirectly determine the contribution of reactive oxygen species delivered by the plasma towards bacterial elimination.

5.4.1 Organic molecules present during treatment reduced bactericidal action of plasma

In the previous section, experiments demonstrated that the presence of nutrients affected the amount of RNOS found in plasma-treated solutions. To determine the effect of such RNOS on bacteria, *S.* Typhimurium suspensions were treated with the AP-DBD plasma jet and the reduction of CFU after treatment was assessed, as described in Section 2.5.2. Bacterial suspensions were prepared using the same solutions analysed by EPR and UV-Vis spectroscopy and exposed to the AP-DBD plasma jet, as described in Section 2.5.1. The number of CFU surviving the plasma treatment was quantified and analysed considering the RNOS measured in plasma-treated liquids.

These experiments demonstrated a statistically significant difference in the number of CFU found with plasma-treated and untreated samples in H_2O and PBS, as demonstrated by the analysis with one-way ANOVA ($P<0.0001$; **Figure 5.7**). Bacteria in H_2O presented a 1.5-log reduction after plasma treatment, which corresponds to a percent reduction between 90 and 99 %. Plasma-treated bacteria in PBS presented a 3.5-log reduction, corresponding to a percent

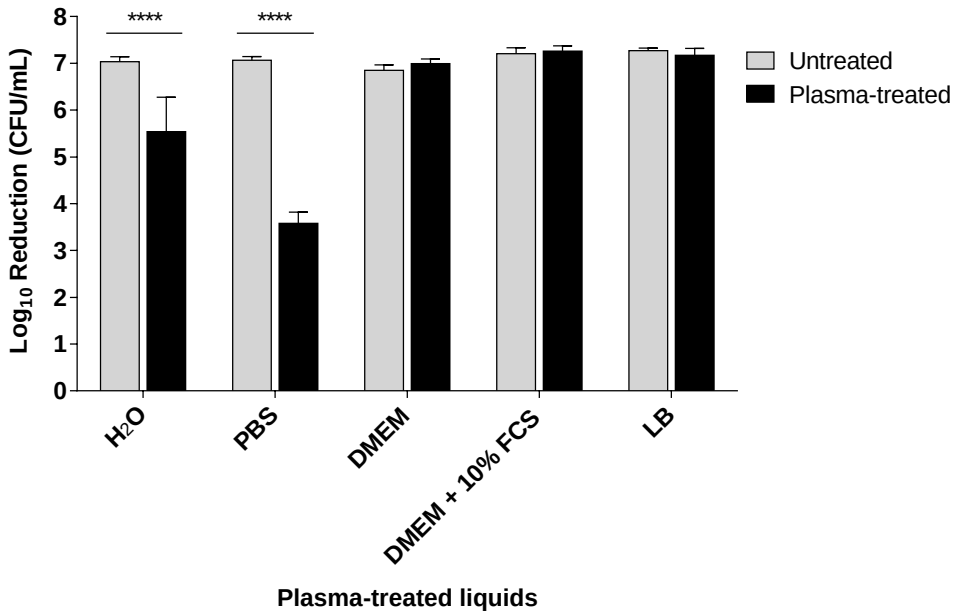

Figure 5.7. ***Log$_{10}$ reduction of CFU in plasma-treated bacterial suspensions in the presence of organic molecules.*** *S.* Typhimurium suspended in 500 µL H_2O, PBS, DMEM, DMEM + 10 % (v/v) FCS and LB were treated with the AP-DBD plasma jet for 90 seconds. Data presented as Log_{10} reduction (CFU/mL) of two independent experiments ($n \geq 4$). ****: $P<0.0001$.

reduction between 99.9 and 99.99 %. The number of CFU recovered from samples in nutrient-rich media exposed to plasma were similar to those found in the corresponding untreated samples.

The results of these experiments suggest that the bactericidal activity of the AP-DBD plasma jet was reduced in the presence of nutrients, as no decrease in the bacterial load was achieved in bacteria treated in nutrient-rich solutions. In contrast, more than 99 % of bacteria exposed to plasma in PBS and 90 % of those exposed in H_2O were eliminated, respectively.

5.4.2 Plasma treatment in the presence of organic molecules induced non-lethal membrane damage in *Salmonella*

The Live/Dead Assay is a method used to determine cell viability in bacteria that relies on the integrity of the cell membrane to prevent the passage of the membrane-impermeable propidium iodide (PI) inside the cells. The dye can access the cytoplasmic space to stain nucleic acids only when the cell membrane presents damage to a degree that allows the diffusion of PI molecules. This method was used here to determine the damage induced by the AP-DBD plasma jet in the bacterial cell membrane of *S.* Typhimurium in liquid suspensions in the presence of nutrients. Samples were prepared and treated with the plasma jet as described in Section 2.5.1. Bacterial cells were stained with a mixture of the nucleic acid stains green-fluorescent SYTO9 dye (that always enters the cell and therefore stain both live and dead cells) and red-fluorescent membrane-impermeant PI (that stain only cells with compromised membrane integrity and dead cells). The Live/Dead assay was performed as described in Section 2.5.3.

The flow cytometry gating strategy used for the analysis of plasma-treated bacterial suspensions is described in **Figure 5.8a** where the positive control of membrane damage (heat-inactivated bacteria) is presented as an example. Samples were gated from SSC/FSC plot. The frequency of bacteria with damage to the cell membrane were calculated from PI/SYTO9 dot plot and presented as the percentage of cells gated from SSC/FSC plots. Three populations of cells were identified: cells with no damage (right gate) with a dominating SYTO9 stain; cells with intermediate damage (middle gate) that are stained with similar levels of PI and SYTO9; and cells with high damage to the cell membrane (left gate), where PI dominates the stain. Each of the five bacterial suspensions used for this experiment presented a characteristic distribution in the plots. Therefore, the gates in PI/SYTO9 plots were adjusted according to the characteristics of the distribution of each population (**Figure 5.8b**).

Results showed that untreated bacterial samples in H_2O suspension presented a statistically significant difference in the percentage of cells with membrane damage than in those treated in PBS and nutrient-rich solutions, as demonstrated by the analysis with one-way ANOVA

($P<0.0001$; **Figure 5.8c**). Bacteria suspended in PBS and DMEM treated with the AP-DBD plasma jet presented a decrease in the percentage of cells with no damage to the cell membrane when compared to the corresponding untreated samples ($P<0.05$ and $P<0.0001$, respectively;

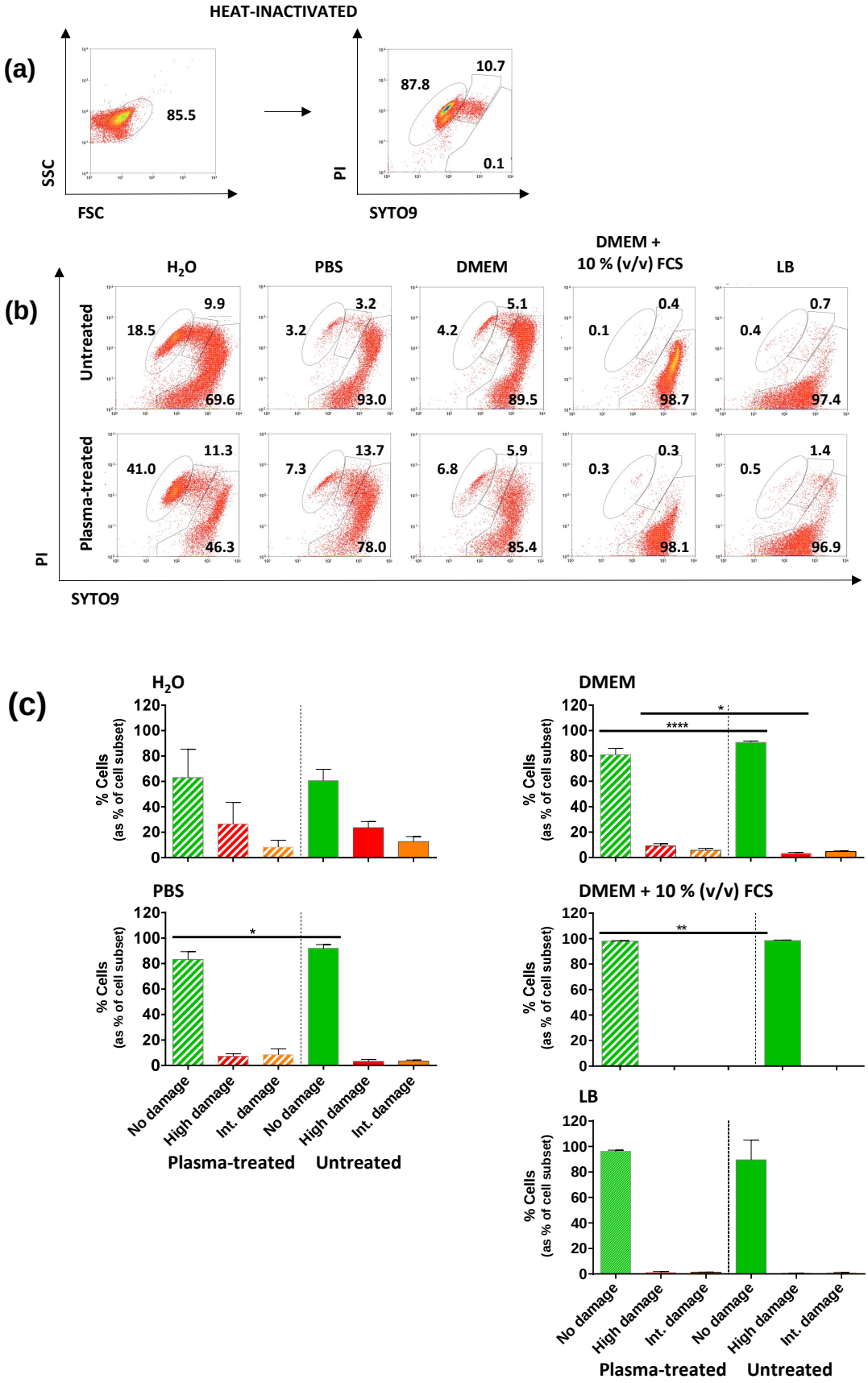

Figure 5.8. (Caption overleaf.)

Figure 5.8. ***Nutrient-rich media ameliorated the damage induced to the cell membrane of S. Typhimurium by plasma.*** Five hundred microliters of each liquid containing approximately 0.8 x 10^7 CFU were treated with the AP-DBD plasma jet for 90 seconds. Bacterial cells were stained with SYTO9 and PI. **(a)** Flow cytometry gating strategy for the analysis of membrane damage in plasma-treated *S.* Typhimurium. ***Left:*** SSC/FSC gate. ***Right:*** Dot plot showing the gating of heat-inactivated bacterial cells presenting intact membrane (right gate), intermediate damage (middle gate) and high damage (left gate). **(b)** PI/SYTO9 dot plots for untreated and plasma-treated *S.* Typhimurium in H_2O, PBS, DMEM, DMEM + 10 % (v/v) FCS and LB. Gate numbers in the plots represent frequency of cells as a percentage of the indicated population gated from SSC/FSC plots. Data from one of three biological replicates are shown, representative of two independent experiments. **(c)** Quantification of the three populations of cells shown in **(b)**. Data presented as mean + S.D. ****: P<0.0001; **: P<0.01; *: P<0.05.

Figure 5.8c). A corresponding increase in the percentage of cells with high and intermediate damage to the cell membrane was observed in plasma-treated cells, but a statistically significant difference was only observed for bacteria in DMEM ($P<0.05$). A statistically significant difference was also observed between plasma-treated and untreated bacteria in DMEM + 10 % (v/v) FCS ($P<0.01$). However, this did not translate into an increase in the percentage of cells with intermediate and high damage to the cell membrane.

In general, the percentages of untreated bacteria with no membrane damage was the highest in samples in nutrient-rich solutions, as expected. Membrane integrity was compromised in samples suspended in H_2O and to a lesser extent in PBS due to the osmotic pressure in H_2O and lack of nutrients. In the same way, few or no bacterial cells with damaged cell membranes were observed in nutrient-rich bacterial suspensions. A statistically significant decrease in the percentage of cells without membrane damage after plasma treatment was observed in bacteria suspended in PBS, DMEM and DMEM + 10 % (v/v) FCS. The statistical significance of the difference observed in bacteria treated in DMEM + 10 % (v/v) FCS could be due to the small SD in these samples (mean ± SD: 98.6±0.3 % untreated bacteria vs. 98.0±0.3 % plasma-treated bacteria).

These results suggest that the presence of nutrients during plasma treatment reduced the levels of membrane damage in *S.* Typhimurium caused by plasma treatment. The reduction of the percentage of cells with intact membrane achieved in the buffered solutions PBS, DMEM and DMEM + 10 % (v/v) FCS does not correspond to bacterial elimination, since only *S.* Typhimurium treated with the plasma in the presence of PBS were killed, as observed in Section 5.4.1.

5.4.3 H_2O_2 produced in the gas phase participated in bacterial elimination

Antioxidant enzymes can confer protection from oxidative stress to bacteria. The specificity of these enzymes for their substrate is used to establish the involvement of the substrate in a particular biological process (21). For example, if catalase inhibits or reduces bacterial elimination, it is assumed that H_2O_2 is involved in this process. This principle could be applied to antioxidant enzymes and compounds, such as superoxide dismutase (SOD) and D-Mannitol, known scavengers of $O_2^{\cdot -}$ and $^{\cdot}OH$, respectively.

To determine the participation of H_2O_2, $O_2^{\cdot -}$ and $^{\cdot}OH$ in bacterial elimination caused by plasma treatments, LB agar plates were supplemented with 2000 U Catalase/plate, 400 U SOD/plate and 20 mM D-Mannitol/plate, respectively. All agar plates treated with the AP-DBD plasma jet presented a zone of inhibition with the same area (1590 mm^2) (**Figure 5.9**). Plates supplemented with SOD presented a similar number of CFU in the zone of inhibition (269 CFU) to the plates exposed to plasma without the addition of scavengers (270 CFU; **Figure 5.9a,e**). Plates supplemented with catalase prior to plasma treatment presented an increase in the number of CFU that survived the treatment in the zone of inhibition (> 400 CFU; **Figure 5.9b**). The

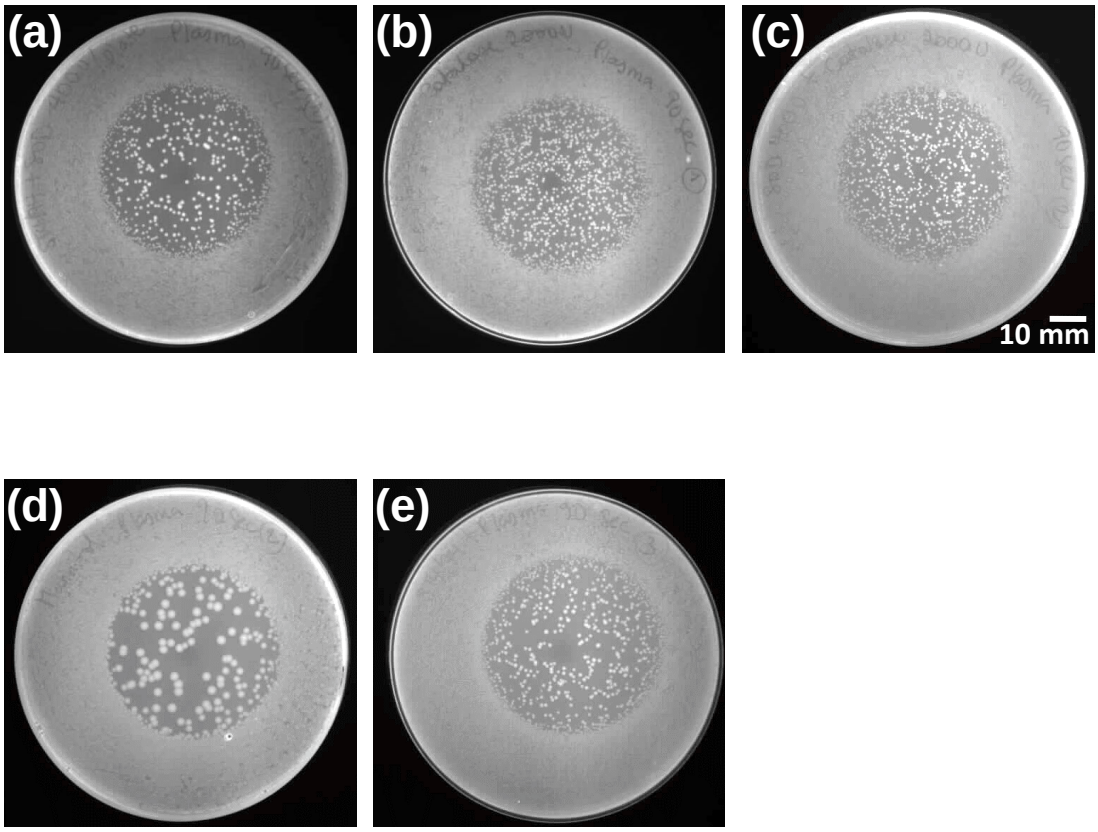

Figure 5.9. ***Effect of scavengers on plasma treatment of agar plates.*** Representative agar plates with *S.* Typhimurium treated with the AP-DBD plasma jet. Plates supplemented with **(a)** 400 U SOD/plate; **(b)** 2000 U catalase/plate; **(c)** 400 U SOD and 2000 U Catalase/plate; **(d)** 20 mM D-Mannitol; **(e)** without scavengers. Scavengers were added to agar plates prior to the addition of bacteria for treatment. Plates were exposed to plasma for 90 seconds. Scale bar 10 mm.

combined addition of SOD and catalase to agar plates did not further improve the survival of *S.* Typhimurium to plasma treatment (**Figure 5.9c**). The colonies present on plates supplemented with catalase were smaller than those present in plates treated without scavengers. In contrast, plates supplemented with D-Mannitol presented bigger colonies, but fewer in number compared to plates treated without scavengers (118 CFU; **Figure 5.9d,e**).

These results suggest that the addition of catalase to agar plates improved the survival of *S.* Typhimurium to plasma treatment. SOD did not improve the survival of bacteria to plasma treatment and did not provide additional protection when present in combination with catalase. Also, D-mannitol did not contribute to the survival to treatment, as plates supplemented with this scavenger presented less CFU in the zone of inhibition than plates without scavengers. In addition, D-mannitol could act as an additional source of nutrients since *Salmonella* can metabolize this sugar (241), which could explain the increased size of the surviving colonies in the kill zone. Thus, the amount of $O_2^{\cdot -}$ and ·OH delivered to bacterial cells might not be sufficient to be detected by this method. The participation of other RNOS produced by the plasma such as NO, O, $O_2(a^1\Delta g)$, among others in the gas phase not assessed here could contribute to the bactericidal activity observed.

5.5 DISCUSSION

The aim of this chapter was to determine the effect of organic molecules during plasma treatment on the amount of RNOS available and to investigate whether their presence during plasma treatment reduced the ability of the AP-DBD plasma jet to eliminate bacteria. For this purpose, two approaches were taken: **(a)** a chemical approach to identify the short- and long-lived species formed in plasma-treated liquids; **(b)** a biological approach to determine whether the antibacterial action of plasma was affected by the presence of organic molecules. With this combined approach, the role of interfering agents during plasma treatment (such as organic molecules and salts) was determined for elimination of *S.* Typhimurium in liquid environments.

The results presented here suggest that short-lived ROS formed in plasma-treated liquids interacted with the organic matter in nutrient-rich media and therefore, could mediate the bactericidal action of plasmas observed in plasma-treated *S.* Typhimurium. More than 90 % and 99% of bacteria in H_2O and PBS, respectively, exposed to the AP-DBD plasma jet for 90 seconds were eliminated. The EPR results for the analysis of plasma-treated liquids demonstrated that solutions with the highest content of organic matter presented the lowest levels of O/O_3, $O_2(a^1\Delta g)$ and ·OH (Section 5.2.1). Interestingly, the concentration of ·OH was higher in PBS and DMEM than in water. This could be due to the presence of salts that provide buffering in these liquids that could favour the formation of additional hydroxyl radicals, as suggested by Tresp *et al.* (231). An increase in the ·OH formed in DMEM supplemented with FCS was masked by the reaction of ·OH with the abundant organic matter present in the

solution. This increase in the amount of ·OH radical available in plasma-treated PBS could contribute to the bactericidal action of this liquid.

It has been demonstrated that the AP-DBD plasma jet used for this study generates a significant amount of O_3 in the gas phase, and this reactive species was also found to be abundant in plasma-treated liquids. This indicates that part of the O_3 formed in the gas phase is effectively delivered to the liquid. O_3 reacts with proteins, DNA and lipids in solution (as in culture media shown here) and in biological systems and could mediate the damage inflicted to bacterial cells exposed to plasma. However, in reaction with lipids, O_3 can generate H_2O_2 (83). Considering that the H_2O_2 found in plasma-treated water originates in the gas phase (Gorbanev *et al.*, unpublished data), the reaction of O_3 with lipids in nutrient-rich solutions could explain the increase in the amount of H_2O_2 measured for these solutions (Section 5.3.2). In fact, this could explain the reduced bactericidal effect of plasma-treated *S.* Typhimurium observed in suspensions with high organic content, where part of the toxic O_3 delivered to the liquids led to the formation of H_2O_2 at concentrations that did not affect the viability of bacterial cells. This could be due to the effective and redundant detoxifying mechanisms that *S.* Typhimurium possess against peroxides, which contributes to the survival of cells under oxidative stress (80).

The results presented here could explain the findings of Sears *et al.*, who described an increase in the amount of H_2O_2 in plasma-treated DMEM with increasing treatment time and voltage (242), as the formation of peroxides in the liquid could contribute to the amounts of H_2O_2 detected. In addition, Nosenko *et al.* reported that *E. coli* in PBS suspensions required shorter treatments with a plasma torch to achieve 100% elimination than *E. coli* in LB suspension (203). However, the authors attributed the bactericidal action to the synergistic activity of NO and H_2O_2. The results presented here provide a new interpretation of the data presented by Nosenko *et al.*, suggesting that the reduced bactericidal action in plasma-treated LB could be a consequence of the reduction of O_3 in the liquid and the associated increase in the concentration of H_2O_2 is not relevant for the induction of bacterial cell death.

Opposite to what was found for ROS, the amount of NO/NO_2^- detected by EPR during plasma treatment of liquids was independent of the presence or absence of organic molecules in the solution during treatment (Section 5.2.2). However, it was highest in solutions without buffering properties, suggesting that the acidification of the solution contributes to the formation and stability of RNS. Plasma-treated water has been reported to acidify upon plasma treatment (116, 243). Lukes *et al.* attributed the bactericidal action of plasma treatment of *E. coli* to the acidification of the plasma-treated liquid and corresponding increase of nitrogen-centred species in acidified solutions (220). In addition, the authors indicated that the participation of O_3 in bacterial elimination was negligible. In contrast to this publication, the results obtained here support the participation of ROS in bacterial elimination, especially O_3 and ·OH, and under the conditions used here, the presence of nitrogen-centred species measured were not related to

bacterial cell death. Other biologically relevant species such as peroxinitrite (53, 220) that are known to induce significant damage to biomolecules were not assessed in the present work and could also participate in the elimination of bacteria. However, the amount of RNOS measured in the liquid corresponds to more complex chemical reactions that occur upon interaction of plasma and liquids. Factors such as the pH, ionic strength, presence of organic matter and interaction with other RNOS in the solution determine the formation and degradation of reactive species that affect the total amount available to interact with the spin trap or bacteria.

The multiple RNOS generated during plasma treatment of liquids can attack various cell targets in bacteria. One of the mechanisms of action that contribute to bacterial elimination induced by LTPs is damage to the cell membrane, the first barrier that protects the cells from external insults such as oxidative stress (244). LTP treatment of bacterial cells have demonstrated to induce etching (104), lipid peroxidation (44) and damage to the cell membrane (245). Short treatments of up to 30 seconds with a nonthermal plasma induced membrane permeability in *Pseudomonas aeruginosa* and *Candida albicans* deposited on membranes, as demonstrated by fluorescence microscopy (14). Using a similar approach, Dolezalova *et al.* demonstrated that an argon plasma jet induced membrane damage in *E. coli* exposed to plasma for 45 minutes in water suspensions, also by fluorescence microscopy (71). Although fluorescent microscopy is a very useful technique, it is difficult to obtain quantifiable data. Here, the Live/Dead assay was used in combination with flow cytometry to quantify the percentage of cells with or without cell membrane damage in plasma-treated bacteria in the presence or absence of organic molecules. The experiments demonstrated a reduction in the percentage of viable bacteria with intact cell membrane when treated in PBS, DMEM and DMEM + 10 % (v/v) FCS. These three solutions possess buffering properties, but whereas the long-lived species H_2O_2 and NO_2^- were detected in higher concentrations in the nutrient-rich solutions, PBS was rich in short- and long-lived ROS. Thus, a direct correlation between the RNOS detected in plasma-treated liquids and membrane damage in these three solutions cannot be determined. However, the acidification of the plasma-treated solutions would not be responsible for the bactericidal properties of LTPs on planktonic cultures as suggested by other authors (220, 246), since the highest bactericidal action was observed in PBS.

It is interesting to notice that the reduction in cell membrane integrity in plasma-treated bacteria in nutrient-rich solutions did not correlate with bacterial elimination, as more than 99 % of cells treated in such solutions recovered from treatment, as described above. In the case of cells treated in PBS, a reduction in the percentage of viable bacteria with intact cell membrane was followed by the elimination of more than 99 % of treated cells. These results are comparable, since bacteria was cultured in LB and prior to experiments, bacterial suspensions were prepared in the corresponding solution. In addition, to determine bacterial elimination in plasma-treated solutions, samples were plated in LB agar plates immediately after treatment, where all samples grew in the same nutrient-rich media to promote recovery. Thus, these results suggest that the

damage to the cell membrane induced in bacterial cells right after treatment could be repaired. However, plasma-treated cells in PBS could have other cellular components in the intracellular compartment (such as nucleic acids and proteins) irreversibly damaged by RNOS produced in the plasma-treated PBS. Although *S.* Typhimurium is known to be resistant to oxidative stress due to the presence of redundant antioxidant enzymes (247), the simultaneous and irreversible damage of multiple biological components induced by RNOS would exceed the ability of cells to recover, leading to bacterial death.

In the field of low temperature plasmas, the degradation of purified organic molecules in liquid suspension has been reported (43, 102, 114, 181), but little is known about their effect in biological systems. In plasma-treated liquids, some of the RNOS generated in the gas phase are delivered to the sample which can react with molecules present in the liquid to originate new reactive species (229). Therefore, the composition of RNOS in plasma-treated liquids and in the gas phase are not comparable and the biological effects of LTP treatment of samples in liquid environments should not be directly attributed to the RNOS detected in the gas phase. Considering the possible biomedical application of LTP treatments in skin wounds, surgical site infections and neoplasias, it is necessary to determine how the presence of organic molecules in the surrounding of the target of the treatment (i.e. wound exudate, blood, non-target bacterial cells and non-target host cells) affects the treatment outcome. In this chapter, results have demonstrated that the presence of organic molecules during plasma treatment of *S.* Typhimurium with the AP-DBD plasma jet decreased the efficacy of the antibacterial treatment. Specifically, here it is demonstrated that the highest levels of bacterial elimination were achieved in samples treated in the absence of organic molecules that presented short- and long-lived reactive oxygen species. The reactive nitrogen species measured here may not be key to the elimination of bacteria under these conditions. However, the RNOS measured here represent only a small fraction of all the possible species present in plasma-treated liquids (248) and the bactericidal effects observed in *S.* Typhimurium should not be solely attributed to the RNOS found here.

As *in vitro* studies for the application of biomedical plasmas to treat eukaryotic and prokaryotic cells are carried out in different solutions with and without organic molecules (13, 220, 236, 249, 250), it is important to consider the participation of such molecules in the overall process for the correct interpretation of results. Here, it is demonstrated that organic molecules present in solutions used for eukaryotic and prokaryotic cell culture can interact with RNOS formed during plasma treatment and this affects the levels of short- and long-lived reactive species in treated solutions. Moreover, this effect appears to outweigh the role of ionic strength or pH of the solution. Biological and chemical approaches were combined to provide valuable information on the interference of organic molecules with the bactericidal activity of LTPs. These results allow the identification of a trend in the formation of RNOS in the presence of organic molecules that can be used to understand the mechanisms leading to bacterial

inactivation and membrane damage in *S.* Typhimurium exposed to plasma. The data presented here highlight the importance of acknowledging that these compounds are present during treatments *in vivo* and should be considered during the development of effective therapies.

6 GENERAL DISCUSSION

6.1 PLASMA: A TOOL WITH ANTIMICROBIAL APPLICATIONS

The current approaches used to assess the effect of LTP sources on bacterial cells have limitations in their ability to explain the biological effect that underpin bacterial elimination. Reports in the literature are based on the study of the effect of plasma at the population level and do not reflect the oxidative damage induced in individual cells (13, 71, 91). In addition, the lack of information on the effect of the spatial distribution of RNOS in the plasma effluent and how it correlates with the bactericidal properties of the plasma poses limitations for the correct assessment of the efficacy of plasma treatments. Furthermore, the use of purified DNA and proteins that are not representative of the effect induced in living bacterial cells cannot be extrapolated to the effect on molecular targets contained in living cells (44, 102, 121). Therefore these approaches contribute only partially to the elucidation of antimicrobial mechanisms of plasmas. Finally, there is a lack of studies addressing the interaction of plasma-generated RNOS with external organic molecules in the surroundings of the target cells, even when it is well-known that biomolecules can undergo redox reactions (21). These factors are important because they could lead to the exposure of bacterial cells to sub-lethal doses of RNOS. This has the potential to promote the adaptation of microorganisms to oxidative stress induced by the plasma and induce mutations in the bacterial genome that could favour resistance to treatment.

The conditions described above that were overlooked in the past have been studied in this body of work. This research has shown that the mechanisms leading to bacterial death are influenced by the spatial distribution of RNOS in the plasma effluent, as demonstrated for the atmospheric-pressure dielectric-barrier discharge (AP-DBD) plasma jet. The results obtained in Chapter 3 and 4 suggest that this characteristic is inherent to plasma jets generated in open air. This was demonstrated by the comparison of the ability of the AP-DBD plasma jet (generating charged and neutral species) and the μAPPJ (generating mostly neutral species) to induce DNA damage in *S.* Typhimurium. Although the plasma source or conditions chosen for the generation of plasma will determine its composition in interaction with ambient air, the concentration and spatial distribution of RNOS at different regions of the plasma effluent will have a direct impact on the level of damage induced in bacterial DNA. These findings were only possible due to the use of a quantitative assay for the identification of the plasma-induced DNA damage at the single cell level modified and improved here for this purpose, in combination with the measurement of spatial distribution of ozone in the plasma.

The results presented in Chapter 5 suggest that redox reactions between plasma-generated RNOS and organic molecules in the environment where the target population is contained reduce the efficacy of the treatment. In addition, it is possible that only small amounts of individual RNOS produced by the plasma are necessary to act synergistically on bacteria to

induce cell death, as suggested by the reduced amounts of RNOS detected in plasma-treated liquids. Altogether, these experiments provide evidence of the variability in the oxidative damage induced at the single cell level by low temperature plasmas.

The data presented in Chapters 3, 4 and 5 can be brought together to provide a model for the elimination of bacteria, considering the spatial location of the sample to the centre of the plasma effluent and the presence of organic matter different from the target population (**Figure 6.1**). Given the potential application of LTP treatments to disinfect wounds and promote wound healing, treatment outcome could be affected by several factors. For example, a plasma jet could be used to treat polymicrobial infections of skin wounds. The treatment delivers multiple RNOS to the wound site and induce damage to the cell membrane and DNA of bacterial cells, among others. However, the presence of debri and wound exudate (rich in organic molecules) could decrease the efficacy of the treatment. In the same way, considering the spatial distribution of RNOS in the plasma jet, it could be expected that the levels of cell membrane and DNA damage will vary according to the location of the bacterial cells, i.e. directly under the plasma jet or at the periphery where the levels of RNOS are two low to be effective. The exposure of bacterial cells to sub-lethal concentrations of RNOS could lead to the development of resistance to treatment or induce mutations and in bacteria. This could increase the chance of failure to treatment since these bacteria could recolonize the wound, if unattended.

These results were only possible due to the interdisciplinary quantitative approaches considered for this project. This body of work provides valuable information for the development of successful antimicrobial plasma treatments, as it presents evidence of the importance of the spatial distribution of RNOS in the effluent, presence of organic molecules during treatment and analysis at the single cell level for the understanding of the mechanisms leading to bacterial elimination.

6.2 STATE OF THE FIELD

Although the first reports on the application of atmospheric-pressure plasmas for bacterial elimination appeared almost 20 years ago (251), it was not until recently that the mechanisms of action involved in bacterial elimination and factors affecting the bactericidal activity of plasmas started to be investigated in depth. Because LTP is a technology that originated from the plasma field, much attention was paid to the development of new plasma sources and the characterization of the physical and chemical parameters affecting the overall bactericidal action of plasmas during the early years (11, 52, 111, 252). However, little attention was paid to study how plasma mediated this killing. The most used approaches to assess the bactericidal action of LTPs were to detect changes in cell morphology and measure the reduction of the bacterial load after LTP treatments (253, 254). Purified proteins and nucleic acids where also studied in this context to demonstrate the ability of plasma to inactivate toxins and plasmid DNA (44, 51, 255).

(a)

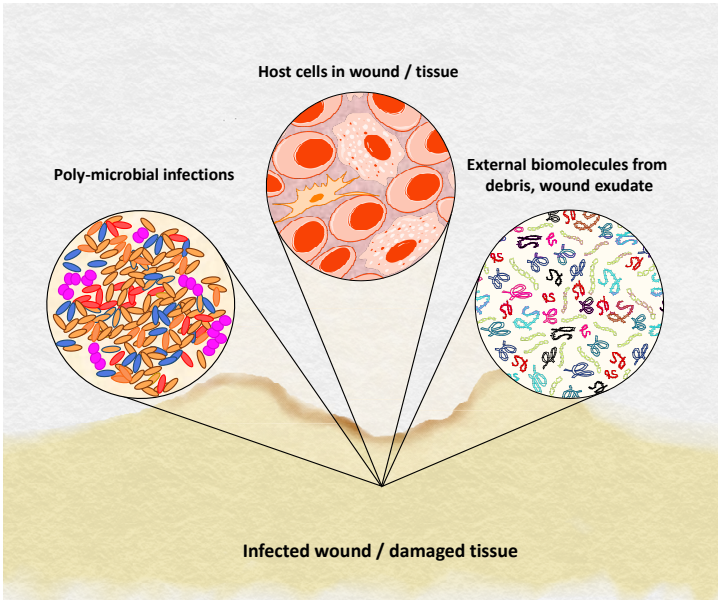

(b)

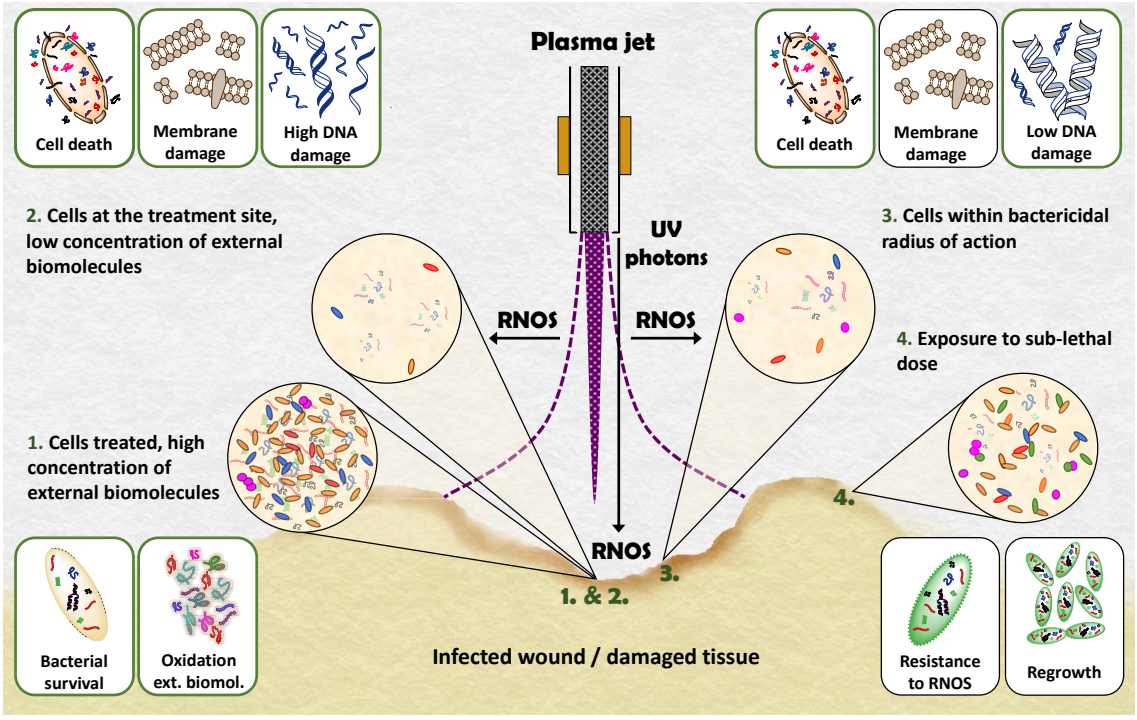

Figure 6.1. (Caption overleaf.)

Figure 6.1. ***Role of the spatial distribution of RNOS in plasma and presence of external biomolecules in the outcome of biomedical LTP treatments.*** Hypothetical application of LTP treatments of an infected surface, such as a skin wound. **(a)** A skin wound with a poly-microbial infection and host cells in the wound bed, where the presence of wound exudate and debris provides the ideal conditions for bacterial proliferation. **(b)** Different outcomes of LTP treatment to kill bacteria according the conditions present at the moment of treatment: **1.** When high concentrations of external biomolecules are present during LTP treatment, plasma-generated RNOS can react with these molecules instead of with target cells, reducing the efficacy of the treatment and leading to bacterial survival. **2.** In the presence of low concentrations of external biomolecules, LTP treatment kill microbes more effectively. The multitarget action of LTP induces damage to the cell membrane and DNA in bacterial cells more effectively in cells directly located under the plasma jet, where the amount of RNOS delivered to the sample is the highest. UV photons generated in the plasma participate mostly in the generation of RNOS. **3.** Microbes located within the bactericidal radius of action of LTP are eliminated, but due to the spatial distribution of RNOS in the plasma effluent, low levels or no DNA damage is induced in bacterial cells and other mechanisms of action will lead the killing. **4.** Microbes located outside the radius of action of LTP could be exposed to sub-lethal doses of RNOS. This could lead to development of resistance to plasma-generated RNOS. Microbes could proliferate and recolonize the wound, if unattended. Boxes outlined in green represent the contribution of this piece of work to the field of low temperature plasmas for biomedical applications.

However, most of these studies carried out by non-biologists lacked understanding of the biological effects of oxidative damage in cells. This presented a challenging scenario for the use of this technology in biomedical applications (e.g. to treat wounds and surgical site infections), as the variability in the plasma sources used and poorly reported biological effects made it difficult to identify the mechanisms responsible.

During the period that the work described in this thesis was carried out, the number and quality of the publications focusing on the biological effects of application of LTPs for bacterial elimination has significantly increased. The bactericidal properties of plasma has been ascribed mainly to the presence of reactive nitrogen and oxygen species and LTPs have proved to be effective against several bacterial species in liquid suspensions, biofilms, fresh produce and medical equipment (256). *In silico* and *in vivo* studies have demonstrated that LTPs can induce damage to the bacterial cell membrane due to lipid peroxidation (44, 71); to the DNA due to oxidation of nucleotide bases and induction of DNA breaks (104, 257) and to the cell wall due to damage to the peptidoglycan structure (258). These publications provide a good foundation for the study of the biological effects of biomedical LTP sources on microbes. However, studies in the field of physics that characterize the spatial distribution of RNOS in the gas phase (112, 122) are dissociated from the study of the mechanisms that cause cell death in bacteria. This is a link that has never been established before in the study of bactericidal LTP treatments and that is relevant to understand the consequences of LTP treatments on bacterial populations exposed to spatially-distributed RNOS.

Considering the possible applications of LTPs in biomedicine to treat skin wounds or surgical-site infections, this study used an interdisciplinary quantitative approach for the elucidation of the mechanisms involved in bacterial elimination with LTP treatments. For this purpose, three topics not addressed in the past were studied here: **(a)** determination of the impact of the spatial distribution of RNOS in the mechanisms of action of LTPs; **(b)** determination of the impact of external organic molecules present during treatment on the efficacy of plasma for bacterial elimination; **(c)** determination of the impact of plasma treatment of bacteria at the single cell level.

6.3 RESEMBLING THE WOUND ENVIRONMENT: PRESENCE OF ORGANIC MOLECULES

As mentioned above, LTP treatments have been suggested as an alternative or complementary therapy to eliminate pathogens in infected wounds (93). The fluid found in a wound (wound exudate) contains all the nutrients required by the tissue to promote healing, such as inorganic salts to buffer the pH in the wound, glucose, cytokines, proteolytic enzymes, plasma proteins and globulins and cells of the immune system (87). Even more, wound debris formed during the healing process and opportunistic microorganisms that colonize the wound can be found, in addition to the cells forming the damaged tissue. Therefore, the application of plasma treatments

to eliminate bacteria from infected wounds should consider the presence of this complex environment rich in organic matter of different origin that can react with plasma-generated RNOS.

In this study, *Salmonella* cultures were prepared in a set of solutions with different organic compositions to resemble the environment of an infected wound exudate (see Chapter 5). The application of the AP-DBD plasma jet to these bacterial suspensions demonstrated that solutions with high nutrient content were more likely to present some damage to the cell membrane that did not affect their viability. In contrast, plasma was able to eliminate 90 to 99 % and 99.9 to 99.99 % of bacterial cells treated in H_2O and PBS, respectively, although a reduction in the percentage of viable cells with no damage in the cell membrane was only observed in PBS-treated samples. These results correlate with the findings of Ferrell *et al.* that used a similar selection of liquids to treat the Gram-positive bacteria *S. aureus* with a spark-based non-thermal plasma (259). The authors described a 2-log reduction in bacterial load after 2 minutes of plasma treatment of *S. aureus* in samples treated in water and PBS, whereas bacteria treated in the nutrient-rich media tryptic soy broth, DMEM and brain heart infusion broth did not produce a statistically significant difference in the number of surviving cells compared to the controls. In this study, they ascribed the reduced bactericidal action of plasma to oxidation of the organic content of the solutions. The bactericidal action of a DBD plasma was also reduced in *E. coli* in maximum recovery diluent suspension (containing nutrients) in comparison to PBS-treated samples (260). In contrast, Rowen *et al.* suggested that the inactivation of *S.* Typhimurium and *S.* Enteritidis in poultry wash water was more efficient compared to treatments in distilled water due to the formation of nitric and carbonic acids originated from fatty acids, lipids and proteins in poultry wash water during plasma treatment (133). However, Rowen *et al.* conducted plasma treatments at 4 °C. The efficacy of the plasma treatment in the presence of biomolecules described by the author could be explained by the increased stability (or reduced decomposition rate) of reactive species at lower temperatures and the reduced metabolism of bacterial cells. The results presented in this thesis together with the existing literature evidence the adverse effect of external organic molecules on the bactericidal action of LTPs administered at room temperature, a key point that should be considered when developing strategies for individual or combined antibacterial LTP treatments in the clinical setting.

It is well-known that organic molecules such as proteins, lipids and carbohydrates can undergo redox reactions (21, 74). In the field of biomedical plasmas, individual reports have described the damaging effects of LTP treatments on biomolecules due to induction of oxidative damage. For example, treatment of lysozyme in aqueous solution with an atmospheric pressure helium plasma jet decreased its enzymatic activity and induced changes of the secondary structure (103). Other plasma sources have been shown to inactivate and degrade the heme group of horseradish peroxidase in PBS (261), oxidize and inactivate the catalytic cysteine in the catalytic centre of glyceraldehyde 3-phosphate dehydrogenase (104), reduce the enzymatic

activity of proteinase K (44) and induce single- and double-strand DNA breaks in purified plasmid DNA in PBS (51, 121). Analysis at the molecular level have demonstrated that LTP treatments can induce structural modifications in proteins and amino acids (181), being aromatic and sulphur-containing amino acids preferentially affected by RNOS (102). However, considering that LTP treatments could be used in biomedicine and that currently clinical trials to clear infections and promote healing in patients with chronic wounds are ongoing, it is fundamental to acknowledge that plasma-generated RNOS interact with organic molecules of any origin and that their presence can determine the success or failure of the treatment.

In contrast to the study carried out by Ferrell *et al.* in plasma-treated *S. aureus* in liquids with different nutrient content (259), the work presented in this thesis on plasma-treated *S.* Typhimurium in liquids with organic content not only describes the reduction in bacterial load but also presents a quantitative analysis of membrane damage of bacterial cells and identification of RNOS formed in plasma treated liquids. Here it is demonstrated that the local environment alters the ability of LTPs to induce oxidative damage to targeted cells. Whereas membrane damage was induced in plasma-treated bacteria in PBS, DMEM and DMEM + 10 % FCS (**Figure 5.8**), bacterial elimination was abrogated by the presence of organic molecules in the culture media (**Figure 3.6** and **Figure 5.7**) when exposed to plasma in both solid and liquid environments. The presence of external organic molecules during treatment also correlates with a decrease in the levels of DNA damage induced in *S.* Typhimurium (**Figure 4.9**). Thus, it is likely that the interaction of plasma-generated RNOS with non-target organic matter is responsible for the decrease in the bactericidal activity of LTPs.

The complex interactions between reactive species and organic molecules in biological systems such as *S.* Typhimurium generate additional reactive species and toxic by-products that cause oxidative damage to the cell. Thus, the damage observed in plasma-treated *S.* Typhimurium is a consequence of a sum of events at the molecular level caused by the synergistic effect of RNOS. This damage cannot be ascribed only to one or more specific species measured but to the synergistic effect of short- and long-lived species. In addition, other biologically relevant species such as peroxynitrite, superoxide and hydroperoxyl radical not analysed here could participate in the induction of oxidative damage to bacteria.

In this study, the highest antibacterial activity was obtained in bacterial suspensions in PBS. Plasma-treated PBS presented ·OH radicals, O_3/O, $O_2(a^1\Delta g)$ and NO/NO_2^-. Machala *et al.* demonstrated that direct current-driven positive transient spark discharge plasma treatments of *E. coli* in PB and PBS buffers were less effective that treatments in water and saline solution (117). The authors attributed the bactericidal action of the plasma to the interaction of acidified nitrites and hydrogen peroxide in non-acidic pH solutions. In the same way, plasma-activated PBS was demonstrated to be less effective in eliminating *E. coli* than plasma-activated water (116) or N-acetyl-cysteine (262), which suggest that the long-lived species formed in PBS that

remain in the solution after treatment might not be present in high enough concentration to induce cell death. However, Joshi *et al.* demonstrated the antibacterial properties of plasma-activate PBS and its effect on gene transcription (107), where long-lived species would be responsible for the effect measured. However, the bactericidal activity of plasma-activated PBS described in these publications is mainly due to the long-lived species that remain in the solution for several hours or even days after treatment and therefore does not benefit from the synergistic action of short- and long-lived species formed during exposure to plasma. In the work presented for this thesis, bacterial cells in PBS were directly exposed to plasma and therefore exposed to the short- and long-lived species generated during the discharge. In contrast to the findings of Machala *et al.*, for the experiments presented in this body of work the pH of plasma-treated PBS did not decrease more than 0.5 after treatment and the concentration of nitrogen-centred species measured during and after plasma treatment were reduced. These results suggest that under the conditions used here, variations in the pH and the resulting formation of RNS favoured by the acidification of the plasma-treated solution would not be responsible for the bacterial elimination observed in *S.* Typhimurium in PBS. The data presented here suggest that in plasma-treated PBS, the combination of short- and long-lived species makes this solution effective against bacteria, specifically by the presence of reactive oxygen species. It has been suggested that the salts present in PBS contribute to the formation of additional ·OH radicals in plasma-treated solutions (231), which could explain the enhanced bactericidal action of PBS observed here.

The chemical reactions that lead to the formation of RNOS in plasma-treated liquids are complex and besides being determined by plasma source and parameters chosen, the liquid used, pH and presence of organic and inorganic molecules can also affect the type and concentration of RNOS formed. In plasma-treated liquids, Tresp *et al.* reported that plasma-treated RPMI (culture media similar to DMEM) presented lower levels of ·OH and O_2·$^-$ than plasma-treated PBS (222, 231), whereas Winter *et al.* described that the levels found between plasma-treated PBS and RPMI were comparable (263). In the thesis presented here, the highest concentration of ·OH was measured in plasma-treated PBS and DMEM, and it decreased in the nutrient-rich solutions DMEM + 10 % FCs and LB (**Figure 5.2a,b**). These results are in line with the findings reported by Tresp *et al.*, since the organic molecules present in the solutions could be degraded by RNOS produced by the plasma. In addition, the salt composition of PBS could favour the formation of additional ·OH radicals that could mediate bacterial elimination (231). Although the spin traps used here to detect ·OH can react with both, O_2·$^-$ and ·OH radicals, no O_2·$^-$ was detected. This could indicate that although O_2·$^-$ might be formed in the solution, the transformation of DMPO-OOH adduct into DMPO-OH adduct due to the short half-life time of the former could occur in plasma-treated samples.

The reduction in the concentration of O_3/O, $O_2(a^1\Delta g)$ and ·OH found here in plasma-treated solutions with high organic matter content could represent the loss of ROS in liquid due to

reaction with biomolecules. Ozone was largely produced in the gas phase of the AP-DBD plasma jet (**Figure 5.2**) and it was also abundant in plasma-treated liquids, specifically in solutions without organic molecules (**Figure 5.2**). O_3 reacts with unsaturated aromatic and aliphatic compounds in cells but also in nutrient-rich solutions as shown here. This reaction promotes the formation of peroxides and H_2O_2 in the solution:

$$HO_2\cdot + ROOH \rightarrow RO_2\cdot + H_2O_2$$

This reaction could explain the increase in the levels of H_2O_2 measured in nutrient-rich solutions exposed to plasma, given that most of the H_2O_2 found in plasma-treated water originates in the gas phase (Gorbanev *et al.*, unpublished data). Although H_2O_2 was increased in solutions with high nutrient content, its presence did not correlate with bacterial elimination, suggesting that H_2O_2 and derived peroxides formed upon oxidation of biomolecules would not be one of the main reactive species responsible for bacterial death.

In addition to lipids, O_3 also oxidises proteins and amino acids by attacking –SH groups and reacts with polysaccharides (84) and this could be another mechanism of direct damage by O_3 to bacterial cells exposed to plasma. Indirectly, O_3 decomposition in liquids could contribute to further induction of damage in bacterial cells, giving origin to the highly reactive ·OH (264):

$$O_3 + OH^- \rightarrow HO_2^- + O_2$$

$$O_3 + HO_2^- \rightarrow \cdot OH + O_2\cdot^- + O_2$$

·OH is considered to be the only oxygen species that can cause direct damage to most organic molecules (74). However, because of its high reactivity, ·OH reacts only with molecules present within 1 to 5 molecular diameters of their site of formation (265, 266). H_2O_2 present in plasma-treated liquids could promote the formation of additional ·OH via Fenton reaction in the intracellular compartment, especially in reaction with iron bound to the DNA:

$$H_2O_2 + Fe^{2+} \rightarrow OH^- + FeO^{2+} + H^+ \rightarrow Fe^{3+} + OH^- + \cdot OH$$

The most significant impact of ·OH is upon DNA, since it attacks the sugar or base moieties by abstracting electrons, as well as adding to the unsaturated bases producing a broad spectrum of potentially mutagenic or lethal lesions (74). Although it is believed that most of the damage induced by H_2O_2 is mediated by the formation of ·OH (21), plasma-treated liquids with abundant organic content presented high levels of H_2O_2 that did not correlate with the bacterial elimination observed (**Figure 5.6**). In fact, more than 99% of the population of *S.* Typhimurium exposed to plasma in nutrient-rich solutions that presented the highest levels of H_2O_2 recovered from treatment. Thus, it is likely that the redundant mechanisms that *S.* Typhimurium possess to respond to oxidative damage induced by H_2O_2 and other RNOS play an important role in the survival of bacteria to plasma treatment. Even more, it highlights that H_2O_2 is not the main reactive species responsible for bacterial death under the conditions used here.

In the case of nitrogen-centred species, the concentrations of NO and NO_2^- in aqueous solutions was dependent on the pH of the treated solution (**Figure 5.4**). In addition, the increase in the treatment time demonstrated a consumption of the species that upon acidification of the solution, could result in the formation of NO_2^- and NO_3^-. At neutral pH in buffered solutions, the nitrites were less oxidized, which could explain the increase in the concentration measured by EPR (**Figure 5.4**). However, in liquids without buffering properties such as H_2O and LB, nitrites are not stable and can be converted to nitrates *via* nitrogen oxide, nitrous acid and nitrogen dioxide. The reaction of nitrites and hydrogen peroxide at low pH or NO and $O_2^{\cdot -}$ can lead to the formation of the highly cytotoxic peroxynitrite (21). The presence of NO and NO_2^- however was not related to membrane damage or bacterial elimination, as described above. It is possible that nitrogen-centred species participated in the formation of other reactive species such as peroxynitrite and hydroperoxyl radical which are cytotoxic (267), but that were not measured here.

Treatments using single RNOS to eliminate bacteria in liquid and solid environments usually require high concentrations to be effective and the exposure to sub-optimal concentrations can induce resistance (268, 269). For example, it has been reported that 20 µM O_3 in water is required to induce a 3.8 $\log_{10}$ reduction in treated *E. coli*, whereas 135 µM O_3 would be required to achieve similar results in O_3-treated *S. enteritidis* (270). Christman *et al.* described that the exposure of *S.* Typhimurium to the sub-lethal concentration of 60 µM H_2O_2 for 60 minutes induced resistance to killing with 10 mM H_2O_2 (22), whereas Carlsson *et al.* demonstrated that 400 µM could induce a significant reduction in the bacterial load (271). In the same way, treatments of 5 minutes with 3.3 x 10^{-6} mol $O_2(a^1\Delta g)$ generated in the air eliminated 50 % of *S.* Typhimurium sample with an activity, described by the authors, as non-mutagenic but cytotoxic (272). In the piece of work presented here, the levels of ·OH, O_3/O and $O_2(a^1\Delta g)$ were found highest in solutions with low-nutrient content and it decreased in high-nutrient content solutions exposed to plasma (**Figure 5.2c,d**). However, the concentration for each of these species was below the values found to be toxic for individual treatments. These results indicate that the bactericidal action of plasma is indeed improved by its multicomponent nature and synergistic activity on bacterial cells. Nevertheless, genetic modifications in bacteria that survived LTP treatment were not investigated in this study and further studies on this topic could be very valuable for the determination of induction of resistance to plasma and antibiotic treatments in bacteria exposed to sub-lethal concentrations of RNOS.

It is clear that the increase in the survival of *S.* Typhimurium to LTP treatment in the presence of external biomolecules observed is due to the scavenging activity of such molecules present during treatment. Although the composition and concentration of RNOS present in plasma-treated liquid differ from those existing in the gas phase, the results presented here demonstrate the interference of organic matter on LTP treatments that is expected to occur in either liquid or solid environments. It could be proposed that external biomolecules consume the plasma-

generated RNOS and compete with the biomolecules in the bacterial cells. In view of the impact of this factor on the outcome of the treatment, it should be taken into consideration when applying LTP treatments in biomedicine, e.g. treatment of infected wounds. In this scenario, the rich environment of the wound could determine the success or failure of the treatment. Therefore, the conditions for the generation of LTPs could be tailored to provide optimal treatments, where a sufficient dose of RNOS to effectively eliminate pathogens from chronic and acute wounds and surgical site infections can be delivered.

6.4 ELIMINATION OF BACTERIA IN DRY/SEMI-DRY ENVIRONMENTS

6.4.1 Role of the spatial distribution of RNOS in the plasma

The elucidation of the effect of external biomolecules on the efficacy of antibacterial plasma treatments in liquids demonstrated the importance of the environment on the efficacy of LTP treatments. However, the application of plasma treatments in environments with reduced or no liquid content would rely mostly on the RNOS formed in the plasma. In this context, it would be expected that the oxidative damage induced in plasma-treated bacteria depends directly on the composition of the plasma. Although there is evidence that the density of oxygen species vary in the plasma effluent (108, 112, 122) and these variations could determine the molecular targets of oxidative damage in plasma-treated cells and the level of damage produced, the effect of the spatial distribution of RNOS in the plasma on bacterial elimination has never been addressed before. Considering the possible applications of LTP treatments in biomedicine, it is crucial to acknowledge the variations in the mechanisms of action used by LTPs to eliminate microorganisms are influenced by the spatial distribution of RNOS.

This study has demonstrated for the first time that the spatial distribution of RNOS in the plasma effluent has a direct effect on the mechanisms leading to bacterial elimination. For this purpose, a single cell assay to determine DNA damage in plasma-treated bacteria was used, since DNA damage is one of the most damaging lesions caused by oxidative stress (205). This method was complemented by study of the composition of the gas phase of the AP-DBD plasma jet and bactericidal action of plasma on agar plates. Here, combined approaches were taken to determine the effect of plasma treatments at the population and single-cell level, considering their relationship with the spatial distribution of reactive species in the plasma effluent, specifically O_3. This study provides crucial information for the development of antibacterial plasma therapies and has demonstrated five critical points: **(a)** the level of DNA damage induced in plasma-treated bacterial cells is dependent on the spatial distribution of RNOS in the plasma effluent and is not a consequence of damage caused exclusively by plasma-generated UV photons (**Figure 4.1** and **Figure 4.7**); **(b)** this damage occurs in DNA sugar-phosphate backbone and nucleotide bases in plasma-treated bacterial cells (**Figure 4.3**); **(c)** the level of such DNA damage is reduced in the presence of biomolecules during the

treatment (**Figure 4.9**); **(d)** the spatial distribution of O_3 correlates with bacterial elimination in agar plates but not with the induction of DNA damage (**Figure 4.10 – 4.13**); **(e)** other RNOS present in the plasma effluent such as H_2O_2 contributes to bacterial elimination (**Figure 5.9**). To the best of my knowledge, this is the first report addressing the effect of LTP treatments on the integrity of DNA in bacterial cells at the single cell level that considers the distribution of RNOS in the plasma effluent.

In silico (113, 147, 216) and experimental studies have demonstrated the variation in the spatial distribution of RNOS in the plasma effluent (108, 112, 122, 273) and on the surface of plasma-treated materials (274). This study has demonstrated that the level of DNA damage induced by LTP treatments (both, AP-DBD plasma jet and µAPPJ) on *S.* Typhimurium was inversely correlated to the distance to the treatment site. The damage inflicted to DNA in bacterial cells was likely originated by the high concentration of RNOS at the treatment site that are carried away due to diffusion and advection mechanisms with increasing distance to the treatment site. The participation of UV photons produced in the plasma sources used here was demonstrated to be minimal. The high levels of DNA damage obtained at the treatment site cannot be ascribed solely to UV photons, although in combination with plasma species, UV photons can participate in the generation of RNOS. Because the amount of UV radiation emitted with different plasma sources vary, its participation in the induction of DNA damage and bacterial elimination must be addressed for every plasma source.

The damage to bacterial DNA was used to demonstrate that the spatial distribution of RNOS determines the damage inflicted by the plasma in biological samples depending on their location relative to the jet. To date, there are only two publications addressing the effect of such distribution on biomolecules exposed to plasma, specifically purified DNA (121, 208). The results presented here are in agreement with the findings reported by the authors and provide information on the damage induced in DNA in the context of living cells. Regarding other biomolecules present in cells during treatment, it could be expected that the damage to bacterial proteins, lipids and carbohydrates would be determined in the same way by the spatial distribution of RNOS in the plasma effluent. This statement is supported by the recent findings of Birer (275). The author describes the existence of reactivity zones in a plasma-treated polyethylene surface due to the chemical changes dependent on the spatial distribution of species in the plasma effluent. Although in this study only the spatial distribution of O_3 in the plasma effluent was assessed and it is not possible to extrapolate the data obtained for other plasma sources, it is expected that other RNOS present specific patterns of distribution in the plasma effluent.

It can be concluded that the mechanisms of action used by LTPs to treat cells (prokaryotic or eukaryotic cells) is affected by the spatial distribution of RNOS in the plasma effluent. This effect has proved to be inherent to the generation of plasma jets in ambient air, as described

here. It could be expected that the level of damage inflicted on other biomolecules in the target cell will be affected in the same way by the spatial distribution of reactive species. It should be noted that the exposure of bacteria to sub-lethal doses of RNOS can promote their adaptation to oxidative stress and induce mutations that could result in the development of resistance to treatment. Thus, this is an important characteristic of LTP treatment that should be taken into consideration for the development of plasma therapies, not only for biomedical applications but also for food disinfection.

6.4.2 Identifying reactive species responsible for bacterial elimination

The O_3 density measured in the gas phase depends on the formation and destruction processes of O_3. Thus, both processes determined the concentration of O_3 detected in the effluent of the AP-DBD plasma jet. One of the main processes associated with the formation of O_3 is a ternary reaction that involves molecular oxygen (215):

$$O + O_2 + M \rightarrow O_3 + M$$

Where M represents a third particle that is not changed in the reaction but participates in the energy and momentum transfer. The dissociation of O_3 can be mediated by the reactions with O and H, as occurring in the core of a RF-driven DBD plasma jet (143):

$$O + O_3 \rightarrow 2\ O_2$$

$$H + O_3 \rightarrow O_2 + {\cdot}OH$$

The formation and destruction of O_3 is limited by the abundance of O, O_2, H, NO and singlet oxygen, as well as by temperature, as increasing temperature accelerates the dissociation of O_3 (143, 216). In other plasma sources similar to the µAPPJ used for part of this study, it has been reported that O_3 forms in the effluent and builds up as it leaves the nozzle, whereas O decays (215). The same trend was reported by Ellerweg *et al.* for O_3 in the axial direction of the plasma effluent (108). The results presented in this study are in agreement with the trends described in the literature. In addition, the data shown here provide further understanding on the effect of such distribution on the elimination of bacteria with LTP treatments.

The present study demonstrated that there is a correlation between the spatial distribution of O_3 in the gas phase with the biological effects in a bacterial cell. It was observed that concentrations of 3 – 5 ppm O_3 in the plasma effluent correlated with the edges of the zones of inhibition in plasma-treated *S.* Typhimurium agar plates. Therefore, a minimum concentration of O_3 in this range was required to kill bacterial cells with the AP-DBD plasma jet. Treatments using exclusively gaseous O_3 to kill bacteria have been demonstrated to require high concentrations of O_3 (ranging from 5.3 to 100 – 500 ppm), longer treatment times (ranging from 5 to 240 minutes) or a combination of both to achieve reduction in the bacterial load (214, 218, 219, 276, 277). Thus, from the results obtained here, it could be inferred that short LTP treatments with a minimum of 3 – 5 ppm O_3 (in addition to other RNOS present in the gas

phase) are effective at eliminating *S.* Typhimurium in agar plates. As described above, plasma-generated RNOS including O_3 can attack directly lipids in the cell membrane and initiate the process of lipid peroxidation, which results in a decrease in membrane fluidity and disruption of membrane-bound proteins, formation of secondary radicals and indirect oxidation of intracellular targets (244). Due to the complex composition of charged and neutral species in the plasma effluent that reach bacterial cells, it is likely that one of the mechanism of action of LTPs is damage to the cell membrane as suggested before (13, 42), and that O_3 mediates this damage. However, outside the edge of the zone of inhibition where confluent growth of bacteria was observed, it is possible that bacterial cells were exposed to sub-lethal concentrations of plasma-generated RNOS. Thus, further studies addressing the effect of the exposure of bacteria to sub-lethal concentrations of RNOS on the development of mutations and resistance to plasma and other antibiotic treatments that rely on the induction of oxidative damage should be considered.

In addition to O_3, it was indirectly determined that H_2O_2 was formed in the gas phase and it contributed to the elimination of *S.* Typhimurium. This was concluded by the study done with agar plates supplemented with scavengers (**Figure 5.9**), where it was demonstrated that catalase added to plates prior to treatment improved the number of bacteria that survived the treatment. Agar plates supplemented with superoxide dismutase (SOD) did not improve the survival of *S.* Typhimurium to plasma treatment. Even more, the addition of both SOD and catalase to agar plates did not contribute to the survival of bacterial cells exposed to plasma. These results could be explained by the possible antagonistic activity of H_2O_2 and $O_2^{\bullet -}$ over SOD and catalase, respectively. Catalase decomposes H_2O_2 into water and molecular oxygen:

$$2\ H_2O_2 \rightarrow 2\ H_2O + O_2$$

In turn, SOD dismutates $O_2^{\bullet -}$ and releases H_2O_2 and molecular oxygen:

$$2\ H^+ + 2\ O_2^{\bullet -} \rightarrow H_2O_2 + O_2$$

Interestingly, the activity of these two enzymes is limited or inhibited by the presence of the opposite enzymatic substrate. Thus, Cu/Zn and Fe in SOD enzymes can be inactivated by H_2O_2 and in the same way, $O_2^{\bullet -}$ can inactivate catalase (278). When both enzymes are present at the same time, they can enhance the activity of each other by removing the opposite substrates that cause their inhibition. However, this was not observed in the experiments where both enzymes were present during plasma treatment.

The fact that the addition of SOD to agar plates did not confer protection to plasma treatment in *S.* Typhimurium has three possible explanations: **(a)** H_2O_2 was present in the plasma effluent at high concentrations that inhibited the activity of SOD, even in the presence of catalase; **(b)** there was little or no $O_2^{\bullet -}$ in the plasma effluent to be scavenged by SOD; **(c)** the reaction of $O_2^{\bullet -}$ with biological targets in the sample was favoured over the reaction with SOD. Agar plates

supplemented with catalase improved the survival of *S.* Typhimurium to plasma treatment, indicating that H_2O_2 is indeed present in the gas phase, as suggested by Gorbanev *et al.* (unpublished data). The author demonstrated that H_2O_2 originates in the gas phase and thus this could be delivered to bacterial cells and contribute to the killing observed.

The third scavenger used, D-mannitol (21), was used to scavenge ·OH radical produced in the plasma effluent. D-mannitol failed to provide protection against plasma treatment. Because D-mannitol can be used by *S.* Typhimurium as an additional source of carbon (241), this could explain the increase in size of bacterial colonies that survive to the treatment. However, this scavenger promoted the elimination of bacteria in the zone of inhibition, possibly due to degradation of the scavenger and formation of secondary toxic species. The presence or absence of ·OH in the gas phase cannot be indirectly determined with this assay and therefore its participation in bacterial elimination cannot be pinned down. However, given the fact that most of the damage caused by H_2O_2 is mediated by the formation of ·OH (21), it is possible that this radical participates in the events that lead to damage to intracellular targets. Further studies to determine the spatial distribution of ·OH could provide information about its participation in bacterial elimination or to the chemical reactions for the generation of other toxic RNOS.

From the results presented here, it could be inferred that H_2O_2 produced in the gas phase participates in the elimination of *S.* Typhimurium, but its concentration and distribution in the plasma effluent is unknown. Norberg *et al.* suggested that the increase in the concentration of H_2O_2 in the effluent at distance from the nozzle was accompanied by the reduction of its precursor ·OH (216). It is possible that H_2O_2 presents a spatial distribution similar to the one described here for O_3, where H_2O_2 builds up over time and its density increases at the surface of the sample. If this was the case, it could be expected that both O_3 and H_2O_2 will not only damage the biomolecules at the cell surface, but also cross the cell membrane to directly and indirectly damage intracellular molecules such as DNA and proteins. In this hypothetical situation, long-lived species such as H_2O_2 and O_3 (described here) delivered by the AP-DBD plasma jet would play a major role in bacterial elimination.

Although these results suggest the participation of H_2O_2 in bacterial elimination in solid surfaces, contrasting results were obtained in plasma-treated bacterial suspensions (**Figure 5.6 – Figure 5.8**), where bacterial elimination was not achieved in nutrient-rich solutions in the presence of increased levels of H_2O_2. These contradictory results could be explained by the different chemical reactions occurring in gas and liquid phase and concentration of H_2O_2 in both environments. Further experiments to determine the spatial distribution of H_2O_2 and other RNOS in the gas phase could help to test the hypothesis stated above and to determine the participation of H_2O_2 in the mechanisms leading to bacterial elimination.

6.5 OTHER FACTORS AFFECTING THE TREATMENT OUTCOME

6.5.1 Population heterogeneity and relevance of single cell approaches

A factor that should be considered in the analysis of plasma treatments is the variability in the response due to the heterogeneity of the population (279). Heterogeneity in cell populations can occur due to the impact of the surroundings on the physiology of the cell, charge and structure of the cell membrane (280), but also due to stochastic events in the population during cell division of bacterial communities (281). Even in apparently homogenous environments, heterogeneity can be observed (280) and such heterogeneity facilitates the survival of the species under adverse conditions. This heterogeneity in a bacterial population could be due to the development of subpopulations of dormant persister cells, for example. Persister cells can be described as bacteria with the same genotype but different phenotype from regular cells (282) that are highly tolerant to the mechanisms used by antibacterial treatments (283). All the pathogens studied so far can form persister cells (284) and they can exhibit a reduced growth rate already before the antibacterial treatment and they have been linked to failure of antibiotics (281). In addition, genotypic changes in the population can lead to the formation of resistant bacteria that can effectively survive antibacterial treatments through adaptation (285). Thus, although the study of antibacterial treatments at the population level provide insight on the overall effect of the treatment, it is clear that it is also important to consider the heterogeneity of the cell population. For biomedical plasmas, the analyses at the single cell level could provide more accurate representation of the effect of plasma treatments on bacterial cells.

In this study, a quantitative analysis at the single cell level was sought with the purpose of identifying the variability in the response of the bacterial population to LTP treatments. One of these approaches was the functional Live/Dead assay by flow cytometry to determine membrane integrity in plasma-treated cells. This method uses a functional dye that penetrates both intact and permeabilized cells and the exclusion probe PI that can only access and stain the DNA in cells with compromised membrane. Fröhling *et al.* (286, 287) described the use of flow cytometry to determine membrane permeabilization, depolarization and esterase inactivation in plasma-treated *E. coli*, *P. carotovorum* and *L. innocua*. This approach can be applied to the study of plasma-treated eukaryotic cells (288, 289) and can be combined with EPR analysis for the identification of intracellular and extracellular RNOS formed during plasma treatment (290).

The second approach was the use of the modified DDD assay for the study of DNA damage induced by plasma treatments in single cells. This method uses a similar principle to the Comet assay for eukaryotic cells (291). Treated cells are prepared in agarose over a microscope slide where DNA fragments from individual damaged cells diffuse around the core, as described in **Figure 2.1**. This method was used in the past for the study of DNA damage in bacteria exposed to antibiotic treatments (137, 292-294). The DDD assay used here was modified to study the

effect of the spatial distribution of RNOS in the plasma effluent on bacterial DNA damage. For this purpose, the method presents three modifications: **(a)** bacterial cells are transferred to agarose-coated slides with the use of an agar section prior to plasma treatment and are covered with a thin layer of LMP agarose post-treatment; **(b)** the addition of the enzyme FPG to the protocol after cell lysis to identify oxidized purines in plasma-treated *S.* Typhimurium; **(c)** the quantitative and objective analysis of images independently of the absolute level of illumination, described in Section 2.6.4.

The modifications to the DDD assay improved the amount of information that can be obtained from plasma-treated bacteria. Firstly, the effect of the spatial distribution of RNOS in the plasma effluent can be determined on the levels of DNA damage induced in bacteria. This method can be modified to study DNA damage in Gram-positive bacteria as well (137). Combined with studies of the spatial distribution of RNOS in the gas phase ((112, 122) and findings described in Chapter 4), this can be used to identify the main species responsible of such damage. Secondly, it provides information not only on the damage inflicted on the sugar-phosphate backbone that cause DNA breaks, but also on the oxidation of purines, a type of lesion that can induce spontaneous mutations in the DNA. The detection of oxidised purines is mediated by the addition of FPG enzyme to the protocol. FPG excises the ROS-induced 7,8-dihydro-8-oxoguanine (oxo8G), 8-oxoadenine and 5-hydroxy-uracil among others, and works in combination with other enzymes of the base excision repair pathway to prevent the induction of mutations by these lesions (295). Therefore, this constitutes a specific mechanism to identify damaged purines by the DDD Assay. Alternatively, other enzymes of the base excision repair pathway (such as endonuclease III, for example) could be used to determine the presence of oxidized pyrimidines. Thirdly, the quantitative method used here has the advantage of the use of an algorithm that identifies the presence or absence of bright pixels in the image (corresponding to DNA fragments stained with SYBR Gold). This characteristic is an improvement to the current methods to analyse DNA fragmentation in bacterial cells that rely on the intensity of the fluorescence of the DNA sample (292). The low fluorescence of small DNA fragments could result in the underestimation of the levels of DNA damage induced. In contrast, the method used here evidence the presence of small fragments and therefore allows a more accurate representation and analysis of the diffusion of DNA fragments in the samples.

Altogether, the techniques used in this body of work have provided valuable additional insight for the study of plasma treatments in bacteria at the single cell level in both, liquid and solid environments. As described above, heterogeneity in bacterial populations can occur, and therefore the assessment of LTP treatments at the population level does not evidence the different responses to oxidative damage produced in each cell. When analysing the effect of plasma treatment at the population level, it was clear that the response to plasma treatment was not homogeneous, as some bacteria survived the treatment and were observed in the zone of inhibition. With the use of these approaches at the single cell level, the different levels of DNA

and membrane damage in plasma-treated bacteria became evident. Specifically, the results of flow cytometry to detect membrane damage revealed the presence of an 'intermediate' population that presented some degree of membrane damage (**Figure 5.8**), but could still be considered viable. For future studies, flow cytometry could be complemented with cell sorting to isolate bacterial cells with different levels of membrane damage to assess culturability and recovery to plasma treatment.

The approaches described in this piece of work can be combined with other methods to further determine the damage induced in plasma-treated cells at the single cell level. Considering that the main target of biomedical plasmas are prokaryotic and eukaryotic cells, approaches in the context of living cells is paramount for a proper identification of the mechanisms leading to bacterial inactivation. The results obtained with purified molecules (such as proteins, lipids and nucleic acids) should not be assumed to reflect the expected response in living cells.

6.5.2 Reproducibility, variability and comparability of LTP sources

The results presented in this body of work have demonstrated that the bactericidal action of LTP treatments can be affected by several intrinsic and extrinsic factors. As described in Chapter 3, the generation of plasma by LTP sources can be modulated by adjusting the physical parameters to improve the delivery of RNOS. In the same way, the biological parameters such as the type of target sample, concentration and environment in which the sample is exposed to treatment (e.g. liquid/solid, nutrient-free/nutrient-rich environment) can determine the outcome of the treatment. Within the results presented here, it became evident that small variations in any of these parameters have a direct impact on the outcome of the treatment and reproducibility of the results. This is observed in the realization that these parameters are not independent from each other. These data highlighted the importance of optimizing and characterizing the conditions for plasma generation and the need of common and standardized guidelines to assess the bactericidal properties of low temperature plasmas.

The plasticity of the generation of plasma treatments presents advantages and disadvantages for the development of biomedical LTPs. On one hand, plasma treatments could be tailored to develop specific treatments against a range of pathogens of biomedical interest. In this scenario, discrete changes in the physical parameters or electrical arrangement of the plasma source could be made to increase the delivery of specific RNOS to effectively eliminate Gram-negative and Gram-positive bacteria and even drug-resistant pathogens. Tailored treatments with specific RNOS produced could be further adjusted to treat infections in solid/semi-solid or liquid environments that could anticipate and compensate for the interference of external organic and water molecules during treatment. The composition of the RNOS in the plasma effluent could be therefore controlled and treatments could be administered under safe conditions. It is possible that with the contribution of interdisciplinary approaches, as the one used in this piece of work, an 'ideal' plasma treatment could be developed. With this objective, several

biomedical LTP sources have been developed, specifically for the treatment of microbial infections and chronic wounds (55, 296, 297). These studies have contributed to the understanding of the mechanism of action of LTPs on target cells and their relationship with the trends in type and concentration of RNOS produced by LTPs.

On the other hand, this same plasticity in the selection of parameters for plasma generation can represent a problem for the reproducibility and comparability of results. Taking the two plasma sources used in this study as an example, it is clear that the chemistry of the plasma delivered to the biological sample differs due to the conditions used for the generation of plasma and inherent characteristics of each plasma source. This was evidenced by the different abilities of both plasma sources to induce DNA damage and eliminate bacteria (see Chapter 4). Therefore, the mechanisms of action used to kill bacteria might rely on different RNOS present in the gas phase. The existence of multiple plasma sources for biomedical applications to treat a wide range of eukaryotic and prokaryotic cell targets under non-standardized conditions makes it difficult to determine what is needed to obtain successful treatments. This poses a challenge for data interpretation and reproducibility of scientific results with different plasma sources. Thus, the task for scientists working on the development of LTP therapies is to identify the key optimal parameters for specific treatments (e.g. antibacterial, antifungal, anticancer), rather than developing universal treatments that might not be effective due to the specific characteristics of resistance and response to oxidative damage of each cell population.

At the time of this thesis, there is not a common biomedical plasma source that could be used as a reference to compare and contrast the results obtained with the many plasma sources available. Even more, a set of methods to characterize the composition of the plasma and the effects on target cells at the single cell and population level has not been established yet. However, this variability has been acknowledged and an interdisciplinary collaborative work (European COST Action MP 1101) to develop a reference plasma source and a biological reference protocol for the study and comparison of plasma treatments across laboratories is ongoing. If adopted by the scientific community, this reference plasma source could provide a baseline for the standardized assessment of biomedical LTPs. Alternatively, the existing commercial and portable devices could be fully characterised and adopted as reference sources.

6.5.3 Electric fields in plasma

Pulsed electric fields are used for decontamination and relies on the permeabilization of the cell membrane of bacteria upon the application of high electric fields (298). Although some authors have shown that electric fields generated in the plasma can induce damage to the cell membrane of bacterial cells (99, 100), their effect has not been addressed in this study. The data obtained in this study suggest the participation of reactive oxygen species in the mechanisms leading to the elimination of bacteria in liquids and solid surfaces, but it is possible that the increased damage observed in cells exposed to plasma is a consequence of the combined effect of

oxidative stress and electric fields acting over bacterial cells. Further studies to determine the effect of this factor on the efficacy of LTP treatments should be carried out in the future to determine their role in bacterial elimination.

6.6 FINAL CONCLUSIONS

Altogether, the results presented here demonstrate that low temperature plasma is a promising multitarget antibacterial therapy. Treatments can be improved with the knowledge of the effect of intrinsic and extrinsic factors on the efficacy of the treatment. In this body of work, O_3 was shown to be spatially distributed in the plasma effluent and have a direct impact on the level of damage induced in biomolecules in living bacterial cells. This variation in O_3 density could reflect the variation in the spatial distribution of other RNOS formed in the plasma. Therefore, such spatial distribution of RNOS could determine the mechanisms of action used by LTPs to induce cell death in bacteria. In addition, the data shown here demonstrated that the external organic molecules present during plasma treatment of bacteria in solid and liquid environments consume part of the RNOS generated by the plasma, as they can also undergo redox reactions. Therefore, the presence of external biomolecules have a direct effect on the level and type of damage induced in the molecular targets in bacterial cells and can determine the treatment outcome. Finally, the present study highlights the importance of single cell approaches to understand the discrete differences in the response of a population to LTP treatments.

This body of work contributes to the knowledge on the biomedical applications of LTPs and illustrates the importance of integrating understanding from plasma physics with biological and chemical analysis for the development of plasma therapies that can be effective and safe for the treatment of patients. LTP treatments applied individually or in combination with other antimicrobial therapies could be effectively used to treat infected wounds, including infections with drug-resistant pathogens. In addition to the parameters already known to affect the antimicrobial activity of plasmas, the factors described here can also contribute to the success or failure of LTP treatments. The spatial distribution of RNOS in the plasma, presence of external biomolecules during treatment and heterogeneity of the target population will equally affect the treatment of bacteria, fungi or cancer cells with LTP therapies. Therefore, the importance of these factors should be acknowledged and considered in the development of successful LTP therapies.

The research presented in this thesis could be extended in the future by studying the effect of the parameters described here for LTPs in the context of wound infections, considering the spatial distribution of RNOS in the plasma, presence of organic matter, the complex topography of the wound and the presence of polymicrobial infections. For this purpose, it is important to determine the minimum concentrations of RNOS produced in the plasma that are required to eliminate specific pathogens. The spatial distribution of other RNOS in the plasma effluent (in

addition to O_3 density shown here) in combination with biological assays should be studied to determine their correlation with the bactericidal action of LTPs. Thus, UV absorption spectroscopy could be used to measure ·OH density (299), combined with laser induced fluorescence to measure NO density, and two-photon absorption laser-induced fluorescence to measure O density (300). In addition, this information could help to predict the main biomolecules affected in cells exposed to plasma located at different distances from the plasma jet. Further analysis of damage to the cell membrane and DNA region in plasma-treated bacteria at the single cell level (located at different distances from the plasma jet) could be done using transmission and scanning electron microscopy (301). Thus, the discovery of trends in the composition of LTPs and the mechanisms of action for bacterial elimination could help in elucidating the main molecular targets in bacterial cells. In the long term, this information could assist the design of more effective therapies, where tailored LTP treatments for specific pathogens (that deliver a desired set of RNOS in sufficient quantity) could be used in biomedicine.

The future application of LTP treatments in biomedicine depends on the development of treatments that are effective against pathogens but safe for human patients. From this angle, the ability of external biomolecules to scavenge the RNOS produced by the plasma could be used to develop 'barriers' to protect sensitive tissues or non-targeted cells from plasma-generated RNOS. In the future, it should be explored whether the application of organic compounds (e.g. non-toxic natural products without cytotoxic or antibacterial properties) in the surroundings of the target region to be exposed to plasma (such as an infected topic wound) could confer protection against plasma-generated RNOS to the host cells and natural bacterial flora present on the skin. This could reduce the side effects of LTP treatments on non-targeted cells. *In vitro* and *in vivo* experiments (e.g. mouse model) assessing not only the induction of physical damage to biological structures such as DNA and cell membrane as described here, but also the viability and induction of mutations should be carried out in both- targeted and non-targeted cells (host cells and pathogens). In particular, the appearance of induced mutations could lead to the development of resistance to LTP treatments in both- host and bacterial cells, and carcinogenesis in eukaryotic cells. This information would contribute to the development of more effective and safer LTP treatments.

In addition, the complex architecture of the infected wound and its impact on the efficacy of antibacterial LTP treatments should be considered. *In silico* approaches could be used to model the delivery of plasma-generated RNOS at surfaces with complex topography such as damaged skin (302), as well as the development of resistance in bacteria exposed to low levels of RNOS (303). Since LTPs can deliver small concentrations of multiple RNOS to hidden grooves in the tissue where common antibacterial treatments (such as ointments and antiseptic solutions) do not reach, this would be valuable for the elimination of drug-resistant microorganisms in skin wounds.

Finally, since Gram positive and Gram negative bacteria (*S. aureus* and *P. aeruginosa*, for example) are commonly found in infected skin wounds, the efficacy of LTP treatments should be studied in the context of polymicrobial infections. Based on previous results obtained by Matthes *et al.* (164), differences in the sensitivity of Gram positive and Gram negative bacteria to LTP treatments can be expected. Besides studying the effect of LTPs on the bacterial load of mixed populations, changes in the population dynamics (304), effect of suboptimal doses of plasma (305) and the generation of small-colony variants of *S. aureus* (306) (i.e. variations in phenotype accompanied by development of aminoglycoside resistance and persistence in chronic infections (307)) should be explored both *in vitro* and *in vivo*. In addition, combinatorial treatments of traditional antimicrobials (such as antibiotics and antiseptics) and LTP therapies to eliminate drug resistant pathogens should be studied.

Ongoing research is increasing our understanding of the physical properties of plasmas and engineering of plasma delivery with the aim of developing plasmas sources that are both well-defined and controlled. In light of what is currently known, the use of LTP treatments in biomedicine has immense potential, as individual or combined treatments could be routinely used to effectively treat acute and chronic infections without negative side effects in patients. To reach this long-term objective, further interdisciplinary approaches are needed to better understand the mechanisms of action, the dynamic composition of plasmas and the limitations of these therapies. This is paramount for the successful translation of this technology to the biomedical setting. The development of new treatments is always challenging, but with the cooperation of the scientific community working in the field, the application of LTP treatments in multiple areas of biomedicine could materialize in the next ten or twenty years.

APPENDIX 1

(a)

```
$HistoryLength = 0;
RGBtable =
  Import["http://www-users.york.ac.uk/~rglv500/colortable_rgb.txt", "Table"] / 255.0;
RGBtable2 = Table[{(i - 1) / 255, RGBtable[[i]]}, {i, 256}];
myColourFunction = Interpolation[RGBtable2];
IDLColour[w_] := RGBColor[myColourFunction[w]]
f[x_] := UnitStep[x - threshold]
g[x_?MatrixQ] := N[Total[f[x], 2] / Dimensions[x][[1]] / Dimensions[x][[2]]]
TIFFGetData[filename_?StringQ] := Import[SubDir <> filename, "Data"]
```

(b)

```
SubDir = "/Users/Angelline/Documents/Angela/CIDCATS/PhD
    project/RESULTS/Salmonella/DDDA/Salmonella/08.03.2013 O2
    curve/08.03.2013/Plasma Helium only/Slide 7 120 sec/";
b = TIFFGetData["Slide 7 He 120sec origin 2 bw.tif"];
Print["The size of the image is ", Dimensions[b], " pixels."]
ΔN = 3; (* Average over a square ΔN x ΔN pixels. *)
c = N[Table[Sum[b[[i + i0, j + j0]], {i0, 0, ΔN - 1}, {j0, 0, ΔN - 1}],
   {i, 1, Dimensions[b][[1]] - ΔN + 1, ΔN}, {j, 1, Dimensions[b][[2]] - ΔN + 1, ΔN}]];
c = c / Max[c];
Print["The size of the reduced image is ", Dimensions[c], " pixels."]
threshold = 0.2
Print["The proportion of the reduced image with intensity ≥ ",
 100 threshold, "% of the maximum value is ", 100 g[c], "%."]
p1 = ArrayPlot[Log[c], ColorFunction → IDLColour, FrameTicks → Automatic];
{Slider[Dynamic[Rmax], {0, 500}], Dynamic[Rmax]}
{Slider[Dynamic[i0], {0, 500}], Dynamic[i0]}
{Slider[Dynamic[j0], {0, 500}], Dynamic[j0]}
Dynamic[Show[p1, Graphics[{Thick, Circle[{j0, Dimensions[c][[1]] - i0 + 1}, Rmax]}]]]
```

(c)

```
The size of the image is {1040, 1388} pixels.

The size of the reduced image is {346, 462} pixels.

0.2

The proportion of the reduced image with intensity ≥
 20.% of the maximum value is 0.186422%.

{ , 61.5}
{ , 197.}
{ , 244.}
```

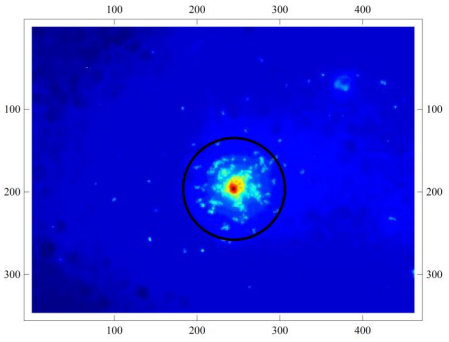

Appendix A.1. ***Algorithm used for the quantitative analysis of DNA damage in single cells with the DDD Assay.*** **(a)** Code that establishes the format of the false colour picture to be displayed. **(b)** Instructions to locate and import the file. The image size was reduced to one third of the original size to facilitate the analysis. The bottom part contains the instructions to generate slider buttons to adjust size and position of circular selection area. **(c)** Slider buttons and false colour image. The size and position of the area to be analysed is adjusted according to each cell in the image. ***(Continues in the following page.)***

(d)

```
c2 = Table[If[Sqrt[(i - i0)^2 + (j - j0)^2] < Rmax, c[[i, j]], 0],
    {i, Dimensions[c][[1]]}, {j, Dimensions[c][[2]]}];
{i0, j0} = N[Mean[Position[c2, Max[c2]]]]
Clear[c2]
ΔR = 3
W = Sort[Flatten[Table[{Sqrt[(i - i0)^2 + (j - j0)^2], c[[i, j]]},
      {i, Dimensions[c][[1]]}, {j, Dimensions[c][[2]]}], 1]];
W3 = Table[WT = Transpose[Select[W, R ≤ #[[1]] < R + ΔR &]];
    {Mean[WT[[1]]], Mean[WT[[2]]]}, {R, 0, Rmax, ΔR}];
W3a = Table[{W3[[i, 1]], Log[W3[[i, 2]] - W3[[Length[W3], 2]]]}, {i, Length[W3] - 1}];
Wx = Fit[W3a, {1, x}, x]
Show[ListPlot[W3a], Plot[Wx, {x, 0, Rmax}]]
Print["Radio of halo is ", -ΔN / D[Wx, x], " (original) pixels."]
Print["Radio of halo is ", -ΔN / D[Wx, x] * 0.063, " (original) um."]
{197., 244.}
3
-0.714645 - 0.111405 x
```

(e)

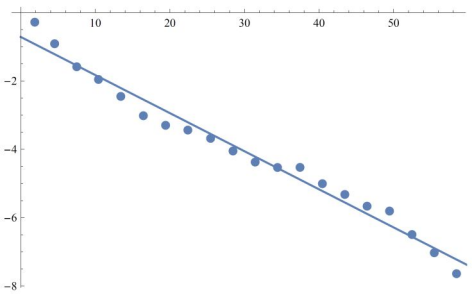


```
Radio of halo is 26.9287 (original) pixels.
Radio of halo is 1.69651 (original) um.
```

Appendix 1. (cont.). (d) Code for the analysis of mean pixel brightness of the selected area. The selected area repositions to have the brightest region located in the centre. The analysis starts in the centre of the selected area and the radial bin size increases 3 pixels at the time to determine the mean pixel brightness in each region. **(e)** The result of the analysis is shown in a plot of the logarithm of mean pixel brightness vs. radial distance. The radius of the halo formed by DNA fragments is determined in μm of the original file. The results fit the model shown in Section 2.6.4.

ABBREVIATIONS

°C	Degrees Celsius
ACS	Agarose-coated slide
ANOVA	Analysis of variance
AP-DBD	Atmospheric-pressure dielectric barrier discharge
CFU	Colony forming units
cm	Centimetre
DC	Direct current
DEPMPO	5-(Diethoxyphosphoryl)-5-methyl-1-pyrroline-N-oxide
DMEM	Dulbecco's modified Eagle's medium
DMPO	5,5-dimethy-1-pyrroline-N-oxide
DNA	Deoxyribonucleic acid
ELISA	Enzyme-linked immunosorbent assay
EPR	Electron paramagnetic resonance
FCS	Foetal calf serum
FE-DBD	Floating-electrode dielectric-barrier discharge
FITC	Fluorescein isothiocyanate
FPG	Formamidopyrimidine-DNA glycosylase
FSC	Forward scatter
x *g*	Times gravity
H_2O	Water
H_2O_2	Hydrogen peroxide
He	Helium

Hz	Hertz
kHz	Kilohertz
kV	Kilovolts
LB	Lennox Broth
LMP	Low melting point
LTP	Low temperature plasma
M	Mole
M9	Minimal medium M9
MGD	N-Methyl-D-glucamine dithiocarbamate
MgF_2	Magnesium fluoride
MHz	Megahertz
min	Minute
mL	Millilitre
mM	milliMole
mm	Millimetre
mm^2	Square millimetre
ms	Millisecond
mW	Microwave power
N_2	Molecular nitrogen
NaCl	Sodium chloride
NaN_3	Sodium azide
nm	nanometre
NO	Nitric oxide

NO_2^-	Nitrite ion
NO_3^-	Nitrate ion
O	Atomic oxygen
O_2	Molecular oxygen
$O_2^{\bullet -}$	Superoxide radical
$O_2(a^1\Delta g)$	Singlet oxygen
O_3	Ozone
OD	Optical density
OES	Optical emission spectroscopy
·OH	Hydroxyl radical
PBS	Phosphate buffered saline
PE	Phycoerythrin
pF	Picofarad
PI	Propidium iodide
ppm	Parts per million
RNOS	Reactive nitrogen and oxygen species
RNS	Reactive nitrogen species
ROS	Reactive oxygen species
S. Typhimurium	*Salmonella enterica* subspecies enterica serovar Typhimurium
sec	Second
slm	Standard litres per minute
SSC	Side scatter
TBE	Tris-botate-EDTA buffer

TEMP	2,2,6,6-Tetramethylpiperidine
TEMPO	2,2,6,6-Tetramethylpiperidine 1-oxyl
U	Units
U/mL	Units per millilitre
µAPPJ	Radio-frequency atmospheric-pressure plasma jet
µL	Microlitre
µM	microMole
µm	Micrometre
µW/cm²	Microwatts per square centimetre
UV	Ultraviolet
vol	Volume
v/v	Volume/volume
w/v	Weight/volume

REFERENCES

1. **WHO** 2014. Antimicrobial resistance: global report on surveillance. World Health Organization. http://www.who.int/drugresistance/documents/surveillancereport/en/.

2. **Levy SB.** 1982. Microbial resistance to antibiotics. An evolving and persistent problem. Lancet **2:**83-88.

3. **Watanabe T.** 1963. Infective heredity of multiple drug resistance in bacteria. Bacteriol Rev **27:**87-115.

4. **WHO.** 2002. Prevention of hospital-acquired infections. A practical guide. **WHO/CDS/CSR/EPH/2002.12**. http://www.who.int/csr/resources/publications/whocdscsreph200212.pdf.

5. **Bowler PG, Duerden BI, Armstrong DG.** 2001. Wound microbiology and associated approaches to wound management. Clin Microbiol Rev **14:**244-269.

6. **Morita Y, Tomida J, Kawamura Y.** 2012. MexXY multidrug efflux system of *Pseudomonas aeruginosa*. Front Microbiol **3:**408. doi:10.3389/fmicb.2012.00408.

7. **Chambers HF, Deleo FR.** 2009. Waves of resistance: *Staphylococcus aureus* in the antibiotic era. Nat Rev Microbiol **7:**629-641.

8. **Patterson MJ.** 1996. *Streptococcus*. *In* Baron S (ed.), Medical Microbiology, 4th ed. University of Texas Medical Branch at Galveston, Galveston, Texas. Available from: http://www.ncbi.nlm.nih.gov/books/NBK7611/.

9. **Siegel JD, Rhinehart E, Jackson M, Chiarello L.** 2007. Management of multidrug-resistant organisms in health care settings, 2006. Am J Infect Control **35**(10)**:**S165-S193. doi:10.1016/j.ajic.2007.10.006.

10. **Lipsky BA, Hoey C.** 2009. Topical antimicrobial therapy for treating chronic wounds. Clin Infect Dis **49:**1541-1549.

11. **Moreau M, Orange N, Feuilloley MG.** 2008. Non-thermal plasma technologies: new tools for bio-decontamination. Biotechnol Adv **26:**610-617.

12. **Ermolaeva SA, Varfolomeev AF, Chernukha MY, Yurov DS, Vasiliev MM, Kaminskaya AA, Moisenovich MM, Romanova JM, Murashev AN, Selezneva II, Shimizu T, Sysolyatina EV, Shaginyan IA, Petrov OF, Mayevsky EI, Fortov VE, Morfill GE, Naroditsky BS, Gintsburg AL.** 2011. Bactericidal effects of non-thermal argon plasma *in vitro*, in biofilms and in the animal model of infected wounds. J Med Microbiol 60:75-83.

13. **Joshi SG, Cooper M, Yost A, Paff M, Ercan UK, Fridman G, Friedman G, Fridman A, Brooks AD.** 2011. Nonthermal dielectric-barrier discharge plasma-induced

inactivation involves oxidative DNA damage and membrane lipid peroxidation in *Escherichia coli*. Antimicrob Agents Chemother **55:**1053-1062.

14. **Kvam E, Davis B, Mondello F, Garner AL.** 2012. Nonthermal atmospheric plasma rapidly disinfects multidrug-resistant microbes by inducing cell surface damage. Antimicrob Agents Chemother **56:**2028-2036.

15. **Brehmer F, Haenssle HA, Daeschlein G, Ahmed R, Pfeiffer S, Gorlitz A, Simon D, Schon MP, Wandke D, Emmert S.** 2015. Alleviation of chronic venous leg ulcers with a hand-held dielectric barrier discharge plasma generator (PlasmaDerm((R)) VU-2010): results of a monocentric, two-armed, open, prospective, randomized and controlled trial (NCT01415622). J Eur Acad Dermatol Venereol **29:**148-155.

16. **Haertel B, von Woedtke T, Weltmann KD, Lindequist U.** 2014. Non-thermal atmospheric-pressure plasma possible application in wound healing. Biomol Ther (Seoul) **22:**477-490.

17. **Newsom SWB, Ridgway GL.** 2013. The history of decontamination in hospitals. *In* Walker J (ed.), Decontamination in hospitals and healthcare, 1st ed. Woodhead Publishing Ltd.

18. **Kohanski MA, Dwyer DJ, Collins JJ.** 2010. How antibiotics kill bacteria: from targets to networks. Nat Rev Microbiol **8:**423-435.

19. **Awad SS, Elhabash SI, Lee L, Farrow B, Berger DH.** 2007. Increasing incidence of methicillin-resistant *Staphylococcus aureus* skin and soft-tissue infections: reconsideration of empiric antimicrobial therapy. Am J Surg **194:**606-610.

20. **McDonnell G, Russell AD.** 1999. Antiseptics and disinfectants: activity, action, and resistance. Clin Microbiol Rev **12:**147-179.

21. **Halliwell B, Gutteridge JMC.** 2007. Free radicals in biology and medicine, 4th ed. Oxford University Press, Oxford; New York.

22. **Christman MF, Morgan RW, Jacobson FS, Ames BN.** 1985. Positive control of a regulon for defenses against oxidative stress and some heat-shock proteins in *Salmonella* Typhimurium. Cell **41:**753-762.

23. **Hugo WB, Longworth AR.** 1966. The effect of chlorhexidine on the electrophoretic mobility, cytoplasmic constituents, dehydrogenase activity and cell walls of *Escherichia coli* and *Staphylococcus aureus*. J Pharm Pharmacol **18:**569-578.

24. **Russell AD, Day MJ.** 1993. Antibacterial activity of chlorhexidine. J Hosp Infect **25:**229-238.

25. **Russell AD, Tattawasart U, Maillard JY, Furr JR.** 1998. Possible link between bacterial resistance and use of antibiotics and biocides. Antimicrob Agents Chemother **42:**2151-2151.

26. **Capriotti K, Capriotti JA.** 2012. Topical iodophor preparations: chemistry, microbiology, and clinical utility. Dermatol Online J **18:**1.

27. **Lansdown ABG.** 2010. A pharmacological and toxicological profile of silver as an antimicrobial agent in medical devices. Adv Pharmacol Sci **2010:**910686. doi:10.1155/2010/910686.

28. **Jung WK, Koo HC, Kim KW, Shin S, Kim SH, Park YH.** 2008. Antibacterial activity and mechanism of action of the silver ion in *Staphylococcus aureus* and *Escherichia coli*. Appl Environ Microbiol **74:**2171-2178.

29. **Percival SL, McCarty SM.** 2015. Silver and alginates: Role in wound healing and biofilm control. Adv Wound Care (New Rochelle) **4:**407-414.

30. **Russell AD.** 1997. Plasmids and bacterial resistance to biocides. J Appl Microbiol **83:**155-165.

31. **Zasloff M.** 2002. Antimicrobial peptides of multicellular organisms. Nature **415:**389-395.

32. **Kavanagh K, Dowd S.** 2004. Histatins: antimicrobial peptides with therapeutic potential. J Pharm Pharmacol **56:**285-289.

33. **Gordon YJ, Romanowski EG, McDermott AM.** 2005. A review of antimicrobial peptides and their therapeutic potential as anti-infective drugs. Curr Eye Res **30:**505-515.

34. **Guilhelmelli F, Vilela N, Albuquerque P, Derengowski LD, Silva-Pereira I, Kyaw CM.** 2013. Antibiotic development challenges: the various mechanisms of action of antimicrobial peptides and of bacterial resistance. Front Microbiol **4:**353. doi:10.3389/Fmicb.2013.00353.

35. **Yeaman MR, Yount NY.** 2003. Mechanisms of antimicrobial peptide action and resistance. Pharmacol Rev **55:**27-55.

36. **Gunaydin M, Esen S, Karadag A, Unal N, Yanik K, Odabasi H, Birinci A.** 2014. *In vitro* antimicrobial activity of Medilox$^{(R)}$ super-oxidized water. Ann Clin Microbiol Antimicrob **13:**29. doi:10.1186/1476-0711-13-29.

37. **Tanaka H, Hirakata Y, Kaku M, Yoshida R, Takemura H, Mizukane R, Ishida K, Tomono K, Koga H, Kohno S, Kamihira S.** 1996. Antimicrobial activity of superoxidized water. J Hosp Infect 34:43-49.

38. **Mai-Prochnow A, Murphy AB, McLean KM, Kong MG, Ostrikov KK.** 2014. Atmospheric pressure plasmas: Infection control and bacterial responses. Int J Antimicrob Agents **43:**508-517.

39. **Daeschlein G, Scholz S, Ahmed R, von Woedtke T, Haase H, Niggemeier M, Kindel E, Brandenburg R, Weltmann KD, Juenger M.** 2012. Skin decontamination by low-temperature atmospheric pressure plasma jet and dielectric barrier discharge plasma. J Hosp Infect **81:**177-183.

40. **Lademann J, Ulrich C, Patzelt A, Richter H, Kluschke F, Klebes M, Lademann O, Kramer A, Weltmann KD, Lange-Asschenfeldt B.** 2013. Risk assessment of the application of tissue-tolerable plasma on human skin. Clin Plasma Med 1:5-10.

41. **Kramer A, Lademann J, Bender C, Sckell A, Hartmann B, Münch S, Hinz P, Ekkernkamp A, Matthers R, Koban I, Partecke I, Heidecke CD, Masur K, Reuter S, Weltmann KD.** 2013. Suitability of tissue tolerable plasmas (TTP) for the management of chronic wounds. Clin Plasma Med 1:11-18.

42. **Deng XT, Shi JJ, Kong MG.** 2006. Physical mechanisms of inactivation of *Bacillus subtilis* spores using cold atmospheric plasmas. IEEE T Plasma Sci **34:**1310-1316.

43. **Park JH, Kumar N, Uhm HS, Lee W, Choi EH, Attri P.** 2015. Effect of nanosecond-pulsed plasma on the structural modification of biomolecules. RSC Advances **5:**47300-47308.

44. **Alkawareek MY, Gorman SP, Graham WG, Gilmore BF.** 2013. Potential cellular targets and antibacterial efficacy of atmospheric pressure non-thermal plasma. Int J Antimicrob Agents **43:**154-160.

45. **Boxhammer V, Li YF, Köritzer J, Shimizu T, Maisch T, Thomas HM, Schlegel J, Morfill GE, Zimmermann JL.** 2013. Investigation of the mutagenic potential of cold atmospheric plasma at bactericidal dosages. Mutat Res **753:**23-28.

46. **Heinlin J, Morfill G, Landthaler M, Stolz W, Isbary G, Zimmermann JL, Shimizu T, Karrer S.** 2010. Plasma medicine: possible applications in dermatology. J Dtsch Dermatol Ges **8:**968-976.

47. **Conrads H, Schmidt M.** 2000. Plasma generation and plasma sources. Plasma Sources Sci Technol **9:**441-454.

48. **Boulos M, Fauchais P, Pfender E.** 1994. Thermal plasmas. Fundamentals and applications. Springer New York, USA.

49. **Galeev A, Sudan RN.** 1983. Basic Plasma Physics, p. xiii, Handbook of Plasma Physics, vol. 1. North-Holland Pub., Amsterdam ; New York, N.Y.

50. **Fridman AA.** 2008. Plasma Chemistry. Cambridge University Press, Cambridge ; New York.

51. **O'Connell D, Cox LJ, Hyland WB, McMahon SJ, Reuter S, Graham WG, Gans T, Currell FJ.** 2011. Cold atmospheric pressure plasma jet interactions with plasmid DNA. Appl Phys Lett **98:**043701. doi:10.1063/1.3521502.

52. **Moisan M, Barbeau J, Crevier MC, Pelletier J, Philip N, Saoudi B.** 2002. Plasma sterilization. Methods mechanisms. Pure Appl Chem **74:**349-358.

53. **Graves DB.** 2012. The emerging role of reactive oxygen and nitrogen species in redox biology and some implications for plasma applications to medicine and biology. J Phys D: Appl Phys **45:**263001. doi:10.1088/0022-3727/45/26/263001.

54. **Laroussi M, Akan T.** 2007. Arc-free atmospheric pressure cold plasma jets: A review. Plasma Process Polym **4:**777-788.

55. **Scholtz V, Pazlarova J, Souskova H, Khun J, Julak J.** 2015. Nonthermal plasma - A tool for decontamination and disinfection. Biotechnol Adv **33:**1108-1119.

56. **Uhm HS, Lim JP, Li SZ.** 2007. Sterilization of bacterial endospores by an atmospheric-pressure argon plasma jet. Appl Phys Lett **90:**261501. doi:10.1063/1.2747177.

57. **Park GY, Hong YJ, Lee HW, Sim JY, Lee JK.** 2010. A global model for the identification of the dominant reactions for atomic oxygen in He/O_2 atmospheric-pressure plasmas. Plasma Process Polym **7:**281-287.

58. **Fernandez A, Thompson A.** 2012. The inactivation of *Salmonella* by cold atmospheric plasma treatment. Food Res Int **45:**678-684.

59. **Ehlbeck J, Schnabel U, Polak M, Winter J, von Woedtke T, Brandenburg R, von dem Hagen T, Weltmann KD.** 2011. Low temperature atmospheric pressure plasma sources for microbial decontamination. J Phys D: Appl Phys **44:**013002. doi:10.1088/0022-3727/44/1/013002.

60. **Bussiahn R, Brandenburg R, Gerling T, Kindel E, Lange H, Lembke N, Weltmann KD, von Woedtke T, Kocher T.** 2010. The hairline plasma: An intermittent negative DC-corona discharge at atmospheric pressure for plasma medical applications. Appl Phys Lett **96:**143701. doi:10.1063/1.3380811.

61. **Heinlin J, Isbary G, Stolz W, Morfill G, Landthaler M, Shimizu T, Steffes B, Nosenko T, Zimmermann J, Karrer S.** 2011. Plasma applications in medicine with a special focus on dermatology. J Eur Acad Dermatol Venereol **25:**1-11.

62. **Lee HW, Kang SK, Won IH, Kim HY, Kwon HC, Sim JY, Lee JK.** 2013. Distinctive plume formation in atmospheric Ar and He plasmas in microwave frequency band and suitability for biomedical applications. Phys Plasmas **20:**123506. doi:10.1063/1.4841295.

63. **Gregorio J, Leroy O, Leprince P, Alves LL, Boisse-Laporte C.** 2009. Design of a microwave microplasma source at atmospheric pressure. IEEE T Plasma Sci **37:**797-808.

64. **Iza F, Kim GJ, Lee SM, Lee JK, Walsh JL, Zhang YT, Kong MG.** 2008. Microplasmas: Sources, particle kinetics, and biomedical applications. Plasma Process Polym **5:**322-344.

65. **Choi J, Iza F, Do HJ, Lee JK, Cho MH.** 2009. Microwave-excited atmospheric-pressure microplasmas based on a coaxial transmission line resonator. Plasma Sources Sci Technol **18:**025029. doi:10.1088/0963-0252/18/2/025029.

66. **Isbary G, Heinlin J, Shimizu T, Zimmermann JL, Morfill G, Schmidt HU, Monetti R, Steffes B, Bunk W, Li Y, Klaempfl T, Karrer S, Landthaler M, Stolz W.** 2012. Successful and safe use of 2 min cold atmospheric argon plasma in chronic wounds: results of a randomized controlled trial. Br J Dermatol 167:404-410.

67. **Fridman A.** 2004, p 410. The 31st IEEE International Conference on Plasma Science (ICOPS 2004)

68. **Park GY, Park SJ, Choi MY, Koo IG, Byun JH, Hong JW, Sim JY, Collins GJ, Lee JK.** 2012. Atmospheric-pressure plasma sources for biomedical applications. Plasma Sources Sci Technol **21:**043001. doi: 10.1088/0963-0252/21/4/043001.

69. **Laroussi M, Tendero C, Lu X, Alla S, Hynes WL.** 2006. Inactivation of bacteria by the plasma pencil. Plasma Process Polym **3:**470-473.

70. **Lackmann JW, Bandow JE.** 2014. Inactivation of microbes and macromolecules by atmospheric-pressure plasma jets. Appl Microbiol Biotechnol **98:**6205-6213.

71. **Dolezalova E, Lukes P.** 2015. Membrane damage and active but nonculturable state in liquid cultures of *Escherichia coli* treated with an atmospheric pressure plasma jet. Bioelectrochemistry **103:**7-14.

72. **Saša L, Nevena P, Maja M, Dušan P, Milena J, Diana B, Slavko M, Dejan M, Gordana M, Pavle M, Zoran P.** 2010. The effect of a plasma needle on bacteria in planktonic samples and on peripheral blood mesenchymal stem cells. New J Phys **12:**083037. doi:10.1088/1367-2630/12/8/083037.

73. **Ureyen Kaya B, Kececi AD, Guldas HE, Cetin ES, Ozturk T, Oksuz L, Bozduman F.** 2014. Efficacy of endodontic applications of ozone and low-temperature atmospheric pressure plasma on root canals infected with *Enterococcus faecalis*. Lett Appl Microbiol **58:**8-15.

74. **Imlay JA.** 2003. Pathways of oxidative damage. Annu Rev Microbiol **57:**395-418.

75. **Fang FC.** 2004. Antimicrobial reactive oxygen and nitrogen species: concepts and controversies. Nat Rev Microbiol **2:**820-832.

76. **Bienert GP, Chaumont F.** 2014. Aquaporin-facilitated transmembrane diffusion of hydrogen peroxide. Biochim Biophys Acta **1840:**1596-1604.

77. **Imlay JA, Chin SM, Linn S.** 1988. Toxic DNA damage by hydrogen peroxide through the Fenton reaction *in vivo* and *in vitro*. Science **240:**640-642.

78. **Imlay JA.** 2013. The molecular mechanisms and physiological consequences of oxidative stress: lessons from a model bacterium. Nat Rev Microbiol **11:**443-454.

79. **Dizdaroglu M.** 2012. Oxidatively induced DNA damage: mechanisms, repair and disease. Cancer Lett. **327:**26-47.

80. **Farr SB, Kogoma T.** 1991. Oxidative stress responses in *Escherichia coli* and *Salmonella* Typhimurium. Microbiol Rev **55:**561-585.

81. **Agnez-Lima LF, Melo JT, Silva AE, Oliveira AH, Timoteo AR, Lima-Bessa KM, Martinez GR, Medeiros MH, Di Mascio P, Galhardo RS, Menck CF.** 2012. DNA damage by singlet oxygen and cellular protective mechanisms. Mutat Res 751:15-28.

82. **Cadet J, Douki T, Ravanat JL.** 2010. Oxidatively generated base damage to cellular DNA. Free Radical Bio Med **49:**9-21.

83. **Victorin K.** 1992. Review of the genotoxicity of ozone. Mutat Res **277:**221-238.

84. **Menzel DB.** 1984. Ozone: An overview of its toxicity in man and animals. J Toxicol Env Health **13:**183-204.

85. **O'Donnell VB, Chumley PH, Hogg N, Bloodsworth A, Darley-Usmar VM, Freeman BA.** 1997. Nitric oxide inhibition of lipid peroxidation: kinetics of reaction with lipid peroxyl radicals and comparison with alpha-tocopherol. Biochemistry **36:**15216-15223.

86. **Lundberg JO, Weitzberg E, Gladwin MT.** 2008. The nitrate-nitrite-nitric oxide pathway in physiology and therapeutics. Nat Rev Drug Discov **7:**156-167.

87. **Cutting KF.** 2003. Wound exudate: composition and functions. Br J Community Nurs **8:**S4-S9. doi:10.12968/bjcn.2003.8.Sup3.11577.

88. **Bertesteanu S, Triaridis S, Stankovic M, Lazar V, Chifiriuc MC, Vlad M, Grigore R.** 2014. Polymicrobial wound infections: Pathophysiology and current therapeutic approaches. Int J Pharm **463:**119-126.

89. **Giacometti A, Cirioni O, Schimizzi AM, Del Prete MS, Barchiesi F, D'Errico MM, Petrelli E, Scalise G.** 2000. Epidemiology and microbiology of surgical wound infections. J Clin Microbiol 38:918-922.

90. **O'Connor N, Cahill O, Daniels S, Galvin S, Humphreys H.** 2014. Cold atmospheric pressure plasma and decontamination. Can it contribute to preventing hospital-acquired infections? J Hosp Infect **88:**59-65.

91. **Alkawareek MY, Algwari QT, Laverty G, Gorman SP, Graham WG, O'Connell D, Gilmore BF.** 2012. Eradication of *Pseudomonas aeruginosa* biofilms by atmospheric pressure non-thermal plasma. PLoS ONE **7**(8)**:**e44289. doi:10.1371/journal.pone.0044289.

92. **Bayliss DL, Shama G, Kong MG.** 2013. Restoration of antibiotic sensitivity in meticillin-resistant *Staphylococcus aureus* following treatment with a non-thermal atmospheric gas plasma. Int J Antimicrob Agents **41:**398-399.

93. **Isbary G, Morfill G, Schmidt HU, Georgi M, Ramrath K, Heinlin J, Karrer S, Landthaler M, Shimizu T, Steffes B, Bunk W, Monetti R, Zimmermann JL, Pompl R, Stolz W.** 2010. A first prospective randomized controlled trial to decrease bacterial load using cold atmospheric argon plasma on chronic wounds in patients. Br J Dermatol 163:78-82.

94. **Moisan M, Barbeau J, Moreau S, Pelletier J, Tabrizian M, Yahia LH.** 2001. Low-temperature sterilization using gas plasmas: a review of the experiments and an analysis of the inactivation mechanisms. Int J Pharm **226:**1-21.

95. **Laroussi M, Mendis DA, Rosenberg M.** 2003. Plasma interaction with microbes. New J Phys **5:**41. doi:10.1088/1367-2630/5/1/341.

96. **Yu H, Perni S, Shi JJ, Wang DZ, Kong MG, Shama G.** 2006. Effects of cell surface loading and phase of growth in cold atmospheric gas plasma inactivation of *Escherichia coli* K12. J Appl Microbiol **101:**1323-1330.

97. **Heise M, Neff W, Franken O, Muranyi P, Wunderlich J.** 2004. Sterilization of polymer foils with dielectric barrier discharges at atmospheric pressure. Plasmas Polym **9:**23-33.

98. **Park SR, Lee HW, Hong JW, Lee HJ, Kim JY, Choi BB, Kim GC, Jeon YC.** 2014. Enhancement of the killing effect of low-temperature plasma on *Streptococcus mutans* by combined treatment with gold nanoparticles. J Nanobiotechnology **12:**29. doi:10.1186/s12951-014-0029-5.

99. **Leduc M, Guay D, Leask RL, Coulombe S.** 2009. Cell permeabilization using a non-thermal plasma. New J Phys **11:**115021. doi:10.1088/1367-2630/11/11/115021.

100. **Pervez MR, Begum A, Laroussi M.** 2014. Plasma based sterilization: Overview and the stepwise inactivation process of microbial by non-thermal atmospheric pressure plasma jet. IJET-IJENS **14:**7-16.

101. **Marr AG, Ingraham JL.** 1962. Effect of temperature on the composition of fatty acids in *Escherichia Coli*. J Bacteriol **84:**1260-1267.

102. **Takai E, Kitamura T, Kuwabara J, Ikawa S, Yoshizawa S, Shiraki K, Kawasaki H, Arakawa R, Kitano K.** 2014. Chemical modification of amino acids by atmospheric-pressure cold plasma in aqueous solution. J Phys D: Appl Phys **47**(28)**:**285403. doi:10.1088/0022-3727/47/28/285403.

103. **Takai E, Kitano K, Kuwabara J, Shiraki K.** 2012. Protein inactivation by low-temperature atmospheric pressure plasma in aqueous solution. Plasma Process Polym **9:**77-82.

104. **Lackmann JW, Schneider S, Edengeiser E, Jarzina F, Brinckmann S, Steinborn E, Havenith M, Benedikt J, Bandow JE.** 2013. Photons and particles emitted from cold atmospheric-pressure plasma inactivate bacteria and biomolecules independently and synergistically. J R Soc Interface **10:**20130591. doi: 10.1098/Rsif.2013.0591.

105. **Bjelland S, Seeberg E.** 2003. Mutagenicity, toxicity and repair of DNA base damage induced by oxidation. Mutat Res **531:**37-80.

106. **Sharma A, Collins G, Pruden A.** 2009. Differential gene expression in *Escherichia coli* following exposure to nonthermal atmospheric pressure plasma. J Appl Microbiol **107:**1440-1449.

107. **Joshi SG, Yost A, Joshi SS, Addya S, Ehrlich G, Brooks A.** 2015. Microarray analysis of transcriptomic response of *Escherichia coli* to nonthermal plasma-treated PBS solution. Adv Biosci Biotechnol **6:**49-62.

108. **Ellerweg D, Benedikt J, von Keudell A, Knake N, Schulz-von der Gathen V.** 2010. Characterization of the effluent of a He/O_2 microscale atmospheric pressure plasma jet by quantitative molecular beam mass spectrometry. New J Phys **12:**013021. doi:10.1088/1367-2630/12/1/013021.

109. **Niemira BA, Sites J.** 2008. Cold plasma inactivates *Salmonella* Stanley and *Escherichia coli* O157:H7 inoculated on golden delicious apples. J Food Prot **71:**1357-1365.

110. **Li YF, Zimmermann JL, Morfill GE.** 2012. Optimizing the distance for bacterial treatment using surface micro-discharge plasma. New J Phys **14:**023058. doi:10.1088/1367-2630/14/2/023058.

111. **Schutze A, Jeong JY, Babayan SE, Park J, Selwyn GS, Hicks RF.** 1998. The atmospheric-pressure plasma jet: A review and comparison to other plasma sources. IEEE T Plasma Sci **26:**1685-1694.

112. **Niemi K, Reuter S, Schaper L, Knake N, Schulz-von der Gathen V, Gans T.** 2007. Diagnostics on an atmospheric pressure plasma jet. J Phys Conf Ser **71:**012012. doi:10.1088/1742-6596/71/1/012012.

113. **Niemi K, Waskoenig J, Sadeghi N, Gans T, O'Connell D.** 2011. The role of helium metastable states in radio-frequency driven helium-oxygen atmospheric pressure plasma jets: measurement and numerical simulation. Plasma Sources Sci T **20:**055005. doi:10.1088/0963-0252/20/5/055005.

114. **von Keudell A, Awakowicz P, Benedikt J, Raballand V, Yanguas-Gil A, Opretzka J, Flotgen C, Reuter R, Byelykh L, Halfmann H, Stapelmann K, Denis B, Wunderlich J, Muranyi P, Rossi F, Kylian O, Hasiwa N, Ruiz A, Rauscher H, Sirghi L, Comoy E, Dehen C, Challier L, Deslys JP.** 2010. Inactivation of bacteria and biomolecules by low-pressure plasma discharges. Plasma Process Polym 7:327-352.

115. **Fridman A.** 2012. Plasma biology and plasma medicine, p. 175-215. *In* Laroussi M, Kong MG, Morfill G, Stolz W (ed.), Plasma medicine: applications of low-temperature gas plasmas in medicine and biology. Cambridge University Press, Cambridge ; New York.

116. **Traylor MJ, Pavlovich MJ, Karim S, Hait P, Sakiyama Y, Clark DS, Graves DB.** 2011. Long-term antibacterial efficacy of air plasma-activated water. J Phys D: Appl Phys **44:**472001. doi:10.1088/0022-3727/44/47/472001.

117. **Machala Z, Tarabova B, Hensel K, Spetlikova E, Sikurova L, Lukes P.** 2013. Formation of ROS and RNS in water electro-sprayed through transient spark discharge in air and their bactericidal effects. Plasma Process Polym **10:**649-659.

118. **Sato T, Yokoyama M, Johkura K.** 2011. A key inactivation factor of HeLa cell viability by a plasma flow. J Phys D: Appl Phys **44:**372001. doi:10.1088/0022-3727/44/37/372001.

119. **Hoentsch M, Bussiahn R, Rebl H, Bergemann C, Eggert M, Frank M, von Woedtke T, Nebe B.** 2014. Persistent effectivity of gas plasma-treated, long time-stored liquid on epithelial cell adhesion capacity and membrane morphology. PLoS ONE **9:**e104559. doi:10.1371/journal.pone.0104559.

120. **Tanaka H, Mizuno M, Ishikawa K, Nakamura K, Kajiyama H, Kano H, Kikkawa F, Hori M.** 2011. Plasma-activated medium selectively kills glioblastoma brain tumor cells by down-regulating a survival signaling molecule, AKT kinase. Plasma Med **1:**265-277.

121. **Han X, Cantrell WA, Escobar EE, Ptasinska S.** 2014. Plasmid DNA damage induced by helium atmospheric pressure plasma jet. Eur Phys J D **68:**46. doi:10.1140/Epjd/E2014-40753-Y.

122. **Schulz-von der Gathen V, Schaper L, Knake N, Reuter S, Niemi K, Gans T, Winter J.** 2008. Spatially resolved diagnostics on a microscale atmospheric pressure plasma jet. J Phys D: Appl Phys **41:**194004. doi:10.1088/0022-3727/41/19/194004.

123. **Awakowicz P, Bibinov N, Born M, Busse B, Gesche R, Helmke A, Kaemling A, Kolb-Bachofen V, Kovacs R, Kuehn S, Liebmann J, Mertens N, Niemann U, Oplaender C, Porteanu HE, Scherer J, Suschek C, Vioel W, Wandke D.** 2009. Biological stimulation of the human skin applying health-promoting light and plasma sources. Contrib Plasma Phys 49:641-647.

124. **Heinlin J, Zimmermann JL, Zeman F, Bunk W, Isbary G, Landthaler M, Maisch T, Monetti R, Morfill G, Shimizu T, Steinbauer J, Stolz W, Karrer S.** 2013. Randomized placebo-controlled human pilot study of cold atmospheric argon plasma on skin graft donor sites. Wound Repair Regen 21:800-807.

125. **Coburn B, Grassl GA, Finlay BB.** 2007. *Salmonella*, the host and disease: a brief review. Immunol Cell Biol **85:**112-118.

126. **Brenner FW, Villar RG, Angulo FJ, Tauxe R, Swaminathan B.** 2000. *Salmonella* nomenclature. J Clin Microbiol **38:**2465-2467.

127. **Pui CF, Wong WC, Chai LC, Tunung R, Jeyaletchumi P, Noor Hidaya MS, Ubong A, Farinazleen MG, Cheah YK, Son R.** 2011. *Salmonella*: A foodborne pathogen. Int Food Res J 18:465-473.

128. **Ohl ME, Miller SI.** 2001. *Salmonella*: a model for bacterial pathogenesis. Annu Rev Med **52:**259-274.

129. **Miller AF.** 2012. Superoxide dismutases: ancient enzymes and new insights. FEBS Lett **586:**585-595.

130. **Henard CA, Vazquez-Torres A.** 2011. Nitric oxide and *Salmonella* pathogenesis. Front Microbiol **2:**84. doi:10.3389/fmicb.2011.00084.

131. **De Groote MA, Ochsner UA, Shiloh MU, Nathan C, McCord JM, Dinauer MC, Libby SJ, Vazquez-Torres A, Xu Y, Fang FC.** 1997. Periplasmic superoxide dismutase protects *Salmonella* from products of phagocyte NADPH-oxidase and nitric oxide synthase. PNAS **94:**13997-14001.

132. **Chen L, Xie QW, Nathan C.** 1998. Alkyl hydroperoxide reductase subunit C (AhpC) protects bacterial and human cells against reactive nitrogen intermediates. Mol Cell **1:**795-805.

133. **Rowan NJ, Espie S, Harrower J, Anderson JG, Marsili L, MacGregor SJ.** 2007. Pulsed-plasma gas-discharge inactivation of microbial pathogens in chilled poultry wash water. J Food Protect **70:**2805-2810.

134. **Fernandez A, Noriega E, Thompson A.** 2013. Inactivation of *Salmonella enterica* serovar Typhimurium on fresh produce by cold atmospheric gas plasma technology. Food Microbiol **33:**24-29.

135. **Fernandez A, Shearer N, Wilson DR, Thompson A.** 2012. Effect of microbial loading on the efficiency of cold atmospheric gas plasma inactivation of *Salmonella enterica* serovar Typhimurium. Int J Food Microbiol **152:**175-180.

136. **WHO Expert Committee on the Control of the Leishmaniases. Meeting (2010 : Geneva), World Health Organization.** 2010. Control of the leishmaniases: report of a meeting of the WHO Expert Committee on the Control of Leishmaniases, Geneva, 22-26 March 2010. World Health Organization, Geneva.

137. **Fernandez JL, Cartelle M, Muriel L, Santiso R, Tamayo M, Goyanes V, Gosalvez J, Bou G.** 2008. DNA fragmentation in microorganisms assessed *in situ*. Appl Environ Microbiol **74:**5925-5933.

138. **Duling DR.** 1994. Simulation of multiple isotropic spin-trap EPR spectra. J Magn Reson Ser B **104:**105-110.

139. **Sellers RM.** 1980. Spectrophotometric determination of hydrogen-peroxide using potassium titanium(IV) oxalate. Analyst **105:**950-954.

140. **Twomey B, Nindrayog A, Niemi K, Graham WG, Dowling DP.** 2011. Correlation between the electrical and optical properties of an atmospheric pressure plasma during siloxane coating deposition. Plasma Chem Plasma P **31:**139-156.

141. **Orphal J.** 2003. A critical review of the absorption cross-sections of O_3 and NO_2 in the ultraviolet and visible. J Photoch Photobio A **157:**185-209.

142. **Schulz-von der Gathen V, Buck V, Gans T, Knake N, Niemi K, Reuter S, Schaper L, Winter J.** 2007. Optical diagnostics of micro discharge jets. Contrib Plasma Phys 47:510-519.

143. **Zhang SQ, van Gaens W, van Gessel B, Hofmann S, van Veldhuizen E, Bogaerts A, Bruggeman P.** 2013. Spatially resolved ozone densities and gas temperatures in a time modulated RF driven atmospheric pressure plasma jet: An analysis of the production and destruction mechanisms. J Phys D: Appl Phys **46:**205202. doi:10.1088/0022-3727/46/20/205202.

144. **Winter J, Dunnbier M, Schmidt-Bleker A, Meshchanov A, Reuter S, Weltmann KD.** 2012. Aspects of UV-absorption spectroscopy on ozone in effluents of plasma jets operated in air. J Phys D: Appl Phys **45:**385201. doi:10.1088/0022-3727/45/38/385201.

145. **Álvarez R, Rodero A, Quintero MC.** 2002. An Abel inversion method for radially resolved measurements in the axial injection torch. Spectrochim Acta B **57:**1665-1680.

146. **Pretzier G.** 1991. A new method for numerical Abel-inversion. Z Naturforsch **46:**639-641.

147. **Niemi K, Reuter S, Graham LM, Waskoenig J, Knake N, Schulz-von der Gathen V, Gans T.** 2010. Diagnostic based modelling of radio-frequency driven atmospheric pressure plasmas. J Phys D: Appl Phys **43:**124006. doi:10.1088/0022-3727/43/12/124006.

148. **Wagenaars E, Gans T, O'Connell D, Niemi K.** 2012. Two-photon absorption laser-induced fluorescence measurements of atomic nitrogen in a radio-frequency atmospheric-pressure plasma jet. Plasma Sources Sci Technol **21:**042002. doi:10.1088/0963-0252/21/4/042002.

149. **Niemi K, Reuter S, Graham LM, Waskoenig J, Gans T.** 2009. Diagnostic based modeling for determining absolute atomic oxygen densities in atmospheric pressure helium-oxygen plasmas. Appl Phys Lett **95:**151504. doi:10.1063/1.3242382.

150. **Knake N, Reuter S, Niemi K, Schulz-von der Gathen V, Winter J.** 2008. Absolute atomic oxygen density distributions in the effluent of a microscale atmospheric pressure plasma jet. J Phys D: Appl Phys **41:**194006. doi: 10.1088/0022-3727/41/19/194006.

151. **Walsh JL, Kong MG.** 2008. Contrasting characteristics of linear-field and cross-field atmospheric plasma jets. Appl Phys Lett **93:**1-3.

152. **Boeuf JP, Yang LL, Pitchford LC.** 2013. Dynamics of a guided streamer ('plasma bullet') in a helium jet in air at atmospheric pressure. J Phys D: Appl Phys **46:**015201. doi:10.1088/0022-3727/46/1/015201.

153. **Algwari QT, O'Connell D.** 2011. Electron dynamics and plasma jet formation in a helium atmospheric pressure dielectric barrier discharge jet. Appl Phys Lett **99**(12)**:**121501 doi:10.1063/1.3628455.

154. **Stoffels E, Kieft IE, Sladek REJ, van den Bedem LJM, van der Laan EP, Steinbuch M.** 2006. Plasma needle for *in vivo* medical treatment: recent developments and perspectives. Plasma Sources Sci T **15:**S169-S180.

155. **Shimizu T, Steffes B, Pompl R, Jamitzky F, Bunk W, Ramrath K, Georgi M, Stolz W, Schmidt HU, Urayama T, Fujii S, Morfill GE.** 2008. Characterization of microwave plasma torch for decontamination. Plasma Process Polym 5:577-582.

156. **Dobrynin D, Fridman G, Friedman G, Fridman A.** 2009. Physical and biological mechanisms of direct plasma interaction with living tissue. New J Phys **11:**115020. doi:10.1088/1367-2630/11/11/115020.

157. **Jiang N, Ji AL, Cao ZX.** 2009. Atmospheric pressure plasma jet: Effect of electrode configuration, discharge behavior, and its formation mechanism. J Appl Phys **106:**013308. doi: 10.1063/1.3159884.

158. **Uljas HE, Ingham SC.** 1999. Combinations of intervention treatments resulting in 5-log10-unit reductions in numbers of *Escherichia coli* O157:H7 and *Salmonella* Typhimurium DT104 organisms in apple cider. Appl Environ Microbiol **65:**1924-1929.

159. **Jorgensen JH, Ferraro MJ.** 2009. Antimicrobial susceptibility testing: a review of general principles and contemporary practices. Clin Infect Dis **49:**1749-1755.

160. **Alagumaruthanayagam A, Pavankumar AR, Vasanthamallika TK, Sankaran K.** 2009. Evaluation of solid (disc diffusion)- and liquid (turbidity)-phase antibiogram methods for clinical isolates of diarrheagenic *E. coli* and correlation with efflux. J Antibiot **62:**377-384.

161. **Sousa JS, Niemi K, Cox LJ, Algwari QT, Gans T, O'Connell D.** 2011. Cold atmospheric pressure plasma jets as sources of singlet delta oxygen for biomedical applications. J Appl Phys **109**(12)**:**123302. doi:10.1063/1.3601347.

162. **Perni S, Liu DW, Shama G, Kong MG.** 2008. Cold atmospheric plasma decontamination of the pericarps of fruit. J Food Protect **71:**302-308.

163. **Matthes R, Bender C, Schluter R, Koban I, Bussiahn R, Reuter S, Lademann J, Weltmann KD, Kramer A.** 2013. Antimicrobial efficacy of two surface barrier discharges with air plasma against in vitro biofilms. PLoS ONE **8:**e70462. doi:10.1371/journal.pone.0070462.

164. **Matthes R, Bekeschus S, Bender C, Koban I, Hubner NO, Kramer A.** 2012. Pilot-study on the influence of carrier gas and plasma application (open resp. delimited) modifications on physical plasma and its antimicrobial effect against *Pseudomonas aeruginosa* and *Staphylococcus aureus*. GMS Krankenhhyg Interdiszip **7:**Doc02.

165. **Li S, Tang ZC, Gu F.** 2010. Experimental study on temperature characteristics and energy conversion in packed bed reactor with dielectric barrier discharge. Heat Mass Transfer **46:**851-857.

166. **Kim SJ, Chung TH, Bae SH, Leem SH.** 2009. Bacterial inactivation using atmospheric pressure single pin electrode microplasma jet with a ground ring. Appl Phys Lett **94:**141502. doi:10.1063/1.3114407.

167. **Sands BL, Ganguly BN, Tachibana K.** 2008. Time-resolved imaging of "Plasma Bullets" in a dielectric capillary atmospheric pressure discharge. IEEE T Plasma Sci **36:**956-957.

168. **Jiang N, Ji AL, Cao ZX.** 2010. Atmospheric pressure plasma jets beyond ground electrode as charge overflow in a dielectric barrier discharge setup. J Appl Phys **108:**033302. doi:10.1063/1.3466993.

169. **Jansky J, Algwari QT, O'Connell D, Bourdon A.** 2012. Experimental-modeling study of an atmospheric-pressure helium discharge propagating in a thin dielectric tube. IEEE T Plasma Sci **40:**2912-2919.

170. **Hirst AM, Frame FM, Maitland NJ, O'Connell D.** 2014. Low temperature plasma: a novel focal therapy for localized prostate cancer? Biomed Res Int **2014:**878319. doi:10.1155/2014/878319.

171. **Sompolinsky D, Samra Z.** 1968. Mechanism of high-level resistance to chloramphenicol in different *Escherichia coli* variants. J Gen Microbiol **50:**55-66.

172. **Dempsey DJ, Thirucote RR.** 1989. Sterilization of medical devices: a review. J Biomater Appl **3:**454-523.

173. **Deng XT, Shi JJ, Shama G, Kong MG.** 2005. Effects of microbial loading and sporulation temperature on atmospheric plasma inactivation of *Bacillus subtilis* spores. Appl Phys Lett **87:**153901. doi:10.1063/1.2103394.

174. **McKinlay AF, Bernhardt JH, Ahlbom A, Cesarini JP, de Gruijl FR, Hietanen M, Owen R, Sliney DH, Soderberg P, Swerdlow AJ, Taki M, Tenforde TS, Vecchia P, Veyret B, Matthes R, Repacholi MH, Diffey B, Mainster MA, Okuno T, Stuck BE, Radiati ICN.** 2004. Guidelines on limits of exposure to ultraviolet radiation of wavelengths between 180 nm and 400 nm (incoherent optical radiation). Health Phys 87:171-186.

175. **Shimizu K.** 2013. Metabolic regulation of a bacterial cell system with emphasis on *Escherichia coli* metabolism. ISRN Biochem **2013:**645983.

176. **McDougald D, Rice SA, Kjelleberg S.** 1999. New perspectives on the viable but nonculturable response. Biologia **54:**617-623.

177. **McDougald D, Gong L, Srinivasan S, Hild E, Thompson L, Takayama K, Rice SA, Kjelleberg S.** 2002. Defences against oxidative stress during starvation in bacteria. Antonie Van Leeuwenhoek **81:**3-13.

178. **Poole K.** 2012. Bacterial stress responses as determinants of antimicrobial resistance. J Antimicrob Chemoth **67:**2069-2089.

179. **Poole K.** 2012. Stress responses as determinants of antimicrobial resistance in Gram-negative bacteria. Trends Microbiol **20:**227-234.

180. **Faure P, Oziol L, Le Bihan ML, Chomard P.** 2004. Cell culture media are potent antioxidants that interfere during LDL oxidation experiments. Biochimie **86:**373-378.

181. **Attri P, Kumar N, Park JH, Yadav DK, Choi S, Uhm HS, Kim IT, Choi EH, Lee W.** 2015. Influence of reactive species on the modification of biomolecules generated from the soft plasma. Sci Rep **5:**8221. doi:10.1038/srep08221.

182. **Seshasayee AS, Bertone P, Fraser GM, Luscombe NM.** 2006. Transcriptional regulatory networks in bacteria: from input signals to output responses. Curr Opin Microbiol **9:**511-519.

183. **Tao H, Bausch C, Richmond C, Blattner FR, Conway T.** 1999. Functional genomics: Expression analysis of *Escherichia coli* growing on minimal and rich media. J Bacteriol **181:**6425-6440.

184. **Battesti A, Majdalani N, Gottesman S.** 2011. The Rpos-mediated general stress response in *Escherichia coli*. Annu Rev Microbiol **65:**189-213.

185. **Nair S, Finkel SE.** 2004. Dps protects cells against multiple stresses during stationary phase. J Bacteriol **186:**4192-4198.

186. **Kram KE, Finkel SE.** 2015. Rich medium composition affects *Escherichia coli* survival, glycation, and mutation frequency during long-term batch culture. Appl Environ Microbiol **81:**4442-4450.

187. **Davies MJ, Fu SL, Dean RT.** 1995. Protein hydroperoxides can give rise to reactive free-radicals. Biochem J **305:**643-649.

188. **Gebicki S, Gebicki JM.** 1993. Formation of peroxides in amino acids and proteins exposed to oxygen free radicals. Biochem J **289:**743-749.

189. **Kalghatgi S, Fridman A, Azizkhan-Clifford J, Friedman G.** 2012. DNA damage in mammalian cells by non-thermal atmospheric pressure microsecond pulsed dielectric barrier discharge plasma is not mediated by ozone. Plasma Process Polym **9:**726-732.

190. **Schneider S, Dünnbier M, Hübner S, Reuter S, Benedikt J.** 2014. Atomic nitrogen: a parameter study of a micro-scale atmospheric pressure plasma jet by means of molecular beam mass spectrometry. J Phys D: Appl Phys **47:**505203. doi:10.1088/0022-3727/47/50/505203.

191. **Miao H, Yun G.** 2011. The sterilization of *Escherichia coli* by dielectric-barrier discharge plasma at atmospheric pressure. Appl Surf Sci **257:**7065-7070.

192. **Yarmolenko PS, Moon EJ, Landon C, Manzoor A, Hochman DW, Viglianti BL, Dewhirst MW.** 2011. Thresholds for thermal damage to normal tissues: an update. Int J Hyperthermia **27:**320-343.

193. **Tian Y, Sun P, Wu H, Bai N, Wang R, Zhu W, Zhang J, Liu F.** 2010. Inactivation of *Staphylococcus aureus* and *Enterococcus faecalis* by a direct-current, cold atmospheric-pressure air plasma microjet. J Biomed Res **24:**264-269.

194. **Nijdam S, van Veldhuizen E, Bruggeman P, Ebert U.** 2012. An Introduction to Nonequilibrium Plasmas at Atmospheric Pressure, p. 1-44, Plasma Chemistry and Catalysis in Gases and Liquids. Wiley-VCH Verlag GmbH & Co. KGaA. doi:10.1002/9783527649525.ch1.

195. **Bensasson RV, Land EJ, Truscott TG.** 1993. Excited states and free radicals in biology and medicine: Contributions from flash photolysis and pulse radiolysis. Oxford University Press, Oxford.

196. **Lu XP, Laroussi M.** 2005. Optimization of ultraviolet emission and chemical species generation from a pulsed dielectric barrier discharge at atmospheric pressure. J Appl Phys **98:**023301. doi:10.1063/1.1980530.

197. **Pipa AV, Hoder T, Brandenburg R.** 2013. On the role of capacitance determination accuracy for the electrical characterization of pulsed driven dielectric barrier discharges. Contrib Plasma Phys **53:**469-480.

198. **Sretenovic GB, Krstic IB, Kovacevic VV, Obradovic BM, Kuraica MM.** 2014. Spatio-temporally resolved electric field measurements in helium plasma jet. J Phys D: Appl Phys **47**(10)**:**102001. doi:10.1088/0022-3727/47/10/102001.

199. **Schneider S, Lackmann JW, Narberhaus F, Bandow JE, Denis B, Benedikt J.** 2011. Separation of VUV/UV photons and reactive particles in the effluent of a He/O_2 atmospheric pressure plasma jet. J Phys D: Appl Phys **44**(37)**:**379501. doi:10.1088/0022-3727/44/37/379501.

200. **Schneider S, Lackmann JW, Ellerweg D, Denis B, Narberhaus F, Bandow JE, Benedikt J.** 2012. The role of VUV radiation in the inactivation of bacteria with an atmospheric pressure plasma jet. Plasma Process Polym **9:**561-568.

201. **Zhang XH, Huang J, Liu XD, Peng L, Guo LH, Lv GH, Chen W, Feng KC, Yang SZ.** 2009. Treatment of *Streptococcus mutans* bacteria by a plasma needle. J Appl Phys **105:**063302. doi:10.1063/1.3080249.

202. **Udekwu KI, Parrish N, Ankomah P, Baquero F, Levin BR.** 2009. Functional relationship between bacterial cell density and the efficacy of antibiotics. J Antimicrob Chemoth **63:**745-757.

203. **Nosenko T, Shimizu T, Morfill GE.** 2009. Designing plasmas for chronic wound disinfection. New J Phys **11:**115013. doi:10.1088/1367-2630/11/11/115013.

204. **Young KD.** 2006. The selective value of bacterial shape. Microbiol Mol Biol Rev **70:**660-703.

205. **Imlay JA, Linn S.** 1988. DNA damage and oxygen radical toxicity. Science **240:**1302-1309.

206. **Lu H, Patil S, Keener KM, Cullen PJ, Bourke P.** 2014. Bacterial inactivation by high-voltage atmospheric cold plasma: influence of process parameters and effects on cell leakage and DNA. J Appl Microbiol **116:**784-794.

207. **Oehmigen K, Hahnel M, Brandenburg R, Wilke C, Weltmann KD, von Woedtke T.** 2010. The role of acidification for antimicrobial activity of atmospheric pressure plasma in liquids. Plasma Process Polym **7:**250-257.

208. **Bahnev B, Bowden MD, Stypczynska A, Ptasinska S, Mason NJ, Braithwaite NS.** 2014. A novel method for the detection of plasma jet boundaries by exploring DNA damage. Eur Phys J D **68:**140. doi:10.1140/epjd/e2014-40844-9.

209. **Reed NG.** 2010. The history of ultraviolet germicidal irradiation for air disinfection. Public Health Rep **125:**15-27.

210. **Pfeifer GP.** 1997. Formation and processing of UV photoproducts: effects of DNA sequence and chromatin environment. Photochem Photobiol **65:**270-283.

211. **Santos AL, Oliveira V, Baptista I, Henriques I, Gomes NC, Almeida A, Correia A, Cunha A.** 2013. Wavelength dependence of biological damage induced by UV radiation on bacteria. Arch Microbiol **195:**63-74.

212. **Shee C, Cox BD, Gu F, Luengas EM, Joshi MC, Chiu LY, Magnan D, Halliday JA, Frisch RL, Gibson JL, Nehring RB, Do HG, Hernandez M, Li L, Herman C, Hastings PJ, Bates D, Harris RS, Miller KM, Rosenberg SM.** 2013. Engineered proteins detect spontaneous DNA breakage in human and bacterial cells. Elife 2:e01222. doi:10.7554/eLife.01222.

213. **Ellerweg D, von Keudell A, Benedikt J.** 2012. Unexpected O and O_3 production in the effluent of He/O_2 microplasma jets emanating into ambient air. Plasma Sources Sci Technol **21:**034019. doi:10.1088/0963-0252/21/3/034019.

214. **Ingram M, Haines RB.** 1949. Inhibition of bacterial growth by pure ozone in the presence of nutrients. J Hyg (Lond) **47:**146-158, tab.

215. **Hemke T, Wollny A, Gebhardt M, Brinkmann RP, Mussenbrock T.** 2011. Spatially resolved simulation of a radio-frequency driven micro-atmospheric pressure plasma jet and its effluent. J Phys D: Appl Phys **44:**285206. doi:10.1088/0022-3727/44/28/285206.

216. **Norberg SA, Johnsen E, Kushner MJ.** 2015. Formation of reactive oxygen and nitrogen species by repetitive negatively pulsed helium atmospheric pressure plasma jets propagating into humid air. Plasma Sources Sci T **24:**035026. doi:10.1088/0963-0252/24/3/035026.

217. **Waskoenig J, Niemi K, Knake N, Graham LM, Reuter S, Gathen VS-vd, Gans T.** 2010. Atomic oxygen formation in a radio-frequency driven micro-atmospheric pressure plasma jet. Plasma Sources Sci T **19:**045018.

218. **Wani S, Maker J, Thompson J, Barnes J, Singleton I.** 2015. Effect of ozone treatment on inactivation of *Escherichia coli* and *Listeria sp.* on spinach. Agriculture **5:**155.

219. **Alexandre EM, Brandao TR, Silva CL.** 2011. Emerging technologies to improve safety and quality of fruits and vegetables. *In* McElhatton A, do Amaral Sobral PJ (ed.), Novel Technologies in Food Science: Their impact on products, consumer trends and the environment. Springer Science & Business Media, New York, USA.

220. **Lukes P, Dolezalova E, Sisrova I, Clupek M.** 2014. Aqueous-phase chemistry and bactericidal effects from an air discharge plasma in contact with water: evidence for the formation of peroxynitrite through a pseudo-second-order post-discharge reaction of H_2O_2 and HNO_2. Plasma Sources Sci Technol **23:**015019. doi:10.1088/0963-0252/23/1/015019.

221. **Duan J, Kasper DL.** 2011. Oxidative depolymerization of polysaccharides by reactive oxygen/nitrogen species. Glycobiology **21:**401-409.

222. **Tresp H, Hammer MU, Weltmann K-D, Reuter S.** 2013. Effects of atmosphere composition and liquid type on plasma-generated reactive species in biologically relevant solutions. Plasma Med **3:**45-55.

223. **Bryan NS, Grisham MB.** 2007. Methods to detect nitric oxide and its metabolites in biological samples. Free Radical Bio Med **43:**645-657.

224. **Nakamura K, Ishiyama K, Ikai H, Kanno T, Sasaki K, Niwano Y, Kohno M.** 2011. Reevaluation of analytical methods for photogenerated singlet oxygen. J Clin Biochem Nutr **49:**87-95.

225. **Gomes A, Fernandes E, Lima JLFC.** 2006. Use of fluorescence probes for detection of reactive nitrogen species: A review. J Fluoresc **16:**119-139.

226. **Halliwell B, Whiteman M.** 2004. Measuring reactive species and oxidative damage *in vivo* and in cell culture: how should you do it and what do the results mean? Brit J Pharmacol **142:**231-255.

227. **Hawkins CL, Davies MJ.** 2014. Detection and characterisation of radicals in biological materials using EPR methodology. BBA-Gen Subjects **1840:**708-721.

228. **Villamena FA, Zweier JL.** 2004. Detection of reactive oxygen and nitrogen species by EPR spin trapping. Antioxid Redox Signal **6:**619-629.

229. **Takamatsu T, Uehara K, Sasaki Y, Miyahara H, Matsumura Y, Iwasawa A, Ito N, Azuma T, Kohno M, Okino A.** 2014. Investigation of reactive species using various gas plasmas. RSC Advances 4:39901-39905.

230. **Takamatsu T, Kawano H, Miyahara H, Azuma T, Okino A.** 2015. Atmospheric nonequilibrium mini-plasma jet created by a 3D printer. AIP Advances **5:**077184. doi:10.1063/1.4928034.

231. **Tresp H, Hammer MU, Winter J, Weltmann K-D, Reuter S.** 2013. Quantitative detection of plasma-generated radicals in liquids by electron paramagnetic resonance spectroscopy. J Phys D: Appl Phys **46:**435401. doi:10.1088/0022-3727/46/43/435401.

232. **Kohno M.** 2010. Applications of electron spin resonance spectrometry for reactive oxygen species and reactive nitrogen species research. J Clin Biochem Nutr **47:**1-11.

233. **Betterton EA, Craig D.** 1999. Kinetics and mechanism of the reaction of azide with ozone in aqueous solution. J Air Waste Manag Assoc **49:**1347-1354.

234. **Tsuchiya K, Yoshizumi M, Houchi H, Mason RP.** 2000. Nitric oxide-forming reaction between the iron-N-methyl-D-glucamine dithiocarbamate complex and nitrite. J Biol Chem **275:**1551-1556.

235. **Ivanov VM.** 2004. The 125th anniversary of the Griess reagent. J Anal Chem+ **59:**1002-1005.

236. **Gibson AR, McCarthy HO, Ali AA, O'Connell D, Graham WG.** 2014. Interactions of a non-thermal atmospheric pressure plasma effluent with PC-3 prostate cancer cells. Plasma Process Polym **11:**1142-1149.

237. **Emerit J, Michelson AM.** 1982. Free-radicals in medicine and biology. Sem Hop Paris **58:**2670-2675.

238. **Laroussi M, Alexeff I, Kang WL.** 2000. Biological decontamination by nonthermal plasmas. IEEE T Plasma Sci **28**.

239. **Gutteridge JMC, Halliwell B.** 1992. Comments on review of free radicals in biology and medicine. Free Radical Bio Med **12:**93-95.

240. **Fridman G, Brooks AD, Balasubramanian M, Fridman A, Gutsol A, Vasilets VN, Ayan H, Friedman G.** 2007. Comparison of direct and indirect effects of non-thermal atmospheric-pressure plasma on bacteria. Plasma Process Polym **4:**370-375.

241. **Steeb B, Claudi B, Burton NA, Tienz P, Schmidt A, Farhan H, Mazé A, Bumann D.** 2013. Parallel exploitation of diverse host nutrients enhances *Salmonella* virulence. PLoS Pathog **9:**e1003301. doi:10.1371/journal.ppat.1003301.

242. **Sears J, Mohades S, Razavi H, Laroussi M.** 2015. Measurement of hydrogen peroxide concentrations in plasma activated media, 22nd International Symposium on Plasma Chemistry. http://www.ispc-conference.org/ispcproc/ispc22/P-I-3-11.pdf.

243. **Ikawa S, Kitano K, Hamaguchi S.** 2010. Effects of pH on bacterial inactivation in aqueous solutions due to low-temperature atmospheric pressure plasma application. Plasma Process Polym **7:**33-42.

244. **Kong MG, Kroesen G, Morfill G, Nosenko T, Shimizu T, van Dijk J, Zimmermann JL.** 2009. Plasma medicine: an introductory review. New J Phys **11:**115012. doi:10.1088/1367-2630/11/11/115012.

245. **Eisenberg GM.** 1943. Colorimetric determination of hydrogen peroxide. Ind Eng Chem Anal Ed **15:**327-328.

246. **Oehmigen K, Winter J, Hahnel M, Wilke C, Brandenburg R, Weltmann KD, von Woedtke T.** 2011. Estimation of possible mechanisms of *Escherichia coli* inactivation by plasma treated sodium chloride solution. Plasma Process Polym **8:**904-913.

247. **Hebrard M, Viala JP, Meresse S, Barras F, Aussel L.** 2009. Redundant hydrogen peroxide scavengers contribute to *Salmonella* virulence and oxidative stress resistance. J Bacteriol **191:**4605-4614.

248. **Liu DX, Bruggeman P, Iza F, Rong MZ, Kong MG.** 2010. Global model of low-temperature atmospheric-pressure He + H_2O plasmas. Plasma Sources Sci Technol **19:**025018. doi:10.1088/0963-0252/19/2/025018.

249. **Hirst AM, Simms MS, Mann VM, Maitland NJ, O'Connell D, Frame FM.** 2015. Low-temperature plasma treatment induces DNA damage leading to necrotic cell death in primary prostate epithelial cells. Br J Cancer **112:**1536-1545.

250. **Kaushik N, Uddin N, Sim GB, Hong YJ, Baik KY, Kim CH, Lee SJ, Kaushik NK, Choi EH.** 2015. Responses of solid tumor cells in DMEM to reactive oxygen species generated by non-thermal plasma and chemically induced ROS systems. Sci Rep **5:**8587. doi:10.1038/srep08587.

251. **Laroussi M.** 1996. Sterilization of contaminated matter with an atmospheric pressure plasma. IEEE T Plasma Sci **24:**1188-1191.

252. **Moreau S, Moisan M, Tabrizian M, Barbeau J, Pelletier J, Ricard A, Yahia L.** 2000. Using the flowing afterglow of a plasma to inactivate *Bacillus subtilis* spores: Influence of the operating conditions. J Appl Phys **88:**1166-1174.

253. **Muranyi P, Wunderlich J, Heise M.** 2007. Sterilization efficiency of a cascaded dielectric barrier discharge. J Appl Microbiol **103:**1535-1544.

254. **Choi JH, Han I, Baik HK, Lee MH, Han D-W, Park J-C, Lee I-S, Song KM, Lim YS.** 2006. Analysis of sterilization effect by pulsed dielectric barrier discharge. J Electrostat **64:**17-22.

255. **Pankaj SK, Misra NN, Cullen PJ.** 2013. Kinetics of tomato peroxidase inactivation by atmospheric pressure cold plasma based on dielectric barrier discharge. Innov Food Sci Emerg **19:**153-157.

256. **Guo J, Huang K, Wang JP.** 2015. Bactericidal effect of various non-thermal plasma agents and the influence of experimental conditions in microbial inactivation: A review. Food Control **50:**482-490.

257. **Arjunan KP, Sharma VK, Ptasinska S.** 2015. Effects of atmospheric pressure plasmas on isolated and cellular DNA: a review. Int J Mol Sci **16:**2971-3016.

258. **Yusupov M, Bogaerts A, Huygh S, Snoeckx R, van Duin ACT, Neyts EC.** 2013. Plasma-induced destruction of bacterial cell wall components: A reactive molecular dynamics simulation. J Phys Chem C **117:**5993-5998.

259. **Ferrell JR, Galov AS, Gostev VA, Banks BA, Weeks SP, Fulton JA, Woolverton CJ.** 2013. Characterization, properties and applications of nonthermal plasma: A novel pulsed-based option. J Biotechnol Biomater **3:**155. doi:10.4172/2155-952X.1000155.

260. **Ziuzina D, Patil S, Cullen PJ, Keener KM, Bourke P.** 2013. Atmospheric cold plasma inactivation of *Escherichia coli* in liquid media inside a sealed package. J Appl Microbiol **114:**778-787.

261. **Ke ZG, Huang Q.** 2013. Inactivation and heme degradation of horseradish peroxidase induced by discharge plasma. Plasma Process Polym **10:**731-739.

262. **Ercan UK, Wang H, Ji HF, Fridman G, Brooks AD, Joshi SG.** 2013. Nonequilibrium plasma-activated antimicrobial solutions are broad-spectrum and retain their efficacies for extended period of time. Plasma Process Polym **10:**544-555.

263. **Winter J, Tresp H, Hammer MU, Iseni S, Kupsch S, Schmidt-Bleker A, Wende K, Dünnbier M, Masur K, Weltmann K-D, Reuter S.** 2014. Tracking plasma generated H_2O_2 from gas into liquid phase and revealing its dominant impact on human skin cells. J Phys D: Appl Phys **47**(28)**:**285401. doi:10.1088/0022-3727/47/28/285401.

264. **Battino R, Rettich TR, Tominaga T.** 1983. The solubility of oxygen and ozone in liquids. J Phys Chem Ref Data **12:**163-178.

265. **Singh A, Singh H.** 1983. Time-scale and nature of radiation biological damage: Approaches to radiation protection and post-irradiation therapy. Prog Biophys Mol Bio **39:**69-107.

266. **Pryor WA.** 1986. Oxy-radicals and related species: their formation, lifetimes, and reactions. Annu Rev Physiol **48:**657-667.

267. **Luc R, Vergely C.** 2008. Forgotten radicals in biology. Int J Biomed Sci **4:**255-259.

268. **Chamnongpol S, Willekens H, Moeder W, Langebartels C, Sandermann H, Jr., van Montagu M, Inze D, van Camp W.** 1998. Defense activation and enhanced pathogen tolerance induced by H_2O_2 in transgenic tobacco. PNAS **95:**5818-5823.

269. **Watson JA, Schubert J.** 1969. Action of hydrogen peroxide on growth inhibition of *Salmonella* Typhimurium. J Gen Microbiol **57:**25-34.

270. **Khadre MA, Yousef AE, Kim JG.** 2001. Microbiological aspects of ozone applications in food: A review. J Food Sci **66:**1242-1252.

271. **Carlsson J, Berglin EH, Claesson R, Edlund MBK, Persson S.** 1988. Catalase inhibition by sulfide and hydrogen peroxide-induced mutagenicity in *Salmonella* Typhimurium strain TA102. Mutat Res **202:**59-64.

272. **Dahl TA, Midden WR, Hartman PE.** 1988. Pure exogenous singlet oxygen: nonmutagenicity in bacteria. Mutat Res **201:**127-136.

273. **Jiang WM, Tang J, Wang YS, Zhao W, Duan YX.** 2014. Characterization of argon direct-current glow discharge with a longitudinal electric field applied at ambient air. Sci Rep **4:**6323. doi:10.1038/Srep06323.

274. **Yonemori S, Ono R.** 2014. Flux of OH and O radicals onto a surface by an atmospheric-pressure helium plasma jet measured by laser-induced fluorescence. J Phys D: Appl Phys **47:**125401. doi:10.1088/0022-3727/47/12/125401.

275. **Birer Ö.** Reactivity zones around an atmospheric pressure plasma jet. Applied Surface Science**:**In-press. doi:10.1016/j.apsusc.2015.04.100.

276. **Torlak E, Sert D, Ulca P.** 2013. Efficacy of gaseous ozone against *Salmonella* and microbial population on dried oregano. Int J Food Microbiol **165:**276-280.

277. **Akbas MY, Ozdemir M.** 2006. Effectiveness of ozone for inactivation of *Escherichia coli* and *Bacillus cereus* in pistachios. Int J Food Sci Tech **41:**513-519.

278. **Kono Y, Fridovich I.** 1982. Superoxide radical inhibits catalase. J Biol Chem **257:**5751-5754.

279. **Muller S, Nebe-von-Caron G.** 2010. Functional single-cell analyses: flow cytometry and cell sorting of microbial populations and communities. FEMS Microbiol Rev **34:**554-587.

280. **Muller S, Harms H, Bley T.** 2010. Origin and analysis of microbial population heterogeneity in bioprocesses. Curr Opin Biotech **21:**100-113.

281. **Lewis K.** 2007. Persister cells, dormancy and infectious disease. Nat Rev Microbiol **5:**48-56.

282. **Willenborg J, Willms D, Bertram R, Goethe R, Valentin-Weigand P.** 2014. Characterization of multi-drug tolerant persister cells in *Streptococcus suis*. BMC Microbiol **14:**120. doi:10.1186/1471-2180-14-120.

283. **Gefen O, Balaban NQ.** 2009. The importance of being persistent: heterogeneity of bacterial populations under antibiotic stress. FEMS Microbiol Rev **33:**704-717.

284. **Lewis K.** 2010. Persister cells. Annu Rev Microbiol **64:**357-372.

285. **Nikaido H.** 2009. Multidrug resistance in bacteria. Annu Rev Biochem **78:**119-146.

286. **Fröhling A, Schlüter OK.** 2015. Flow cytometric evaluation of physico-chemical impact on Gram-positive and Gram-negative bacteria. Front Microbiol **6:**939. doi:10.3389/fmicb.2015.00939.

287. **Frohling A, Baier M, Ehlbeck J, Knorr D, Schluter O.** 2012. Atmospheric pressure plasma treatment of *Listeria innocua* and *Escherichia coli* at polysaccharide surfaces: Inactivation kinetics and flow cytometric characterization. Innov Food Sci Emerg **13:**142-150.

288. **Lunov O, Zablotskii V, Churpita O, Chanova E, Sykova E, Dejneka A, Kubinova S.** 2014. Cell death induced by ozone and various non-thermal plasmas: therapeutic perspectives and limitations. Sci Rep **4:**7129. doi:10.1038/Srep07129.

289. **Haertel B, Strassenburg S, Oehmigen K, Wende K, von Woedtke T, Lindequist U.** 2013. Differential influence of components resulting from atmospheric-pressure plasma on integrin expression of human HaCaT keratinocytes. Biomed Res Int **2013:**761451. doi:10.1155/2013/761451.

290. **Uchiyama H, Zhao Q-L, Hassan MA, Andocs G, Nojima N, Takeda K, Ishikawa K, Hori M, Kondo T.** 2015. EPR-spin trapping and flow cytometric studies of free radicals generated using cold atmospheric argon plasma and X-ray irradiation in aqueous solutions and intracellular milieu. PLoS ONE **10:**e0136956. doi:10.1371/journal.pone.0136956.

291. **Collins AR.** 2004. The comet assay for DNA damage and repair: principles, applications, and limitations. Mol Biotechnol **26:**249-261.

292. **Tamayo M, Santiso R, Gosalvez J, Bou G, Fernandez JL.** 2009. Rapid assessment of the effect of ciprofloxacin on chromosomal DNA from *Escherichia coli* using an *in situ* DNA fragmentation assay. BMC Microbiol **9:**69. doi:10.1186/1471-2180-9-69.

293. **Santiso R, Tamayo M, Fernandez JL, Fernandez MD, Molina F, Villanueva R, Gosalvez J, Bou G.** 2009. Rapid and simple determination of ciprofloxacin resistance in clinical strains of *Escherichia coli*. J Clin Microbiol **47:**2593-2595.

294. **Tamayo M, Santiso R, Otero F, Bou G, Lepe JA, McConnell MJ, Cisneros JM, Gosalvez J, Fernandez JL.** 2013. Rapid determination of colistin resistance in clinical strains of *Acinetobacter baumannii* by use of the micromax assay. J Clin Microbiol **51:**3675-3682.

295. **Michaels ML, Cruz C, Grollman AP, Miller JH.** 1992. Evidence that MutY and MutM combine to prevent mutations by an oxidatively damaged form of guanine in DNA. PNAS **89:**7022-7025.

296. **von Woedtke T, Reuter S, Masur K, Weltmann KD.** 2013. Plasmas for medicine. Phys Rep **530:**291-320.

297. **Isbary G, Zimmermann JL, Shimizu T, Li YF, Morfill GE, Thomas HM, Steffes B, Heinlin J, Karrer S, Stolz W.** 2013. Non-thermal plasma — More than five years of clinical experience. Clin Plasma Med 1:19-23.

298. **Griffiths S, Smith S, MacGregor SJ, Anderson JG, Van Der Walle C, Beveridge JR, Helen Grant M.** 2008. Pulsed electric field treatment as a potential method for microbial inactivation in scaffold materials for tissue engineering: the inactivation of bacteria in collagen gel. J Appl Microbiol **105:**963-969.

299. **Hong YJ, Nam CJ, Song KB, Cho GS, Uhm HS, Choi DI, Choi EH.** 2012. Measurement of hydroxyl radical density generated from the atmospheric pressure bioplasma jet. JINST **7:**C03046. doi:10.1088/1748-0221/7/03/C03046.

300. **Van Gaens W, Bruggeman PJ, Bogaerts A.** 2014. Numerical analysis of the NO and O generation mechanism in a needle-type plasma jet. New J Phys **16:**063054. doi:10.1088/1367-2630/16/6/063054.

301. **Hartmann M, Berditsch M, Hawecker J, Ardakani MF, Gerthsen D, Ulrich AS.** 2010. Damage of the bacterial cell envelope by antimicrobial peptides gramicidin S and PGLa as revealed by transmission and scanning electron microscopy. Antimicrob Agents Chemother **54:**3132-3142.

302. **Babaeva NY, Kushner MJ.** 2013. Reactive fluxes delivered by dielectric barrier discharge filaments to slightly wounded skin. J Phys D: Appl Phys **46**(2)**:**025401. doi:10.1088/0022-3727/46/2/025401.

303. **Gopalakrishnan V, Kim M, An G.** 2013. Using an agent-based model to examine the role of dynamic bacterial virulence potential in the pathogenesis of surgical site infection. Adv Wound Care (New Rochelle) **2:**510-526.

304. **Rogers GB, Hoffman LR, Whiteley M, Daniels TWV, Carroll MP, Bruce KD.** 2010. Revealing the dynamics of polymicrobial infections: implications for antibiotic therapy. Trends Microbiol **18:**357-364.

305. **McVicker G, Prajsnar TK, Williams A, Wagner NL, Boots M, Renshaw SA, Foster SJ.** 2014. Clonal expansion during *Staphylococcus aureus* infection dynamics reveals the effect of antibiotic intervention. PLoS Pathog **10:**e1003959.

306. **Hoffman LR, Deziel E, D'Argenio DA, Lepine F, Emerson J, McNamara S, Gibson RL, Ramsey BW, Miller SI.** 2006. Selection for *Staphylococcus aureus* small-colony variants due to growth in the presence of *Pseudomonas aeruginosa*. PNAS **103:**19890-19895.

307. **Biswas L, Biswas R, Schlag M, Bertram R, Gotz F.** 2009. Small-colony variant selection as a survival strategy for *Staphylococcus aureus* in the presence of *Pseudomonas aeruginosa*. Appl Environ Microbiol **75:**6910-6912.